SETTLEMENT OF STRIP FOOTING ON SAND MAT PLACED OVER THICK SOFT CLAY DEPOSIT

by

SHARIFULLAH AHMED

A thesis submitted to the Department of Civil Engineering,
Bangladesh University of Engineering and Technology,
Dhaka, in partial fulfillment of the degree of

MASTER OF SCIENCE IN ENGINEERING (CIVIL & GEOTECHNICAL)

DEPARTMENT OF CIVIL ENGINEERING

BANGLADESH UNIVERSITY OF ENGINEERING AND TECHNOLOGY

DHAKA, BANGLADESH

DECEMBER, 2016

The thesis titled **"Settlement of Strip Footing on Sand Mat Placed over Thick Soft Clay Deposit"**, submitted by **Sharifullah Ahmed,** Roll Number: **0409042234**, Session: **April, 2009**, has been accepted as satisfactory in partial fulfillment of the requirement for the degree of **Master of Science in Engineering (Civil & Geotechnical)** on **December 31, 2016.**

BOARD OF EXAMINERS

Dr. Sarwar Jahan Md. Yasin
Professor
Department of Civil Engineering
Bangladesh University
of Engineering and Technology
Dhaka - 1000.

Chairman
(Supervisor)

Dr. Abdul Muqtadir
Professor and Head
Department of Civil Engineering
Bangladesh University
of Engineering and Technology
Dhaka - 1000.

Member
(Ex-officio)

Dr. Md. Zoynul Abedin
Professor
Department of Civil Engineering,
Bangladesh University
of Engineering and Technology
Dhaka-1000.

Member

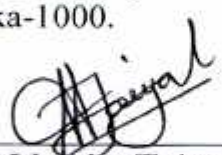

Dr. Md. Abu Taiyab
Professor
Department of Civil Engineering
Dhaka University of Engineering
and Technology
Gazipur-1700.

Member
(External)

DECLARATION

It is hereby declared that this thesis or any part of it has not been submitted elsewhere for the award of any degree or diploma.

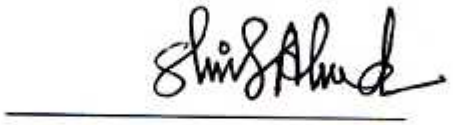

(Signature of the Student)

(Sharifullah Ahmed)

ACKNOWLEDGEMENT

The author wishes to express his deep appreciation to the almighty Allah for allowing him to bring an end of this thesis. Then he desires to convey his admiration to his supervisor Sarwar Jahan Md. Yasin, Professor, Department of Civil Engineering, Bangladesh University of Engineering and Technology (BUET), for his keen interest, valuable suggestions, proper guidance, cordial association and supervision throughout the project work. In the different stages of study and report making, his appropriate opinion and suggestions helped to avoid omissions, confusions and inconsistency.

The author gratefully acknowledges the constructive criticisms and valuable suggestions made by Professor Dr. Abdul Muqtadir, Professor Dr. Md. Zoynul Abedin and Professor Dr. Md. Abu Taiyab.

ABSTRACT

Shallow foundations on soft soils deposit without any improvement can undergo a high reduction in volume after consolidation and secondary settlement. For low and medium rise building projects on such soil condition, a deep foundation may not be economically feasible. For such a case an alternative to deep foundations may be shallow strip footings placed on a double layer foundation system in which the upper layer is untreated or cement treated compacted sand.

This research work deals with the specific case of the bearing capacity of a rigid plane-strain footing placed on the surface of a soil consisting of a uniform clean or treated sand layer overlying a thick, homogeneous bed of soft clay. The study considered both the cases where the thickness of the sand layer is thin or thick compared to the footing width. In all cases the ground surface and the interface between the two soil layers is taken as horizontal. It is assumed that the response of the clay layer is undrained for plastic loading stages and drained in consolidation stages and the response of the sand layer is drained in all loading stages.

The settlement of the shallow strip foundation resting on layered soils, where upper layer as untreated or treated sand layer and bottom clay layer has been analyzed in this research work. Parametric study has been conducted to determine the effect of thickness, density, cementation of sand mat and density, shear strength of the soft clay layer on the settlement of strip foundation. A better insight of elasto-plastic, consolidation and creep settlements of a strip footing on sand mat under different footing pressure equivalent to low or moderately loaded low to medium rise residential or commercial building loads has been developed. Guidelines has been established for designing shallow strip footing with sand mat on thick soft clay deposit determining the thickness of sand mat for different material characteristics to avoid punching shear failure and to limit the settlement to an allowable level.

The relative settlement (S/S_o) at the center point of the footing for both untreated or cement treated upper sand mat was calculated, where S_o is the settlement for the case with H_i= 0.25m and S is the settlement for other thickness of upper sand mat. A larger value of relative settlement S/S_o indicates larger difference of settlement between the

cases of small and larger thickness of sand layer. From this study it is concluded that the relative settlement S/S_0 may be considered as the index of the effectiveness of sand layer.

A guideline is developed for strip footing on soft inorganic *NC* soil of Bangladesh having void ratio from 1.0 to 1.45. The research work was limited to a single value of E' and ϕ' of soft clay layer and also a single ϕ' value of sand mat. These design charts may be used to obtain total settlement for a given value of footing pressure, sand mat thickness, footing width and initial void ratio. For untreated or cement treated sand as upper layer, settlement of strip footing may be calculated for particular value of H_i, q, B and γ_{sat} using developed design chart or equations. For a specific value of settlement the design thickness of sand mat may be obtained using the proposed charts. The permissible settlement as per BNBC 2015 is 50mm. Design thickness of sand mat for 50mm settlement may be directly obtained from these charts.

For H_i/B =0.6 or above, settlement of Untreated Sand as upper layer into bottom clay layer is very small which represented the distribution of major deformation within upper layer and the influence zone of footing is limited in upper layer which indicates complete effectiveness of upper layer in bearing the foundation effectively. For H_i =0.75 or above settlement of footing with cement treated sand as upper layer and soft clay as bottom layer is very small which means the distribution of major deformation within upper layer and the function of footing is limited in upper layer which also indicates complete effectiveness of upper layer in bearing the foundation effectively. Brittle behavior of cemented sand and fracture or cracks is not considered in this analysis.

TABLE OF CONTENTS

CHAPTER-7
CONCLUSIONS

LIST OF FIGURES

LIST OF TABLES

NOTATIONS

c	Cohesion
C_u , S_u	Undrained shear-strength
$\underline{\underline{D}}_e$	Elastic material matrix representing Hooke's law
e	Void ratio
E	Young's modulus
EA	Axial stiffness
EI	Bending stiffness
E_{50}^{ref}	Reference secant modulus for deviatoric loading
E_{oed}^{ref}	Reference secant modulus for primary compression
E_{ur}^{ref}	Reference secant modulus for unloading/reloading
E_{oed}	Oedometer modulus
f	Yield function
g	Plastic potential function
G	Shear modulus
K	Bulk modulus
K_0	Coefficient of lateral earth pressure at rest
m	Power in stress-dependent stiffness relation
M	Slope of critical state line in p'-q space
n	Porosity
OCR	Overconsolidation ratio
p	Isotropic stress or mean stress, positive for pressure; negative for tension
p_p	Isotropic preconsolidation stress, positive for pressure
POP	Pre overburden pressure
q	Equivalent shear stress or deviatoric stress
R_f	Failure ratio
t	Time
$\underline{u}$	Vector with displacement components
γ	Volumetric weight
Δ	Increment

$\underline{\varepsilon}$	Vector with Cartesian strain components, normal components, positive for extension; negative for compression
ε_v	Volumetric strain, negative for compression; positive for extension
κ	Cam-Clay swelling index
κ^*	Modified swelling index
λ	Plastic multiplier
λ	Cam-Clay compression index
λ^*	Modified compression index
μ^*	Modified creep index
ν	Poisson's ratio
$\underline{\sigma}$	Vector with Cartesian stress components, normal components, positive
for	tension; negative for pressure
σ_p	Vertical preconsolidation stress, negative for pressure
ϕ	Friction angle
ψ	Dilatancy angle
k	Coefficient of permeability, m/s
k_1	Coefficient of permeability at initial state, m/s
n	Porosity, %
p	Mean stress, kPa
p'	Mean effective stress, kPa
q	Deviator stress, kPa
S_r	Degree of Saturation, %
S_t	Sensitivity
u_w	Pore water pressure, kPa
v	Specific Volume
w	Water content, %
w_L	Liquid Limit, %
w_P	Plastic Limit, %
z	Depth, m
σ_v	Reference pressure of Tangent modulus method, 100 kPa
m	Modulus number, Tangent modulus method
β	Stress exponent, Tangent modulus method
λ	Slope of the normal compression line in ln p' : v plane

κ	Slope of the swelling line in ln p' : v plane
γ	Unit weight, kN/m^3
γ_w	Unit weight of water, kN/m3
φ'	Effective friction angle, ^{o}
ψ	Dilatancy angle, ^{o}
v	Poisson ratio
E	Young's modulus
c	Cohesion
σ_p	Preconsolidation pressure, kPa
σ'_1, σ'_3	Principal effective stresses, kPa
ε	Strain
M_t	Tangent modulus, kPa
M_s	Secant modulus, kPa
M	Slope of Critical State line
c_v	Coefficient of consolidation (vertical flow), m^2/s
c_h	Coefficient of consolidation (horizontal flow), m^2/s
kPa	kN/m^2
r_k	Permeability ratio k_h / k_v
θ	Lode angle, ^{o}

CHAPTER- 1

INTRODUCTION

1.0 Introduction

In most of the parts of Bangladesh, urban and industrial developments often take place in region where the underlying soils are soft with high void ratios. Shallow foundations on such soft soil deposit without any improvement can undergo a high reduction in volume after consolidation and secondary settlement. For low and medium rise building projects on such soil condition, a deep foundation may not be economically feasible. For such case an alternative to deep foundations may be shallow strip footings placed on a double layer foundation system in which the upper layer is untreated or cement treated compacted sand to reduce the settlement.

The bearing capacity of a vertically loaded footing placed on the surface of a homogeneous soil may be estimated relatively easily using conventional Terzaghi's bearing capacity theory in which appropriate values of the bearing capacity factors are adopted. This type of calculation is based on the implicit assumption that the soil is rigid-perfectly plastic with the strength characterized by a cohesion and an angle of friction. Whilst this approach is highly successful for homogeneous soils, it cannot, in general, be used for cases where the soil properties vary with depth. If a foundation is placed on the surface of a layered soil for which the thickness of the top layer is large compared with the width of the foundation, then realistic estimates of the bearing capacity may be obtained using conventional bearing capacity theory based on the properties of the two soil layer. If the thickness of the top layer is comparable to the foundation width, however, this approach may not be appropriate.

This research work deals with the specific case of the bearing capacity of a rigid plane-strain footing placed on the surface of a soil consisting of a uniform clean or treated sand layer overlying a thick, homogeneous bed of clay. The study considered both the cases where the thickness of the sand layer is thin or thick comparable to the footing width and in all cases the ground surface and the interface between the two soil layers is horizontal. It is assumed that the response of the clay layer is undrained for plastic loading stages and drained in consolidation stages and the response of the sand layer is drained in all loading stages.

The settlement of the shallow foundation resting on layered soils, with an upper untreated or treated sand layer and bottom clay layer, depends on related parameters. The relative settlement (S/S_o) of the center point of the footing was calculated, where S_o is the settlement for the case with thickness of upper sand mat 0.25m and S is the settlement for others values of thickness of upper sand mat. The effect of these parameters on settlement has been presented through plotting these parameters against relative settlement. A detailed study has been carried out to investigate into the settlements of foundation, the plane strain displacement field in the foundation soil for various parameter ranges and to identify influence of the parameters. In this study, design guideline including design charts and design equations were developed using the results of finite element numerical analysis.

1.2 Objectives of the Study

This research attempts to focus on the following objectives:

a. Investigate and quantify the effect of dense sand mat on soft soil on the settlement of strip footings and deformation pattern or strain field of layered soil underlying the strip footings placed on this.

b. Conduct a parametric study to determine the effect of thickness, density, cementation of sand mat and density, shear strength of the soft clay layer on the settlement of strip foundation.

c. Develop a better insight of elasto-plastic, consolidation & creep settlements of a strip footing on sand mat under different footing pressure equivalent to low or moderately loaded low to medium rise residential or commercial building.

d. Determine the thickness of sand mat for different material characteristics to avoid punching shear failure and to limit the settlement to an allowable level.

e. Establish guidelines for designing shallow strip footing with sand mat on thick soft clay deposit.

1.3 Organization of the Thesis

FEM analyses of a plain strain 2D model of a strip footing on a sand mat over thick soft clay strata has been performed using PLAXIS 8.0. Footing pressure, sand mat thickness and stiffness, density and strength of the soft clay layer has been varied in the analyses. Soil models that has been used are Hardening Soil Model (for elasto-plastic settlement of clay layer and sand mat), Soft Soil Model (for consolidation settlement of soft clay) and Soft Soil Creep Model (for creep settlement of soft clay). A standard fixity and close consolidation boundary has been applied on the model geometry. The sand mat and top part of clay layer has been meshed more finely than the bottom part of soft clay layer with 15 noded finite elements. Footing settlement due to elasto-plastic, consolidation and creep deformation of the soil layers has been determined.

Obtained settlement of the plain strain strip footings has been presented in the form of non-dimensional charts incorporating the parameters of sand mat and clay layer.

The primary focus of this thesis is to provide a rigorous study into the behaviour of strip footings(Length>>Width), on a two layered soil system. A brief review of research into the bearing capacity and load-settlement response of footings on layered soil has been presented in Chapter 2.

Chapter 3 provides background to selected aspects of elasticity, plasticity and numerical method, as well as few constitutive models. It also includes detailed discussion on the numerical formulations adopted in this study.

Chapter 4 presents interpretation of materials parameters used in this research work. This includes problem definition and a discussion on geometric models used in this thesis which has been studying using numerical method. Analysis of has been made with two different Sand mat and their properties are mentioned in Chapter 4.

Chapter 5 includes operational procedure of PLAXIS relevant to the analysis made in this research work and a discussion on finite element models used in PLAXIS.

Parametric Study has been done using PLAXIS and the results are presented in graphical form in Chapter 6. Establishing design guideline including charts and equations to obtain thickness of upper sand mat to keep the settlement within permissible limit also presented in this chapter. Vertical displacement fields for different thickness of upper sand layer are also presented here for untreated and cement treated sand. Conclusions have been drawn on the basis of these parametric study and displacement fields in this chapter.

Chapter 7 presents conclusions and recommendation of further research.

CHAPTER-2
LITERATURE REVIEW

2.1 Introduction

In this chapter, literature related to bearing capacity and load settlement response of shallow foundation on layered sub-soil is discussed. Earlier analysis have been divided in two categories. One is limit analysis and another is continuum numerical analysis. Elasticity, plasticity and constitutive material models are also discussed here. Drained and undrained analysis, effective stress, consolidation and creep settlement concepts of soft soil are also discussed in this chapter.

2.2 Settlement of Foundation

Settlement is the vertical subsidence of the ground or structure as the soil is compressed. Excessive settlement, particularly when it is unevenly distributed beneath the foundation, can result in structural damage to building frame and excessive wear or equipment failure from misalignment resulting from foundation settlements. Uniform settlements-even if relatively large-can usually be tolerated for either rigid mats beneath buildings. Total settlement may be divided into - Immediate, Consolidation, creep Settlement etc.

Immediate settlement are those that take place as the load is applied or within a time period of about 7 days. Immediate settlement analyses are used for all fine-grained soils including silts and clays with a degree of saturation $S < 90$ percent and for all coarse-grained soils with a coefficient of permeability above 10^{-3} m/s (Bowles, 1996).

Consolidation settlement analyses are used for all saturated, or nearly saturated, fine grained soils. When the pores of soils are filled with water, compression is impossible because the void volume is totally occupied. The increase in load upon the saturated clay during a consolidation test or actual field situation is initially balanced by an increase in fluid pressure in the pores of the soil. Higher fluid pressure in the clay causes the pore water to flow out of the clay toward any direction where fluid pressure is lower. Only after pore fluid is removed, can the soil compress to a lower void ratio. This process is called consolidation. Consolidation settlement is those that are time-dependent and take months to years even hundreds of years to occur.The movement of pore water out of the soil is a function of the permeability, and clay has the lowest permeability of any soil. Therefore, it may take years for the soil to reach equilibrium under the load imposed. The consolidation settlements for most projects occur in 3 to 10 years.

Secondary settlement or creep occurs after primary settlements (Immediate and Consolidation) due to rearrangement of soil particle without any addition of load.

2.3 Bearing Capacity of Footing on Multiple-Layered Soils

In layered soil profiles, the unit weight of the soil, the angle of friction and the cohesion are not constant throughout the depth. The ultimate surface of failure may extend through two or more of the soil layers. Within each layer in layered soil deposits, the soil can be assumed to be homogeneous while the strength properties of adjacent layers are generally different. Because estimating bearing capacity of foundation on layered soil is more difficult than homogeneous one, two-layer soil system has been used to characterize heterogeneity of soil and the bearing capacity of such foundation has been investigated extensively as found literature which are presented in the following sections.

Button (1953) presented a solution for strip footings on two-layer clayey soil of different cohesion based on the limit equilibrium method with a cylindrical failure surface. This author also presented many other related studies which were conducted for clayey soil layers and on the ultimate bearing capacity for a sand layer overlaying a clay layer and for footings resting over a two-layer c-ø soil.

Meyerhof and Hanna (1978) proposed a semi-empirical technique, based on small scale tests, to solve the bearing capacity of a sand layer overlaying a clay layer. As referred by Murthy *et al*. (1995), finite element method or numerical limit analysis were utilized by Burd and Frydman (1997), Michalowski (2002) and Merifield *et al*. (1999) to obtain the bearing capacity of two-layer clay foundation with distinctly different strength.

Soils and rocks are heterogeneous materials created by complex geological processes. Because of the uncertainties associated with inherent variability of the engineering properties of soil from point to point, even within the same stratum, as well as limited information from site investigation, soil and rock properties may be regarded as random variables.

2.4 Limit Analysis of Bearing Capacity of Shallow Foundation

The lower bound theorem of limit analysis states that if a distribution of stress, over the domain in question, can be found which satisfies the equations of equilibrium, the stress

boundary conditions and the yield condition, the load associated with this stress distribution is less than or at best equal to the true ultimate or limit load.

The upper bound theorem of limit analysis states that if the power of the external load is greater than or equal to the rate of internal energy dissipation associated with a kinematically admissible velocity field, then the load must be greater than or at best equal to the true ultimate or limit load. The upper bound technique of limit analysis may be employed here to generate approximate solutions to the bearing capacity problem. If the upper and lower bounds coincide, the limit load is the true collapse load.

2.4.1 Footing Foundations on Firm or Dense Soil above Soft Layers

Figure 2.1 shows the stress conditions beneath a footing that rests on a firm stratum *A* located above a soft stratum *B.* If the upper boundary of the soft stratum is located close to the base of the footing, failure may occur, the footing breaking through the firm layer into the soft deposit (Skempton, 1942). These can be avoided by giving the footing such dimensions that the pressure on the upper boundary (computation methods may be Boussinesq's Equations) of stratum *B* does not exceed the allowable bearing value for the soil in that stratum. Less accurately, the total footing load can be assumed to be uniformly distributed over the base of a truncated pyramid whose sides slope from the edges of the footing to the upper surface of *B* at an angle of 60^{o} with the horizontal.

If the upper boundary of the soft stratum *B* is located at a considerable depth below the base of the footings, failure by breaking into the ground cannot occur because stratum A acts like a thick raft that distributes the weight of the building uniformly over the surface of *B.* The flexural rigidity of this raft prevents the surface of *B* from heaving beyond the loaded area.

Nevertheless, the settlement may be very large. For example, the weight of the building represented in Fig. 2.2 is transmitted by continuous footings onto a stratum of dense sand and gravel that rests at a depth of 7m, on a layer of soft clay 15m thick.

The footings were designed for a soil pressure of 250 kPa, a conservative value for dense sand and gravel. The greatest pressure on the surface of the clay due to the weight of the building was 110 kPa. During the construction period of 1 year, the footings settled between 25 and 100 mm. During the following 40 years the settlement increased to about

1 m. Since the basement floor, is rested on the sand between the footings, neither crack nor displacement had been occurred to the footings. Thus it is evident that the layer of sand and the footings settled together.

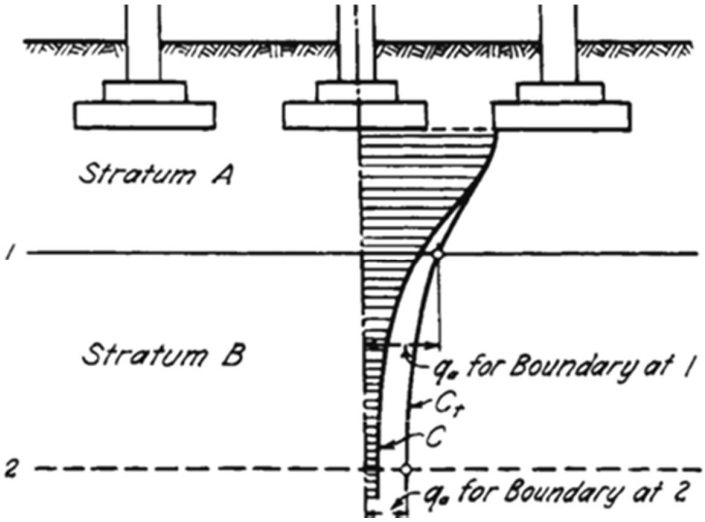

Figure 2.1 Method of calculation to ascertain whether allowable soil pressure is exceeded for members of stratified clay subsoil. Curve C represents variation with depth of vertical pressure beneath single footing neglecting influence of adjacent footings and curve C_t represents this considering influence of adjacent footings (Skempton, 1942).

In spite of the symptoms mentioned previously, it was not suspected that the seat of settlement was located below the sand. Hence, the "strengthening" was accomplished by increasing the width of the footings so that the intensity of the pressure exerted by the footings was reduced about 30%. However, since the pressure on the clay remained unchanged, the expensive alterations did not have the slightest effect on the trend of the time settlement curves shown in Fig. 2.2c.

At a later date undisturbed samples were taken from the clay at some distance A, B, C, D etc. On the basis of the results of consolidation tests on undisturbed clay samples taken from nearer to the building the average rate of building settlement as a whole was computed. The theoretical trend of the primary settlement, represented by the dash curve in Fig. 2.2c is very similar to the real one. On account of the secondary compression, however, the real settlement was of a rate from 3 to 8 mm per year, for different parts of the structure and the curve of computed primary settlement then approaches a horizontal asymptote.

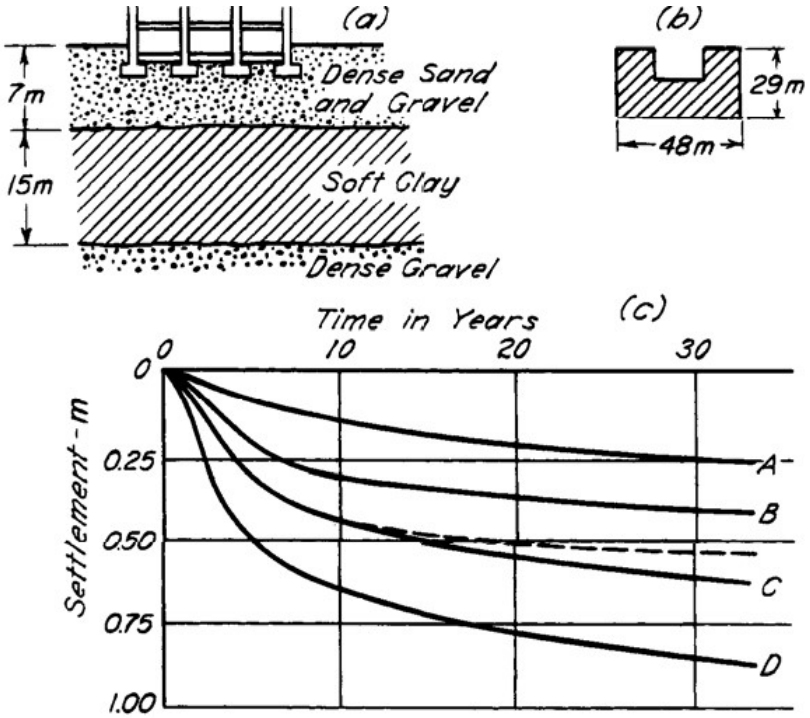

Figure 2.2 (a) Cross-section through foundation of structure supported by dense sand and gravel underlain by soft clay. (b) Plan of structure. (c) Observed time-settlement curves. Dash curve represents time-settlement relation for primary settlement computed from results of consolidation tests (after Terzaghi, 1935).

This observations clearly show that the consolidation settlement of soft layers located at a considerable depth below the footings is in reality practically independent of the distribution of pressure on the base of the footings, because the firm stratum supporting the footings acts like a natural raft that distributes the load from the footings over the softer strata. Methods for reduction of the consolidation settlements of the lower layers related to raft foundations are discussed here. If the foundation is designed such a way that the consolidation settlement of the soft layers will be tolerable, the footings can be designed considering the soft strata did not exist. Hence, the presence of the soft strata may compel the designer to change the entire layout of the foundation, but it has no bearing on the allowable soil pressure for the footings.

2.4.2 Bearing Capacity for Footings on Layered Soils

A footing placed on stratified deposits where the thickness of the top stratum from the base of the footing d_1 is less than the H distance computed as in Fig. 2.3. In this case the rupture zone will extend into the lower layer(s) depending on their thickness and require some modification of q_{ult} in three general cases as follows:

Case 1. Footing on layered clays (all $\phi = 0$) as in Fig. 2.3a.

a. Top layer weaker than lower layer *($c_1 < c_2$)*

b. Top layer stronger than lower layer *($c_1 > c_2$)*

Case 2. Footing on layered *c-ø* soils with *a, b* same as case 1.

Case 3. Footing on layered sand and clay soils as in Fig. 2.3b.

a. Sand overlying clay and

b. Clay overlying sand

Experimental work to establish methods to obtain q_{ult} for these three cases seems to be based mostly on models – often with B<75 mm. Apparently at the first Button (1953), used a circular arc to search for an approximate minimum, which was found (for the trial circles all in the top layer) to give $N_c = 5.5 < 2\pi$.

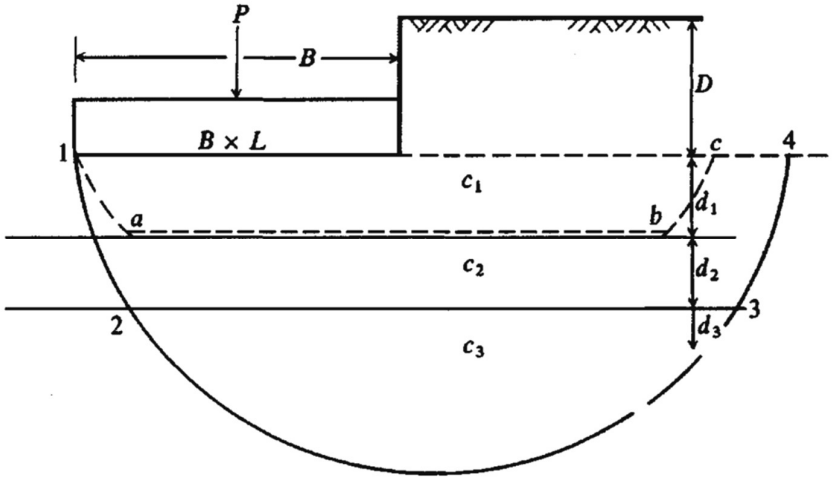

Fig 2.3(a) Footing on layered clay soil. For very soft c_1 failure may occur along sliding block 1*abc* and not a circular arc and reduce N_c to a value less than 5.14.

A guideline for ϕ-c soils with a number of thin layers is to use average values of c and ϕ in the Meyerhof, Hansen, and Vesic bearing capacity equations obtained as

$$c_{av} = \frac{c_1 H_1 + c_2 H_2 + c_3 H_3 + \cdots\cdots\cdots + c_n H_n}{\sum H_1}$$

$$\phi_{av} = \tan^{-1} \frac{H_1 \tan\phi_1 + H_2 \tan\phi_2 + H_3 \tan\phi_3 + \cdots\cdots\cdots + H_n \tan\phi_n}{\sum H_1}$$

where c_i = cohesion and ϕ_i = angle of internal friction in stratum of thickness H_i; c or ϕ may be zero. H_i may be multiplied by a weighting factor (1.0 is used here) if desired. The effective shear depth of interest is limited to approximately $0.5B \tan(45° + \phi/2)$.

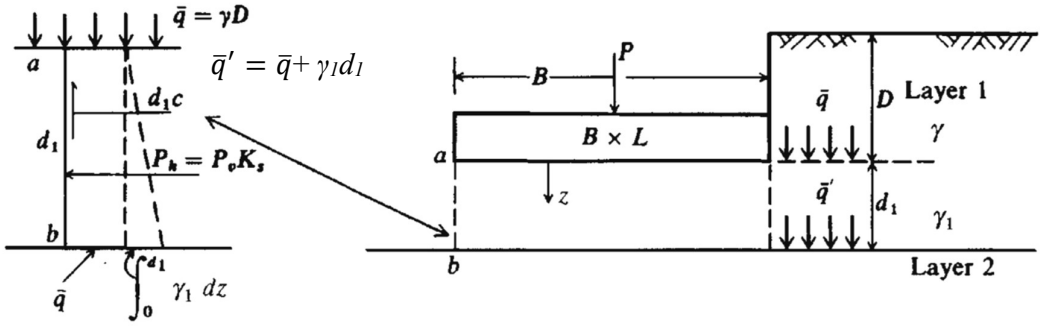

Figure 2.3(b) Footings on layered soil.

2.4.3 Experimental Work on Bearing Capacity Theories of Footings on Multi Layered Soil

Meyerhof and Hanna (1978) developed a theory to estimate the ultimate bearing capacity of a shallow rough continuous foundation supported by a strong soil layer underlain by a weaker soil layer as shown in Fig. 2.4. According to their theory, at ultimate load per unit area, q_u , the failure surface in soil will be as shown in Fig. 2.4. If the ratio H/B is relatively small, a punching shear failure is occured in the top (stronger) soil layer followed by a general shear failure in the bottom (weaker) layer which is the upper limit for the ultimate bearing capacity.

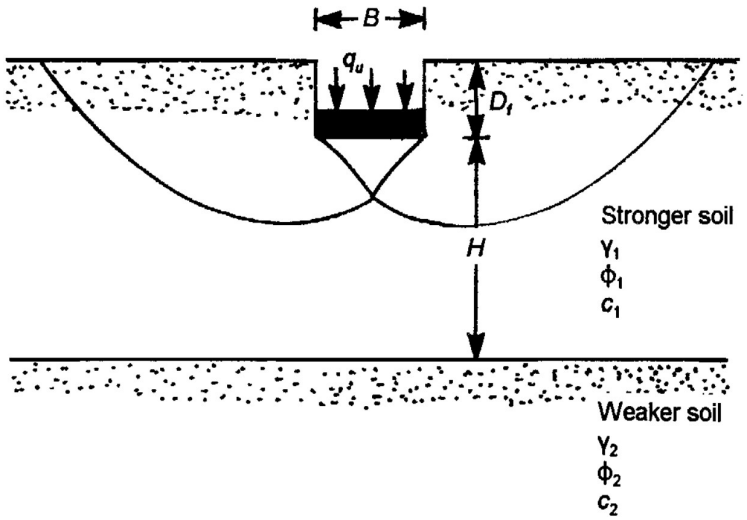

Figure 2.4 Punching shear models on layered soil (*Das, 1997*).

Considering the unit length of the continuous foundation, the ultimate bearing capacity can be given as (*Das, 1997*):

$$q_u = q_b + \frac{2c_a H}{B} + \gamma_1 H^2 \left(1 + \frac{2D_f}{H}\right) \frac{K_s \tan\phi_1}{B} - \gamma_1 H$$

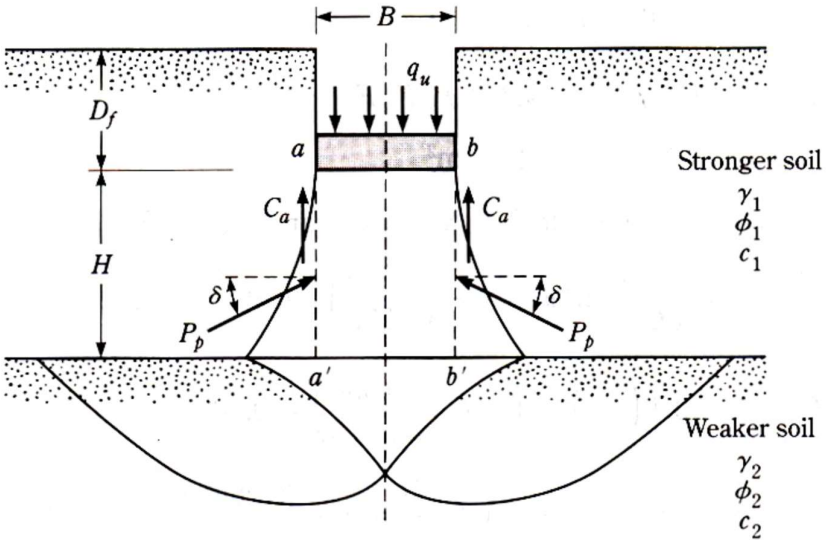

Figure 2.5 Punching shear models of rough continuous footing on layered soil - stronger over weaker (*Das, 1997*).

The relationship between K_s and ϕ_1 is plotted and presented by Hanna and Meyerhof (1980) as a function of c_1 and the ratio δ/ϕ_1. However, these charts are not presented in non-dimensional form and useful only for the values of sand unit weight and layer thickness that was adopted in the analysis. Alternatively, useful design charts that cover a broad range of parameters are given by Michalowski and Shi (1995) using limit equilibrium method, which was not experimentally. These solutions, by their very nature, were upper bounds, and they may overestimate the bearing capacity by a significant amount. (Burd and Frydman, 1997)

Figure 2.6 gives the variation of K_s with q_2/q_1 and ϕ_1. In such case, the upper limit for q_u is $q_u = q_t = c_1 N_{c(1)} + qN_{q(1)} \frac{1}{2}\gamma_1 B N_{\gamma(1)}$ (2.1)

For Stronger Sand Layer Over Weaker Saturated Clay ($\phi_2 = 0$), $c_1 = 0$ and, hence, $c_a = 0$. Also for $\phi_2 = 0$, $N_{c\,(2)} = 5.14$, $N''_{(2)} = 0$, $N_{q\,(2)} = 1$. So the ultimate bearing capacity of the foundation q_{ult}

$$q_u = 5.14c_2 + \left(1 + \frac{B}{L}\right)\gamma_1 H^2 \left(1 + \frac{2D_f}{H}\right)\frac{K_s \tan\phi_1}{B} + \gamma_1 H \le q_t \qquad (2.2)$$

where

$$q_t = \gamma_1 D_f N_{q(1)} \left[\tan^2\left(45^\circ + \frac{\phi_1}{2}\right)\right] + \frac{1}{2}\gamma_1 B N_{\gamma(1)} \left[\tan^2\left(45^\circ + \frac{\phi_1}{2}\right)\right] \qquad (2.3)$$

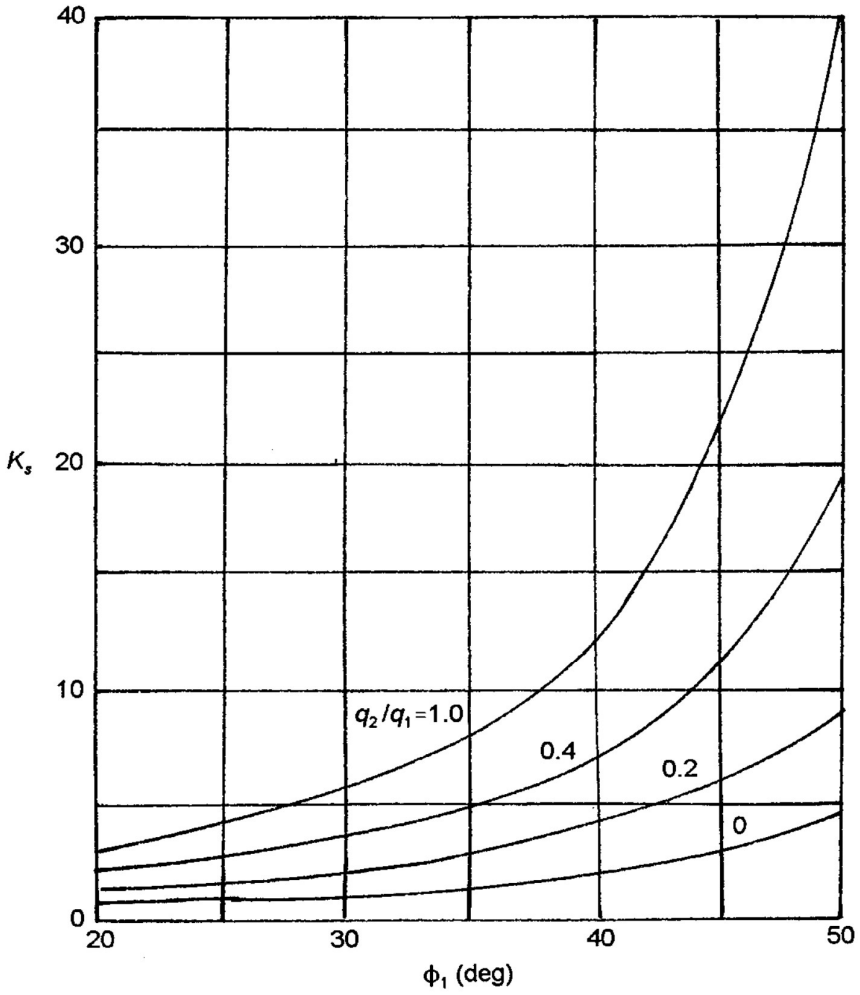

Figure 2.6 Meyerhof and Hanna(1980) - variation of K_s with ϕ_1 and q_2/q_1

For rectangular foundations, the preceding equation can be modified as

$$\frac{q_2}{q_1} = \frac{c_2 N_{c(2)}}{\frac{1}{2}\gamma_1 B N_{\gamma(1)}} = \frac{5.14 c_2}{\frac{1}{2}\gamma_1 B N_{\gamma(1)}} \quad (2.4)$$

The shape factor for a strip foundation can be taken as one. For square or circular foundations, as per the experimental work for Hanna and Meyerhof (1980), this magnitude was appears to vary between 1.1 and 1.27. Based on this concept, Hanna and Meyerhof (1980) developed some alternative design charts to determine the punching shear coefficient K_s.

2.4.4 Bearing Capacity of Footings on a Sand Layer Overlying Soft Clay

B. R. Srinivasa Murthy, A. Sridharan and P. Vinod (1995) have devised a method for estimation of the bearing capacity of two-layer soil systems beneath rigid circular footings. The layered system was considered to be divided into distinct elastic and plastic zones and a spatial variation of deformation moduli was adopted within the defined plastic zone. The bearing capacity of a two-layer soil system was defined in terms of a modified influence coefficient which was evaluated by obtaining the spatial variation of deformation moduli which simultaneously satisfied the two conditions, namely the defined contact pressure distribution pattern at the soil-footing interface and the uniform-vertical-displacement constraint condition of rigid footing at the ultimate state.

Using the finite-element method of analysis, modified influence coefficients was evaluated and the results was presented in Fig. 2.7. Although such solutions cannot be applied directly to plane-strain footings, it can be seen from Fig. 2.7 that the predicted critical depth did not exceed a value of about H/B =2.0, even for bearing-capacity ratios as high as q_s/q_c =20.

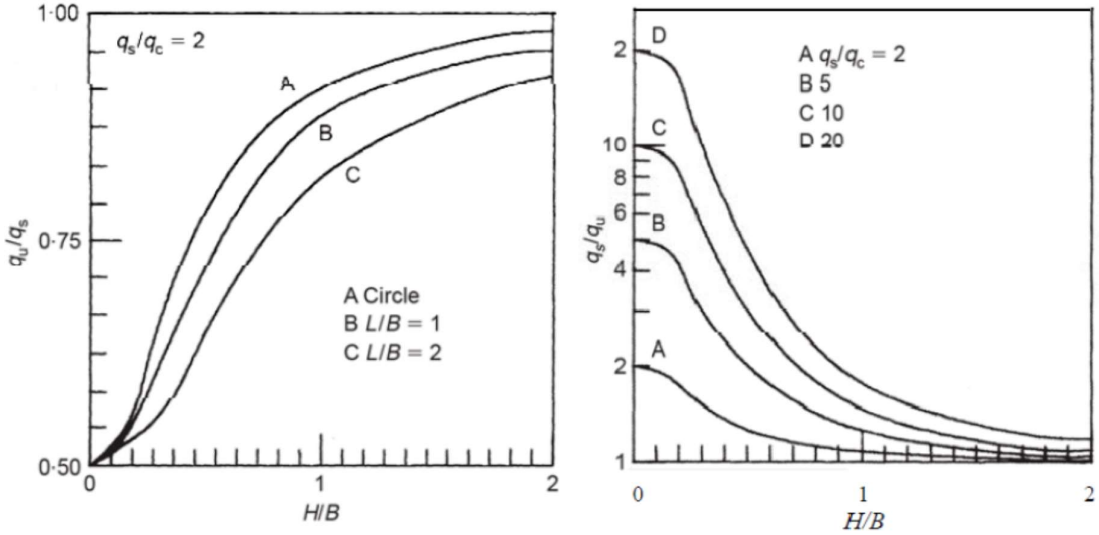

Figure 2.7 Variation of q_s/q_u versus H/B for different values of q_s/q_c and Variation of q_u/q_s versus H/B for different footings.

This method was viable compared to data available in the literature of Meyerhof & Hanna (1978). For the solution of the settlement problem of rigid circular footings on sand over-lying clay use existing method of Sridharan et al., 1997 was possible to estimate the settlement of the footing at various values of bearing pressure up to 90% of the bearing capacity.

H. J. Burd, and S. Frydman (1997) discussed the use of relatively straightforward load-spreading analysis to calculate the bearing capacity of a sand layer overlying soft clay but it ignored important details of the mechanics of the problem. The authors referred to the suggestion by Jacobsen et al. (1977) that the load-spreading angle α depended only on the bearing-capacity ratio q_s/q_c, and established appropriate values of this for any particular application. For a strip footing, with zero surcharge, this ratio was

$$q_s \frac{q_s}{q_c} = \frac{\lambda B N_\lambda}{2 N_c c_u} \tag{2.5}$$

where N_c is the bearing-capacity factor for the clay.

The bearing-capacity ratio (taking N_c to be constant) was therefore a function only of ϕ' and $c_u/\gamma B$. Although these two variables were the same for all of the reported model tests, the values of α back calculated from the measured q_u data show a significant variation; this indicated that the Jacobsen assumption is fundamentally flawed. This deficiency was evident in other published data e.g. Michalowski & Shi (1995), Burd & Frydman (1997).

The H/B=0 test may be used to select an appropriate value for c_u, although the curve is difficult to interpret because it does not reach a well-defined limit. The authors recorded a limit stress of 46.6 kPa; however, a lower value was propose corresponding to the point at which the slope of the curve reduces markedly. A value of 31 kPa is proposed and adopted in analysis.

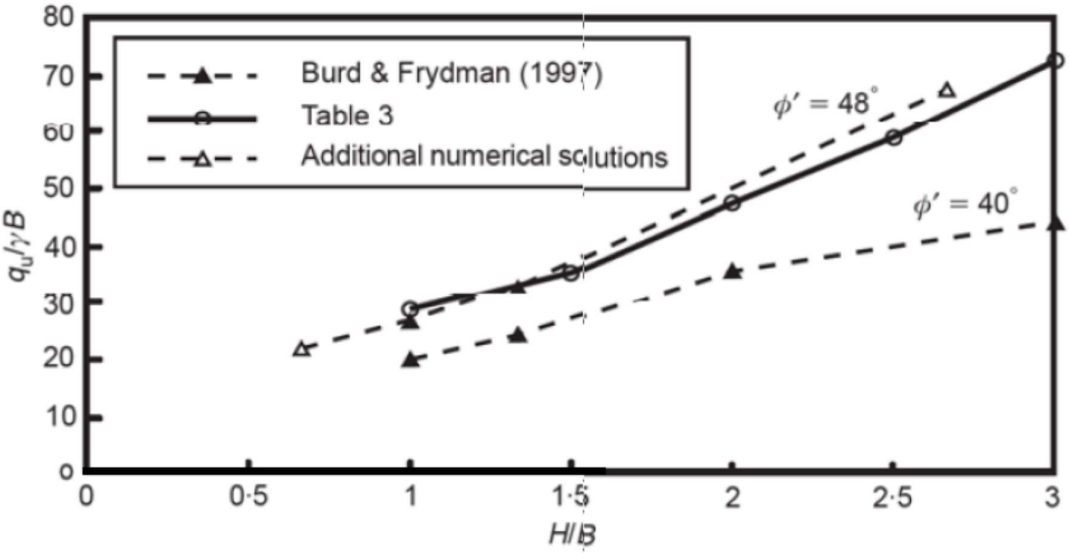

Figure 2.8 Numerical and experimental values of $q_u/\gamma B$

Numerical solution to this problem by Michalowski & Shi (1995), used a kinematic analysis method and obtained charts of upper-bound solutions. Unfortunately, the range of ϕ' covered by these charts was limited and the solutions was not be applied directly to these model tests. These charts could be used cautiously for design (noting that they are upper bounds). Alternatively, Burd & Frydman (1997) used finite-difference and finite-element methods to obtain solutions for $\phi' = 40°$and 48° in the top layer. From which values of $q_u/\gamma B$ obtained by interpolation (Fig. 2.8). The numerical solutions for $\phi' = 48°$ were seen to provide a reasonable fit to the experimental data.

2.4.5 Derivation of Bearing Capacity Equation for a Two Layered System of Weak Clay Layer Overlain by Dense Sand Layer

Using the punching shear model of Hanna and Meyerhof (1980), Abdulhafiz O. Al-Shenawy & Awad A. Al-Karni (2005) derived the ultimate bearing capacity equation as a function of the properties of soils, the footing width, and the top layer thickness and design charts were developed in dimensionless form for very wide ranges of design parameters through a detailed parametric study of the design parameters including the effect of angle of friction, the ratio of the thickness of sand layer to the footing width, the ratio of the depth of embedment to the footing width, and the ratio of the clay soil cohesion to the product of the clay unit weight by the footing width the available method based on the limit equilibrium analysis and is useful in overcoming the problem of the design charts of Michalowski and Shi (1995) which may overestimate the bearing capacity by a significant amount because of the very nature of the upper bound solution on which the derivation is based. Derived Bearing Capacity Equation is:

$$\frac{q_u}{\gamma B} = 5.14\frac{c_u}{\gamma B} + \frac{D}{B} + K_p \tan\delta\left(\frac{H}{B}\right)^2 + 2K_p \tan\delta\left(\frac{D}{B}\right)\left(\frac{H}{B}\right) \qquad (2.6)$$

Fig. 2.9 shows a comparison between the results of the variation of $(H/B)_{\text{Critical}}$ with D/B at δ/ϕ of 1.0 and 0.67, where $(H/B)_{\text{critical}}$ is the ratio of the depth of the sand layer below the footing base to the footing width at which the clay layer has no effect on the bearing capacity. The $(H/B)_{\text{Critical}}$, at D/B=0 is increased from 3.5 to 4.77 when δ/ϕ is decreased from 1.0 to 0.67, respectively. The figure also shows a comparison with the results of Michalowski and Shi (1995) which show that the value of δ/ϕ is close to one when H/B is small and reduces as H/B increases which is in agreement with Meyerhof (1974). By using the lower values of δ/ϕ suggested by Hanna and Meyerhof (1980) is

$$\delta/\emptyset = a + b\,(q_2/q_1) + c(q_2/q_1)^2 \quad (2.7)$$

where, a =0.00829(q_2/q_1) −0.00872, b = 0.000744(q_2/q_1)+1.0621

and c =−0.00900(q_2/q_1) −0.0515.

By using the relationship in Eq. (2.7), the variation of $(H/B)_{critical}$ with D/B is shown in *Fig.* 2.14. The value of $(H/B)_{critical}$ based on Eq. (2.7) gives even more conservative results for the bearing capacity. The results also showed the variation of $(H/B)_{critical}$ with $c_u/\gamma B$ and compare the results of Michalowski and Shi (1995) with the results of Eq. (2.19) at $\delta/\emptyset$ equal to one and $\delta/\emptyset$ from Eq. (2.20), respectively. The results are close in values but differ in trend since those of Michalowski and Shi (1995) are concave up, while the curves of $\delta/\emptyset$ equal to one are concave down. However, in *Fig.* 2.9 the results are different in values but agree in trend as the results of Michalowski and Shi (1995) are concave up, and the ones for $\delta/\emptyset$ from Eq. (2.7) are concave up also.

It was concluded that using Eq. (2.7) to calculate $\delta/\emptyset$ and using it in Eq. (2.6) is more reliable since the difference in values is due to the overestimation associated with the upper bound solution. Ultimate Bearing Capacity, q_u depends mainly on parameters include $\emptyset$, *H/B, D/B,* and $\delta/\emptyset$ and $c_u/\gamma B$. According to Eq. (2.6), in general, increasing the values of these parameters is increased the bearing capacity of the layered soil.

An example showed that an increase in *H/B* by 200% caused an increase in $q_u/\gamma B$ by 300%. By comparing the results the effect of ϕ on the increase in $q_u/\gamma B$ is more pronounced when the overburden pressure *(D/B)* becomes larger. Since the bearing capacity of the top layer increases as ϕ increases, the value of $q_u/\gamma B$ also increases and becomes constant at a critical value of *H/B.* Since the effect of the bottom layer on the bearing capacity is diminished. This critical value of *H/B* increases as ϕ increases. From the effect of the angle of friction *(*ϕ*)* on $q_u/\gamma B$ can be neglected at small values of *H/B* and this becomes more significant as *H/B* becomes greater than 1. Fig.2.11 showed that the difference between the values of $q_u/\gamma B$ at different *D/B* increases as *H/B* increases. *D/B* increases the critical value of *H/B* which means an increase in the values of $q_u/\gamma B$ of the two layer combined system. Another representation of the results in Fig.2.11 was shown in Fig. 2.12 as a linear variation between $q_u/\gamma B$ and *D/B* with different slopes for each line of each value of *H/B.* The slope of these relationships increases with the increase of *H/B.*

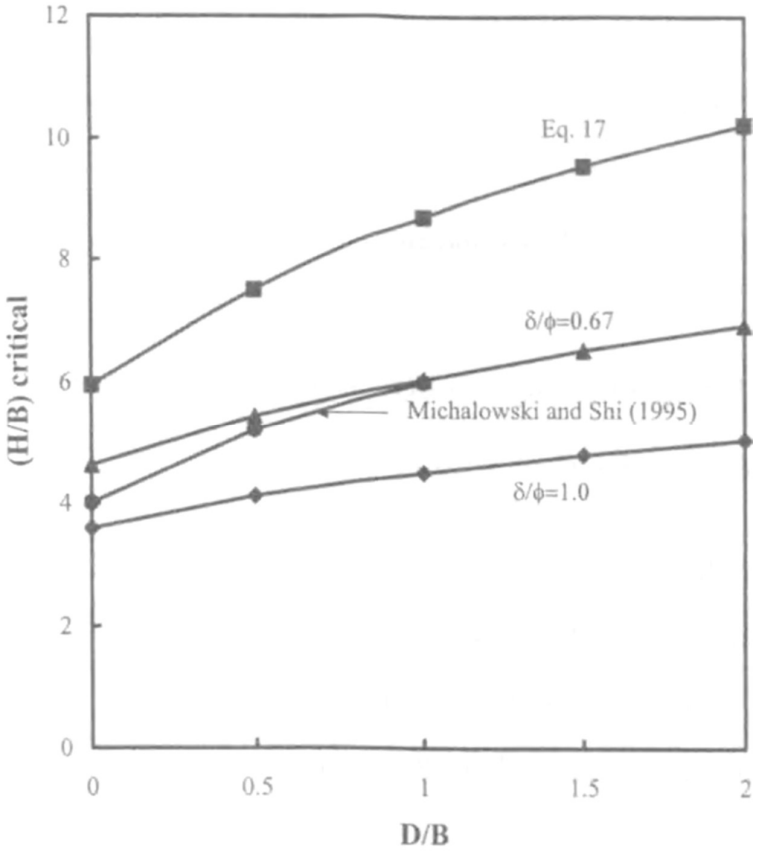

Figure 2.9 Effect of δ/ϕ on the variation of $(H/B)_{critical}$ with D/B

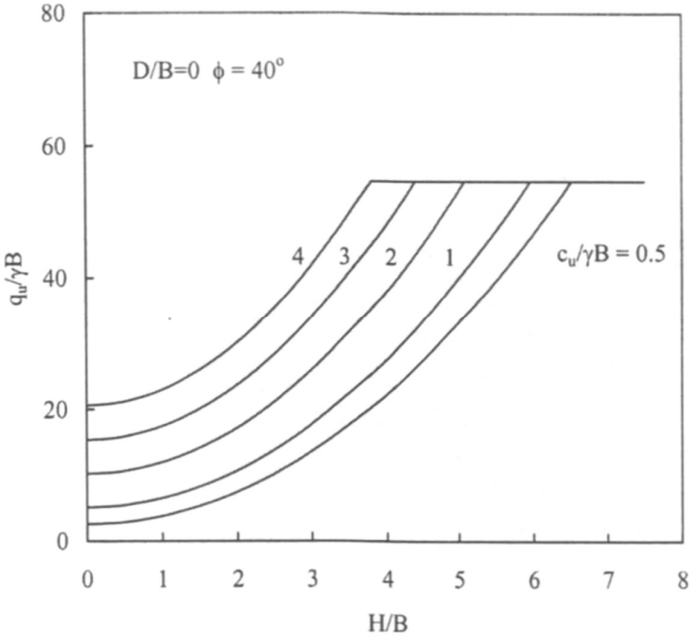

Figure 2.10 Variation of $q_u/\gamma B$ with $c_u/\gamma B$ at different value of H/B at $\phi = 40^0$ and $D/B = 0$

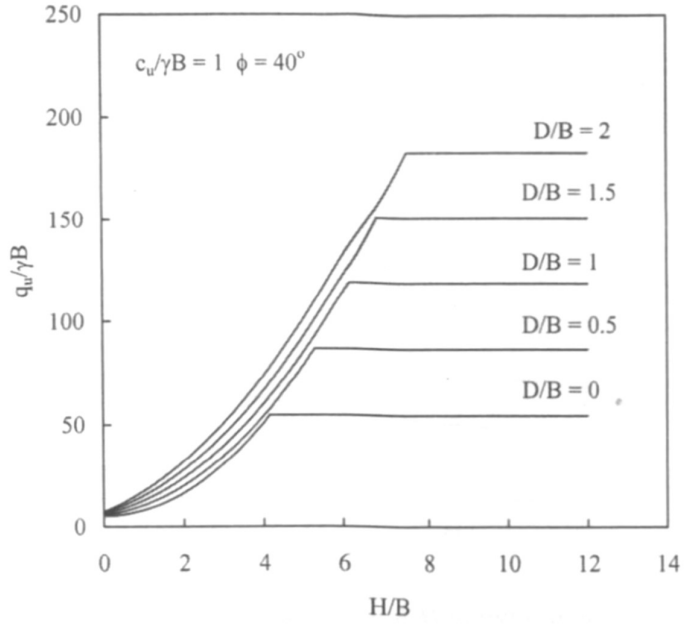

Figure 2.11 Effect of *D/B* on the variation of $q_u/\gamma B$ with *H/B* at angle of friction $\phi = 40^0$ and $c_u/\gamma B = 1$

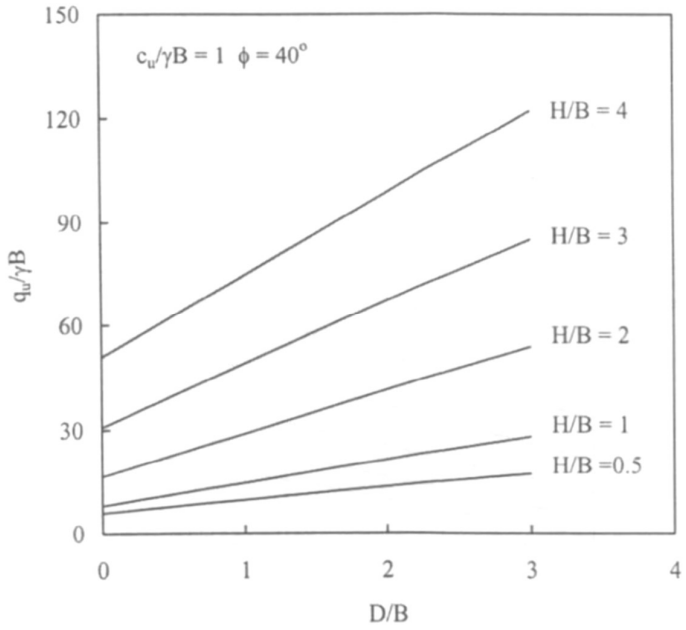

Figure 2.12 Variation of $q_u/\gamma B$ with *D/B* at different value of *H/B* at angle of friction $\phi = 40^0$ and $c_u/\gamma B = 1$

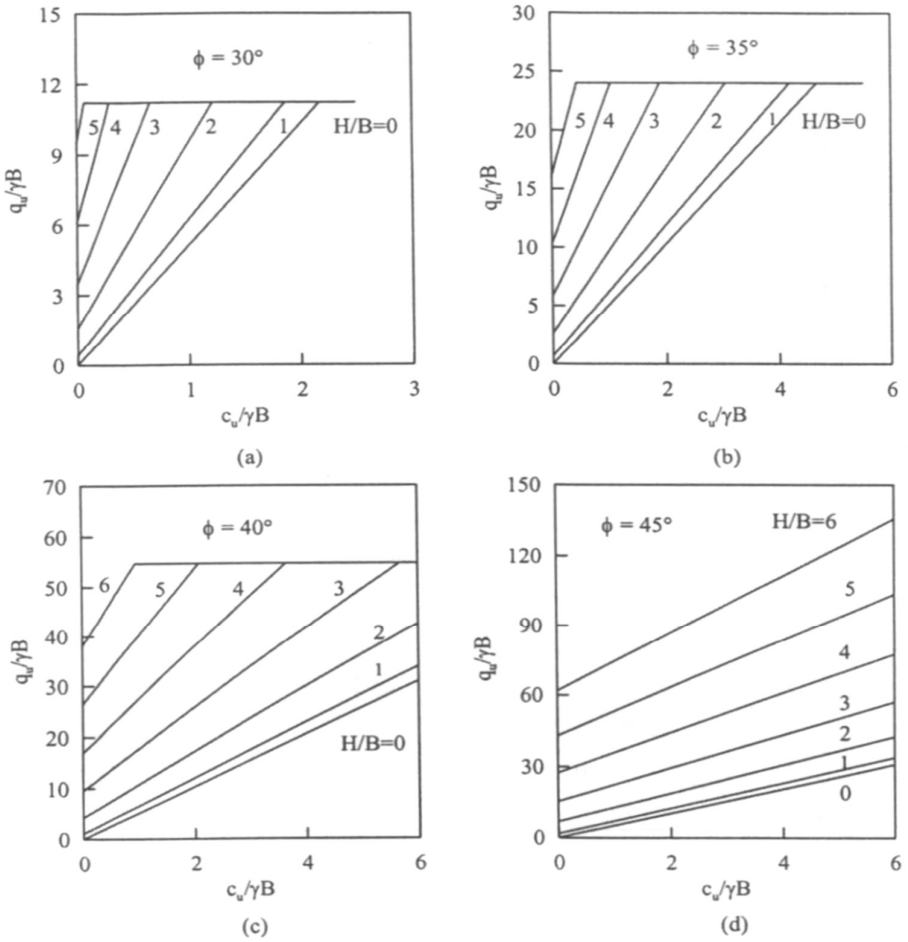

Figure 2.13 Variation of $q_u/\gamma B$ with $c_u/\gamma B$ for sand-clay foundation soil at D/B = 0:
(a) ϕ = 30°, (b) ϕ = 35°, (c) ø = 40° and (d) ϕ = 45°

The parameter $c_u/\gamma B$ represented the effect of the strength of the bottom layer on the bearing capacity of the two-layered system. The results show that the values of $q_u/\gamma B$ increase linearly with the increase of $c_u/\gamma B$. The greatest effect of the parameter $q_u/\gamma B$ on the bearing capacity of the layered system is its effect on the value of the critical value of *H/B*. Unlike the effect of the angle of friction, the critical value of *H/B* is reduced as the value of $q_u/\gamma B$ increases as shown in Fig. 2.10.

It may be concluded that a thicker sand layer is needed for a weaker clay layer to reach the maximum value of $q_u/\gamma B$.

Design charts were divided into groups with different values of *D/B* of 0, 0.5, 1.0, 1.5, 2, 2.5, and 3. In each group there are four charts for ø equal to 30°, 35°, 40°, and 45° (Fig. 2.13). Each chart shows the variation of $q_u/\gamma B$ with $c_u/\gamma B$ for different values of *H/B*.

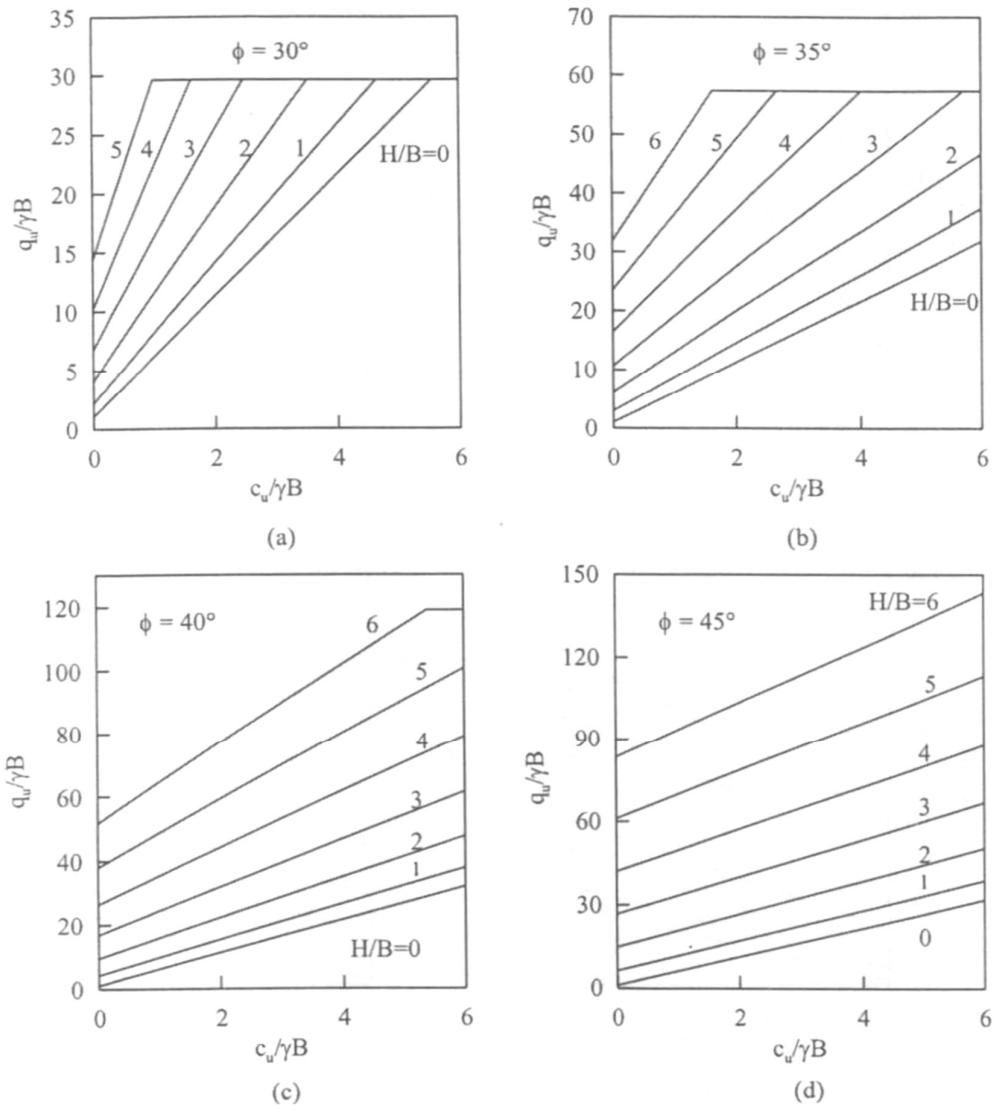

Figure 2.14 Variation of $q_u/\gamma B$ with $c_u/\gamma B$ for sand-clay foundation soil at D/B = 1.0: (a) ϕ = 30°, (b) ϕ = 35°, (c) ϕ = 40° and (d) ϕ = 45°

The effect of the punching shear parameter *(δ)* was considered and evaluated from empirical relationships that were developed based on the experimental results of Hanna and Meyerhof (1980). Based on this analysis, design charts were developed using the punching shear model in a dimensionless form since those of Hanna and Meyerhof (1980). The presented charts here are useful in overcoming the significant overestimate problem of design charts that were developed by Michalowski and Shi (1995).

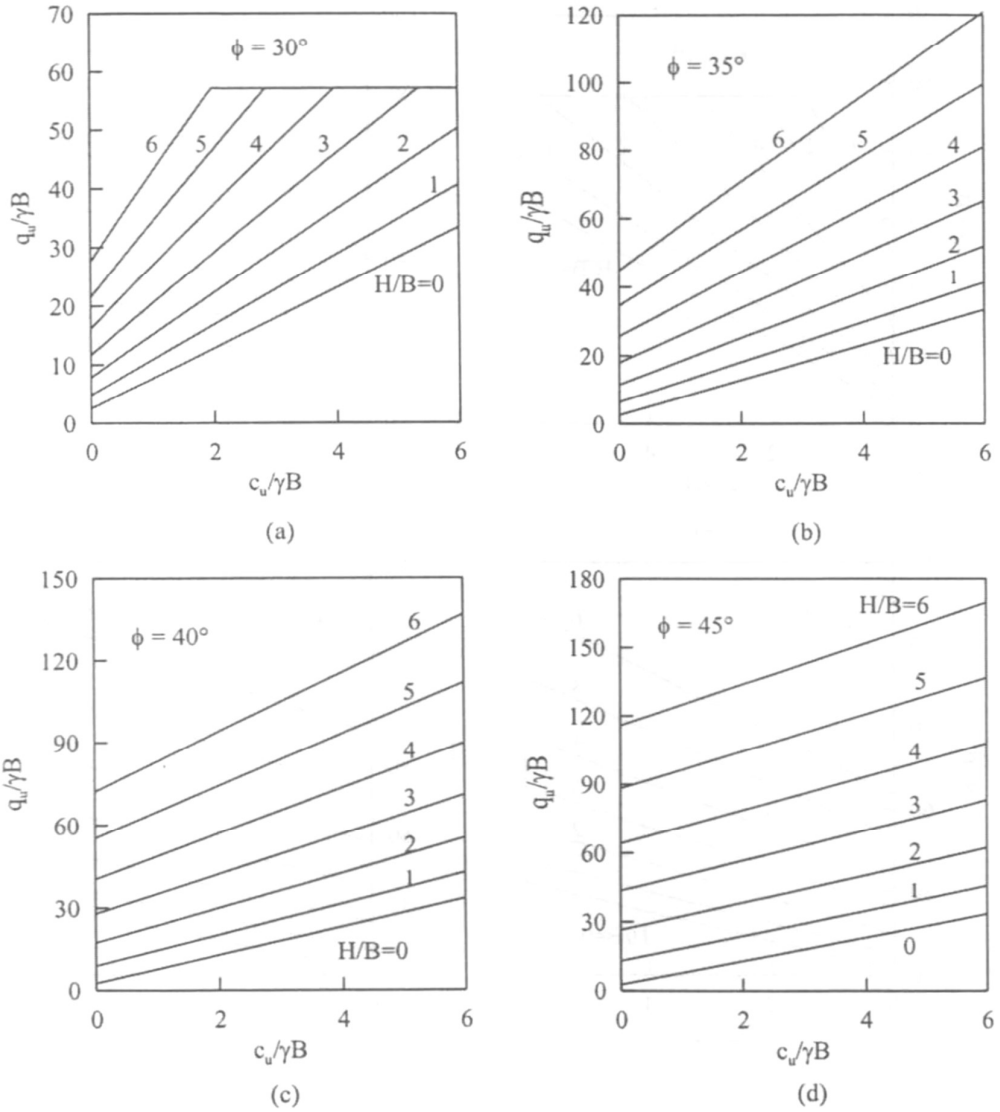

Figure 2.15 Variation of $q_u/\gamma B$ with $c_u/\gamma B$ for sand-clay foundation soil at D/B = 2.5: (a) ϕ = 30°, (b) ϕ = 35°, (c) ϕ = 40° and (d) ϕ = 45°

2.5 Continuum Analysis of Soil

Numerical geotechnical modelling combines uncontroversial laws of equilibrium and of compatibility or continuity of displacement fields through so-called constitutive relations which relate the changes in loads applied to elements of soil to the deformations or gradients of displacement that develop in those elements.

While soils deposited through being transported by air or water they present as dilute particle suspensions with little interaction between individual particles. In case of describing such materials in which the particles interact to appear as strong engineering materials and which are usually so much larger than the individual particles that we have

to smear out the properties and create an equivalent continuum for any analysis. In deciding how we should describe and model the mechanical behaviour of soils we have to come to terms with this particle-continuum duality. Instead of working in terms of forces and relative displacements at particle contacts we now work in terms of continuum concepts such as stress and strain. Stress is only relevant at a scale considerably larger than the individual particles and the network of force chains between particles. Strain is defined in terms of gradient of a field of displacement.

Analyses and observations of particle assemblies show that individual particles rotate and slide at particle contacts and interparticle friction has a lower effect than might have been. Conventional definitions of strain do not admit rotation as a field variable. Particle rotation is a consequence of out of balance moments being imposed on the particles. These too cannot be incorporated in conventional definitions of stress: we assume that only normal and shear tractions (and not moments) can be transmitted across any surface in the *continuum* and the need for moment equilibrium forces the symmetry of the stress tensor. Practically, we have to work in terms of the continuum quantities stress and strain in order to be able to estimate the behaviour of geotechnical systems. It is also inevitable that our understanding of the behaviour of soils as assemblies of individual particles should in general be mediated through observation of the behaviour of samples of soils containing a very large number of particles in the laboratory. The constitutive models are all constructed in terms of components of stress and strain. The most appropriate use of analyses of particulate assemblies seems at present to be to provide inspiration for the continuum constitutive models.While affording a relatively simple means of obtaining the deformation response of the soil, the Winkler model neglects the interaction of one spring with another and, therefore, does not treat the underlying soil as a true continuum. An alternative and improved approach is to treat the soil as an elastic continuum.

2.5.1 Elastic Properties of Soil

Hooke's generalized stress-strain law for any homogeneous, isotropic, elastic material is

$$\varepsilon_x = \frac{1}{E_s}(\sigma_x - \upsilon\sigma_y - \upsilon\sigma_z) \tag{2.8.1}$$

$$\varepsilon_y = \frac{1}{E_s}(\sigma_y - \upsilon\sigma_x - \upsilon\sigma_z) \tag{2.8.2}$$

$$\varepsilon_z = \frac{1}{E_s}(\sigma_z - \upsilon\sigma_x - \upsilon\sigma_y) \tag{2.8.3}$$

The signs here are based on using (+)υ of Eq. (2.8.2) following. In matrix notation Eq. (2.8) can be written as $\varepsilon = D\sigma$, where the matrix D is $\begin{bmatrix} 1 & -\vartheta & -\vartheta \\ -\vartheta & 1 & -\vartheta \\ -\vartheta & -\vartheta & 1 \end{bmatrix}$.

In confined compression tests (consolidation test or compression beneath the tip of a pile in situ) the lateral strain (ε_2, ε_3) is taken as 0.0 and $\varepsilon_v = \varepsilon_1$ has been found. Then from Eqs. (2.8) can be obtained the following:

$$\varepsilon_v = \frac{(1+\nu)(1-2\nu)\sigma_1}{E_s(1-\nu)} \tag{2.9}$$

For υ= 0.5, this equation gives the volumetric strain ε_v = 0; i.e., there is no volume change in the soil. Also, for υ = 0 the volumetric strain is $\varepsilon_v = \sigma_z / E_s = \varepsilon_z$. The volumetric strain was used to plot ε versus log p graph.

In general, a perfectly linear or non-linear elastic isotropic material will retain its original shape and size if its applied stress state is released (Wood, 1990). Soft clays have a high porosity and can hold a large volume of water compared to its bulk volume. As water will dissipate from the voids during compression, a high porosity will result in a high compressibility. The rate of consolidation is governed by the permeability, which for a clay soil often is very low.

The one-dimensional (1D) constrained modulus E_{oed} is another common stiffness parameter and it is obtained from the oedometer test. It is related with Young's modulus E through Poisson's ratio v as

$$E_{oed} = \frac{(1-v)E}{(1-2v)(1+v)} \tag{2.10}$$

2.5.2 Modulus of Elasticity (E_{Young}) and Modulus of Deformation (E_{Def})

The stress-strain behavior soil is elastoplastic. The Modulus of Elasticity, which is an index of the material stiffness and a fundamental material constant, can be graphically defined by the slope of the tangent passing through the origin O(0,0) of a stress-strain diagram (tangent modulus).

During the initial (small) loading increments materials exhibit elastic behavior and the displacements are resilient. An important remark is that the Modulus of Deformation, as

it is defined and represented in Figure 2.18, is dependent on the loading pressure (σ). Graphically it is defined according to the slope of line OA (secant modulus).

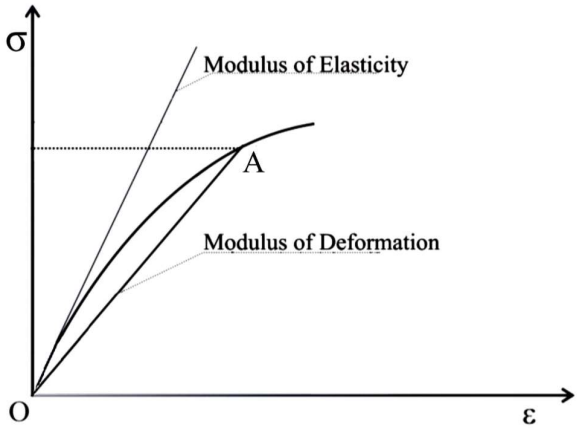

Figure. 2.16 The Modulus of Elasticity and the Modulus of Deformation

2.5.3 Contractancy and Dilatancy

The volume of the soil material which is made up of void filled with single or multi-phase fluid. For a typical medium dense sand about a third of the volume is void; for a normally consolidated clay voids might make up towards half of the volume.

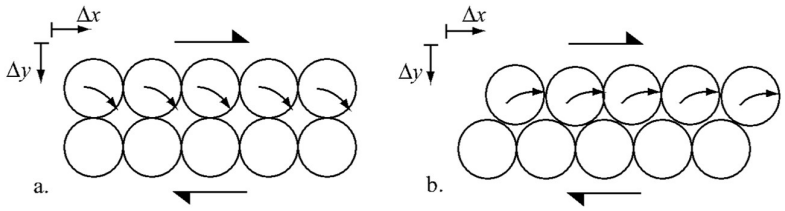

Figure 2.17: a) When sheared, Loosely packed soil grains roll down into the open voids resulting in a decrease in volume b) Shearing of Densely packed soil grains in an over-consolidated state in the state (Axelsson, 1994).

Change in volume of soil which is a result of soil particles rolling into or out of the voids. A normally consolidated soil can contract during shearing, meaning the soil will decrease in volume as loosely packed grain particles roll down into open void spaces (Figure 2.17a). (Axelsson, 1994)

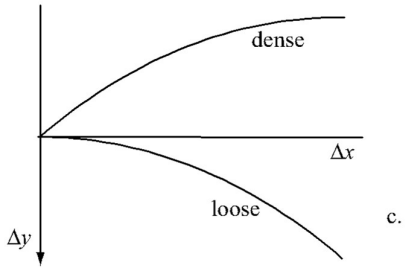

Figure 2.17b Volume change in shearing of loosely and densely packed layers of circular discs

2.5.4 Drained and Undrained Behavior of Soft Soil

If considering a fully saturated soil, subjected to an increase in total vertical stress and assuming zero lateral strain, the volume change will be entirely due to deformation of the soil in the vertical direction. Initially, the pore water pressure will be governed by the position of the water table and is referred to as static pore water pressure. As the vertical stress is increased, the solid particles will try to rearrange into a denser configuration. But with zero lateral strain, and assuming that water is incompressible, there can be no volume change without dissipation of pore water. Immediately, the pore water pressure will increase since it is resisting the rearrangement of soil particles and this increase will be equal to the increase in total vertical stress. The increase in pore water pressure, named excess pore water pressure, creates a pressure gradient resulting in a transient flow of pore water towards a free-draining boundary of the soil layer (Craig, 2004).

As the reduction of excess pore water pressure is complete, i.e. the excess pore water pressure is zero, the soil is said to be in a drained condition. When there is still excess pore water pressure present, the soil is said to be in an undrained condition. The soil volume will reduce as drainage occurs since dissipation of excess pore water pressure results in an increase of effective vertical stress, allowing the soil particles to rearrange is referred to as consolidation.

Drainage is largely depending on the permeability of the soil, and can take a considerable amount of time to complete for clay with low permeability. (Craig, 2004). The use of drained analysis in a finite element analysis should be conducted when permeability is high, rate of loading is slow and the short-term behaviour is not of interest.

On the other hand, an undrained analysis should be performed when permeability is low and the rate of loading is high and assessing short term soil behaviour is of interest. Undrained behavior of soft soil may be understood as the situation of soils under external

loading in which water can't drain out of soil in the short term (Whitlow 1983), because the rate of loading is much quicker than the rate at which pore water is able to dissipate and most of external loading is transferred into pore water, leading to an increase of excess pore pressure. The existence of drained or undrained state depends on types of soil and rate of loading. Normally, undrained state is experienced with fine-grained soil (clay, peat etc.). However, if the rate of loading is fast enough, the coarse-grained soil also experiences undrained behavior. According to Whitman (1979), undrained shear strength of soil s_u is defined as strength of fine-grained soil which describes the capacity to sustain shear stress under undrained condition. In aspect of soil properties, the undrained shear strength only depends on the initial void ratio or the initial water content. Furthermore unlike the critical state of friction angle, ϕ'_{cs} , the undrained shear strength is not a fundamental soil parameter. Its value depends on the value of effective confining stress. It can be considered that an increase of effective confining stress results in an increase of undrained shear strength.

The behavior of saturated soft soils subjected to loading in the short term is considered in undrained state. The failure surface is formulated, along which soil grains slide over each other. The undrained shear strength of soil in this situation is defined as the maximum shear stress at which the soil starts failing.

Another approach is to take account of the whole consolidation process with a coupled consolidation FE analysis. In general, the coupled elastic plastic FE analysis (2 phase model) yields similar results for the long term behaviour of the foundation as the drained FE analysis with the 1 phase model, and the 1 phase model overpredicts the settlements during the loading/construction process.

2.5.5 Effective Stress

The parameter specific volume v is highly useful when designing more advanced constitutive material models and is expressed as the total volume of soil that contains a unit volume of solids, i.e. $V = 1 + e$. A fully saturated soil has the unit weight γ_{sat}. In such a case, the solid soil particles are subjected to a buoyancy force acting upward. This force is equal to the unit weight of water γ_w. The buoyancy reduced unit weight from γ to γ' is thus $\gamma' = \gamma_{sat} - \gamma_w$.Fully saturated soil can be considered as a skeleton of solid particles enclosing voids containing incompressible water. Since the individual soil particles are

also considered incompressible, a reduction in volume of a fully saturated soil is only possible if some water can escape the voids.

The principle divides the total normal stress σ acting on a soil body into two components and can be expressed as $\sigma = \sigma' + u$ (Schofield and Wroth, 1968) where σ' is the normal stress which must effectively be carried by the soil skeleton particles and u is the pore water pressure carried by the incompressible fluid occupying the voids.

Two stress parameters utilized in the constitutive relations is the effective mean stress p' and the deviatoric stress q, which are defined in the triaxial plane as

$$p' = \frac{\sigma_1' + \sigma_2' + \sigma_3'}{3} = \frac{\sigma_a' - 2\sigma_r'}{3} \quad \text{and} \quad q = \sigma_a - \sigma_r \tag{2.11}$$

where σ_1', σ_2' and σ_3' are the three principal stresses, σ_a' is the effective axial stress and σ_r' is the effective radial stress in the triaxial plane. Since the deviatoric stress is defined as the difference between the axial and radial stress, it is not affected whether it is calculated with total or effective stress measures.

2.5.6 Effect of Change in the Coefficient of Permeability on Consolidation Characteristics of Clay

The settlement rate and pore water pressure dissipation rate are mainly controlled by the permeability of soil. Mohammed Y. Fattah, Maysam Th. Al-Hadidi and Ahmed S. al-Shammary (2012) investigated the importance of the decrease of the coefficient of permeability on the time rate of consolidation settlement and pore water pressure using the finite element method. Consolidation process is accompanied by decrease in void ratio which leads to decrease in the coefficient of permeability. After pore pressure dissipation, there is a gain in the shear strength, which should also be considered, but in a long-term stability analysis.

The formula proposed by Taylor (1948) and verified by Tavenas et al. (1983) can be used to represent this variation of the permeability of soft clay during the consolidation:

$$k = k_o .10^{\left[-\frac{(e_o - e)}{c_k}\right]} \tag{2.12}$$

where e_o = the initial void ratio, e = the void ratio at the condition under consideration, k = the permeability, k_o = the initial permeability, and c_k = constant which is equal to $0.5e_o$.

The effect of permeability is clear at later times of consolidation due to decrease in void ratio and hence slower dissipation of pore water pressure.

2.5.7 In Situ Stresses and K_0 Conditions

The soil mass response is heavily dependent on the previous stress history. Any previously applied stresses that are larger than those currently existing have been locked into the soil structure and will affect subsequent stress-response behavior until a new set of larger stresses. The stress history is lost in varying degrees (or completely) when the soil is excavated/remolded or otherwise disturbed as in sample recovery. Vertical locked-in *effective stresses* p'_o would be larger than the effective lateral stresses σ'_h at the same point. We may define the ratio of the horizontal to vertical stresses as $K = \frac{\sigma_h}{p_0}$ which is valid for a particular depth at any time.

Over geological time the stresses in a soil mass at a particular level stabilize into a steady state and strains become zero. When this occurs the vertical and lateral stresses become principal stresses acting on principal planes. This effective stress state is termed the *at-rest* or K_0 condition with K_0 defined as $K_0 = \frac{\sigma'_h}{p'_0}$.

Jaky (1948) presented a derived equation as $K_0 = \frac{1-\sin\phi'}{1+\sin\phi'}\left(1+\frac{2}{3}\sin\phi'\right)$ and in simplified form as $K_0 = 1 - \sin\phi'$ which called "Jaky's equation" and has proved reasonably reliable for normally consolidated soil. For normally consolidated clay K_0 may be expressed as $K_0 = 0.95 - \sin\phi'$ (Brooker and Ireland,1965).

Kezdi (1972) suggests that for sloping ground Jaky's equation can be used as $K_0 = \frac{1-\sin\phi'}{1+\sin\beta}$, where β is the angle with the horizontal.

2.5.8 The Compression Index and Ratio

The amount of primary consolidation settlement is computed using either the compression index C_c obtained from a plot of void ratio ε versus log p or from a compression ratio C'_c obtained from a plot of strain ε versus log σ. The void ratio or strain is computed based on initial sample conditions and the compression ΔH under the current

load increment from D_{10} to D_{100}.This value computes a slightly larger (and more conservative) C_c or C'_c. The plot of ε versus log σ is more rapid than using e versus log σ. The initial branch of the e or ε versus log σ plot represents recompression of the sample back to the in situ state from the expansion that occurred during recovery. This is also called the *preyield* stress range. The approximately linear curve portion beyond the in situ state is called the *postyield* stress range.

The discontinuity between the pre- and postyield curve branches represents the previously consolidated stress state (or previous stress history imprint). The discontinuity is seldom abrupt but usually transitions along a curve that is a characteristic of that particular soil under the test procedure(s) being used. Experience on both "undisturbed" and remolded samples of the same soil, and using loading and unloading curve parts, gives the following:

a. If the discontinuity occurs at approximately the current in situ overburden pressure p'_o, the soil is *normally consolidated (NC).*

b. If the discontinuity occurs at a pressure σ'_c greater than the existing overburden pressure, the soil is *overconsolidated (OC)* and the OCR = $\sigma'_c / p'_o > 1$.

c. If the discontinuity occurs at a pressure σ'_c less than σ'_0, the soil is probably recently (on a geologic scale) deposited and may still be undergoing consolidation.

e. The remolded soil consolidation curve is always below the "undisturbed" soil curve, as shown by the labeled, dashed line. This observation, together with the transition back to the "virgin" curve at the point where an unload curve branch is done, is the basis for defining C_r and locating the preconsolidation pressure p'_c.

If the soil is preconsolidated, that slope between current p'_o and p'_c, drawn by eye as a best fit since it is usually curved, is designated the recompression index C_r or recompression ratio C_r. For computing C_r with rebound data sometimes the average of the initial recompression branch and the reload branch is used.

It should be evident that all stresses involved here are effective stresses. In situ we have K_0 conditions, and in the laboratory by definition the excess pore pressure Δu is zero when we complete the data for any given load increment on the sample. At this pore-

pressure state the soil grain contact points carry the applied stress, and by definition this is the *effective pressure* state.

2.5.9 Consolidation of Soil

Under external loading in undrained state of soil, excess pore water pressure develops. If a fully saturated soil subjected to an increased total stress is allowed to gradually reduce in volume due to dissipation of excess pore pressure, it is said to have primary consolidated. This process might take a long time and when all excess pore pressure has dissipated, the soil is considered fully consolidated.

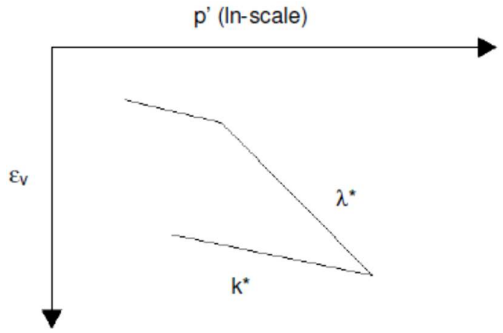

Figure 2.18 Determination of λ^*, κ^* from isotropic compression test

The maximum value of effective stress experienced in the past is referred to as the vertical pre-consolidation stress σ'_{vc}. If the present effective stress is same as σ'_{vc}, the soil is said to be in a state of normal consolidation. If the soil on the other hand at some time in history has experienced a larger effective stress than its current level, the soil is said to be over-consolidated. The present value effective stress is σ'_{v0} the over-consolidation ratio as defines $OCR = \frac{\sigma'_{vc}}{\sigma'_{v0}}$ is usually the result of geological factors such as erosion of overburden or glaciation.

The characteristics of clay during one-dimensional consolidation or swelling can be obtained from an oedometer test. The shape of the curve obtained in *e-log*σ' the space is related to the stress history of the clay. The curve shape for *NC* clay is nearly linear and is named the virgin compression line, tangentially represented by the compression index C_c. If the clay is *OC*, its stress state will be plotted as a point on the left side of the virgin compression line. These points then lie within the area of expansion or recompression and can be represented by the swelling index C_r, which is the tangent of the unloading-reloading line. Ultimately, the recompression curve will join with the virgin compression line and any further compression then occurs along the virgin line.

To predict the consolidation settlement of a layer of saturated clay, one dimensional theory assumes the condition of zero lateral strain within the clay layer and the reduction in unit volume is equal to the reduction in thickness. It is therefore possible to express the full consolidation settlements of a clay layer of thickness *H* as

$$S_c = m_v \Delta\sigma_v' H \tag{2.13.1}$$

where the coefficient of volume compressibility m_v and change in effective vertical stress $\Delta\sigma_v'$ are assumed constant within a layer.

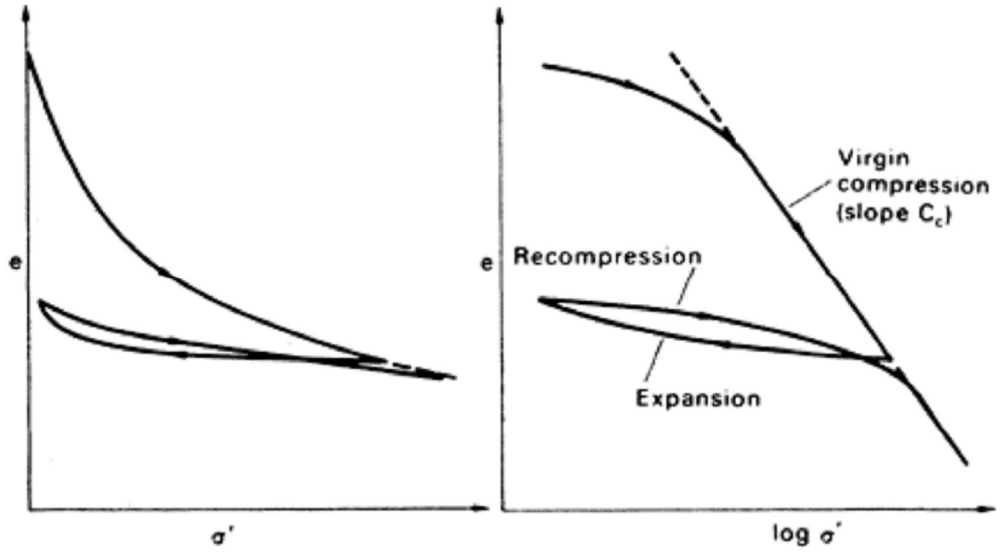

Figure 2.19 Void ratio - effective stress relationship in semi-logarithmic space (Craig, 2004).

It is also possible to express the full consolidation settlement directly from an oedometer test with NC clay as

$$S_c = \frac{C_c \log(\sigma_{v1}'/\sigma_{v0}')}{1 + e_0} H \tag{2.13.2}$$

where σ_{v0}' is the initial state of effective vertical stress, σ_{v1}' is the final state of stress.

For the purpose of this thesis, it is appropriate to express the full settlement in terms of the modified compression and swelling parameters. These parameters can be obtained from the compression index and swelling index to fit into the ε-logσ' space according to PLAXIS, 8.0 as

$$\lambda^* = \frac{C_c}{2.3(1 + e_0)} \quad \text{for } \sigma' > \sigma_c' \tag{2.13.3}$$

$$\kappa^* = \frac{2C_r}{2.3(1 + e_0)} \quad \text{for } \sigma' < \sigma_c' \tag{2.13.4}$$

where the factor 2.3 origins from the ratio between the logarithm of base 10 and the natural logarithm.

The full consolidation settlement expressed with the modified compression index for normally consolidated clay is obtained as

$$S_c = 2.3\lambda^* \log(\sigma'_{v1}/\sigma'_{v0})H \quad (2.13.5)$$

For stress levels below the pre-consolidation stress, the consolidation is governed by the modulus κ^* and the deformations will be mainly elastic, but not necessarily linear elastic. As the stress level exceeds the pre-consolidation stress, the consolidation is instead governed by the modulus λ^*. At this point, the stress path follows the virgin compression line, resulting in larger and irreversible deformations (Axelsson, 1994).

In order to obtain accurate results when dealing with stress-dependent stiffness, the modified compression and modified swelling modulus can be replaced with a parameter β^* which is the tangent of the oedometer curve in ε-logσ'_v space according to equation (2.13.1) for stress below the pre-consolidation stress and according to equation (2.13.2) for stress above the pre-consolidation stress. The tangent of β^* is taken in between the stress-range σ'_{v0} and σ'_{v1} . Thus the full consolidation settlement obtained as a result of the stress state going from σ'_{v0} to σ'_{v1} in a certain layer at a certain depth can be obtained with the expression

$$S_c = 2.3\beta^* \log(\sigma'_{v1}/\sigma'_{v0})H \quad (2.13.6)$$

By introducing a dimensionless number called the time factor T_v it is possible to calculate the progress of consolidation after a certain time period:

$$T_v = \frac{C_v t}{d^2} \quad (2.13.7)$$

where C_v is the coefficient of vertical consolidation, t is the time and d is the length of the longest drainage path.

In this thesis, only the full consolidation settlement is of interest and the consolidation obtained within a certain time period is not concern.

2.5.10 Creep Behavior of Soil

Secondary consolidation or creep, on the other hand, is a viscous behaviour of the soil-water system causing slow-rate compression, mainly observed after primary

consolidation. It is an important component in the consolidation process of clay soils and lies within the scope of this master's thesis and will thus be taken into consideration.

Creep is reasonably understood as the gradual rearrangement of soil grains in more stable configuration. Besides, another understanding is that creep is caused by a very slow drainage of water from micro-pores to macro network. It can be said that the mechanism which causes creep deformation is still not fully understood due to different opinions of previous research.

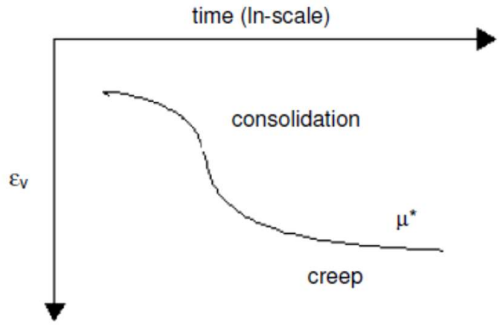

Figure 2.20 Determination of μ^* from isotropic compression test

Everything on this earth has at least one thing in common: everything changes with time, all soils age and change. The principal evidence of time dependency in soils behaviour is the empirical observations of large settlements developing with time in soils subjected to constant effective stress. This phenomenon is referred to as creep behaviour and it is clearly evident mostly in clays but it is observed in sandy soils, as well.

Creep is the phenomenon in which the strain increases at constant effective stress, due to viscous effect involving the soil solid skeleton. The strain is gradually increasing with constant effective stress acting on the specimen, in other words the soil exhibits creep behaviour (Fig 2.21a).

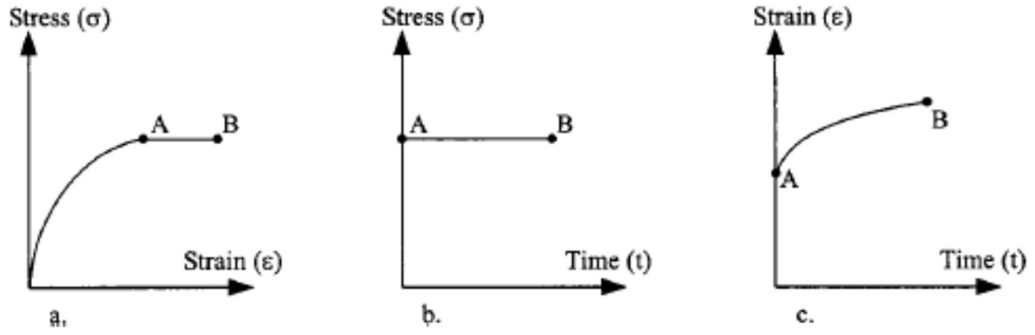

Figure 2.21 Definition of creep test

The creep process is divided into three phases. The primary phase, can be defined as a creep deformation during which the strain rate decreases continuously with time. Deformation at a constant rate (material flow) is denoted as the secondary phase. In the tertiary phase the strain rate is continuously increasing and this leads to the creep rupture. This fact is demonstrated plotting the logarithm of the strain rate against the logarithm of time (Fig 2.22b).

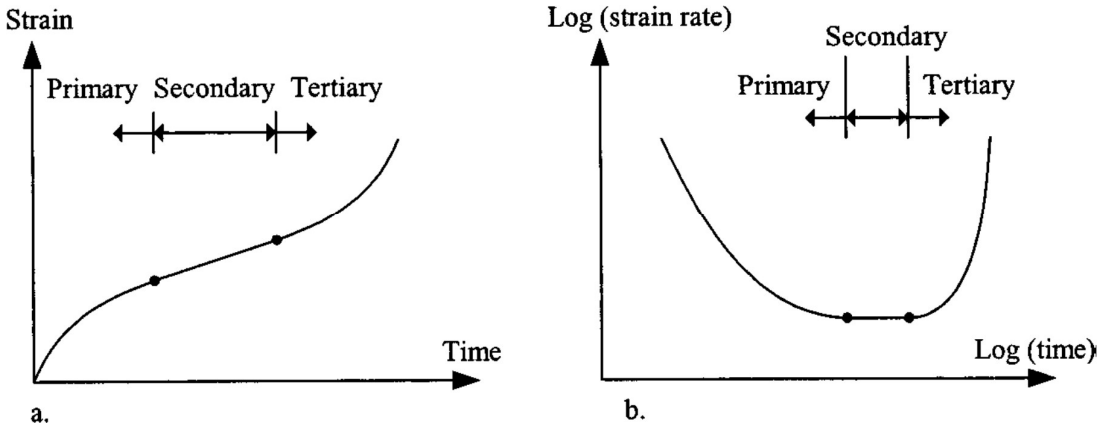

Figure 2.22 Three phases of creep in a triaxial apparatus (Augustesen et. al., 2004).

Volumetric creep consists only of the primary phase of the creep deformation, i.e. it tends to stabilise. Deviatoric creep consists only primary creep phase if the deviatoric stress is low but after crossing some level of the shear mobilisation primary phase will be followed by the secondary phase which can lead to the tertiary phase.

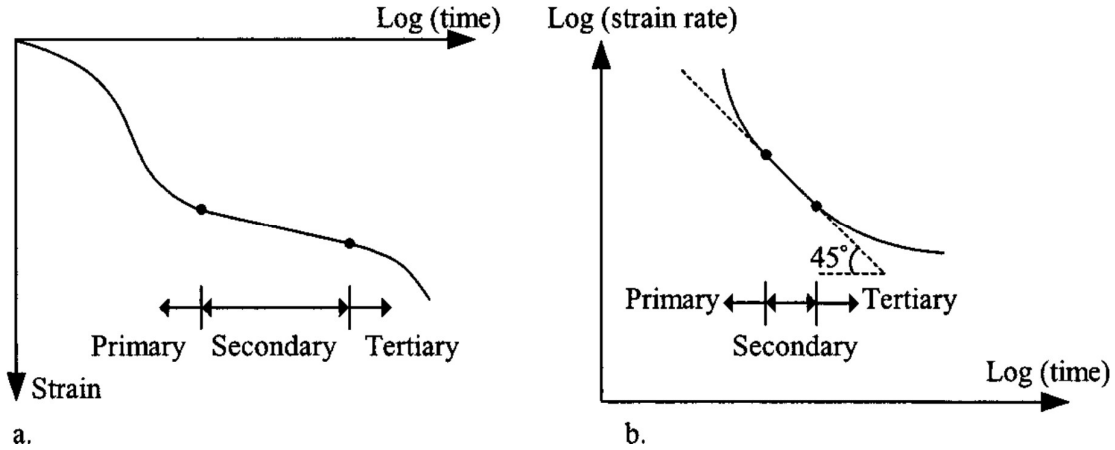

Figure 2.23 Primary, secondary and tertiary compression in an oedometer test (Augustesen et. al., 2004).

For oedometer tests, primary, secondary, and tertiary compression can be defined by plotting strains versus the logarithm of time, as reported in Figure 2.23.

When a fully saturated soil sample (typically a clay sample) is suddenly loaded one-dimensionally, its void ratio decreases producing, at least for normally consolidated samples, the well known S-shaped curve, reported in Figure 2.24.

During primary compression settlement is controlled by dissipation of excess pore pressure and Darcy's law, i.e. it is a consolidation process. However, during secondary compression, the rate of viscosity is controlled by soil viscosity; however, as settlements requires hydraulic gradient, excess pore pressure also exist during that stage.

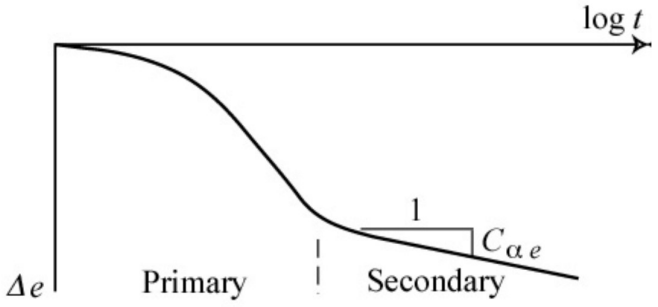

Figure 2.24 S-shaped compression curve in semi-logarithmic plot.

The secondary phase is denoted as secondary consolidation and this phase corresponds to pure creep, i.e., deformations occur due to deformations in the soil skeleton. Tertiary compression also corresponds to pure creep and it is characterized by a nonlinear relationship between the logarithm of time and strain.

2.5.11 Continuum Analysis with Finite Element Method

The study of numerical methods to solve geotechnical problems are increasing tremendously such as finite element method (FEM). Sloan and Randolph 1982, Griffiths (1989) has been widely used to compute the bearing capacity of strip and circular footings. Because of the complex nature of soil, the development of constitutive models capable of capturing ‘real’ soil behavior is a key aspect of analyses of geotechnical structures.

There exists a limit state, the critical state, where the volume change ceases for a large shear deformation while the deviatoric stress approaches a limit value (Axelsson, 1994).

Many numerical and constitutive models of soil behaviour are built around the principles of Critical state soil mechanics highlights the understanding and importance of volume change and the changes in effective stresses when evaluating soil behaviour (Wood, 1990).

Finite element analysis is a method of solving continuous problems governed by differential equations by dividing the continuum into a finite number of parts (elements), which are specified by a finite number of parameters. A problem is solved by dividing the larger geometry into small elements, which are interconnected with nodes. Each element is assigned an element property. In solid mechanics, the properties include stiffness characteristics for each element. This force-displacement relationship is expressed as- the nodal force matrix equal to multiply of the element stiffness matrix and the nodal displacement matrix of the element.

2.5.12 Elasto-Plasticity Theory: The Four Main Ingredients

Elastic material models and solutions based on theory of elasticity may be directly applied in geotechnical engineering for problems where strains are very small. Elastic strains are by definition recoverable and strains are again zero when the load causing them is removed. When involved strain is significant some of the strain will normally be permanent. Permanent strains are called irrecoverable or plastic, hence the name of *elasto-plasticity* associated to the constitutive law that accounts for irreversible behaviour of the material.

The *yield point* (Fig 2.26), or more generically the *yield surface* in three-dimensional conditions, marks the boundary of the region of elastically attainable states of stress. It is described by an equation called *yield criterion*:

$$F(\sigma_{ij},h) = 0 \qquad (2.14)$$

where h represents a set of variables linked to the history of the process (hardening parameters), later described.

Whenever $F(\sigma_{ij},h) < 0$ the soil state represented is inside the yield locus and the response is elastic. Whether $F(\sigma_{ij},h) = 0$ the soil state is in an elasto-plastic condition.

The yield locus can represent either a failure situation (in case of elastic perfectly plastic materials) or simply a yielding condition. In the elastic-perfectly plastic model there is a

region of stress space which can be reached elastically, without incurring any irrecoverable deformations, however, as soon as the boundary of this elastic region is reached then the material fails at constant stress as described in Figure 2.25. Stress points outside the yielding surface ($F(\sigma_{ij},h) > 0$) are not allowed. In the case of prefect plasticity the yield criterion coincides with a failure criterion.

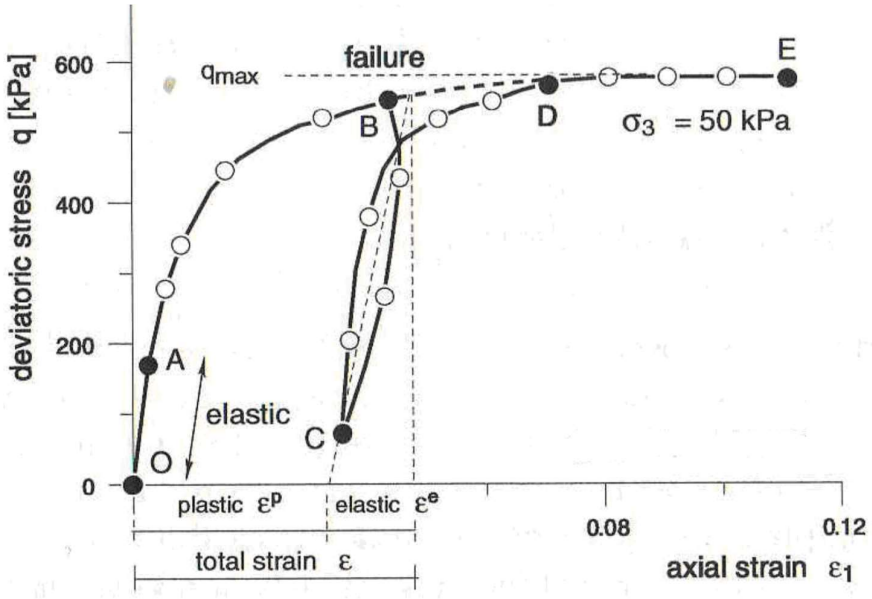

Figure 2.25 The result of a standard triaxial test with one unloading- reloading cycle.

On reloading starting from point C in Figure 2.25, in fact, the primary loading curve is reached at point D and then follows the primary loading curve up to a maximum value q_{max} at point E where the soil fails. Shear stress at point E is known as soil shear resistance under constant confining pressure σ_r .During primary loading along the path OABDE the so called yield point is gradually moved from A to E. This process of increasing the yielding point is known as *hardening*.

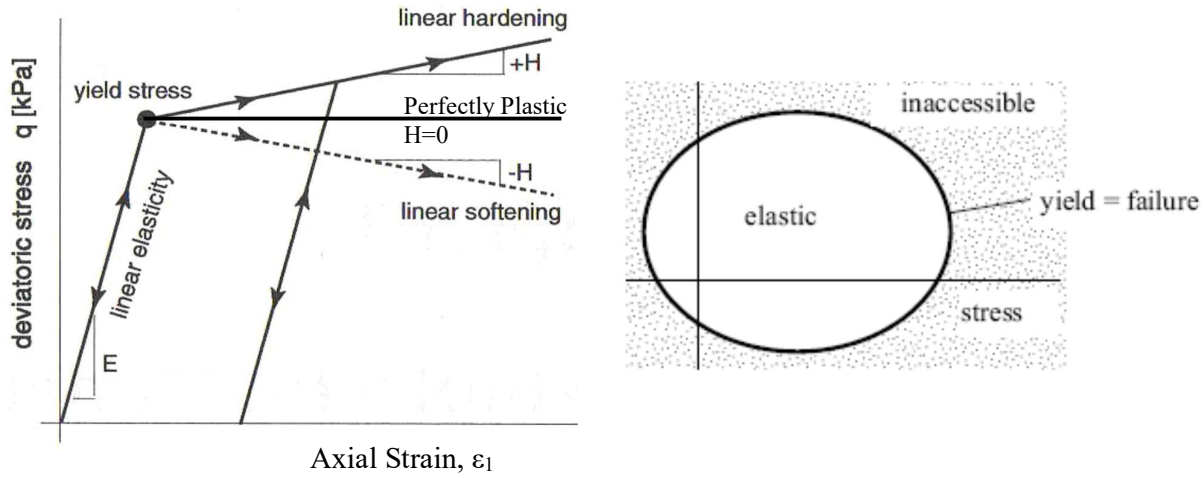

Figure 2.26 Perfect plasticity linear strain hardening or softening plasticity.

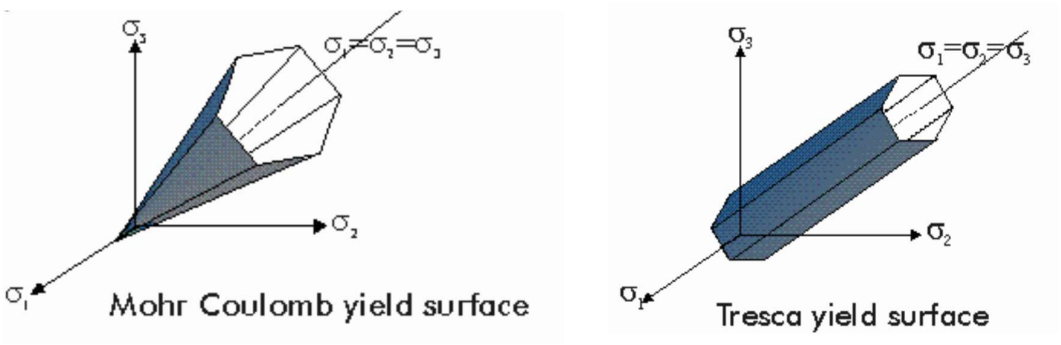

Figure 2.27 Yield surface in principal stress state.

In an elastic perfectly plastic framework, such as depicted in Figure 2.26, the material shows no hardening and the stiffness H of the material reduces to zero. Another type of plastic behaviour is seen in Figure 2.31 where the linear stress-strain is continuous in the plastic range but with a lower stiffness H compared to the stiffness E in the elastic range. If the plastic stiffness $H > 0$ then the behaviour is referred to as *strain hardening* behaviour, otherwise for $H < 0$ it is called *strain softening* behaviour.

2.5.13 The Bearing Capacity of Two Layered Soil using PLAXIS

The PLAXIS Version 8 finite element package was used for analysis of bearing capacity of two-layered subsoil loaded with strip and square foundations whose width B=1.0 m. The foundations were very flexible (EA = 300000 kN/m, EI =1000 kN/m^2) and very rough (no soil sliding in their base). In analysis using PLAXIS for cohesionless sands was assumed c =1 kPa for sands in this paper and $\psi = \phi - 30^o$ for the soils with $\phi > 30^o$, and $\psi = 0$ for the soils with $\phi < 30^o$. The angle of dilatancy of dense sand is greater than that suggested by authors of PLAXIS. The influence of elastic parameters on the bearing capacity is very small, while the strength parameters and angle of dilatancy considerably affect the bearing capacity.

The bearing capacity factors are exclusively the functions of the angle of internal friction. If the weaker soil is deeper than $2B$ below foundation base, then the ultimate limit state has to be checked for the substitute foundation width B' and length L' placed on the surface of a weaker layer. The dimensions of substitute foundations proposed in Polish Standards are denoted by

$B'_n = B + \frac{2h}{m}$ and $L'_n = B + \frac{2h}{m}$ where h is top layer thickness. For cohesive soils, m = 8 if $h \leq B$ and m = 6 if $h > B$ and for cohesionless soils, m = 6 if $h \leq B$ and m = 3 if $h > B$.

Polish Standards proposed, $B'_p = B + \frac{2h}{n}$ and $L'_p = B + \frac{2h}{n}$

where n = 6 for all soils.

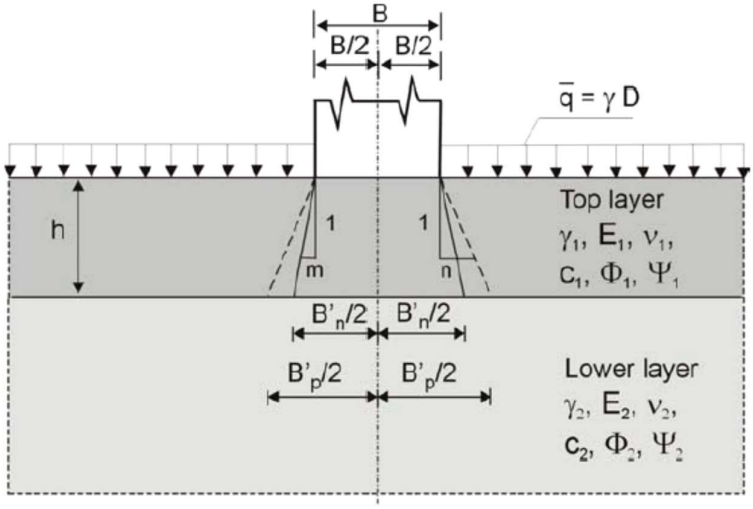

Fig. 2.28 Proposition of substitute foundation width.

2.5.14 Circular Footings on a Cemented Layer above Weak Foundation Soil

This project studied shallow spread footings placed on a double layer foundation system in which the upper layer was artificially cemented through mixing, compaction, and curing. The method identified both the ultimate capacity of the footing and its load–settlement response, particularly the settlement at working loads.

This study produced a design method for the complete pressure–settlement curve of spread footings bearing on a layered system in which the upper layer was cemented and the underlying layer was a weakly bonded residual soil with a high void ratio. Results from normalized plate-loading tests (Thomé et al. 2005) and numerical simulation was combined to produce a method for predicting load–settlement curves for circular footings on these layered systems.

Finite-element analysis of footing behavior on layered soils

The constitutive model used to represent both the cemented upper layer and the lower, weakly bonded residual soil layer was an elastic – perfectly plastic model with the Drucker–Prager failure criterion and a non-associated flow rule. In the simulations, the modeling parameters effective cohesion intercept (c_1'), effective friction angle (ϕ_1'), and

Young's modulus (E_1) of the cemented upper layer; and effective cohesion intercept (c_2'), effective friction angle (ϕ_2'), and Young's modulus (E_2) of the weakly bonded lower layer were used and these were obtained from drained triaxial tests. It is noted that the elasticity has been defined as isotropic, even though compaction of the cemented layer may induce transverse anisotropy.

Parametric analysis

The load–deformation calculations were used to examine the effects of the constitutive parameters in relation to the footing diameter (D) and the thickness (H) of the cemented layer. Referred by Thomé et al. 2005, the strength parameters of the cemented layer, c_1' and ϕ_1', were reduced according to Tessari's (1998) project. For the weakly bonded material in the lower layer, the full measured values of c_2' and ϕ_2' were used. Measured values of the secant Young's modulus (E) at an axial strain of 0.1% were used for both materials.

Poisson's ratio (ν) does not significantly influence the results of the numerical analysis, the study used a constant value of $\nu = 0.25$ for both soil layers. The dilatancy angle in the upper layer (ψ_1) was considered to be $0.3\phi_1'$ that of lower layer (ψ_2) was considered zero in all simulations. Burd and Frydman (1997) showed that bearing capacity does not depend strongly on K_o and natural unit weight (γ_{nat}). So all simulations used initial stresses that assumed isotropic conditions, that is, with an at-rest coefficient (K_o) equal to unity and (γ_{nat})was fixed at 18 kN/m^3.

The finite-element analysis did not permit simulation of the rupture of the plate-loading tests, because the stress domain was treated as a continuum. It was therefore necessary to define a consistent condition that would be treated as a functional or serviceability failure. This "limit bearing pressure" was taken as the loading calculated to produce a maximum displacement equal to 2% of the plate diameter, that is, a relative settlement (displacement divided by footing size) of 2%. The value selected for this critical displacement criterion (2%) arose from several series of plate-loading tests carried out at the experimental field site of the Federal University of Rio Grande do Sul (Thomé et al. 2005) and from the work by Berardi and Lancellotta (1991). The latter authors analyzed the behavior of more than 200 shallow foundations. They found that maximum displacements at working loads were generally of the order of 1% of foundation width. This means that the 2% value for the critical relative displacement in this study—which was

considered to define the maximum, or limit, loading—was approximately double the value observed at working load.

Results of Numerical Analysis

A series of simulations was done for footing diameters ranging from 0.3 to 2.4 m and thickness of the cemented upper layer ranging from 0.15 to 0.60 m. In normalized terms, calculations were performed for H/D ratios of 0.25, 0.5, and 1.0. Three levels of cementation were considered for the cemented upper layer. These were modeled by different cohesion intercepts and classified as strong cementation(S) (c_1' = 450 kPa), medium cementation(M) (c_1'= 100 kPa), or weak cementation(W) (c_1' = 30 kPa) cementation. Values of ϕ_1 ranged from 35° to 50°. Pressure was here taken to be constant over the area of the footing and equal to the applied load divided by the area of the footing. No account was taken of pressure variation over the base of the footing. Curves of pressure versus relative settlement from the simulations listed for H/D = 1.0, 0.25 and 0.50.

It was helpful to normalize the results of plate-loading tests, whether in the field or in computer simulations. Normalization established general tendencies in relation to different plate diameters and the thicknesses of the cemented layer.

It remains to be seen, however, whether results from field plate-loading tests, with their associated variability, can also be normalized in the same way as the simulated results. A figure shows results that have been normalized from data presented by Thomé et al. (2005) for plate-loading tests where the upper layer was mixed with ash–lime. Although the data clearly showed some scatter, which was inherent in all field tests, the normalized experimental curves from the field tests can be readily approximated by a single relationship.

Further verification was obtained by replotting results from two additional sets of plate-loading tests on upper layers that were strengthened with (*i*) bottom ash and Portland cement or (*ii*) clayey soil and Portland cement. Fig. 2.29 and 2.30, respectively, show normalized results from these additional test series. The normalization methodology proposed above applies quite well to these separate test series, in which the upper layers were improved by three different cementing agents.

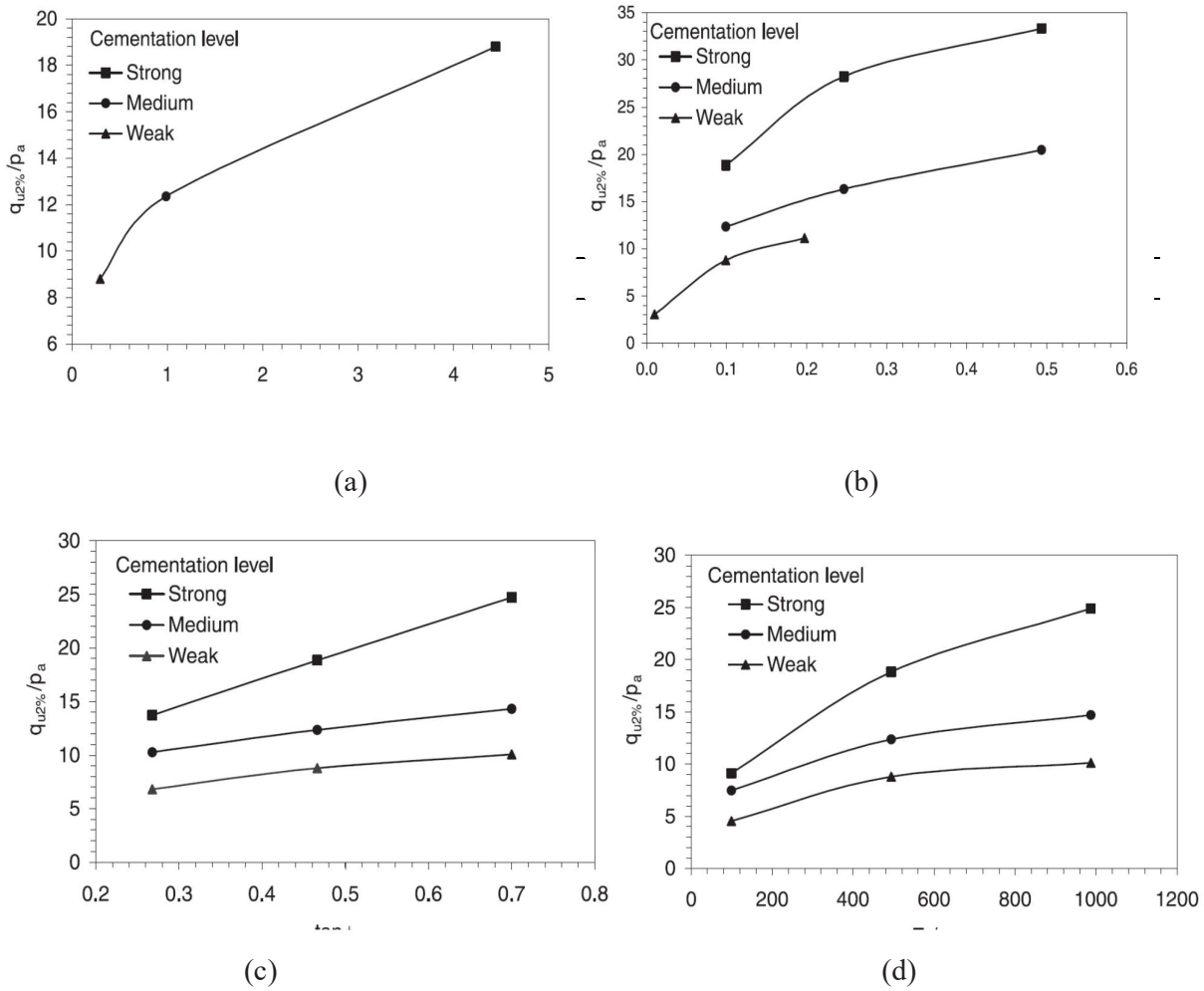

Fig. 2.29 Influence of the materials parameters on value of $q_{u2\%}$ for H/D = 1.

According to the numerical results it is possible to predict load–settlement curves for footings of different diameters bearing on cemented layers of different thickness by using only the results of a single plate-loading test on the layered system in question. What were still needed for design purposes, however, are values of the limit pressure ($q_{u2\%}$) for the particular geometries being considered.

The results showed that the limit pressure ($q_{u2\%}$) for each H/D ratio depended mainly on c_1' and c_2', ϕ_2', and E_2 of the weak bottom layer. The influence of the other soil properties, such as ϕ_1' and E_1, were found to be statistically not significant in contributing to the limit pressure ($q_{u2\%}$). In terms of the thickness of the cemented layer and the footing diameter, the method was valid for $0.25 \leq H/D \leq 1.0$. The method will be presented in a non-dimensional format, where p_a was atmospheric pressure.

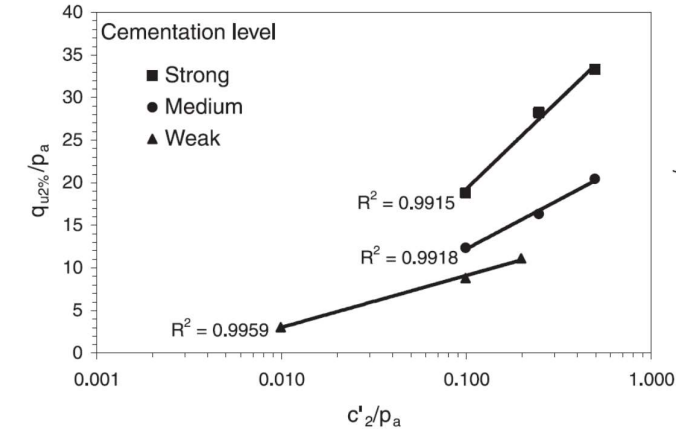

(a)

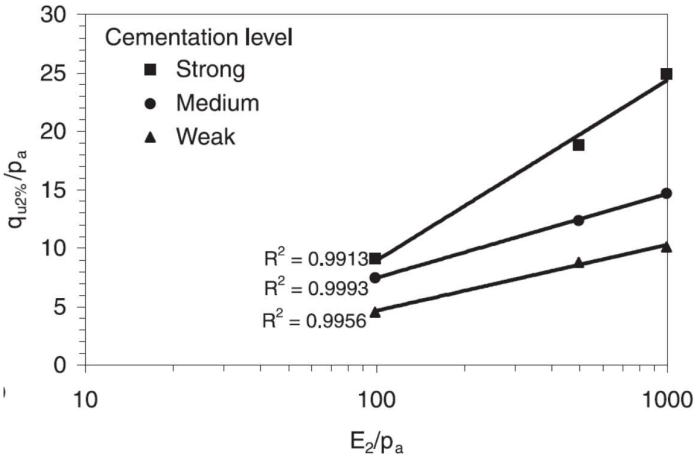

(b)

Figure 2.30 Linear variation of $q_{u2\%}/p_a$ with the logarithms of c_2'/p_a and of E_2/p_a.

The authors propose a semi-empirical method for evaluating $q_{u2\%}/p_a$. It searches for the mathematical function that fits the value of F to the results of the finite-element simulations and simulations were done for cases where the upper layer was strongly, intermediately, and weakly cemented and for H/D values of 1.0, 0.5, and 0.25.

The function F_2 depends on c_2'/p_a (Fig. 2.30*a*). Empirically, the mathematical function for F_1 can be written as follows:

$$F_2 = \ln\left(\frac{c_2'}{p_a}\right) \qquad 2.15.1$$

The function F_2 depended on the three parameters c_2'/p_a, ϕ_2', and E_2/p_a. The finite-element simulations showed that these three parameters influence the value of $q_{u2}\%/p_a$ in the ways shown in Figs. 2.30*b*. In Figs. 2.30*a* and 2.30*b*, the relationships $q_{u2\%}/p_a$ versus c_2'/p_a and $q_{u2\%}/p_a$ versus E_2/p_a are nonlinear. When the results are replotted in terms of

$q_{u2\%}$ /p_a versus ln (c_2'/p_a) and $q_{u2\%}$ /p_a versus ln (E_2/p_a), the relationships are approximately linear (Fig. 2.31). In Fig. 2.30b, $q_{u2\%}/p_a$ varies approximately linearly with tan ϕ_2'.When empirical fittings were being undertaken with the finite-element simulations, the use of the tan (ϕ_2') relationship did not produce good results, because the numerical magnitudes of the values of tan (ϕ_2') were considerably smaller than those of the ln (c_2'/p_a) and ln (E_2/p_a) terms.

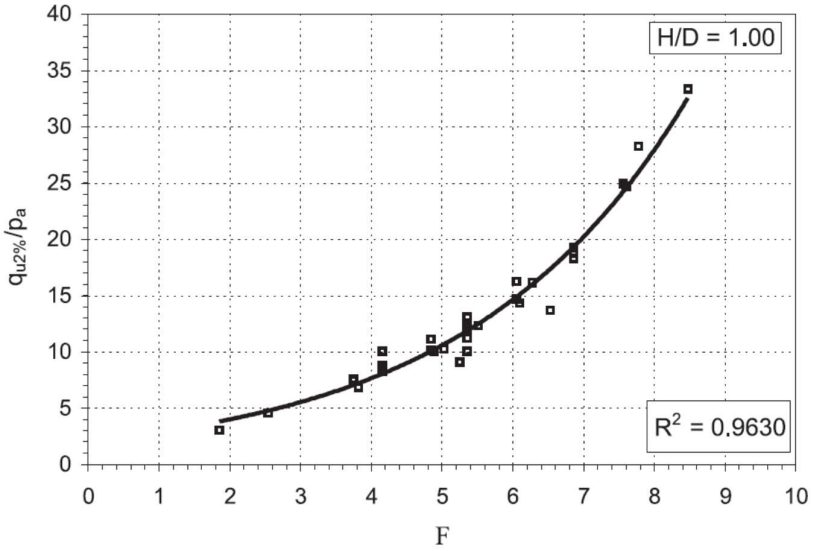

Figure 2.31 Relationship between $q_{u2\%}$ /p_a and F for H/D = 1.0.

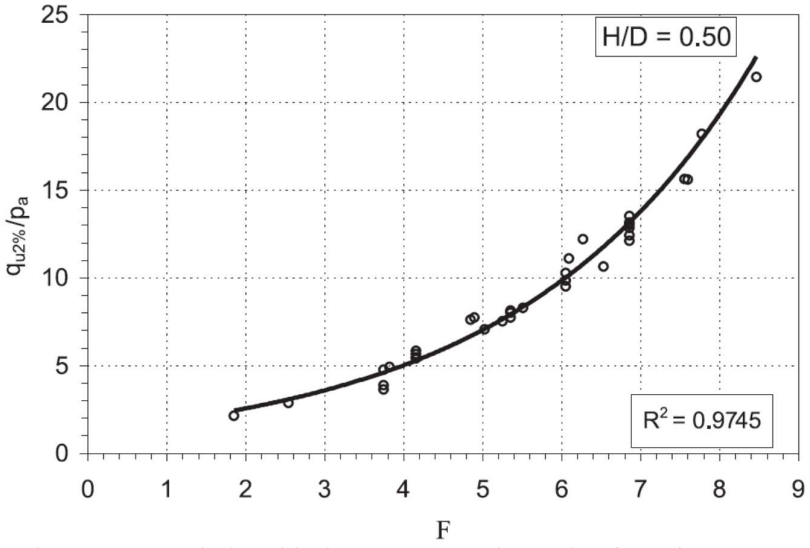

Figure 2.32 Relationship between $q_{u2\%}$ /p_a and F for H/D = 0.5.

Trial solutions showed that a function 1/(cos^4 ϕ_2') would produce a suitable reflection of the influence of ϕ_2' . The equation for F_2 was written as

$$F_2 = \ln\left(\frac{c_2'}{p_a}\right) + \ln\left(\frac{E_2}{p_a}\right) + \frac{1}{\cos^4\phi_2'} \qquad 2.15.2$$

When Eqs. 2.15.1 and 2.15.2 were substituted in Eq. 2.34.4, the value of F becomes

$$F = \ln\left(\frac{c_1'}{p_a}\right) + \ln\left(\frac{c_2'}{p_a}\right) + \ln\left(\frac{E_2}{p_a}\right) + \frac{1}{\cos^4\phi_2'} \qquad 2.34.9$$

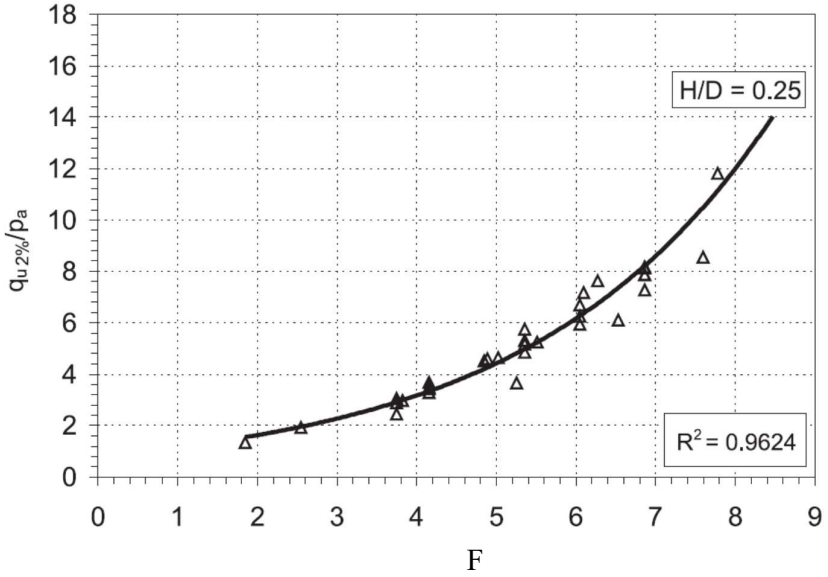

Figure 2.33 Relationship between $q_{u2\%}/p_a$ and F for H/D = 0.25.

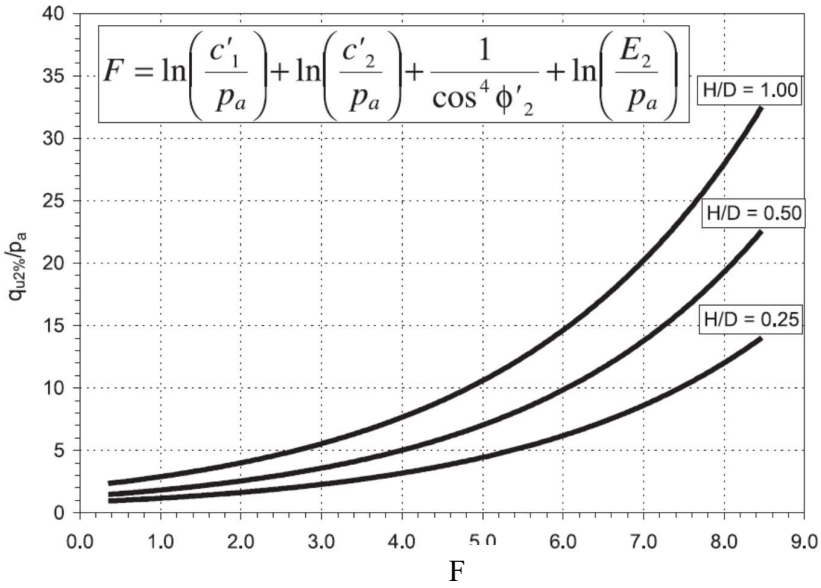

Figure 2.34 Graphical solution for obtaining bearıng capacity at a 2% relative settlement of footings on a layered system with a cemented upper layer.

Figure 2.33 presents values of $q_{u2\%}/p_a$ as a function of factor F for the case H/D = 1.0 and the range of soil properties used in the finite-element simulations. Fitting an exponential curve (Eq. 2.15.3) through the results of the empirical search process

produces a high coefficient of determination, R^2 = 0.96. Figures 2.33 and 2.34 present similar exponential relationships (Eqs. 2.15.4 and 2.15.5 for H/D = 0.5 and H/D = 0.25, respectively, which also have high values of R^2 of around 0.96. Figure 2.50 summarizes these exponential relationships in the form of graphs that can be used for design purposes. The equations for the three curves in Fig. 2.34 are as follows:

for $H/D = 1.0$, $q_{u2\%}/p_a = 2.10\ e^{0.324F}$ 2.15.3

for $H/D = 0.5$, $q_{u2\%}/p_a = 1.31\ e^{0.337F}$ 2.15.4

for $H/D = 0.25$, $q_{u2\%}/p_a = 0.84\ e^{0.333F}$ 2.15.5

To check the method outlined in previous sections, the values of limit loads ($q_{u2\%}$) calculated with Eqs. 2.15.3–2.15.5 were compared with measured values obtained by Consoli et al. (1998), Tessari et al. (1998), and Thomé et al. (2005) from plate-loading tests on three different cemented, layered systems.

For every H/D ratio for a given layered profile, the relationship between applied pressure and relative settlement was unique. As H/D increases, the load–settlement response becomes stiffer and stronger. For a given set of soil parameters for a given layered profile, expressing the applied pressures q in the form $q/q_{u2\%}$ and the settlements δ in the form δ/D produces unique normalized pressure–settlement relationships. A semi-empirical method based on finite-element calculations provides a new way of predicting the limit bearing pressure ($q_{u2\%}$) of footings on a two-layer system in which the upper layer was an improved cemented material. The solution requires the cohesion intercept of the cemented upper layer; and the cohesion intercept, friction angle, and Young's modulus of the weaker compressible lower layer. When the present methodology was used, it was not necessary to make any reductions in the parameters of the cemented upper layer. Such reductions were included in the development of the proposed method. For a given project, the techniques proposed in that paper, when combined with results from one plate-loading test, made it possible to estimate complete pressure– settlement curves (to a relative settlement of 2%) for footings of different sizes on different thicknesses of a cemented upper layer.

2.5.15 Case Study on Settlement of Foundation

Razzaque & Alamgir (1999) have performed a case study on the foundation of low rise building on compressible peat soil deposit of KCC area. They have studied long-Term Settlement of the Building in Fig 2.35. Peat Deposit and represented in Fig 2.36.

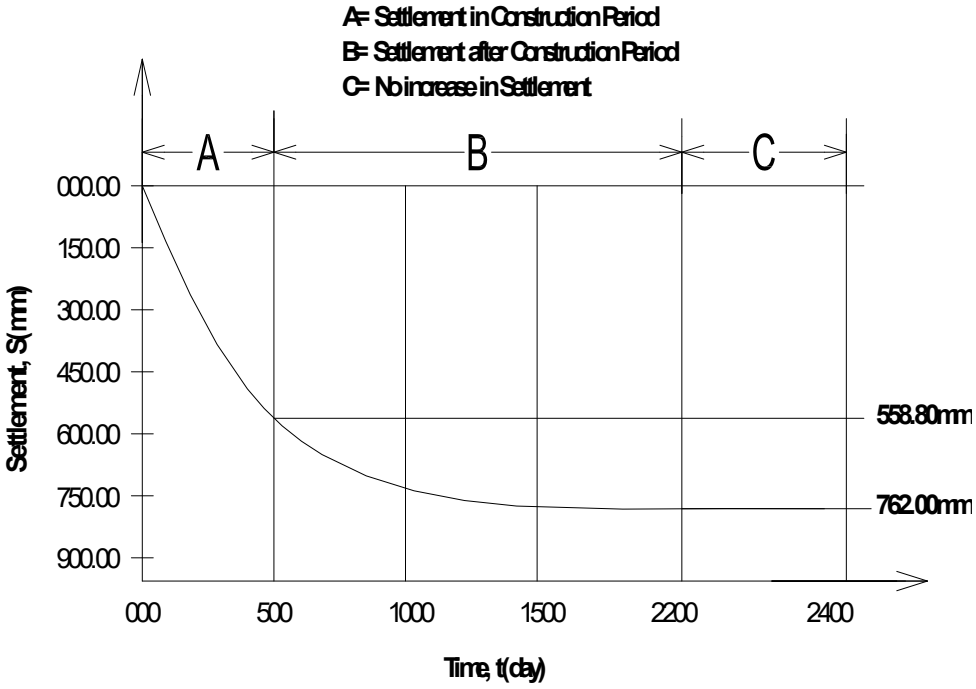

Figure 2.35 Long-Term Settlement of the Building in KCC area.

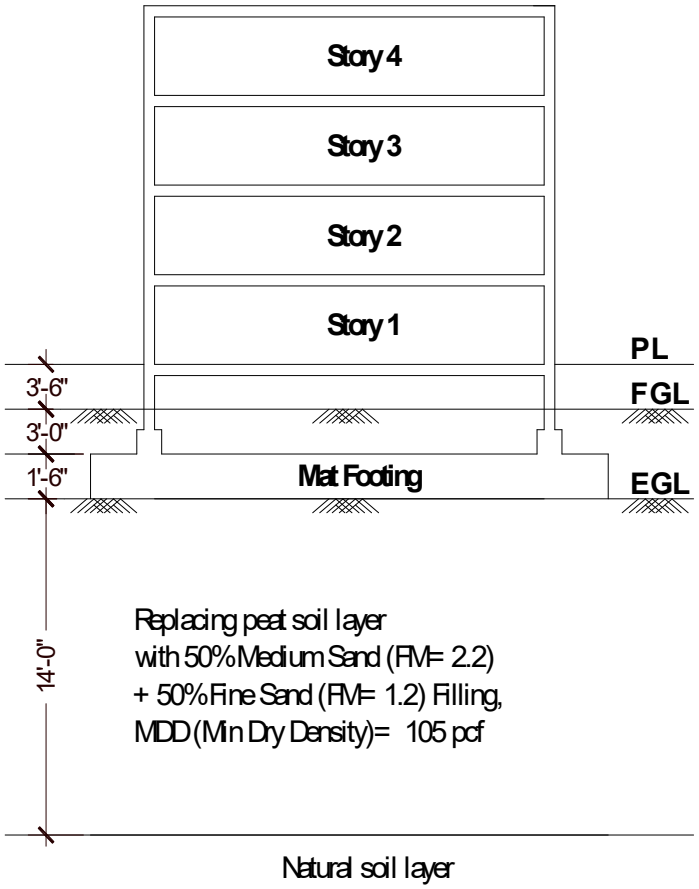

Figure 2.36 The foundation of low rise building on compressible peat soil deposit of KCC area.

2.6 Components of Constitutive Material Model

Constitutive models describe the relationship between stress and strain. The deformation analysis continues to be one the hardest issues to solve in the scope of the geotechnical project regarding the high non-linearity of the soil behaviour.

In order to create a constitutive elasto-plastic material model, it is necessary to define four components, according to the theory of plasticity (Wood, 2004) as shown in Figure 2.53 and Figure 2.54.

Elastic Properties

The elastic behaviour is assumed to be isotropic and defined by two elastic parameters, the bulk modulus *K* and shear modulus *G*. Elastic behavior is the easiest to model since no plastic integration is required.

By using an oedometer, it is possible to visualize the elastic and plastic response of the soil. The oedometer presents semilogarithmic plots where the relationship between stress and volume changes, plotted as the specific volume ν, becomes somewhat linear, both during loading and unloading. As visible in Figure 2.37, the average slope κ of the unload-reload line will characterise the elastic volumetric response of the soil whereas the average slope λ of the normal compression line characterises the plastic volumetric response (Wood, 2004).

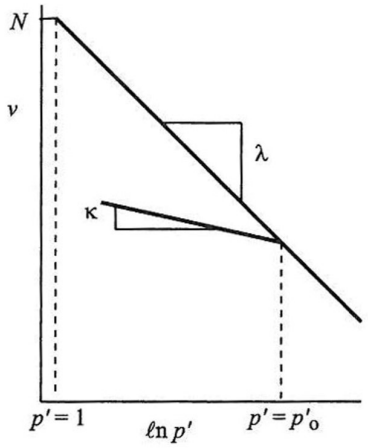

Figure 2.37 The linear normal compression line and the unloading-reloading line in a semi-logarithmic compression plane (Wood, 2004).

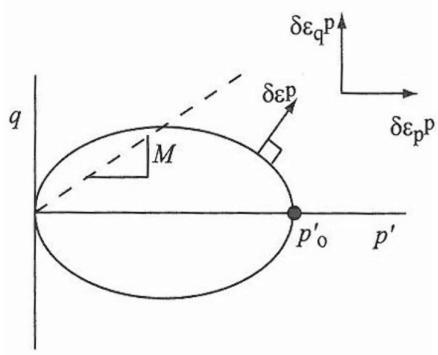

Figure 2.38 Elliptical yield locus for Cam Clay model (Wood, 2004).

Yield Criterion

The Cam Clay yield locus, as it is called in the two-dimensional (2D) space, takes on an elliptical shape in the p′:q-plane. It intersects the p′-axis in the origin and at a value of the mean pre-consolidation pressure, p_0'. The magnitude of p_0' will depend on the stress history of the soil; e.g. the stress history will determine the size of the yield locus (Axelsson, 1994).

Flow Rule

The Cam Clay model is assumed to obey the hypothesis of associated flow. This means that the increments of plastic strain are assumed to be normal to the yield surface at the current stress state, see Figure 2.38.

Hardening Rule

As the yield locus will change in size in plastic loading with a changing effective stress state, the hardening rule describes how the size of the yield locus influences the plastic strain. The Cam Clay is a volumetric hardening model and it is assumed that the size of the yield locus depends only on the plastic volumetric strain (Wood, 2004).

2.7 Constitutive Models for Soil

The following Constitutive Models are used for Simulating Soil Behaviour.

2.7.1 Hyperbolic Soil Model

The well-known hyperbolic model developed by Duncan and Chang (1970) captures soil behavior in a very tractable manner on the basis of only two stiffness parameters. The major inconsistency of this type of model is that in contrast to the elasto-plastic type of model, a purely hypo-elastic model cannot consistently distinguish between loading and unloading. The hyperbolic model is also not suitable for collapse load computations in the fully plastic range (Schanz, Vermeer et al. 1999).

Due to these restrictions of hyperbolic model a model was formulated in an elasto-plastic framework called 'Hardening Soil (HS) model' with so-called isotropic hardening. This model, however, supersedes the hyperbolic model by far: firstly by using the theory of plasticity rather than the theory of elasticity, secondly by including soil dilatancy and thirdly by introducing a yield cap.

2.7.2 The Cam Clay Model

A part of the scope of this master's thesis is to evaluate the results achieved by modelling with the Soft Soil Model (Plaxis manual). It is therefore appropriate to introduce the Cam Clay model, which serves as the foundation of the Soft Soil Model.

K. H. Roscoe and his group implemented the theory of perfect plastic material behaviour into their formulations, such as the Mohr-Coulomb yield criterion or the simpler extended Von Mises criterion. Roscoe group embraced the theory of plasticity since it was discovered that as a granular material soil displaces irreversible deformations combined with hardening or softening, a so-called work hardening material (Wood, 2004). The Roscoe group then started to formulate constitutive equations implementing the flow theory of plasticity into their critical state concept and a yield criterion with a logarithmic yield function was derived on energy considerations. The bullet shaped Cam Clay locus was regarded as somewhat un-realistic and was thus later modified to contain an elliptical yield locus in the effective mean stress – deviatoric stress plane. This model is called the Modified Cam Clay model (Axelsson, 1994).

The fundamental idea with the modified Cam Clay theory is that the soil material will fail as it reaches a certain stress state, known as the critical state. This results in shear deformations without any change in total volume. The model assumes associated plasticity behaviour between the plastic yield function and the plastic potential function. The modified Cam Clay model has been successful when analysing problems involving the loading of soft clays. If a constitutive model is to reproduce the isotropic loading behaviour of soil, it must include a yield function of effective mean stress and include a volumetric response.

2.7.3 Constitutive Modeling of Cemented Soil

Mashad, M., El. and Hashad, A. (2013) have used with plane strain elements with 15 nodes in simulation of improved soil which was soil-cement dust (mixed soil) having properties are shown in Table 2.1 for various mixtures.

A finite element numerical analysis using nonlinear elasto-plastic analysis was performed using PLAXIS 8.2 and Mohr-Coulomb soil model were used. In most FE analyses both lime/cement and clay are modeled as Mohr-Coulomb elasto-plastic materials.

Benjamin Charbit (2009) modeled the plastic behavior of lime/cement with the concrete damaged plasticity model. This model has been successfully used to describe cracking of concrete (Malm, 2009). Sand layer was modeled as a linear elastic material. 4-node tetrahedral element (Dhont, 2007) was used.

Table 2.1 Properties of Soil Mix Elements

Soil Properties	**Nat. Soil**	**Mix 10%**	**Mix 15%**	**Mix 30%**
(c) kN/m^2	12	28	66	104
(ϕ)	13	7	11	16
Young's modulus kN/m^2	13000	13050	13100	13150
Density kN/m^3	18.1	17.5	17.5	17.8
Posson's ratio	0.35	0.34	0.33	0.31
Permeability (k) (cm/sec)	3.7×10^{-6}	5.1×10^{-6}	2.1×10^{-6}	3.7×10^{-6}

The Mohr-Coulomb criterion has been used extensively to characterize the failure of soils. However, as pointed out before, the use of shear strength parameters, c and ø to soils and cement treated soils have led to number of anomalies. Many studies have shown that failure envelope of cement treated soils are curved. Consequently, it is impossible to report a particular internal friction angle (ø) to characterize the strength over the wide range of confining pressures. Several failure criteria such as, Griffith crack theory, modified Griffith crack theory have been presented to improve the strength description of geomaterials. Application of each failure criteria is limited to type of material and stress conditions.

CHAPTER-3

NUMERICAL ANALYSIS IN PLAXIS

3.1 Introduction

The theoretical basis of numerical analysis using PLAXIS and materials models are presented in this chapter.

3.2 Basic Model Parameters in Relation to Real Soil Behaviour

The axial pressure σ_1 on a soil element below a footing is increased whilst the radial isotropic confining stress σ_3 is kept constant. Under this type of foundation loading soil tend to produce curves as shown in Figure 3.1a. The increase in the volume (or volumetric strain) is typical for sands and is also frequently observed for rocks. Figure 3.1b shows the test results put into an idealised form using the Mohr Coulomb model. The figure gives an indication of the meaning and influence of the five basic model parameters. This is to be noted that the dilatancy angle ψ is needed to model the irreversible increase in volume.

PLAXIS uses the Young's modulus as the basic stiffness modulus in the elastic model and the Mohr-Coulomb model, but some alternative stiffness moduli are displayed as well. The values of the stiffness parameters adopted in a calculation require special attention as many geomaterials show a nonlinear behaviour from the very beginning of loading.

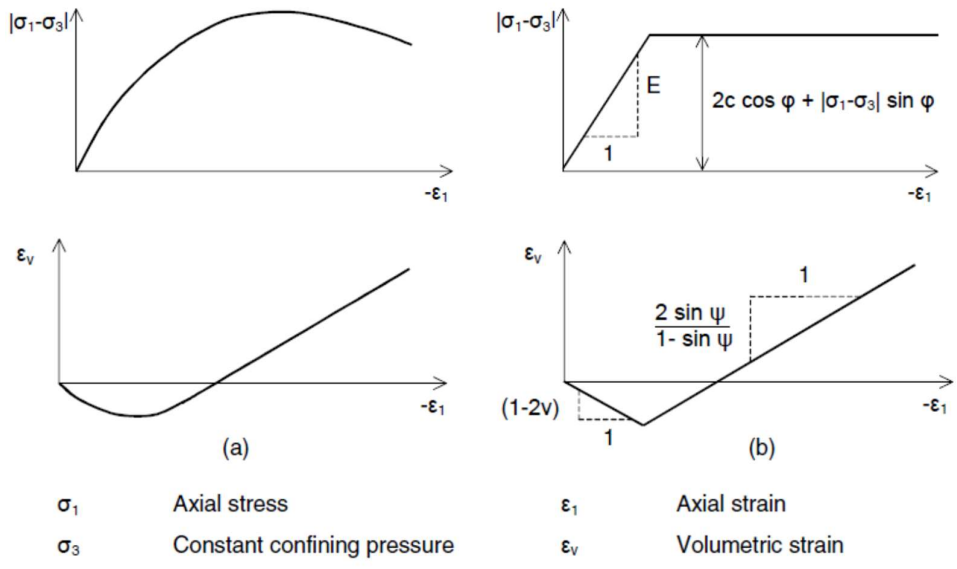

Figure 3.1 Results from (a) standard drained triaxial tests and (b) elastic-plastic model.

In soil mechanics the initial slope is usually indicated as E_0 and the secant modulus at 50% strength is denoted as E_{50} (Figure 3.2). For materials with a large linear elastic range it is realistic to use E_0, but for loading of soils one generally uses E_{50}. For unloading problems, as in the case of tunneling and excavations, one needs E_{ur} instead of E_{50}.

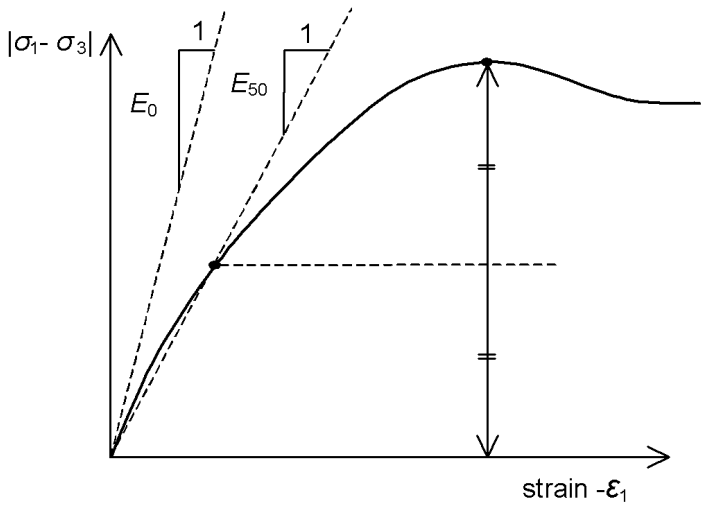

Figure 3.2 Definition of E_0 and E_{50} for standard drained triaxial test results

Also, the observed soil stiffness in terms of a Young's modulus may be lower for (drained) compression than for shearing. Hence, when using a constant stiffness modulus to represent soil behaviour one should choose a value that is consistent with the stress level and the stress path development. For the Mohr-Coulomb Model, PLAXIS offers a special option for the input of a stiffness increasing with depth.

3.3 Undrained Analysis with Effective Parameters in PLAXIS

In the PLAXIS it is possible to specify undrained behaviour in an effective stress analysis using effective model parameters which are available for all material models in the PLAXIS program. This is achieved by identifying the type of material behaviour (*Material type*) of a soil layer as *Undrained*. In this Section, it is explained how PLAXIS deals with this special option.

The presence of pore pressures in a soil body, usually caused by water, contributes to the total stress level. According to Terzaghi's principle, total stresses σ can be divided into

effective stresses σ' and pore pressures σ_w. However, water is supposed not to sustain any shear stress, and therefore the effective shear stresses are equal to the total shear stresses:

$$\sigma_{xx} = \sigma'_{xx} + \sigma_w \quad 3.1a$$

$$\sigma_{yy} = \sigma'_{yy} + \sigma_w \quad 3.1b$$

$$\sigma_{zz} = \sigma'_{zz} + \sigma_w \quad 3.1c$$

$$\sigma_{xy} = \sigma'_{xy} \quad 3.1d$$

$$\sigma_{yz} = \sigma'_{yz} \quad 3.1e$$

$$\sigma_{zx} = \sigma'_{zx} \quad 3.1f$$

This is to be noted that, similar to the total and the effective stress components, σ_w is considered negative for pressure. A further distinction is made between steady state pore stress, p_{steady}, and excess pore stress, p_{excess} as follows:

$$\sigma_w = p_{steady} + p_{excess} \quad 3.2$$

Steady state pore pressures are considered to be input data, i.e. generated on the basis of phreatic levels or groundwater flow. Excess pore pressures are generated during plastic calculations for the case of undrained material behaviour. Since the time derivative of the steady state component equals zero, it follows:

$$\dot{\sigma}_w = \dot{p}_{excess} \quad 3.3$$

Hooke's law can be inverted to obtain:

$$\begin{bmatrix} \dot{\varepsilon}^e_{xx} \\ \dot{\varepsilon}^e_{yy} \\ \dot{\varepsilon}^e_{zz} \\ \dot{\gamma}^e_{xy} \\ \dot{\gamma}^e_{yz} \\ \dot{\gamma}^e_{zx} \end{bmatrix} = \frac{1}{E'} \begin{bmatrix} 1 & -v' & -v' & 0 & 0 & 0 \\ -v' & 1 & -v' & 0 & 0 & 0 \\ -v' & -v' & 1 & 0 & 0 & 0 \\ 0 & 0 & 0 & 2+2v' & 0 & 0 \\ 0 & 0 & 0 & 0 & 2+2v' & 0 \\ 0 & 0 & 0 & 0 & 0 & 2+2v' \end{bmatrix} \begin{bmatrix} \dot{\sigma}'_{xx} \\ \dot{\sigma}'_{yy} \\ \dot{\sigma}'_{zz} \\ \dot{\sigma}_{xy} \\ \dot{\sigma}_{yz} \\ \dot{\sigma}_{zx} \end{bmatrix} \quad 3.4$$

Substituting Eq. (3.1) gives:

$$\begin{bmatrix} \dot{\varepsilon}^e_{xx} \\ \dot{\varepsilon}^e_{yy} \\ \dot{\varepsilon}^e_{zz} \\ \dot{\gamma}^e_{xy} \\ \dot{\gamma}^e_{yz} \\ \dot{\gamma}^e_{zx} \end{bmatrix} = \frac{1}{E'} \begin{bmatrix} 1 & -v' & -v' & 0 & 0 & 0 \\ -v' & 1 & -v' & 0 & 0 & 0 \\ -v' & -v' & 1 & 0 & 0 & 0 \\ 0 & 0 & 0 & 2+2v' & 0 & 0 \\ 0 & 0 & 0 & 0 & 2+2v' & 0 \\ 0 & 0 & 0 & 0 & 0 & 2+2v' \end{bmatrix} \begin{bmatrix} \dot{\sigma}_{xx} - \dot{\sigma}_w \\ \dot{\sigma}_{yy} - \dot{\sigma}_w \\ \dot{\sigma}_{zz} - \dot{\sigma}_w \\ \dot{\sigma}_{xy} \\ \dot{\sigma}_{yz} \\ \dot{\sigma}_{zx} \end{bmatrix} \quad 3.5$$

$$\dot{\sigma}_w = \frac{K_w}{n}\left(\dot{\varepsilon}^e_{xx} + \dot{\varepsilon}^e_{yy} + \dot{\varepsilon}^e_{zz}\right) \quad 3.6$$

Considering slightly compressible water the inverted form of Hooke's law may be written in terms of the total stress rates and the undrained parameters E_u and υ_u:

$$\begin{bmatrix} \dot{\varepsilon}^e_{xx} \\ \dot{\varepsilon}^e_{yy} \\ \dot{\varepsilon}^e_{zz} \\ \dot{\gamma}^e_{xy} \\ \dot{\gamma}^e_{yz} \\ \dot{\gamma}^e_{zx} \end{bmatrix} = \frac{1}{E_u} \begin{bmatrix} 1 & -v_u & -v_u & 0 & 0 & 0 \\ -v_u & 1 & -v_u & 0 & 0 & 0 \\ -v_u & -v_u & 1 & 0 & 0 & 0 \\ 0 & 0 & 0 & 2+2v_u & 0 & 0 \\ 0 & 0 & 0 & 0 & 2+2v_u & 0 \\ 0 & 0 & 0 & 0 & 0 & 2+2v_u \end{bmatrix} \begin{bmatrix} \dot{\sigma}'_{xx} \\ \dot{\sigma}'_{yy} \\ \dot{\sigma}'_{zz} \\ \dot{\sigma}_{xy} \\ \dot{\sigma}_{yz} \\ \dot{\sigma}_{zx} \end{bmatrix} \quad 3.7$$

In order to avoid numerical problems caused by an extremely low compressibility of water, ν_u is by default taken as 0.495, which makes the undrained soil body slightly compressible. In order to ensure realistic computational results, the bulk modulus of the water must be high compared with the bulk modulus of the soil skeleton, i.e. $K_w >> n\,K'$. This condition is sufficiently ensured by requiring $\nu' \leq 0.35$.

When the *Material type* (type of material behaviour) is set to *Undrained*, PLAXIS automatically assumes an implicit undrained bulk modulus, K_u, for the soil as a whole (soil skeleton + water) and distinguishes between total stresses, effective stresses and excess pore pressures:

Total stress, $\Delta p = K_u \Delta\varepsilon_v$

Effective stress, $\Delta p' = (1- B)\Delta p = K'\Delta\varepsilon_v$

Excess pore pressure, $\Delta p_w = B\Delta p = \frac{k_w}{n}\Delta\varepsilon_v$

This is to be noted that effective stress model parameters should be entered in the material data set, i.e. E', ν', c', φ' and not E_u, ν_u, c_u (s_u), φ_u. The undrained bulk modulus is automatically calculated by PLAXIS using Hooke's law of elasticity:

$$K_u = \frac{2G(1+v_u)}{3(1-2v_u)} \text{ where } G = \frac{E}{2(1+v')}$$

and $v_u = 0.495$ (when using the Standard setting)

or $v_u = \frac{3v' + B(1-2v')}{3 - B(1-2v')}$ (when using the Manual setting).

A particular value of the undrained Poisson's ratio, ν_u, implies a corresponding reference bulk stiffness of the pore fluid, $K_{w,ref}/n$:

$$\frac{K_{w,ref}}{n} = K_u - K' \text{where } K' = \frac{E'}{3(1-2v')}$$

$K_{w,ref}/n$ is generally much smaller than the real bulk stiffness of pure water, K_w^0 (2.106 kN/m^2).

If the value of Skempton's *B*-parameter is unknown, but the degree of saturation, *S*, and the porosity, *n*, are known instead, the bulk stiffness of the pore fluid can be estimated from:

$$\frac{K_w}{n} = \frac{K_w^0 K_{air}}{SK_{air} + (1-S)K_w^0} \frac{1}{n} \qquad 3.8a$$

where K_{air} = 200 kN/m^2 for air under atmospheric pressure. Skempton's *B*-parameter can now be calculated from the ratio of the bulk stiffnesses of the soil skeleton and the pore fluid:

$$B = \frac{1}{1+\frac{nK'}{K_w}} \qquad 3.8b$$

The rate of excess pore pressure is calculated from the (small) volumetric strain rate, according to:

$$\dot{\sigma}_w = \frac{K_w}{n} \dot{\varepsilon}_v \qquad 3.8c$$

For soft soil projects, accurate data on effective parameters may not always be available. Instead, in situ tests and laboratory tests may have been performed to obtain undrained soil parameters. In such situations measured E_u obtained from laboratory test can be easily converted into E' by: $E' = \frac{2(1+\nu')}{3} E_u$. Undrained shear strengths, however, cannot easily be used to determine the effective strength parameters φ and c. For such projects PLAXIS offers the possibility of an undrained analysis with direct input of the undrained shear strength (c_u or s_u) and $\varphi = \varphi_u = 0°$. This option is only available for the Mohr-Coulomb Model and the Hardening-Soil model. This is to be noted that whenever the *Material type* parameter is set to Undrained, effective values must be entered for the elastic parameters *E* and ν.

3.4 Material Model Used in PLAXIS

In order to describe the deformations of a soil occurring from changes in the current stress state, a mathematical framework is assigned to the soil. These govern the force displacement relationships and are called material models to simulate the behaviour of soil and other continua. Soil is a non-linear, multi-phase, stress-dependent and time-dependent material. Hence, the material model, i.e. the constitutive relation between stress and strain, is very complex. In PLAXIS, there are eight different material models available for soil and rock behaviour. However, only the Hardening Soil (HS) model,

Soft Soil Creep(SSC) model and Soft Soil(SS) Model have been used for analyses in this research work. The HS model is used for treated or untreated sand. The SS model and SSC models were chosen for the soft clay soils.

3.4.1 Mohr-Coulomb Model

The Mohr-Coulomb model (MC-model) is an elastic perfectly-plastic model. This model represents a 'first-order' approximation of soil or rock behaviour. The general behaviour of an elastic perfectly plastic material is illustrated in Figure 3.3. The model requires five input parameters; E and v for the elasticity, φ and c for plasticity and ψ for the dilatancy. The model is isotropic and does not account for soils stress-dependency, i.e. soils tendency to stiffen with increased pressure. Besides the five model parameters, initial horizontal soil stresses have to be generated by selecting proper K_0-values.

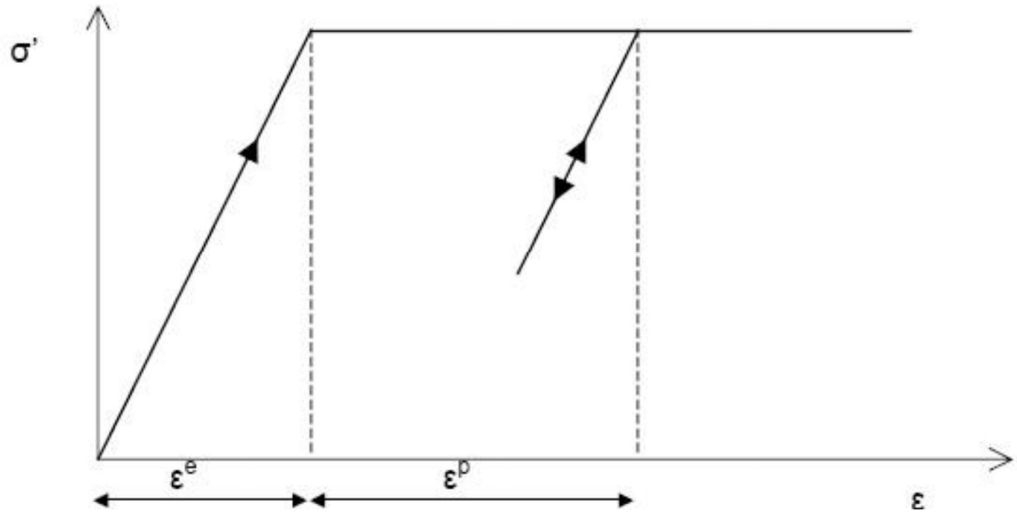

Figure 3.3. Basic idea of an elastic perfectly plastic model.

Plasticity and Yield Functions

When modelling plasticity, PLAXIS introduces functions called yield functions, which are equal to zero when the material behaves plastic. The Mohr-Coulomb yield condition, an extension of the Coulomb friction law, consists of six yield functions, all expressed with principal stresses, the friction angle and the cohesion. When the six functions are set to zero (i.e. acting plastic) they create a surface in the principal stress space called the yield surface, illustrated in Figure 3.4. When the material is exposed to stress states within this surface it acts elastic and Hooke's law obeys.

Perfectly plastic means that the constitutive relation is independent of the plastic strain and fully defined by the model's input parameters. This leads to a fixed yield surface. In

contrast, more advanced models that are plastic or not perfectly-plastic, have a yield surface that expands due to plastic strain.

Input Parameters

When v is unknown, PLAXIS recommends using values in the range 0.3 to 0.4 and 0.15 to 0.25 for loading and reloading, respectively. The cohesive strength has the dimension of stress. When modelling sand without cohesive strength ($c = 0$) PLAXIS will not perform well numerically. To avoid complications the cohesion should therefore be prescribed to a small value, in the order of magnitude $c \approx 0.2kPa$. The computing time increases exponentially with increasing friction angle. Hence, one may avoid prescribing high values for the friction angle.

The dilatancy angle, ψ is specified in degrees. Apart from heavily overconsolidated layers, clay soils tend to show little dilatancy ($\psi \approx 0$). The dilatancy of sand depends on both the density and on the friction angle. The dilatancy angle for sand with high friction angle is roughly $\psi = \varphi - 30^o$. For sand with less friction angle than 30^o the dilatancy is close to zero. A small negative value for ψ is only realistic for extremely loose sands.

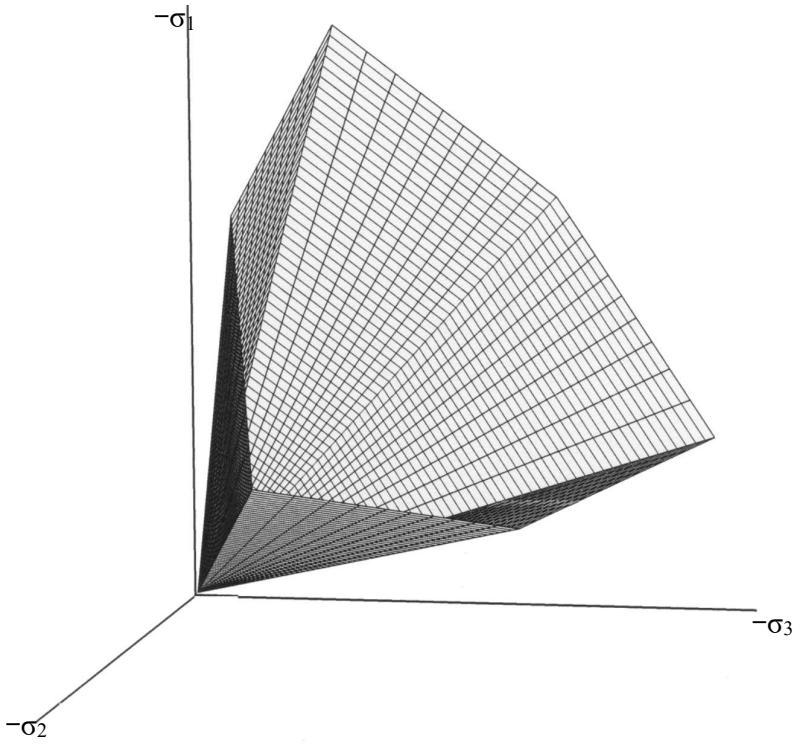

Figure 3.4 The Mohr-Coulomb yield surface in principal stress space ($c = 0$).

Advanced Input Parameters

The advanced features in this model comprise the increase of stiffness and cohesive strength with depth and the use of a tension cut-off. In real soils, the stiffness depends significantly on the stress level, which means that the stiffness generally increases with depth which titled as soil's stress-dependency and is expressing by $E_{increment}$ and y_{ref}, i.e. increase of stiffness per meter and the depth where the increase starts, respectively. This is to be noted that during calculations a stiffness increasing with depth does not change as a function of the stress state. In an analogous way the cohesion is also increased with depth. This can be accountd by using $c_{increment}$ and y_{ref}, i.e. increase of cohesion per meter and the depth where the increase starts, respectively. Tension cut-off implies prescribing soil's tensile-capacity to zero. The basic Mohr-Coulomb Model has this option as default. Tension cut-off is suitable for most soils, such as sand and gravel with no tensile strength. However, in clay it could be adequate to account for tensile strength and tension cut-off could then be deactivated.

3.4.2 Hardening Soil Model

As presented by Plaxis 2D-Version 8.0 Manual, the Hardening Soil (HS) Model proposed by Brinkgreve & Ver meer (1997 and Schanz, (1998) is an advanced true second order model for simulating the behavior of different types of soil, both soft soils and stiff soils. HS model behaving isotropic and hardening plastic and models the soil's stiffness, hardening process and plasticity more accurately than the Mohr-Coulomb Model.

The relation between deviatoric stress q and axial (vertical) strain ε_1 is in this model explained by elastoplastic type hyperbolic curves which have been derived from standard drained triaxial tests, such a relation is illustrated in Figure 3.5. The failure line in the figure is derived from the Mohr-Coulomb failure criterion.

In contrast to the elastic perfectly-plastic model, the HS Model has a yield surface that expands due to plastic strain, thereby describing the plasticity more realistic. Plastic volumetric strain has been observed in soil exposed to isotropic compression. The yield surface described until now does not account for this phenomenon. PLAXIS has introduced a second surface, illustrated in Figure 3.6, closing the elastic region which governs this behaviour. This cap is dependent on the friction angle, the odometer module and the preconsolidation.

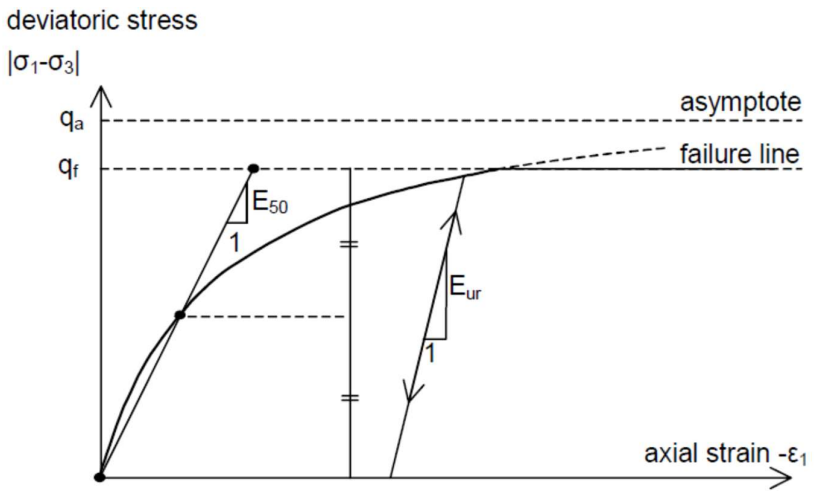

Figure 3.5 Hyperbolic deviatoric stress and axial strain relationship in primary loading for a standard drained triaxial test (Brinkgreve, Broere et al. 2002).

MC-Model explains limiting state of stress in terms of friction angle and the HS Model describes an elastoplastic kind of hyperbolic model. This type of hyperbolic stress-strain relationship was developed for use in nonlinear incremental analyses of deformation in all soils but it does not account for viscous effects. In HS Model the material stiffness matrix is formed and decomposed in each calculation step. When subjected to primary deviatoric loading, soil shows a decreasing stiffness and simultaneously irreversible plastic strains develop.

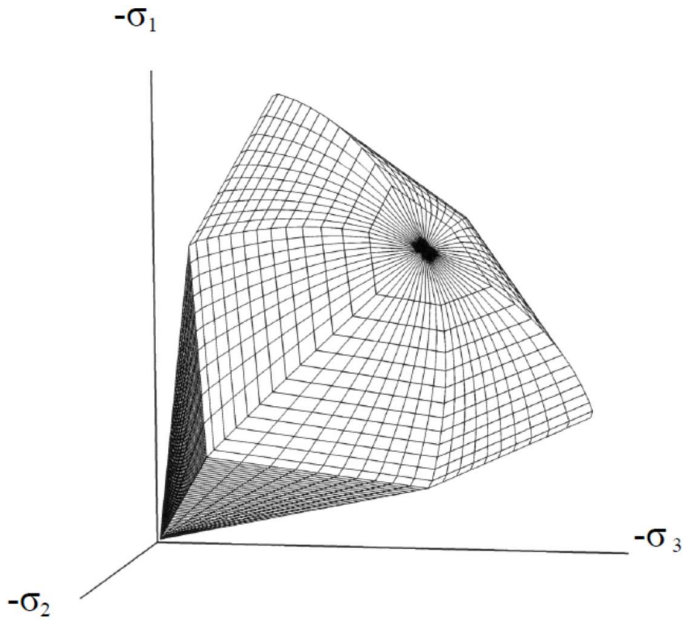

Figure 3.6 Total yield contour or the cap yield surface of Hardening Soil model in principal stress space for cohesionless soil.

The model involves friction hardening to model the plastic shear strain in deviatoric loading, and cap hardening to model the plastic volumetric strain in primary compression. Distinction can be made between two main types of hardening, namely shear hardening and compression hardening. Shear hardening is used to model irreversible strains due to primary deviatoric loading. Compression hardening is used to model irreversible plastic strains due to primary compression in oedometer loading and isotropic loading. Yield contour of the model in three-dimensional space is shown in Fig 3.6. Failure is defined by means of Mohr-Coulomb failure criterion.

With respect to its stiffness behaviour HS Model involves a power law formulation for stress-dependant stiffness, similar as the one used in the Duncan-Chang model. Since this model is based on hardening plasticity rather than non-linear elasticity, it overcomes the limitations and inconsistencies of the Duncan-Chang model with respect to dilatancy and neutral loading. Besides that, this model also by includes soil dilatancy and yield cap.

The HS model describes soils stiffness with three Young moduli, E_{50}^{ref} = triaxial primary loading stiffness or secant stiffness in standard drained triaxial test, E_{oed}^{ref}= oedometer primary loading stiffness or tangent stiffness for primary oedometer loading and E_{ur}^{ref}= triaxial unloading/reloading stiffness. As average values for various soil types, we have $E_{ur} \approx 3\ E_{50}$ and $E_{oed} \approx E_{50}$, but both very soft and very stiff soils tend to give other ratios of $E_{oed}\ /E_{50}$. Strength Parameters are c'_{ref} = effective cohesion, φ'_{ref} = effective angle of internal friction and ψ = angle of dilatancy.

Pre-Consolidation Pressure is governed in the initial stress calculation and is specified by the over consolidation ratio, $OCR = \frac{\sigma_p^{'}}{\sigma_{vertical}^{'}}$ or the preoverburden pressure, $POP = \left|\sigma_p^{'} - \sigma_{vertical}^{'}\right|$ where, $\sigma_p^{'}$ is the pre-consolidation pressure, and $\sigma_{vertical}^{'}$ is the in-situ effective vertical stress.

Hardening Soil Model is built in formulation that makes the stiffness dependent on the effective stress level. Several stiffness parameters are introduced, controlling loading in shear (deviatoric loading), volumetric loading and unloading. Soil is highly stress-dependent. The stress dependency for all stiffness moduli can be expressed by the equation below for deviatoric loading.

$$E_{50} = E_{50}^{ref}\left(\frac{\sigma_3 + a}{P^{ref} + a}\right)^m \text{ or, } E_{50} = E_{50}^{ref}\left(\frac{c\cos\varphi - \sigma_3'\sin\varphi}{c\csc\varphi + P^{ref}\sin\varphi}\right)^m \qquad 3.9$$

where, $p^{ref} = p_a = 100$ kPa is the atmospheric pressure and $a = \frac{c}{tan\phi}$ is the attraction.

Other stiffness moduli parameters can be determined by the following equations:

$$E_{ur} = E_{ur}^{ref}\left(\frac{c\cos\varphi - \sigma_3'\sin\varphi}{c\csc\varphi + P^{ref}\sin\varphi}\right)^m \quad (3.10)$$

and, $$E_{oed} = E_{oed}^{ref}\left(\frac{c\cos\varphi - \sigma_3'\sin\varphi}{c\csc\varphi + P^{ref}\sin\varphi}\right)^m \quad (3.11)$$

where m defines the stress dependency.

In order to simulate a logarithmic compression the power should be taken equal to 1.0. This is ruled with a parameter m coupled to power law, which span from 0.5 to 1(Brinkgreve et al., 2002). Values of 1 for soft clays, and 0.5 for Norwegian sand and silt. The hyperbolic relationship between the vertical strain ε_1 and the deviatoric stress q in primary loading for a triaxial loading

$$\varepsilon_1 = \frac{1}{E_i}\frac{q}{1-\frac{q}{q_a}} \quad \left(q < q_f\right) \quad (3.12)$$

where q_a is the asymptotic value of shear strength which is the ratio of ultimate deviatoric stress and failure ratio R_f and E_i is the initial stiffness. The value of E_i can be calculated by

$$E_i = \frac{2E_{50}}{2 - R_f} \quad (3.13)$$

The ultimate deviatoric stress, $q_f = (c\cot\varphi - \sigma_3')\frac{2\sin\varphi}{1-\sin\varphi}$ and $q_a = \frac{q_f}{R_f}$ where failure ratio $R_f = 1$. In PLAXIS, the suitable default value of R_f is equal to 0.9.

HS model has some advanced parameters that have default values in PLAXIS 2D like, Poisson's ratio for unloading-reloading υ_{ur} ($\upsilon_{ur} = 0.2$), reference stress for stiffness $p_{ref}\left(p_{ref} = 100kPa\right)$ and the K_0 value for a normally consolidated soil is often assumed to be related to the friction angle by Jaky's empirical expression, $K_0 = 1 - \sin\varphi$.

3.4.3 Soft-Soil Creep Model

As presented by Plaxis 2D-Version 8.0 Manual, Buisman (1936) was probably the first to propose a creep law for clay after observing that soft-soil settlements could not be fully explained by classical consolidation theory. This work on 1D-secondary compression was continued by other researchers. More mathematical lines of research on creep were

followed by few researchers. This mathematical 3D-creep modelling was influenced by the more experimental line of 1D-creep modelling, but conflicts exist.

The earlier mentioned Hardening soil model does not account for creep, i.e. secondary time-dependent settlements. This is a phenomenon highly influencing the settlements in soft-soil, i.e. normally consolidated clay, clayed silt and peat, when subjected to high primary compression. Soft-soil creep model is focused on this phenomenon and is therefore suitable for long-time settlement calculation in soft-soil.

The special features of these soft soils materials is their high degree of compressibility. This is best demonstrated by oedometer test data as reported for instance by Janbu in his Rankine lecture (1985). Considering tangent stiffness moduli at a reference oedometer pressure of 100 kPa, he reported for *NC* clays, E_{oed} = 1 to 4 MPa and stiffnesses for non-cemented *NC*-sands are in the range of 10 to 50 MPa.

Besides the extreme compressibility another feature of the soft soils is the linear stress-dependency of soil stiffness. According to the Hardening-Soil model we have:

$E_{oed} = E_{oed}^{ref}(\sigma/p^{ref})^m$

at least for c = 0 and on using an exponent, m =1 equal to one, the above stiffness law reduces to: $E_{oed} = \sigma/\lambda^*$ where, $\lambda^* = p^{ref}/E_{oed}^{ref}$.

Then Hardening-Soil model yields $\dot{\varepsilon} = \lambda^* \dot{\sigma}/\sigma$ which can be integrated to obtain the well-known logarithmic compression law $\varepsilon = \lambda^* \ln\sigma$ for primary oedometer loading.

For many practical soft-soil studies, the modified compression index λ^* will be known and the PLAXIS user can compute the oedometer modulus from the relationship:

$E_{oed}^{ref} = p^{ref}/\lambda^*$.

The secondary compression (for instance during a period of 10 or 30 years) to be a percentage of the primary compression. Large primary settlements are usually followed by substantial creep settlements in later years and it is desirable to estimate the creep from FEM-computations. Dams or buildings may also be founded on initially overconsolidated soil layers that yield relatively small primary settlements. Then, as a consequence of the loading, a state of normal consolidation may be reached and significant creep may follow. This is a treacherous situation as considerable secondary compression is not preceded by the warning sign of large primary compression. Again, computations with a creep model are desirable.

Some basic characteristics of the Soft-Soil-Creep model are:

- Stress-dependent stiffness (logarithmic compression behaviour)
- Distinction between primary loading and unloading-reloading
- Secondary (time-dependent) compression
- Memory of pre-consolidation stress
- Failure behaviour according to the Mohr-Coulomb criterion

3.4.3.1 Basics of One-Dimensional Creep

When reviewing previous literature on secondary compression in oedometer tests, one is struck by the fact that it concentrates on behaviour related to step loading, even though natural loading processes tend to be continuous or transient in nature. Considering such a classical creep test proposed the following equation to describe creep behaviour under constant effective stress:

$$\varepsilon = \varepsilon_c - C_B \log\left(\frac{t}{t_c}\right) \text{ for } t > t_c \tag{3.14}$$

where ε_c is the strain up to the end of consolidation, t is the time measured from the beginning of loading, t_c is the time to the end of primary consolidation and C_B is a material constant. Unlike the soil mechanics convention, compressive stresses and strains are taken to be negative. For further consideration, it is convenient to rewrite this equation as:

$$\varepsilon = \varepsilon_c - C_B \log\left(\frac{t_c + t'}{t_c}\right) \text{ for } t' > 0 \tag{3.15}$$

with $t' = t - t_c$ being the effective creep time.

As presented by Plaxis 2D-Version 8.0 Manual, based on Bjerrum, (1967), Garlanger (1972) proposed a creep equation:

$$e = e_c - C_\alpha \log\left(\frac{\tau_c + t'}{t_c}\right) \quad \text{with } C_\alpha = C_B(1 + e_0) \quad \text{for } t' > 0 \tag{3.16}$$

The engineering strain ε is replaced by void ratio e_0 and the consolidation time t_c is replaced by a parameter τ_c. Eqs. 3.15 and 3.16 are entirely identical when choosing $\tau_c = t_c$. For the case that $\tau_c \neq t_c$ differences between both formulations will vanish when the effective creep time t' increases.

Due to the special assumption that this loading period of the standard oedometer test one day coincides to the consolidation time t_c, it follows that such tests have no effective creep time. Hence one obtains $t' = 0$ and the log-term drops out of Eq. 3.16 it would thus

seem that there is no creep in this standard oedometer test, but this suggestion is entirely false. Even highly impermeable oedometer samples need less than one hour for primary consolidation. Then all excess pore pressures are zero and one observes pure creep for the other 23 hours of the day. Therefore will not be made any assumptions about the precise values of τ_c and t_c.

As presented by Plaxis 2D-Version 8.0 Manual, another slightly different possibility to describe secondary compression is the form adopted by Butterfield (1979):

$$\varepsilon^H = \varepsilon_c^H - C \ln\left(\frac{\tau_c + t'}{\tau_c}\right) \tag{3.17}$$

where ε^H is the logarithmic strain defined as:

$$\varepsilon^H = \ln\left(\frac{V}{V_0}\right) = \ln\left(\frac{1+e}{1+e_0}\right) \tag{3.18}$$

with V_0 is the initial volume.

For small strains it is possible to show that:

$$C = \frac{C_\alpha}{(1+e_0).\ln 10} = \frac{C_B}{\ln 10} \tag{3.19}$$

because then logarithmic strain is approximately equal to the engineering strain.

3.4.3.2 Determination of τ_c

By differentiating Eq. (3.17) with respect to time and dropping the superscript '*H*' to simplify notation, one finds:

$$-\dot{\varepsilon} = \frac{C}{\tau_c + t'} \qquad \text{or inversely: } -\frac{1}{\dot{\varepsilon}} = \frac{\tau_c + t'}{C} \tag{3.20}$$

which allows one to make use of the construction developed by Janbu (1969) for evaluating the parameters *C* and τ_c from experimental data being indicated in Figure 3.7a. Janbu method of Figure 3.7b can be used to determine the parameter *C* from an oedometer test with constant load.

In the Janbu method both τ_c and *C* follow directly when fitting a straight line through the data. In Figure 3.7b, τ_c is the intercept with the (non-logarithmic) time axis of the straight creep line. The deviation from a linear relation for $t < t_c$ is due to consolidation.

Considering the classical literature at the end-of-consolidation strain:

$$\varepsilon_c = \varepsilon_c^e + \varepsilon_c^c = -A \ln\frac{\sigma'}{\sigma_0'} - B \ln\frac{\sigma_{Pc}}{\sigma_{P0}} \tag{3.21}$$

This is to be noted that ε is a logarithmic strain, rather than a classical small strain although we conveniently omit the subscript '*H*'. In the above equation σ_0' represents the

initial effective pressure before loading and σ' is the final effective loading pressure. The values σ_{p0} and σ_{pc} representing the pre-consolidation pressure corresponding to before-loading and end-of-consolidation states respectively. In most literature on oedometer testing, one adopts the void ratio e_0 instead of ε, and log instead of ln, and the swelling index C_r instead of A, and the compression index C_c instead of B. The constants A and B relate to C_r and C_c as:

$$A = \frac{C_r}{(1+e_0).\ln 10} \qquad \text{and} \qquad A = \frac{(C_c - C_r)}{(1+e_0).\ln 10} \tag{3.22}$$

Combining Eqs. 3.20 and 3.21 it follows that:

$$\varepsilon = \varepsilon^e + \varepsilon^c = -A \ln\left(\frac{\sigma'}{\sigma'_0}\right) - B \ln\frac{\sigma_{Pc}}{\sigma_{P0}} - C \ln\left(\frac{\tau_c + t'}{\tau_c}\right) \tag{3.23}$$

where ε is the total logarithmic strain due to an increase in effective stress from σ'_0 to σ' and a time period of t_c+t'.

In Figure 3.8 the terms of Eq. (3.23) are depicted in a ε-lnσ diagram.

3.4.3.3 Differential Law for 1D-Creep

The previous equations emphasize the relation between accumulated creep and time, for a given constant effective stress. For solving transient or continuous loading problems, it is necessary to formulate a constitutive law in differential form. In a first step we will derive an equation for τ_c. Indeed, despite the use of logarithmic strain and ln instead of log, equation (3.23) is classical without adding new knowledge. In fact, we have not been able to find precise information on τ_c in the literature, apart from Janbu's method of experimental determination.

In order to find an analytical expression for the quantity τ_c, we adopt the basic idea that all inelastic strains are time dependent. Hence total strain is the sum of an elastic part ε_e and a time-dependent creep part ε_c. For non-failure situations as met in oedometer loading conditions, we do not assume an instantaneous plastic strain component, as used in traditional elastoplastic modelling. In addition to this basic concept, we adopt Bjerrum's idea that the pre-consolidation stress depends entirely on the amount of creep strain being accumulated in the course of time. In addition to Eq. (3.23) we therefore introduce the expression:

$$\varepsilon = \varepsilon^e + \varepsilon^c = -A \ln\left(\frac{\sigma'}{\sigma'_0}\right) - B \ln\left(\frac{\sigma_P}{\sigma_{P0}}\right)$$

$$\text{and } \sigma_P = \sigma_{P0} \exp\left(\frac{-\varepsilon^c}{B}\right) \tag{3.24}$$

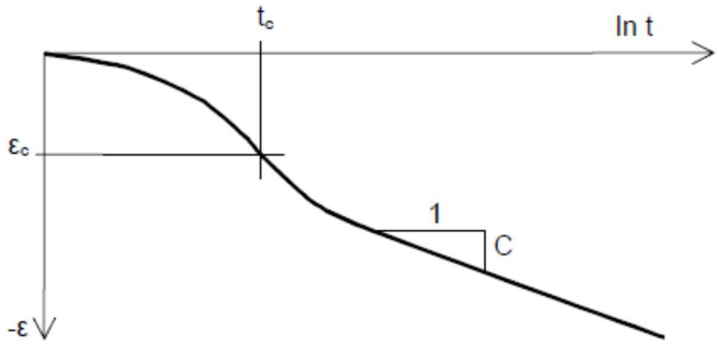

(a)

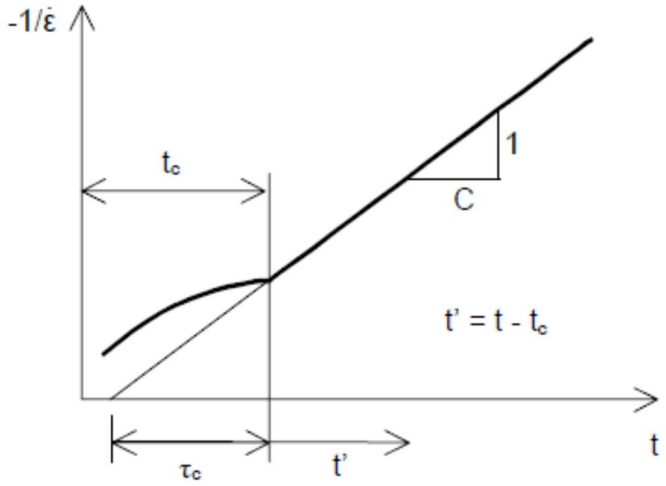

(b)

Figure 3.7 Consolidation and creep behaviour in standard oedometer test

This is to be noted that ε_c is negative, so that σ_p exceeds σ_{p0}. The longer a soil sample is left to creep the larger σ_p grows. The time-dependency of the pre-consolidation pressure σ_p is now found by combining Eqs. 3.23 and 3.24 to obtain:

$$\varepsilon^e - \varepsilon^c = -B \ln \frac{\sigma_p}{\sigma_{Pc}} = -C \ln \left(\frac{\tau_c + t'}{\tau_c} \right) \tag{3.25}$$

In conventional oedometer testing the load is stepwise increased and each load step is maintained for a constant period of $t_c + t' = \tau$, where τ is precisely one day. In this way of stepwise loading the so-called *NC*-line with $\sigma_p = \sigma'$ is obtained. On entering $\sigma_p = \sigma'$ and $t' = \tau - t_c$ into Eq. (3.25) it is found that:

$$B \ln \frac{\sigma'}{\sigma_{Pc}} = C \ln \left(\frac{\tau_c + t' - t_c}{\tau_c} \right) \text{ for: } \quad OCR = 1 \tag{3.26}$$

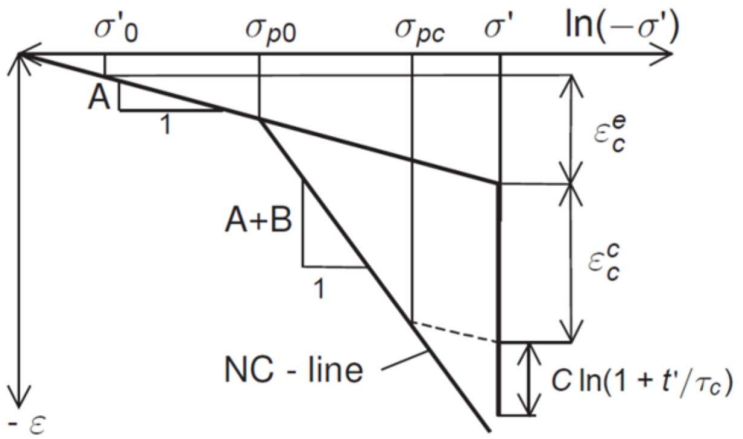

Figure 3.8 Idealised stress-strain curve from oedometer test with division of strain increments into an elastic and a creep component. For $t' + t_c = 1$ day, one arrives precisely on the NC-line (Vermeer & Neher, 1999).

It had been assumed that ($\tau_c - t_c$) << τ. This quantity can thus be disregarded with respect to τ and it follows that:

$$\frac{\tau}{\tau_c} = \left(\frac{\sigma'}{\sigma_{Pc}}\right)^{\frac{B}{C}} \quad \text{or,} \quad \tau_c = \tau \left(\frac{\sigma_{Pc}}{\sigma'}\right)^{\frac{B}{C}} \tag{3.27}$$

Hence τ_c depends both on the effective stress σ' and the end-of-consolidation pre-consolidation stress σ_{pc}. In order to verify the assumption ($\tau_c - t_c$) << τ, it should be realised that usual oedometer samples consolidate for relatively short periods of less than one hour. Considering load steps on the normal consolidation line, we have *OCR*=1 both in the beginning and at the end of the load step. During such a load step σ_p increases from σ_{p0} up to σ_{pc} during the short period of primary consolidation. Hereafter σ_p increases further from σ_{pc} up to σ' during a relatively long creep period. Hence, at the end of the day the sample is again in a state of normal consolidation, but directly after the short consolidation period the sample is under-consolidated with $\sigma_p < \sigma'$. For the usually very high ratios of $B/C \geq 15$, we thus find very small τ_c-values from Eq. (3.27). Hence not only t_c but also τ_c tend to be small with respect to τ. It thus follows that the assumption ($\tau_c - t_c$) << τ is certainly correct. Eq. (3.23) is differentiated to obtain:

$$\dot{\varepsilon} = \dot{\varepsilon}^e + \dot{\varepsilon}^c = -A\frac{\dot{\sigma}'}{\sigma'} - \frac{C}{\tau_c + t'} \tag{3.28}$$

where $\tau_c + t'$ can be eliminated by means of Eq. (3.25) to obtain:

$$\dot{\varepsilon} = \dot{\varepsilon}^e + \dot{\varepsilon}^c = -A\frac{\dot{\sigma}'}{\sigma'} - \frac{C}{\tau_c}\left(\frac{\sigma_{Pc}}{\sigma_P}\right)^{\frac{B}{C}} \qquad \text{with } \sigma_p = \sigma_{p0}\, exp\left(\frac{-\varepsilon^c}{B}\right) \tag{3.29}$$

Again it is recalled that ε_c is a compressive strain, (consider negative) using Eq. (3.29) can be obtained:

$$\dot{\varepsilon} = \dot{\varepsilon}^e + \dot{\varepsilon}^c = -A\frac{\dot{\sigma}'}{\sigma'} - \frac{C}{\tau}\left(\frac{\sigma'}{\sigma_P}\right)^{\frac{B}{C}} \tag{3.30}$$

3.4.3.4 Three-Dimensional-Model

On extending the 1D-model to general states of stress and strain, the well-known stress invariants for pressure p and deviatoric stress q are adopted. These invariants are used to define a new stress measure named p_{eq}:

$$P^{eq} = P' + \frac{q^2}{M^2 P'} \tag{3.31}$$

p_{eq} is constant on ellipses in p-q-plane (Figure 3.10). In fact we have the ellipses from the Modified Cam-Clay-Model as introduced by Roscoe and Burland (1968).

The soil parameter M represents the slope of the so-called 'critical state line' (Figure 3.8). We use the general 3D-definition 3.7b for the deviatoric stress q and:

$$M = \frac{6\ sin\varphi_{cv}}{3 - sin\varphi_{cv}} \tag{3.32}$$

where ϕ_{cv} is the critical-void friction angle, also referred to as critical-state friction angle. On using Eq. (3.7b) for q, the equivalent pressure p^{eq} is constant along ellipsoids in principal stress space. To extend the 1D-theory to a general 3D-theory, attention is now focused on normally consolidated states of stress and strain as met in oedometer testing. In such situations it yields and it follows from Eq. (3.31) that:

$$P^{eq} = \sigma'\left[\frac{1 + 2\ K_0^{NC}}{3} + \frac{3(1 - K_0^{NC})^2}{M^2(1 + 2\ K_0^{NC})}\right]$$

$$P_p^{eq} = \sigma_p\left[\frac{1+2\ K_0^{NC}}{3} + \frac{3\left(1- K_0^{NC}\right)^2}{M^2\left(1+2\ K_0^{NC}\right)}\right] \tag{3.33}$$

where $\sigma' = K_0^{NC}, \sigma_1'$ and P_p^{eq} is a generalised pre-consolidation pressure, being simply proportional to the one-dimensional one. For known values of K_0^{NC}, P^{eq} can thus be computed from σ', and $p_p{}^{eq}$ can thus be computed from σ_p. Omitting the elastic strain in the 1D-equation (3.33), introducing the above expressions for p^{eq} and $p_p{}^{eq}$ and writing ε_v instead of ε it is found that:

$$-\varepsilon_v^c = \frac{C}{\tau}\left(\frac{P^{eq}}{P_p^{eq}}\right)^{\frac{B}{C}} \text{ where: } P_p^{eq} = P_{p0}^{eq}\ exp\left(\frac{-\varepsilon^c}{B}\right) \tag{3.34}$$

For one-dimensional oedometer conditions, this equation reduces to Eq. (3.34), so that one has a true extension of the 1D-creep model. It should be noted that the subscript '0' is once again used in the equations to denote initial conditions and that $\varepsilon_v^c = 0$ for time $t = 0$. Instead of the parameters A, B and C of the 1D-model, we will now change to the material parameters κ^*, λ^* and μ^*, who fit into the framework of critical-state soil mechanics. Conversion between constants follows the rules:

$$k^* = \frac{3(1-v_{ur})}{(1+v_{ur})}A \quad , \qquad \mathrm{B} = \lambda^* - \kappa^* \quad , \quad \mu^* = \mathrm{C} \tag{3.35}$$

On using these new parameters, Eq. (3.21) changes to become:

$$-\dot{\varepsilon}_v^c = \frac{\mu^*}{\tau}\left(\frac{P^{eq}}{P_p^{eq}}\right)^{\frac{\lambda^*-k^*}{\mu^*}} \qquad \text{with:} \quad P_p^{eq} = P_{p0}^{eq}\, exp\left(\frac{-\varepsilon_v^c}{\lambda^*-k^*}\right) \tag{3.36}$$

As yet the 3D-creep model is incomplete, as we have only considered a volumetric creep strain ε_v^c, whilst soft soils also exhibit deviatoric creep strains. For introducing general creep strains, we adopt the view that creep strain is simply a time-dependent plastic strain. It is thus logic to assume a flow rule for the rate of creep strain, as usually done in plasticity theory. For formulating such a flow rule, it is convenient to adopt the vector notation and considering principal directions:

$\underline{\sigma} = (\sigma_1 \quad \sigma_2 \quad \sigma_3)^T$ and $\underline{\varepsilon} = (\varepsilon_1 \quad \varepsilon_2 \quad \varepsilon_3)^T$

where T is used to denote a transpose. Similar to the 1D-model we have both elastic and creep strains in the 3D-model. Using Hooke's law for the elastic part, and a flow rule for the creep part, one obtains:

$$\underline{\dot{\varepsilon}} = \underline{\dot{\varepsilon}}^e + \underline{\dot{\varepsilon}}^c + \underline{\dot{\varepsilon}}^c = \underline{\underline{D}}^{-1}\,\underline{\dot{\sigma}}' + \lambda\frac{\partial g^e}{\partial \underline{\sigma'}} \tag{3.37}$$

where the elasticity matrix and the plastic potential function are defined as:

$$\underline{\underline{D}}^{-1} = \frac{1}{E_{ur}}\begin{bmatrix} 1 & -v_{ur} & -v_{ur} \\ -v_{ur} & 1 & -v_{ur} \\ -v_{ur} & -v_{ur} & 1 \end{bmatrix} \text{ and } g^c = p^{eq} \tag{3.39}$$

Hence we use the equivalent pressure p^{eq} as a plastic potential function for deriving the individual creep strain-rate components. The subscripts '*ur*' are introduced to emphasize that both the elasticity modulus and Poisson's ratio will determine unloading-reloading behaviour.

Now it follows from the above equations that:

$$\dot{\varepsilon}_v^c = \dot{\varepsilon}_1^c + \dot{\varepsilon}_2^c + \dot{\varepsilon}_3^c = \lambda = \frac{\partial p^{eq}}{\partial \sigma_1'} + \frac{\partial p^{eq}}{\partial \sigma_2'} + \frac{\partial p^{eq}}{\partial \sigma_3'} = \lambda = \frac{\partial p^{eq}}{\partial p'} = \lambda = \alpha \tag{3.40}$$

Hence we define $\alpha = \partial p^{eq}/\partial p'$. Together with Eqs. 3.23 and 3.24 this leads to:

$$\underline{\dot{\varepsilon}} = \underline{\underline{D}}^{-1}\,\underline{\dot{\sigma}}' + \frac{\dot{\varepsilon}_v^c}{\alpha}\frac{\partial p^{eq}}{\partial \underline{\sigma'}} = \underline{\underline{D}}^{-1}\,\underline{\dot{\sigma}}' + \frac{1}{\alpha}\frac{\mu^*}{\tau}\left(\frac{p^{eq}}{p_p^{eq}}\right)^{\frac{\lambda^*-\kappa^*}{\mu^*}}\frac{\partial p^{eq}}{\partial \underline{\sigma'}} \tag{3.41}$$

where:

$$p_p^{eq} = p_{p0}^{eq}\exp\left(\frac{-\varepsilon_v^c}{\lambda^*-\kappa^*}\right) \quad \text{or inversely: } -\varepsilon_v^c = \lambda^* - \kappa^* \ln\left(\frac{p_p^{eq}}{p_{p0}^{eq}}\right) \tag{3.42}$$

3.4.3.5 Formulation of Elastic 3D-Strains

The elastic strains as well, the elastic modulus E_{ur} has to been defined as a stress-dependent tangent stiffness according to:

$$E_{ur} = 3(1-2v_{ur})K_{ur} = 3(1-2v_{ur})\frac{p'}{K^*} \tag{3.43}$$

E_{ur} is simply a variable quantity that relates to the input parameter κ^*. υ_{ur} is an additional true material constant. Hence similar to E_{ur}, the bulk modulus K_{ur} is stress dependent according to the rule $K_{ur} = p'/\kappa^*$. Now it can be derived for the volumetric elastic strain that:

$$\dot{\varepsilon}_v^e = \frac{\dot{p}'}{K_{ur}} = k^*\frac{\dot{p}'}{p'} \quad \text{or by integration: } -\varepsilon_v^e = k^* \ln\left(\frac{p'}{p_0'}\right)$$

For one-dimensional compression on the normal consolidation line, we have both $-3p'(1+2K_0^{NC})\sigma'$ and $-3p_0'(1+2K_0^{NC})\sigma_0'$ it follows that $p'/p_0 = \sigma'/\sigma_0$. As a consequence we derive the simple rule $-\varepsilon_v^c = k^* \ln\left(\frac{\sigma'}{\sigma_0'}\right)$,

whereas the $1D-$model involves $-\varepsilon_v^c = A \ln\left(\frac{\sigma'}{\sigma_0'}\right)$.

It would thus seem that κ^* coincides with A. Unfortunately this line of thinking cannot be extended towards overconsolidated states of stress and strain. For such situations, it can be derived that:

$$\frac{\dot{P}'}{P'} = \frac{1+\upsilon_{ur}}{1-\upsilon_{ur}}\;\frac{1}{1+2K_0}\;\frac{\dot{\sigma}'}{\sigma'} \tag{3.44}$$

and it follows that:

$$-\dot{\varepsilon}_v^e = k^*\frac{\dot{P}'}{P'} = \frac{1+\upsilon_{ur}}{1-\upsilon_{ur}}\;\frac{k^*}{1+2K_0}\;\frac{\dot{\sigma}'}{\sigma'} \tag{3.45}$$

where K_0 depends to a great extent on the degree of overconsolidation. For many situations, it is reasonable to assume $K_0 \approx 1$ and together with $v_{ur} \approx 0.2$ one obtains $-2\varepsilon_v^c \approx k^*\, ln\left(\frac{\sigma'}{\sigma_0'}\right)$. Good agreement with the 1D-model is thus found by taking $\kappa^* \approx 2A$.

3.4.3.6 Review of Model Parameters

As soon as the failure yield criterion $f(\underline{\sigma}', c, \varphi) = 0$ is met, instantaneous plastic strain rates develop according to the flow rule $\underline{\dot{\varepsilon}}^p = \lambda\, \partial g/\partial \underline{\sigma}'$ with $g = g(\sigma', \psi)$. This gives as additional soil parameters the effective cohesion, c, the Mohr-Coulomb friction angle, φ, and the dilatancy angle ψ. For fine grained, cohesive soils, the dilatancy angle tends to be small, it may often be assumed that ψ is equal to zero. In conclusion, the Soft-Soil-Creep model requires the following material constants:

Basic stiffness parameters:

κ^*	: Modified swelling index	[-]
λ^*	: Modified compression index	[-]
μ^*	: Modified creep index	[-]

Advanced parameters (it is advised to use the default setting):

ν_{ur}	: Poisson's ratio for unloading-reloading (default 0.15)	[-]
K_0^{NC}	: $\sigma'_{xx}/\sigma'_{yy}$ stress ratio in a state of normal consolidation	[-]
M	: K_0^{NC}-related parameter	[-]

By default, M is calculated from Eq. (2.19), using $\varphi_{cv} = \varphi + 0.1°$, this is not an experimental finding, but just a practical default value. In addition, PLAXIS displays the approximate value of K_0^{NC} that corresponds to the default setting of M. In general, resulting default values of K_0^{NC} tend to be somewhat higher than the ones that follow from Jaky's formula $K_0^{NC} = 1 - \sin\varphi$. Alternatively, values of K_0^{NC} may be entered after which the corresponding value of M is calculated from the relation:

$$M = 3\sqrt{\frac{(1-K_0^{NC})^2}{(1+2K_0^{NC})^2} + \frac{(1-K_0^{NC})(1-2\nu_{ur})(\lambda^*/\kappa^* - 1)}{(1+2K_0^{NC})^2(1-2\nu_{ur})\,\lambda^*/\kappa^* - (1-K_0^{NC})(1+\nu_{ur})}} \qquad (3.46)$$

A particular value of M cannot be entered directly. Values for K_0^{NC} can be chosen.

Modified swelling index, modified compression index and modified creep index

These parameters can be obtained both from an isotropic compression test and an oedometer test. When plotting the logarithm of stress as a function of strain, the plot can be approximated by two straight lines (see Figure 3.2). The slope of the normal consolidation line gives the modified compression index λ^*, and the slope of the unloading (or swelling) line can be used to compute the modified swelling index κ^*. There is a difference between the modified indices κ^* and λ^* and the original Cam-Clay

parameters κ and λ. The latter parameters are defined in terms of the void ratio e instead of the volumetric strain ε_v. The parameter μ^* can be obtained by measuring the volumetric strain on the long term and plotting it against the logarithm of time (see Figure 3.1). These relationships are summarized in Table 3.1.

Table 3.1a Relationship to Cam-Clay parameters		
1. $\lambda^* = \frac{\lambda}{1+e}$	2. $\kappa^* = \frac{\kappa}{1+e}$	----------
Table 3.1b Relationship to internationally normalized parameters		
3. $\lambda^* = \frac{C_c}{2.3(1+e)}$	4. $\kappa^* \approx \frac{2C_r}{2.3(1+e)}$	5. $\mu^* \approx \frac{C_\alpha}{2.3(1+e)}$

In Table 3.1, The isotropic compression index κ and κ^* and the one-dimensional swelling index C_r. For a rough estimate of the model parameters, one might use the correlation $\lambda^* \approx I_p(\%)/500$, the fact that λ^*/μ^* is in the range between 15 to 25 and the general observation $\lambda^*/\kappa^* (=\lambda/\kappa)$ is in the range between 2 to 10. For characterising a particular layer of soft soil, it is also necessary to know the initial pre-consolidation pressure σ_p^0. This pressure may, for example, be computed from a given value of the overconsolidation ratio (*OCR*). Subsequently σ_p^0 can be used to compute the initial value of the generalised pre-consolidation pressure p_p^{eq}.

If the standard setting for the Soft-Soil-Creep model parameters is selected, then the value $\nu_{ur} = 0.15$ is automatically adopted. For loading of *NC* clay, Poisson's ratio plays a minor role, but it becomes important in unloading problems. Hence, Poisson's ratio should not be based on the normally consolidated K_0^{NC}-value, but on the ratio of difference in horizontal stress to difference in vertical stress in oedometer unloading and reloading:

$$\frac{\upsilon_{ur}}{1+\upsilon_{ur}} = \frac{\Delta\sigma_{xx}}{\Delta\sigma_{yy}} \qquad \text{(unloading and reloading)} \qquad (3.47)$$

3.4.3.7 Practical Application of the Soft Soil Creep Model

Creep behaviour depends on the stiffness parameters λ^*, κ^*, μ^* and the initial OCR. when a load step is applied both consolidation and creep will occur simultaneously. At the start of the load application the effect of consolidation on the settlement of the soil sample will

usually be significant. However, at the later the consolidation rate should be low enough so that its contribution on the settlements is minor compared to the contribution of creep or μ^*. The creep rate also depends on the values of λ^* and κ^*, but changing these parameters will also affect the primary loading and unloading-reloading behaviour and thus seriously affect the results of the simulation. The ratio λ^*/κ^*, cannot be smaller than 1 and should normally be between 2 and 10 and for most practical cases this ratio falls within the range of 3 to 7. The creep ratio, $(\lambda^* - \kappa^*)/\mu^*$ can have a wide range of values, normally between 5 and 25, where high values represent stiff soils with little creep and small values represent soft soils with a considerable amount of creep. For most practical cases the ratio falls within the range of 10 to 20, and if it is over 25 creep is not necessary to be considered.

The Soft Soil Creep model distinguishes similarly to in Hardening Soil and Soft Soil Models the distinction between primary loading and unloading/reloading behaviour is made by means of a cap, i.e. a curved plane in stress space that defines the limit stress state between those two modes of loading. The position of this cap is initially determined by the preconsolidation stress. However, in the Soft Soil Creep model the position of the cap is not only determined by the maximum stress state that has been reached in the past, as is the case in the HS and SS models, but it is also a function of time. In the Soft Soil Creep (SSC) model this shift of the cap needs time. If a higher load is applied, the cap will not follow immediately, but will take 1 day to adapt to the new stress state. This value of 1 day is an arbitrarily chosen value used in the model and cannot be varied by the user. Furthermore, when the cap reaches the applied stress state after one day, it will continue to expand with a continuously decreasing expansion rate. Any change in the stress state will cause a change in the cap expansion velocity; an increase in stress, even when the stress remains below the cap, will cause an increased velocity of the cap expansion. Similarly, a decrease of stress will cause a decrease in the cap expansion velocity.

As time is essential for the behaviour of the cap; therefore PLAXIS calculations will give a warning if a project in which the SSC model is used contains phases with a zero time step and can be ignored in a calculation phase where the soil layer that is modelled with the SSC model is not activated yet. The expansion velocity of the cap depends on time. This has consequences for the determination of the initial stresses as the history of the soil plays a major role here.

When we construct a model for an embankment was constructed several months ago, consisting of soft soils which strongly exhibit creep behaviour and assume that the subsoil and the embankment are both drained this could be easily modelled using time independent soil behaviour. In that case the embankment could be activated in the first calculation phase to model the present day situation; whether the embankment was built last week or last year is not important then.

For the SSC model, the position of the cap is also time dependent. So the correct value of the *OCR* should also take into account the time elapsed since the soil was formed and started creeping. *OCR*=1 means there has been creep for only one day. When the stress is increased beyond the cap it will take 1 day for the cap to expand to the new stress state. This also means that the PLAXIS defaults are only suited for a newly applied material which will exhibit large creep deformations. Layers in the subsoil should initially be assigned a proper *OCR* that represents the history of that layer. There are basically two ways to do this. The first possibility is to assign an *OCR* in Initial Conditions by either double-clicking on a cluster or specifying the *OCR* in the table of K_0-values before starting the initial stress procedure (K_0-procedure). Normally one would use undrained material behavior to illustrate creep behavior. Start the calculation and ignore the warning about calculation phases with zero time interval.

3.4.3.8 Creep Behavior of a Soil Block

Soft soils that exhibit creep behavior generally have a low permeability and show undrained behavior under short term loading. Excess pore pressures that developed cannot drain off and effectively consolidation cannot occur, but deformation is not hindered. Now leave the block of soil undisturbed for a considerable time period. The development of excess pore pressures is occured in the absence of external loads or deformation in SSC material. Normally, creep behaviour of the soil causes plastic deformation and, a decrease in volume. As the material is undrained and there is no possibility to consolidate, volume strains are not allowed in SSC model. Therefore, the plastic volume strain that is calculated due to creep has to be compensated by an elastic volume strain of equal magnitude but opposite direction and the total volume strain equal to zero.

The creep rate depends on the effective stress level, and the excess pore pressures decrease the effective stresses the creep rate will decrease at an even higher rate than in

the case of a drained material. The shift of stress from the effective stress part of the total stress to the (excess) pore pressures is also the cause for the very small deformation. The increased pore pressures cause a very small volume strain of the pore water, and thereby of the entire model. An important feature of the SSC model is creep behavior of undrained soils leads to an increase of excess pore pressures. Behavior under the combination of consolidation and creep in a creep sensitive soil depends on whether creep or consolidation is dominant. Over time, creep would tend to increase the pore pressures, reduces the creep velocity and increase the consolidation velocity. Due to consolidation or the pore pressures drop, the consolidation rate is decreased and the creep rate is increased. A simple 1D consolidation test has been performed on four different soil data sets, each with the same strength and stiffness parameters, but with permeabilities varying between 0.1 m/day and 10^{-4} m/day. For this exercise closed consolidation boundaries have been added to the left and right side of the square soil block.

The excess pore pressure in the middle of the soil sample is a function of time. After first loading the sample with 100 kPa over a period of 1 day, the excess pore pressure is 109 kPa in all cases (100 kPa due to the load and 9 kPa due to creep during the first day). For the highest permeability (0.1 m/day) the excess pore pressures immediately drop when consolidation starts, whereas for lower permeabilities the excess pore pressures first increase for a while, until consolidation really becomes the dominant effect and the excess pore pressures finally decrease. This is noted that for a permeability of 10^{-4} m/day the excess pore pressures even rise to a peak value of 130 kPa after 63 days.

3.4.4 Soft Soil Model

When simulating the behaviour of soft soils like normally consolidated clay we use the Soft Soil Model (SS). It is a type of Cam Clay model and it has very good performance for primary compression. In the SS model, there is an assumption of a logarithmic relation between the volumetric strain ε_v and the mean effective stress p' and has strong capabilities when modelling compression behaviour of very soft soils during isotropic virgin compression, along the normal consolidation line, this relation is formulated as

$$\varepsilon_v - \varepsilon_v^0 = -\lambda^* ln\left(\frac{p'}{p^0}\right) \quad \text{(virgin compression)} \qquad (3.48.1)$$

where λ^* is the modified compression index which can be determined from the compressibility of the material in primary loading, p^0 is the initial value of the mean

effective stress and ε_v^0 is the initial volumetric strain. In order to maintain the validity of Expression (3.48) a minimum value of p' is set equal to a unit stress. The parameter λ^* is not the same as the Cam-Clay parameter λ as used by Burland (1965); they differ in the sense that equation (3.48) is a function of volumetric strain instead of void ratio. The relation in equation (3.48) is shown in Figure 3.9.

If the soil however is subjected to isotropic unloading or reloading, its behaviour follows a different path and is formulated as

$$\varepsilon_v^e - \varepsilon_v^{e0} = -\kappa^* ln\left(\frac{p'}{p^0}\right) \tag{3.48.2}$$

where κ^* is the modified swelling index, which determines the compressibility of the material in unloading and subsequent reloading. ε_v^e is the elastic volumetric strain and ε_v^{e0} is the initial elastic volumetric strain. κ^* will determine the compressibility of the soil material during unloading or reloading up to the normal compression line. The distinction between the two parameters $\lambda^*$and κ^* is presented in Figure 3.9.

It is assumed that the soil response during the unloading and reloading is elastic as denoted by the superscription *e* in the equation (3.48). The elastic behaviour which is described by Hooke's Law. In equation (3.49) implies linear stress dependency on the tangent bulk modulus can be determined by

$$K_{ur} = \frac{E_{ur}}{3(1-2\nu_{ur})} = \frac{p'}{\kappa^*} \tag{3.49}$$

in which the subscript *ur* denotes unloading/reloading and effective parameters are considered rather than undrained soil properties, as might be suggested by the subscripts *ur*. K_{ur} is the elastic bulk modulus and E_{ur} is the elastic Young's modulus.

Soft Soil Model is capable to account for both elastic and plastic material behaviour. It is an advanced constitutive material model and the main features of the Soft Soil Model include:

- Failure behaviour according to the Mohr-Coulomb criterion.
- Yield surface adapt from Modified Cam Clay model with associated flow rule for plastic strains.
- Stiffness parameters can be obtained from oedometer-tests.

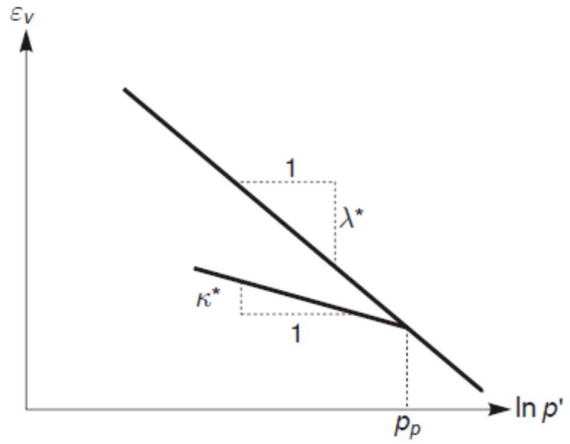

Figure 3.9 Logarithmic relation between the volumetric strain ε_v and the mean effective stress p'(Brinkgreve et al., 2002)

The main strengths of the Soft-Soil model include:

- Stress dependent stiffness (logarithmic compression behaviour).
- Distinction between primary loading and unloading-reloading.
- Memory for pre-consolidation stress.

The main weaknesses of the Soft-Soil model include:

- Not suitable for other types than soft soils, normally or near-normally consolidated.
- Does not take secondary compression (creep) into account.
- Less suited for other than compression stress paths.
- Do not take anisotropy of the soil into account.

3.4.4.1 Yield Function for Triaxial Stress State ($\sigma_2' = \sigma_3'$)

The Soft-Soil model is capable to simulate soil behaviour under general states of stress. However, for clarity, in this section, restriction is made to triaxial loading conditions under which $\sigma_2' = \sigma_3'$. For such a stress state the yield function of the Soft-Soil model is defined as:

$$f = \overline{f} - p_p \tag{3.50}$$

where f is a function of the stress state (p',q) and p_p, the pre-consolidation stress, is a function of plastic strain such that:

$$\overline{f} = \frac{q^2}{M^2\left(p' + c\cot\phi\right)} + p' \tag{3.51}$$

$$p_p = p_p^0 \, exp\left(\frac{-\varepsilon_v^c}{\lambda^* - k^*}\right) \tag{3.52}$$

The yield function *f* describes an ellipse in the p'-q-plane, as illustrated in Figure 3.12. The parameter *M* in Eq. (3.51) determines the height of the ellipse. The height of the ellipse is responsible for the ratio of horizontal to vertical stresses in primary onedimensional compression. As a result, the parameter *M* determines largely the coefficient of lateral earth pressure, K_0^{nc}. Such an interpretation and use of *M* differs from the original critical state line idea, but it ensures a proper matching of K_0^{nc} in primary one − dimensional compression.

The tops of all ellipses are located on a line with slope *M* in the p'-q-plane. In the Modified Cam-Clay model (Burland 1965, 1967) the *M*-line is referred to as the critical state line and represents stress states at post peak failure. The parameter *M* is then based on the critical state friction angle. In the Soft-Soil model, however, failure is not necessarily related to critical state. The Mohr-Coulomb failure criterion is a function of the strength parameters ϕ and *c*, which might not correspond to the *M*-line.

The isotropic pre-consolidation stress, p_p, determines the extent of the ellipse along p' axis. During loading, infinitely many ellipses may exist (Figure 3.12) each corresponds to a particular value of p_p. In tension ($p' < 0$), the ellipse extends to $c\cot\phi$ (Eq. (3.51) and Figure 3.10). In order to make sure that the right hand side of the ellipse (i.e. the 'cap') will remain in the 'compression' zone ($p' > 0$) a minimum value of $c\cot\phi$ is adopted for p_p. For $c = 0$, a minimum value of p_p equal to a stress unit is adopted. Hence, there is a 'threshold' ellipse and the yield contour has the form of an ellipse, where the top intersects with a line having slope *M* (Figure 3.10). In the Soft Soil Model, Mohr-Coulomb failure criterion is introduced to obtain a more realistic failure state. Similar to the Cam-Clay theory, there can exist an unlimited number of ellipses and the mean effective pre-consolidation pressure determines the extent of the ellipse along the p'axis.

The value of p_p is determined by volumetric plastic strain following the hardening relation, Eq. (3.52). This equation reflects the principle that the pre-consolidation stress increases exponentially with decreasing volumetric plastic strain (compaction). p_p^0 can be regarded as the initial value of the pre-consolidation stress. According to Eq. (3.52) the initial volumetric plastic strain is assumed to be zero.

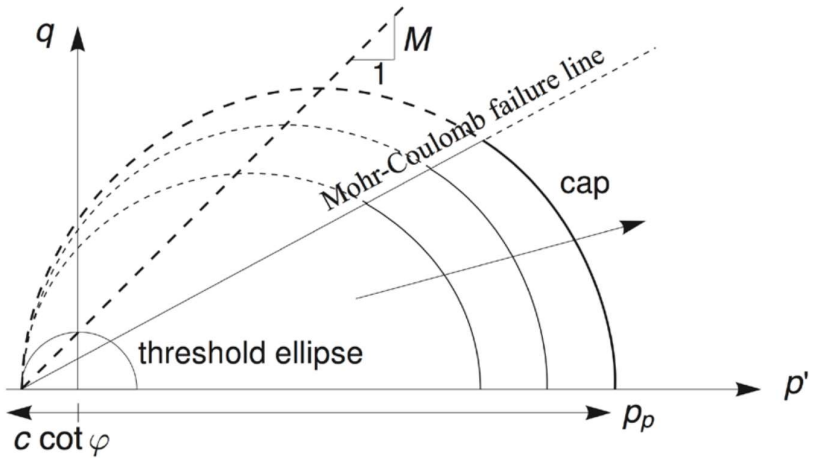

Figure 3.10: Yield surface of the Soft Soil Model in p'-q-plane.

The yield function, describes the irreversible volumetric strain in primary compression, and forms the cap of the yield contour. To model the failure state, a perfectly-plastic Mohr-Coulomb type yield function is used which is a straight line in *p'*-*q*-plane (Figure 3.10). The slope of the failure line is smaller than the slope of the *M*-line.

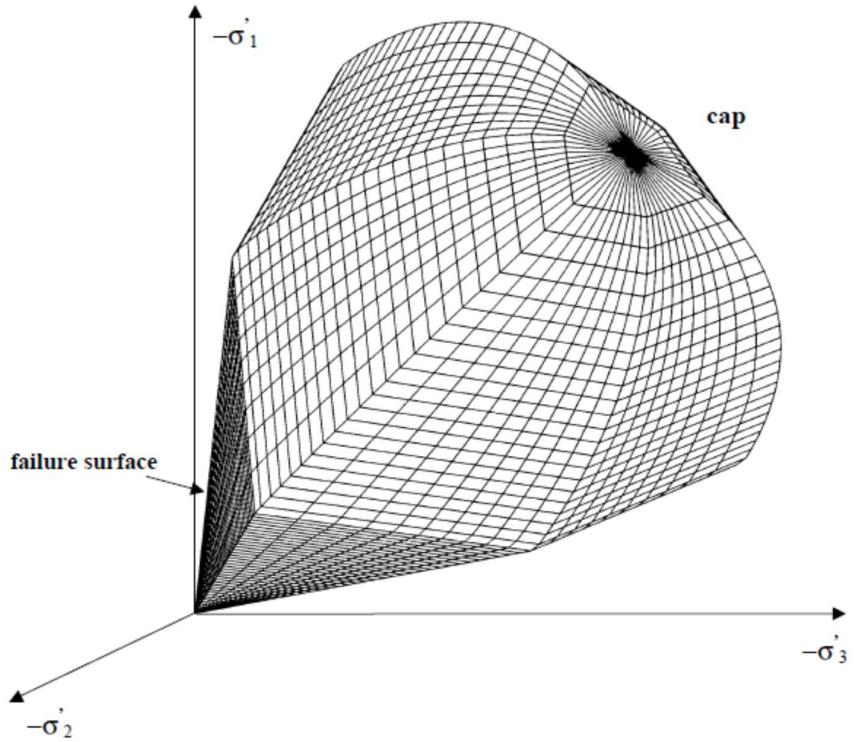

Figure 3.11 Total yield contour of the Soft-Soil model in principal stress space.

The total yield contour, as shown by the bold lines in Figure 3.10, is the boundary of the elastic stress area. The failure line is fixed, but the cap may increase in primary

compression. Stress paths within this boundary give only elastic strain increments, whereas stress paths that tend to cross the boundary generally give both elastic and plastic strain increments.

For general states of stress, the plastic behaviour of the Soft-Soil model is defined by a total of six yield functions; three compression yield functions and three Mohr-Coulomb yield functions. The total yield contour in principal stress space, resulting from these six yield functions, is indicated in Figure 3.11.

The soil parameters required as input for the Soft Soil Model are presented in Table 3.2.

Table 3.2: Input parameters for the Soft Soil material model (PLAXIS, 8.0).

Basic stiffness parameters:

λ^*	: Modified compression index	[-]
φ	: Friction angle	[°]
ψ	: Dilatancy angle	[°]
κ^*	: Modified swelling index	[-]
c	: Cohesion	[kPa]

Advanced parameters:

ν_{ur}	: Poisson's ratio for unloading/reloading	[-]
K_0^{NC}	: $\sigma'_{xx}/\sigma'_{yy}$ stress ratio in a state of normal consolidation	[-]
M	: K_0^{NC}-related parameter	[-]

M is calculated automatically from the coefficient of the lateral earth pressure, K_0^{NC}, by means of Eq. (3.55). Physically, in the current model M differs from that in the Modified Cam-Clay model where it is related to the material friction.

Modified swelling index and modified compression index parameters are discussed in section 3.41 and Table 3.2.

Remarks on Table 3.2:

- In relations 1 and 2, the void ratio, e, is assumed to be constant. In fact, e will change during a compression test, but this will give a relatively small difference in void ratio. For e one can use the average void ratio that occurs during the test or just the initial value.

- In relations 3 there is no exact relation between κ^* and the one-dimensional swelling indices, because the ratio of horizontal and vertical stresses changes during 1-D unloading. For approximation it is assumed that the average stress state during unloading is an isotropic stress state, i.e. the horizontal and vertical stresses are equal.

3.4.4.2 Parameters in SS Model

The cohesion has the dimension of stresses. Any effective cohesion may be used, including a cohesion of zero. When using the standard setting the cohesion is set equal to 1 kPa. Entering a cohesion will result in an elastic region that is partly located in the 'tension' zone, as illustrated in Figure 3.10, the left hand side of the ellipse crosses the p'-axis at a value of $-c\cot\phi$. In order to maintain the right hand side of the ellipse (i.e. the cap) in the 'pressure' zone of the stress space, the isotropic pre-consolidation stress p_p has a minimum value of $c\cot\phi$. This means that entering cohesion larger than zero may result in a state of 'over-consolidation', depending on the magnitude of the cohesion and the initial stress state. As a result, a stiffer behaviour is obtained during the onset of loading. It is not possible to specify undrained shear strength by means of high cohesion and a friction angle of zero. Input of model parameters should always be based on effective values.

The effective angle of internal friction represents the increase of shear strength with effective stress level. Zero friction angle is not allowed. On the other hand, care should be taken with the use of high friction angles. It is often recommended to use ϕ_{cv}, i.e. the critical state friction angle, rather than a higher value increases the computational requirements. based on small strains. For the Soft Soil, the dilatancy can generally be neglected or zero degrees. Poisson's ratio has been discussed earlier.

The parameter M is automatically determined based on the coefficient of lateral earth pressure in normally consolidated condition, K_0^{NC}, as entered by the user. The value of M is indicated in the input window. As can be seen from Eq. (3.55), M is also influenced by the Poisson's ratio v_{ur} and by the ratio λ^*/κ^*. However, the influence of K_0^{NC} is dominant. Eq. (3.55) can be approximated by $M \approx 3.0 - 2.8K_0^{NC}$.

If oedometer data is unavailable and the engineer still would like to model with the Soft Soil Model, a number of empirical relations have been established relating the modified

compression index to different parameters. (Vermeer, 2002) suggests in a PLAXIS 2D news bulletin the following empirical relations as, $\lambda^* \approx 0.3 I_p$ and $\lambda^* \approx 0.2(W_L\text{-}0.1)$.

3.4.4.3 Example of SS Model Analysis

Table 3.3: PLAXIS input parameters for the Soft Soil material model (Subsea 7, 2010).

Parameter		Soil unit I	Soil unit II	Unit
Effective unit weight	γ'	10	12.6	kN/m^3
Effective friction angle	ϕ'	36	36	°
Dilatancy angle	Ψ	0	0	°
Effective cohesion	c'	1	1	kPa
Coefficient of permeability	k	0.0001	0.0001	m/day
Modified compression index	λ^*	0.032	0.02	-
Modified swelling index	κ^*	0.004	0.0057	-
Over-consolidation Ratio	OCR	6	20	-
λ^*/κ^*-ratio	-	8	3.5	-

Table 3.4: Results from 31 days of consolidation from PLAXIS 2D computation with Soft Soil Model (SSM), Mohr-Coulomb Model (MCM), analytical calculation and survey measurements.

Method	Survey	SSM	MCM	Analytical
Consolidation settlements after 31 days, m	0.05	0.05	0.01	0.02

This also seems to be true since a better correlation is achieved with the Soft Soil Model when comparing it to the survey measurements. Virgin compression of soft clay will yield plastic strains, however, plastic strains does not imply that a state of failure has been reached. Adapting a logarithmic compression path, the Soft Soil Model is able to differentiate between virgin compression and elastic recompression, identifying plastic strains in regions that the Mohr-Coulomb Model would otherwise treat as purely elastic.

This will further confirm that consolidation settlement analyses for soft clays experiencing virgin compression should always be computed with an advanced constitutive model that can incorporate a logarithmic compression feature and a plastic hardening behaviour.

CHAPTER-4

MATERIAL AND PROBLEM DEFINITION

4.1 Introduction

This research work aimed at analysis of a two layer sub-soil, where the upper layer is a sand layer (untreated or cement treated) placed over natural soft Inorganic Clay deposit extended to a great depth. Such soft clay deposit exist in many parts of Bangladesh. Sub-soil Characteristics in different regions of Bangladesh as obtained from literature review is presented in this chapter. Material properties used in this research have been taken from those obtained by literature review. Properties of cemented soil is also presented here. The definition of the current problem including model geometry and material properties are also presented in this chapter.

4.2 Geotechnical Characteristics of Bangladeshi Soil

Soft Inorganic Clay Soils of almost all part of Bangladesh is presented here and sand of Dhaka and major river bad has been presented below.

4.2.1 Characteristics of Soft Inorganic Clay Soils

The index properties of cohesive soils in Khulna City Corporation (KCC) was obtained by Adhikari et al. (2006). It has been observed that for the soil at this area the Liquid Limit (*LL*) range from 38% to 59% and Plasticity Index (*PI*) range from 9% to 30% is presented in Table 4.1.

The insitu Void Ratios (e_0) and Compression Index(C_c) values for the soil at this area are given in Table 4.2. This C_c values were determined from test and found to be smaller than those calculated using the Skempton (1944) formula, C_c= 0.009(*LL*-10) and are other measurements including that given by Terzaghi (1943).

Table 4.1. Plasticity values for soil of the Khulna City Area. (after Adhikari et al., 2006)

Depth (m)	Liquid limit, *LL* (%)	Plasticity index, *PI* (%)
1.5	55	28
3.1	44	16
	52	25
	58	29
4.6	43	17
	44	09
	50	25
6.2	38	16
	48	21
	54	28
7.7	47	21
	40	10

Table 4.2. Void ratio and Compression index values of surface soils of the Khulna City Area. (after Adhikari et al., 2006)

Depth (m)	Void Ratio (e_0)	Compression Index (C_c)
2	0.88	0.14
2.5	1.00	0.15
	0.88	0.25
4	0.79	0.14
	0.93	0.17
	1.03	0.22
5.5	1.07	0.34
	0.98	0.14

From the compression index and liquid limit plot it is observed that a valid linear relation exists between the compression index and liquid limit for selected coastal regions soil as represented by the equation, $C_c = 0.009\ (LL - 13)$ (Adhikari et al., 2006).

Anisuzzaman et al. (2013) presented a summary of the properties of selected coastal soil samples which is shown in Table 4.3.

Ranges of various soil parameters such as Unconfined compressive strength (q_u), Cohesion (c), Angle of internal friction (ϕ) etc. for some typical cohesive/ semicohesive inorganic fine-grained soils in different regions of Bangladesh as summarised by Serajuddin (1998) are shown in Table 4.4 and Table 4.5.

Table 4.3 Summary of physical and engineering properties of top coastal soil. (after Anisuzzaman et al., 2013)

Properties	Location		
	Bhola	Chittagong	Noakhili
Physical Properties			
Liquid limit, *LL* (%)	37~55	33~53	41~45
Plastic limit, *PL* (%)	24~29	24~30	22~28
Natural moisture content, W_n (%)	34~45	30~44	45~54
Plasticity index, *PI* (%)	14~30	10~20	14~17
Engineering Properties			
Cohesion, c (kPa)	20~28	18~27	15~22
Angle of Internal Friction, ϕ (degree)	13~15	11~14	16~19
Undrained Shear Strength, c_u (kN/m^2)	15~29	15~19	14~35
Compressibility ratio, $C_c/(1+e_o)$	0.14~0.16	0.13~0.17	0.14~0.18

Table 4.4. Natural Moisture Content, Liquid Limit, Plasticity Index, Over Consolidation Ratio values of Inorganic clays and silts of Bangladesh. (after Serajuddin, 1998)

Brief description of site	*NMC* (%)	*LL* (%)	*PI* (%)	*OCR*	
				CM	SM
Rajshahi around Kaliganghat and Amnura	15-18	47-51	20-29	9.75-10.0	-
Kushtia around Alamdanga and Pabna-Kushtia Ganges river bed Char	27-31	35-84	10-44	1.00-2.22	1.00-2.86
Faridpur around Golabaria, Baliakandi and Amdanga	32-47	45-47	20-47	2.89-4.11	2.89-5.38
Jessore	48-52	64-68	35-36	1.15-2.39	1.28-1.74
Khulna around KalabashuKhali, Hankura, Kewratola, Pachuria and Hasanpur	32-53	35-60	11-29	1.75-4.38	1.78-2.18
Dhaka around DND Project area	25-34	36-41	20-22	2.60-3.36	2.43-3.36
Comilla around Motlab	29-37	35-39	7-11	6.73-7.52	-
Sylhet around Juri	37	46	20	1.72	2.8
Chittagong around Patenga and Dohazari	27-52	36-47	13-20	1.23-7.34	-

NMC – Natural Moisture Content
LL – Liquid Limit
PI – Plasticity Index
CM – Casagrande Method
SM – Schmertman Method
OCR – Over Consolidation Ratio

Table 4.5. Values of various engineering properties of Inorganic clays and silts of Bangladesh. (after Serajuddin, 1998)

Explored zone	Depth (m)	NMC (%)	In-situ γ_d (g/m^3)	e_0	q_u (Kg/ cm^2)	c (Kg/ cm^2)	ϕ (degree)	C_c
North-west Zone	3.5-11	19-52	1.08-1.72	0.558-1.42	0.06-1.94	0.08-0.91	7-34	0.10-0.64
North-East Zone	3.5-8	20-46	1.17-1.77	0.511-1.29	0.20-1.46	0.14-0.98	1-34	0.09-0.29
South-west Zone	3.5-9.5	24-47	1.15-1.56	0.706-1.32	0.02-1.66	0.03-4.43	2-35	0.08-0.52
South-East Zone	5-12.5	24-54	1.09-1.60	0.711-1.463	0.31-1.49	0.006-0.68	2-39	0.15-0.56

Table 4.6. Range of some typical values of laboratory maximum dry density and Optimum Moisture Content for different soils of Bangladesh. (after Serajuddin, 1998)

Location	*LL* (%)	*PI* (%)	UCS symbol	G_s	Maximum Dry Density (g/cm^3)	Optimum Moisture Content (%)
South –East Zone	20-40 NP	1-21 NP	CL, ML, ML-CL SM	2.62-2.69	1.60-1.97 1.85-1.99	11-22 10-12
South –West Zone	24-49 51-72 NP	2-25 25-43 NP	CL, ML, ML-CL CH, MH SM	2.62-2.79	1.64-1.84 1.51-1.75 1.53-1.62	14-21 18-24 15-20
North – West Zone	17-49 51-85	2-30 24-61	CL, ML, ML-CL CL-CH, CH, MH	2.60-2.70	1.42-1.81 1.48-1.66	12-26 17-25
North – East Zone	28-56 NP	2-3 NP	CL, ML, CH, MH SM, SM-ML	2.67-2.71	1.69-1.92 1.72-1.89	12-20 12-16

As mentioned by Terzaghi (1948) and Peck (1967), $q_u = f.N$, where, q_u = Unconfined Compressive Strength in kPa, N=SPT value and f = 12.50 for very soft to soft Clay and f = 13.33 for medium stiff to hard Clay.

Serajuddin and Chowdhury (1998) obtained similar correlation between SPT value and Unconfined Compressive Strength of Cohesive Soil Deposit of Bangladesh and according to their findings –

f = 16, High Plastic Clay and Silt, $w_L \geq 51\%$

f = 15, Medium Plastic Clay and Silt, w_L = 36% – 50%

f = 13, Low Plastic Clay and Silt, $w_L \leq 35\%$, w_L is Liquid Limit.

4.2.2 Characteristics of Bangladeshi Sand

Serajuddin (1970) and Serajuddin and Islam (1985) studied the permeability characteristics of different Bangladeshi sands containing various proportions of nonplastic fines (Particles smaller than 0.075 mm) at different degree of packing. They compared the laboratory measured permeability values with in-situ measured permeability for different size and shape of particle, uniformity, porosity, amount of silts present etc. Permeability values reported by them, presented in Table 4.7, can be used to make an approximate estimate of field permeability of sand beds containing silts.

Densities and void ratios of four Bangladeshi sand namely Teesta Sand, Meghna Sand, Dhaka Sand and Jamuna Sand as reported by Yasin and Shafiullah (2003) are presented in Table 4.8. The angles of internal friction of the soils studied by them were determined from the peak stress data on the deviator stress vs. axial strain curves. These friction angles along with initial void ratio, relative density, deviator stress at peak and major principal stress at peak are presented in Table 4.9.

Table 4.7. Co-efficient of laboratory measured permeability, k_{20} for (a) selected aquifer sands in natural grading and (b) laboratory mixed sands in predetermined proportions of various sand fraction and non-plastic fines. (after Serajuddin, 1998)

Granular composition					Coff. of permeability, K_{20} (cm/sec x 10^{-4}) at the indicated porosity (%)			
% finer than the diameter (mm)				D_{10} (mm)				
4.75	2.0	0.425	0.075		33.3	37.5	41.17	44.44
-	-	99	5	0.100	5	8	13	-
-	98	95	10	0.075	2	4	8	-
-	98	60	10	0.075	5.5	8.5	14	23
78	76	44	2	0.200	32	45	60	-
-	98	78	2	0.150	17	33	60	-
87	77	50	0	0.250	90	200	-	-
-	-	98	8	0.076	-	-	4.4	-
90	88	72	8	0.100	6	12	20	-
98	92	70	8	0.100	17	28	42	-
98	97	58	8	0.100	8	14	20	34
-	-	97	25	0.030	-	5.5	7.5	10
-	100	90	8	0.100	-	4.2	10	25
-	100	70	8	0.090	18	24	30	-

Table 4.8. Sampling location, grain properties, limiting density and void ratio of some Bangladeshi Sands. (Yasin et a., 2003)

Sand Type	Teesta Sand	Meghna Sand	Dhaka Sand	Jamuna Sand
Location	Teesta Barrage Site, Rangpur	Meghna Bridge Site, Dhaka	Rajarbagh, Dhaka	Jamuna Bhuyanpur, Tangail
Approximate depth from ground surface (m)	4.5-6.0	River bed	12-15	River bank
Specific gravity	2.67	2.7	2.66	2.69
Fineness Modulus	2.4	1.35	0.98	0.4
Maximum dry density, kN/m^3	16.66	15.95	13.74	15.31
Maximum dry density, kN/m^3	14.15	13.40	11.05	12.30
Maximum void ratio	0.92	0.97	1.36	1.14
Minimum void ratio	0.57	0.66	0.89	0.72

Table 4.9. Angle of shearing resistance at failure for various initial Void ratio and relative density

Sample	Initial void ratio	Relative density %	Deviator stress psi	Major principal stress, psi	Angle of internal friction at failure (degree)
Teesta	0.76	46	43.0	57.50	36.67
	0.89	8	38.8	53.50	34.91
	0.93	0	37.0	51.50	34.10
Meghna	0.81	52	38.8	53.30	34.90
	0.86	35	37.4	51.90	34.28
	0.97	15	34.1	48.60	32.71
Dhaka	0.92	77	33.2	47.70	32.26
	1.12	42	32.1	46.60	31.69
	1.28	14	29.5	44.00	30.28
Jamuna	0.80	81	47.0	61.50	38.20
	0.93	50	42.4	56.90	36.43
	1.03	26	38.2	52.70	34.65

4.3 Geotechnical Characteristics of Cement Stabilized Sand

The Characteristics of Cemented Clayey soil of Bangladesh was studied by some researcher as has been found in literature but no study could be found on Cemented sand of Bangladesh. For this reason literature related to properties of cement stabilization of sands in other countries have been reviewed and parameters of cement treated sand required for the present analysis have been selected from those found from literature review.

Cement can be applied to stabilize any type of soil, except those with organic content greater than 2% or having *pH* lower than 5.3. Granular soils and clayey materials with low plasticity index are better suited to be stabilized with cement (Muhunthan et al., 2008).

Significant reduction in plasticity index and swell potential, and remarkable increase in strength, modulus of elasticity and resistance against the effects of moisture and freeze-thaw can be achieved by cement stabilization. It is noted that reduction in plasticity index is due to increase of plastic limit, which is highly affected by cement content and curing time (Muhunthan et al., 2008).

The addition of cement was also found to increase optimum water content but decrease the maximum dry density. However, report by ACI committee 230 (1990) states that cement treatment causes changes in maximum dry density and optimum water content, but the direction of changes is not predictable. In addition cement treatment causes immediate decrease in water content (Muhunthan et al., 2008). Cement treated materials behave in a more brittle manner than non-treated materials.

Typically amounts of cement for stabilization of soil vary from 5% to 10% by weight of dry soil. Cement content increases unconfined compressive strength of fine-grained as well as coarse-grained soils (Figure 4.1).

Improvement in unconfined compressive strength due to cement stabilization varies up to 150 times of unconfined compressive strength at fresh condition for coarse-grained soils. In addition, unconfined compressive strength increases with increasing curing time and that amount of improvement is significant. Recent studies have also reported that addition of cement increases the effective cohesion significantly (Muhunthan et al., 2008).

Figure 4.2 (after Mitchell, 1976) shows the effect of cement content on effective cohesion of several coarse-grained and fine-grained soils. It is noted that, this plot was obtained for 90 days curing time and 413.64 kPa (60 psi) confining pressure. According to this study cement treatment leads to an increase in effective cohesion and the increase in cohesion may be expressed as: $c(\text{psi}) = 7.0 + 0.225\sigma_c$, where, σ_c is unconfined compressive strength (psi) and c is effective cohesion.

Internal friction angle remains relatively constant for cement treated soils regardless of cement content and curing time (Muhunthan et al., 2008). The average value of internal friction angle are 43.8° for granular cement treated soils, (Muhunthan et al., 2008). However, referred by Muhunthan et al. (2008), Uddin et al. (1997) stated that cement stabilization leads to significant increase in internal friction angle. In addition, the results of undrained triaxial test have shown that cohesion and friction angle increase with increasing curing time and cement content.

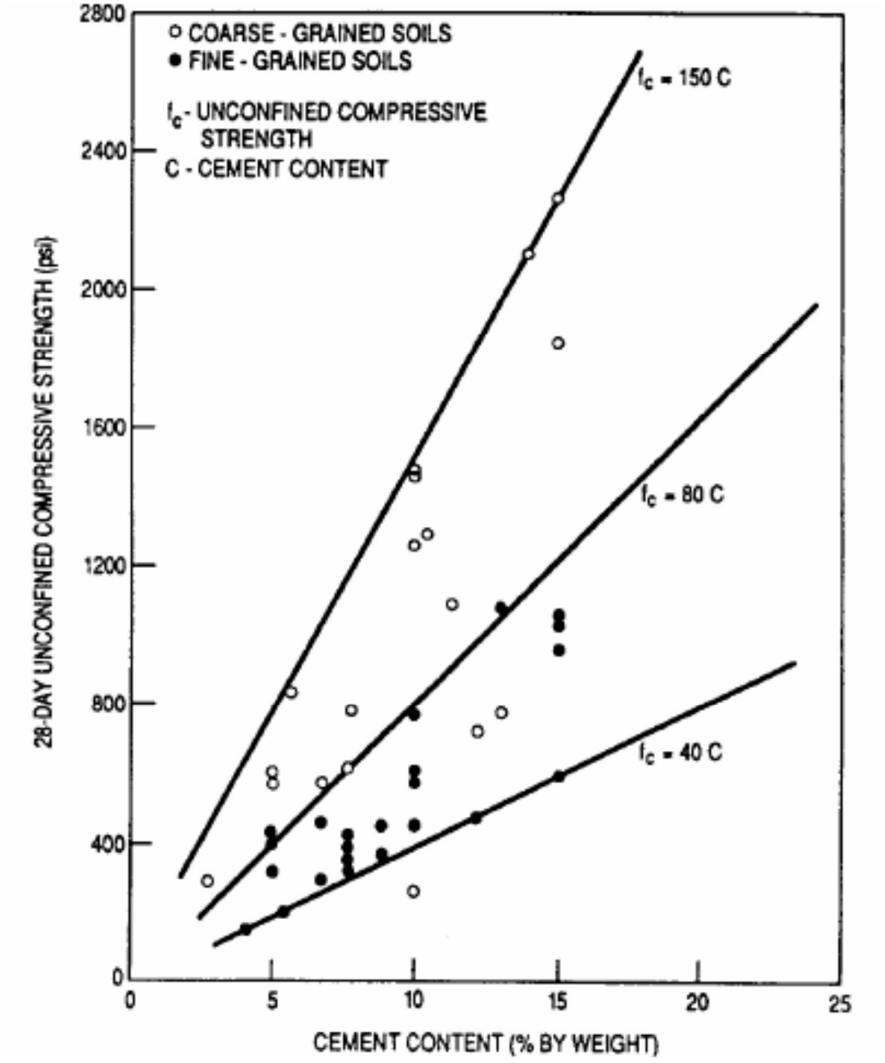

Figure 4.1 Relationship between cement content and unconfined compressive strength for cement treated soils (Mitchell, 1976).

The cohesion of cement treated clay disappears at large strain, and it behaves as purely frictional material (Muhunthan et al., 2008). Muhunthan et al. (2008) presented form report of White et al. (2005) that ignificant (10% to 20%) reduction in unconfined compressive strength for 4 hours delays between mixing and compaction of cement treated material were and for 24 hours delays the reduction was as much as 40%. They also observed each 1% increase in relative compaction leads to about 200 kPa increase in unconfined compressive strength.

From the interpretation of results from unconfined compression tests, drained triaxial compression tests with local strain measurements for cemented sandy soils, it was

concluded that the unconfined compression resistance is a direct measurement of the degree of cementation. Consequently, the triaxial shear strength can be expressed as a function of the internal shear angle of the non-structured material and the unconfined compression resistance. In addition, a logarithmic formulation is adopted to express the relationship between static deformation moduli and axial strain amplitude in axis-symmetric conditions. Data from other reported investigation programs gave the a correlations a broader acceptance to general geotechnical applications.

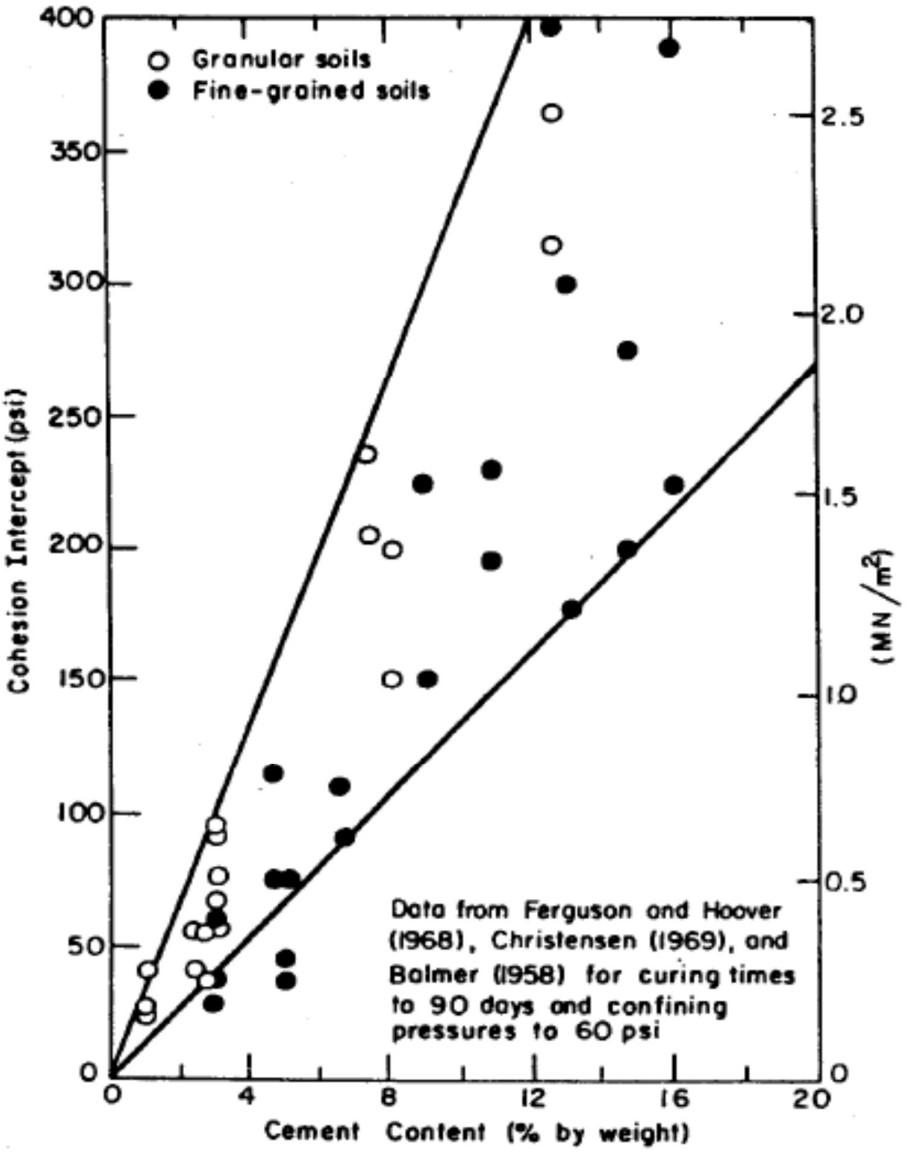

Figure 4.2 Effect of cement content on effective cohesion for several coarse-grained and fine-grained soils (Mitchell, 1976).

Bonded structure of the loaded soil contributes to reduce settlements and increase bearing capacity. Artificially cemented structure of soil significantly reduces soil compressibility. Stress-strain behavior of cemented sands specimens have been used to establish a fundamental understanding of natural soils behavior.

From a mechanical point of view, cemented soils, weak rocks, and similar bonded materials constitute an intermediate class of geomaterials placed between classical soil mechanics and rock mechanics.

For a given range of stresses, shear strength of cemented sands can be represented by straight Mohr-Coulomb envelopes defined by c' which is an unique function of cementation, and ϕ', which seems to be not affected by the cement content. As for deformability, cemented soils show a very stiff behavior before yielding. The brittle behavior changes to a ductile soil response as the stress level changes from low to high. Basically, it comprises an initial stiff behavior followed by increasingly plastic deformation as the soil approaches failure.

Muhunthan et al. (2008) have shown the stress-strain behavior of cemented soils to be basically dependent on their initial state, and its position in relation to the yield curve and the critical state line of the non-structured remolded soil. Muhunthan et al. (2008) describe the idealized behavior of cemented soils, which is divided into three different classes, as illustrated in Figure 4.3. The first class (curve 1 in Figure 4.3) occurs when the soil reaches its yield stress during isotropic compression; in this case, shearing will produce a similar behavior to that observed for an equivalent nonstructured soil. The second class (curve 2 in Figure 4.3) occurs for intermediate stress states, in which the bonds will be broken during shear; the strength is controlled by the frictional component of the equivalent non-structured soil and the stress-strain curve shows a well defined yield point after an apparent linear behavior. In the third class (curve 3 in Figure 4.3) the soil is sheared at low confining stresses compared to the bond strength; a peak in the stress-strain curve occurs at small strains and for stresses outside the limit state surface of the equivalent non-structured soil.

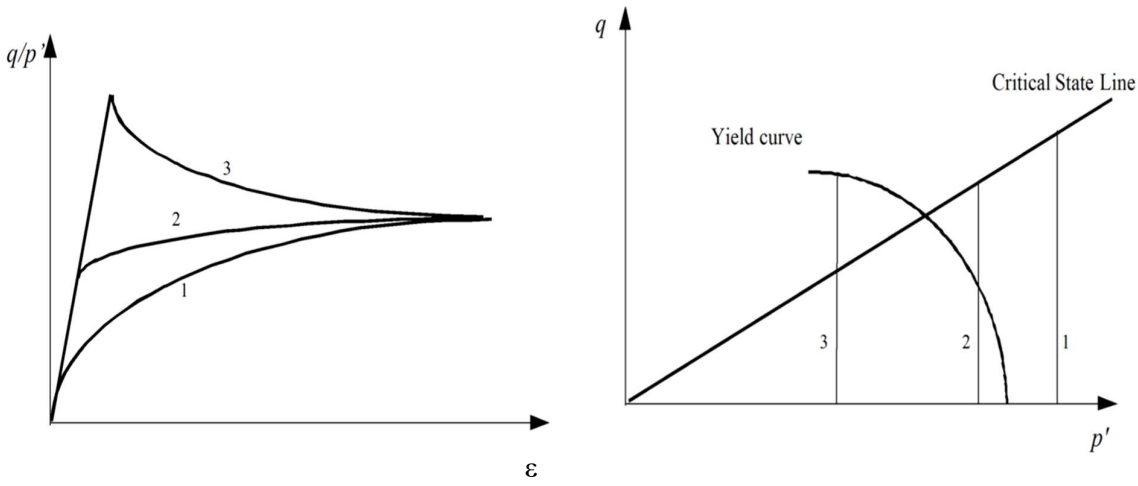

(a) stress-strain

(b) Effective stress paths (after Coop and Atkinson 1993).

Figure 4.3 Idealized behavior of a cemented soil.

The proposal by Muhunthan et al. (2008) for developing constitutive models for cemented soils and weak rocks, within the framework of the hardening plasticity theory is based on (1) the fundamental role played by the yield phenomenon and (2) the necessity of considering the cemented material behavior as being related to the behavior of an equivalent uncemented material.

Muhunthan et al. (2008) presented the approach which is suggested by Gens and Nova (1993) starts from a constitutive law for the uncemented material, which is modified according to the amount of cementation. The material degradation is simulated through the reduction of the degree of cementation as a function of the strain level.

Triaxial tests at confining pressures up to 100 kN/m^2 are consistent with realistic assumptions made in some important engineering applications. Combination of a strong bonded structure with low confining stresses implies that no yielding occurs during isotropic compression; the initial stress state is well inside the yield envelope and peak stresses are outside the state boundary surface of the uncemented soil. In general, the stress-strain behavior of the cemented soil can be described as initially stiff, apparently linear up to a well defined yield point, beyond which the soil suffers increasingly plastic deformations until failure. As the cement content increases, both peak strength and initial stiffness increase. Different from the uncemented soil, cemented specimens show a

marked brittle behavior at failure with well defined shear planes being formed. This brittle response increases with increasing cement content and decreases as the initial mean effective stress increases. The axial strain at failure decreases with increasing cement content and decreasing initial mean effective stresses. As for the volumetric response, the cemented specimens show an initial compression followed by a strong expansion with the maximum dilation rate taking place right after the peak strength. Subsequently, the dilation rate decreases as the soil approaches an ultimate stable condition.

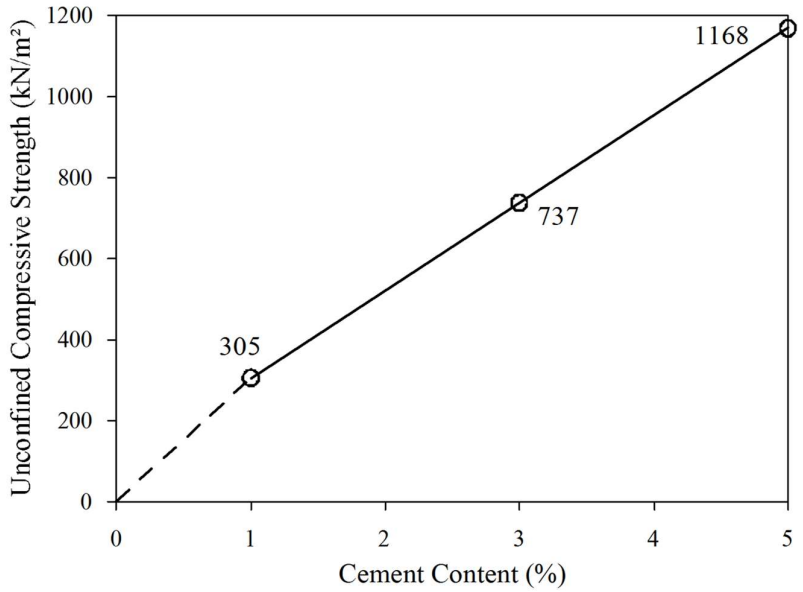

Figure 4.4 Effect of cement content on the unconfined compressive strength (Muhunthan et al., 2008).

Due to cohesive-frictional nature of the cemented soil, the shear strength can be expressed as a function of the internal friction angle (ϕ) and the cohesion intercept, c. The ϕ angle obtained for the uncemented soil was found to be lower than the average value obtained for the cemented specimens. Cement content does not constitute an appropriate parameter to evaluate the degree of cementation. Constitutive model based on the hardening elastoplasticity, incorporating the peculiar characteristics of cemented soils and weak rocks, constitutes the better approach to express modulus degradation. The elastic behavior of geomaterials, the yield phenomenon associated with cemented bonds breakage, the post-peak behavior, and the aspects related to the microstructure of cemented soils, are fundamental.

The complete determination of the ultimate or critical state in a p': q: e space presents some experimental difficulties, given the brittle behavior and the strain localization observed for cemented specimens especially for conventional triaxial tests. The investigation of the critical state line, as well as of the complete state boundary surface, plays a fundamental role in establishing a general theoretical framework for the behavior of cemented soils.

The study of the stress-strain behavior of an artificially cemented sandy soil has allowed to establish the following statements:
a) The unconfined compressive strength seems to be a direct measure of the degree of cementation in triaxial compression; b) The shear strength of the cemented soil measured in conventional triaxial tests can be determined as a function of the unconfined compressive strength and the uncemented friction angle; c) For the range of stresses investigated, the deformation or secant modulus is not significantly affected by the initial mean effective stress; d) The change in the secant deformation modulus with the axial strain can be qualitatively represented by mathematical expressions initially proposed for uncemented granular materials.

Failure envelopes of Weakly Cemented Sands is nonlinear. Mohr-Coulomb theories describe the failure strength as a linear function of stress using one or two parameters commonly known as the cohesion intercept/apparent cohesion (c) and the friction angle ($\varnothing$). However, it has been well recognized that the Mohr envelope becomes nonlinear especially at low confining stress resulting in decreased cohesion intercept and increased friction angle. In particular, forcing a linear Mohr envelope for weakly cemented sands results in significant over estimation of the cohesion.

However, these envelope functions are not continuous in stress space; there is a discontinuity at the transition point from small to large confining stress thus increasing the number of parameters required to define the strength function.

Nonlinear relations in the form of $\tau = a.\sigma^n$ have been used by many researchers (e.g. Charles and Watts, 1980; Hoek and Brown, 1980) to describe the shear strength function over a wide range of effective stresses, for various geomaterials. In this equation, τ is the shear strength for a given normal stress σ, a and n are the nonlinear strength parameters that are determined by curve fitting the experimental data. Based on a sensitivity study conducted on a and n, a method for characterizing the shear strength of weakly cemented sands by just one parameter is suggested.

4.4 Selection of Soil Properties for this Study

For inorganic clay of Bangladesh the value of Liquid Limit (*LL)* rarely exceed 60% and Plasticity Index (*PI)* rarely exceed 30%. For this reason *LL*=60% and *PI*=30% has been selected for this study.

For Normally consolidated clay (after Sture, 2004): $E_u^{50} = \frac{15000 c_u}{I_p\%}$. According to PLAXIS manual for soft soil, E_u may be converted into E' by: $E' = \frac{2(1+\nu')}{3} E_u$ where $\nu' \leq 0.35$. From data presented by Serajuddin and Chowdhury (1998) for soft high plastic (CH) clay c_u = 12kPa, E_u^{50} = 6000 kPa and E' =5000 kPa have been used.

Sorensen K.K., and Okkels N. (2013) provided correlation between drained shear strength and plasticity index of NC clay as ϕ'_{NC} (deg) = 43–10log *PI* (deg). For *PI*=30% this correlation gives as ϕ'_{NC} = 28°. A value of 24° for Bangladeshi soft clay has been considered and used in this analysis.

Drained cohesion of sand and NC clay is zero. PLAXIS does not allow a zero value of drained cohesion and for that a unit value 1.0 kPa for these parameters have been used.

Serajuddin and Ahmed (1967) provided correlation for C_c of Plastic Silt and Clay of different area of Bangladesh which is, C_c = 0.0078(*LL*– 14). According to this correlation for *LL*= 60% we get C_c near to 0.35.

Soil with low density or high void ratio undergoes larger settlement. As shown in Table 4.5 the void ratio for inorganic clay of Bangladesh is as large as 1.463. Liquid limit is the mineralogical properties of a soil while the void ratio is a measure of density and may very keeping the liquid limit fixed. For this reason variable void ratio with fixed Liquid limit have been used in this analysis. Analysis have been carried out with four different value of void ratio and these are 1.00, 1.15, 1.30 and 1.45.

An average value of Dry Density γ_d of soft soil of Bangladesh may be considered as 1.5 g/cm^3 or 14.70 kN/m^3 (Table 4.5) and according to the relationship $\gamma_{sat} = \gamma_d + \gamma_w \frac{e}{1+e}$ an average value of Saturated Unit Weight is 20 kN/m^3 was taken for the present study.

In calculating the consolidation settlement of NC clay Swelling Index C_s is not necessary to be used. In calculating the consolidation settlement by PLAXIS with C_s value greater than zero a Swelling or upward settlement is obtained which should not to have occurred for NC Clay. However, a zero value of C_s is not allowed by PLAXIS and for this reason a very small value of C_s = 0.001 has been used in this analysis.

4.5 Problem Definition

A schematic diagram of the problem is defined as shown in Figure 4.4. The soil is considered as a two layer system. The top layer is a sand layer of thickness H_i. The bottom layer is a homogenous soft clay layer with effective shear strength parameters c' and ϕ'. The footing is of width B=2.5 m and is placed in the sand layer. The length of the finite element model is 7B, and the depth of clay layer is 6B. The size of the finite element model is taken as sufficiently large to avoid boundary effect so that there will be no deformation of ground at the model boundary due to footing pressure.

4.6 Material Properties Data for Analysis of The Problem

The bearing capacity of soil depends on strength parameters c'_{ref} and φ'. The soils were modeled with three material models – Hardening Soil (HS) Model, Soft Soil (SS) Model

and Soft Soil Creep (SSC) Model. The HS model is used to simulate the untreated and cement treated sand layer and the SS and SSC model is used to simulate clay layer. The input parameters used in different models are represented in Table 4.10 & Table 4.11.

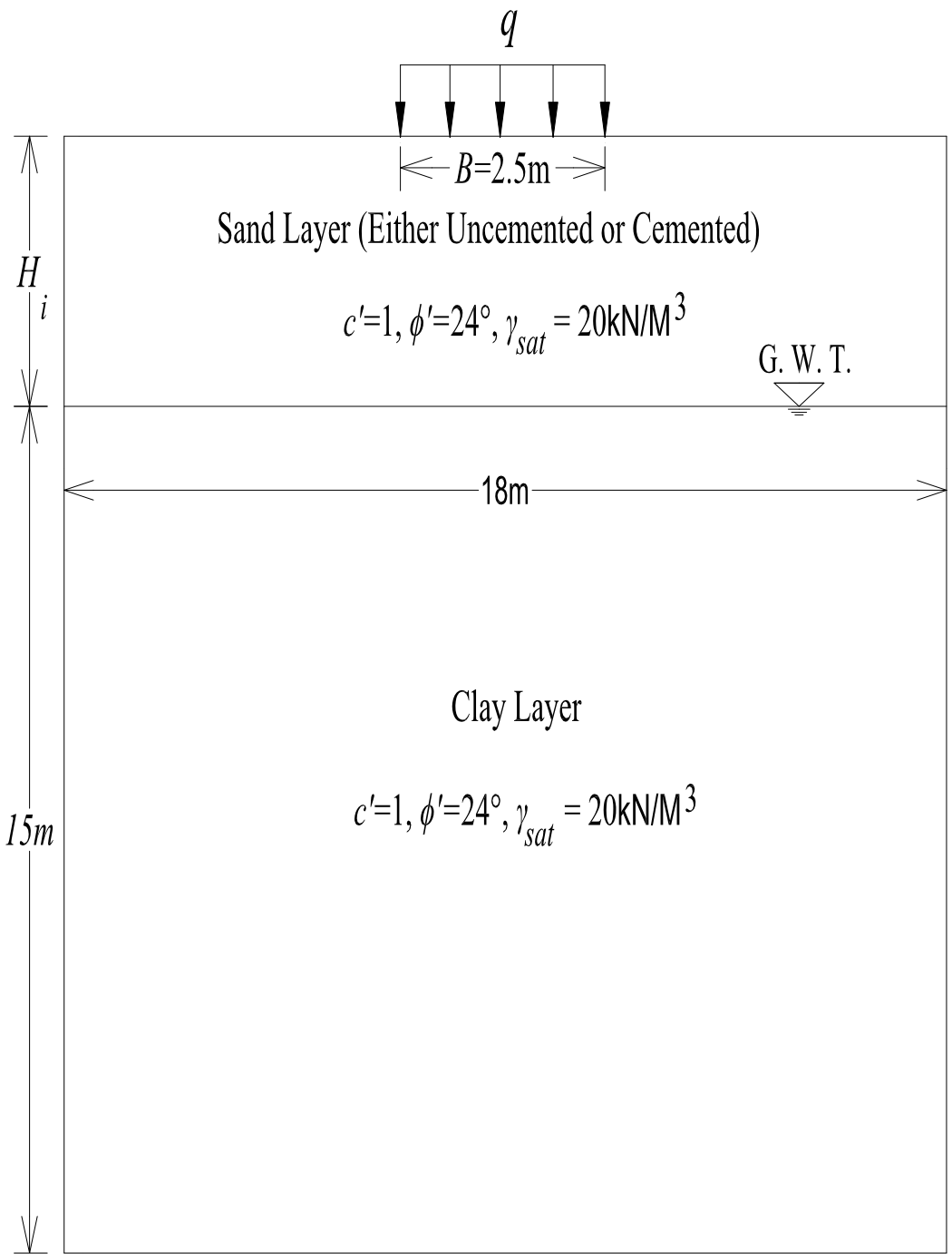

Figure 4.4. Schematic diagram of the problem.

Table 4.10. Material set input parameters for the lower clay layer

Parameter	Material Set			Unit
	Clay (Elastoplastic Stage)	Clay (Consolidation Stage)	Clay (Creep Stage)	
Material model	HS	SS	SSC	-
Drainage Condition	U	U	U	-
Poisson's Ratio, ν' (Note: PLAXIS required value)	0.2	0.15	0.15	-
Saturated Unit Weight (below phreatic level), γ_{sat}	20	20	20	kN/m^3
Unsaturated Unit Weight (above phreatic level), γ_{unsat}	15	15	15	kN/m^3
Drained Cohesion, c'_{ref}	1	1	1	kN/m^2
Drained Friction Angle, ϕ'	24	24	24	degree
Dilatancy Angle, ψ	0	0	0	degree
Initial Stress, K_0=1-sin ϕ'	0.593	0.593	0.593	-
OCR	1	1	1	1
Interface Reduction Factor, R_{inter}	1	1	1	-
Horizontal Permeability, k_x	1.0E-4	1.0E-4	1.0E-4	m/day
Vertical Permeability, k_y	1.0E-4	1.0E-4	1.0E-4	m/day
Triaxial Stiffness, E_{50}^{ref}	5000	-	-	kN/m^2
Oedometer Stiffness, E_{oed}^{ref}	4750	-	-	kN/m^2
Unloading/Reloading Stiffness, E_{ur}^{ref}	15000	-	-	kN/m^2
Power, m (Note: Required for HS Model)	1.00	-	-	-
Compression Index, C_c	-	0.36	0.36	-
Swelling Index, C_s	-	0.001	0.001	-
Creep Index, C_α	-	-	0.018	-
Natural Void Ratio, e_{init}	1.00 1.15 1.30 1.45	1.00 1.15 1.30 1.45	1.00 1.15 1.30 1.45	-
U -Undrained and D -Drained				

Table 4.11. Material set input parameters for the upper sand layers

Parameter	Material Set		Unit
	Sand-I (untreated sand)	Sand-II (cement treated sand)	
Material model	HS	HS	-
Drainage Condition	D	U	-
Poisson's Ration, ν' (Note: PLAXIS required value)	0.2	0.2	-
Saturated Unit Weight (below phreatic level), γ_{sat}	20	20	kN/m^3
Unsaturated Unit Weight (above phreatic level), γ_{unsat}	18	18	kN/m^3
Cohesion(constant or variable), c'_{ref}	1	300	kN/m^2
Friction Angle, φ'	38	38	degree
Dilatancy Angle, ψ	8	8	degree
Interface Reduction Factor, R_{inter}	1	1	-
Horizontal Permeability, k_x	1	1.00E-5	m/day
Vertical Permeability, k_y	1	1.00E-5	m/day
Triaxial Stiffness, E_{50}^{ref}	5.0E+4	6.0E+5	kN/m^2
Oedometer Stiffness, E_{oed}^{ref}	4.75E+4	5.7E+5	kN/m^2
Unloading/Reloading Stiffness, E_{ur}^{ref}	1.5E+5	1.8E+6	kN/m^2
Power, m (Note: Required for HS Model)	0.5	0.5	-
Natural Void Ratio, e_{init}	0.5	0.5	-
U -Undrained and D -Drained			

Table 4.12. Material parameters for the Concrete Strip Footing

Input Parameter	Parameter Value	Unit
Material Type	Plate	-
Material Model	Elastic	-
Drainage Condition	Undrained	-
Normal Stiffness, *EA*	4.5E+07	kN/m
Flexural Rigidity, *EI*	1.35E+06	kNm^2/m
Equivalent Thickness, *d*	0.60	m
Poisson's Ratio, *v′*	0	-
Weight, *w*	0	kN/m/m

CHAPTER-5

FINITE ELEMENT ANALYSIS USING PLAXIS

5.1 Introduction

Finite Element Analysis of the strip footing on double layered soil defined in previous chapter using PLAXIS 2D including general settings, model geometry, soil element, plate element, interface element, boundary conditions, loads, mesh generating, initial condition, calculation and analysis output are illustrated in this chapter. Initial condition, initial stresses generation, different types of calculations, staged construction procedure are also explained in this chapter.

5.2 PLAXIS

A Dutch company has developed the software named PLAXIS, using the finite element method (FEM) for analysis of geotechnical problems. The software portfolio includes two and three dimensional simulation of soil and soil-structure interaction. PLAXIS incorporates three main theories in its FEM-code; deformation, groundwater flow and consolidation. In this thesis work, licensed software "PLAXIS 2D Version 8" has been used.

The program 'PLAXIS' uses the incremental tangent stiffness approach in the analysis, in which the load is divided into a number of small increments, which are applied simultaneously. For each load increment, the stiffness properties appropriate for the current stress level are employed in the numerical analysis. Concepts, methods and criteria of experimental, theoretical and numerical work done by earlier researchers were used in current PLAXIS analysis.

5.3 Elements in PLAXIS

Three types of element are incorporated in a PLAXIS Model. There are Soil element Plate element and Interface element.

5.3.1 Soil Element

There are two different soil elements implemented for soil modelling in PLAXIS 2D. Both of these are triangular elements. One of these is 6 noded triangular element having 3

stress points and other is 15 noded triangular element having 12 stress points i.e. Gaussian integration points, (Figure 5.1).

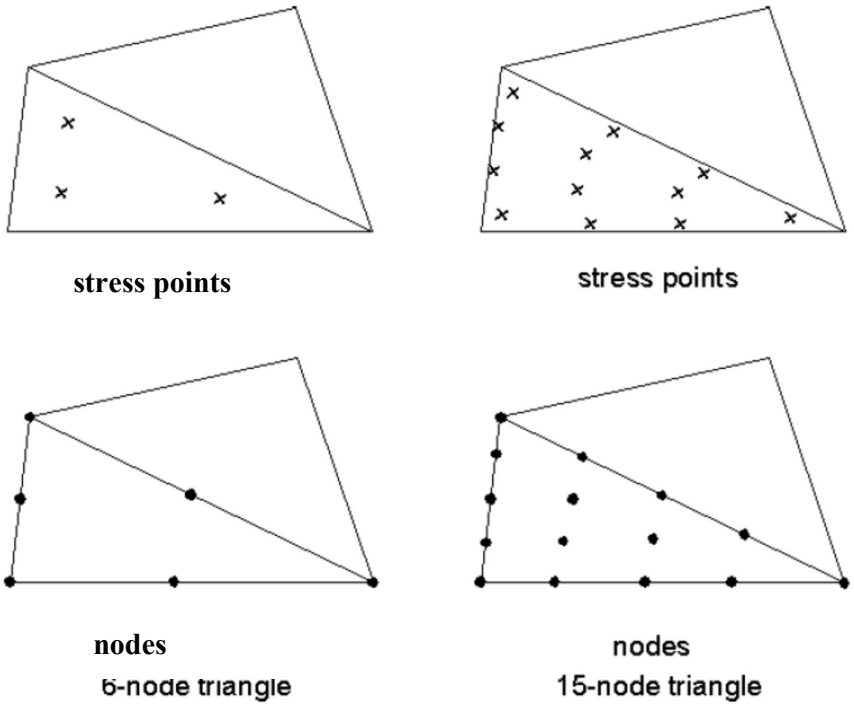

Figure 5.1 Position of nodes and stress points in triangular soil elements.

The user may select either 6-node or 15-node triangular elements (Figure 5.1) to model soil layers and other volume clusters. The 15-node triangle provides a fourth order interpolation for displacements and the numerical integration involves twelve Gauss points (stress points). For the 6-node triangle the order of interpolation is two and the numerical integration involves three Gauss points. The type of element for structural and interfaces elements is automatically taken to be compatible with the selected type of element for adjacent soil.

The 15-node triangle is a very accurate element that has produced high quality stress results for complex problems, as for example in collapse calculations for incompressible soils. The use of 15-node triangles leads to relatively high memory consumption and relatively slow calculation and operation performance. Therefore, a more simple type of elements is also available and this is the 6-node triangle. The 6-node triangle is a fairly accurate element that gives good results in standard deformation analyses, provided that a sufficient number of elements are used. However, care should be taken with axisymmetric models or in situations where (possible) failure plays a role, such as a

bearing capacity calculation or a safety analysis by means of *phi-c reduction*. Failure loads or safety factors are generally overpredicted using 6-noded elements (Plaxis Reference Manual). In those cases the use of 15-node elements is preferred. One 15-node element can be thought of a composition of four 6-node elements, since the total number of nodes and stress points is equal in both case. Nevertheless, one 15-node element is more powerful than four 6-node elements.

5.3.2 Plate element

In addition to the soil elements, compatible plate elements are used to simulate the behaviour of walls, plates and shells. The plate elements are composed of beam elements having three degrees of freedom per node. A plate element has three nodes if it is used with 6 noded soil elements or five nodes if used with 15 noded soil elements. Mindlin's beam theory is used for plate element considering deflection due to both shearing and bending and also change in length due to axial force. The input parameters for plate elements are: i) axial stiffness (*EA*), ii) bending stiffness (*EI*), iii) weight (*w*) and iv) poisson's ratio (*v)*. Elastic or elastoplastic behaviour can be chosen for plate elements. Two limit parameters namely maximum bending moment and maximum axial force are required for obtaining plastic behaviour.

5.3.3 Interface element

Interface elements are used to simulate the interaction between two materials. In FEM calculations, just one displacement is allowed in a specific node. Hence, in a node common for two elements with different material properties, one (or same) displacement must be present. Where soil meets structural elements, this is unrealistic because one expects the soil to slip and also gap relative to the structural element (e.g. a pile slipping relative to the surrounding soil due to external loads). This is achieved in PLAXIS by introducing the interface element, which has two nodes for every stress point. In Figure 5.2 interface element is illustrated, with corresponding volume element.

The interface element is described with an elastic-plastic model, where the Coulomb criterion is used. The properties of the interface element are selected on the basis of adjacent soil.

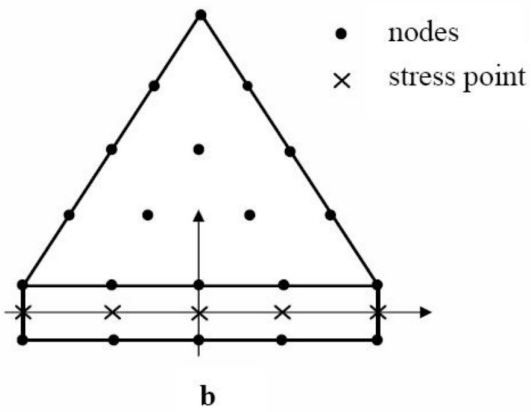

Figure 5.2 15-nodeds soil element coupled to an interface element.

The strength of the interface may be reduced (or increased) with the strength reduction factor R_{inter}, according to the relation $c_i = R_{inter}\, c_{soil}$ or $\tan(\phi_i) = R_{inter} \tan(\phi_{soil})$ where c_i and ϕ_i are the cohesion and friction angle of the interface element. According to PLAXIS R_{inter} is 0.7-0.8 for cohesive soil and 0.9 for frictional soil. *Virtual thickness factor* is used to calculate the Virtual thickness of interface elements. The standard value of the *Virtual thickness factor* is 0.1.

In a consolidation analysis or a groundwater flow analysis, interface elements can be used to block the flow perpendicular to the interface, for example to simulate an impermeable screen. In fact, when interfaces are used in combination with plates, the interface is used to block the flow since plate elements are fully permeable. In situations where interfaces are used in a mesh where they may be fully permeable, it is possible to deactivate the interface. The interface element can also be used to smooth the mesh around areas with high stress and strain gradient (e.g. sharp edges in stiff materials). Standard volume elements have difficulties to produce physical stress oscillation in such areas. Smoothening is created by applying interfaces around the area and activating them during mesh generation, during calculation however these may be deactivated.

5.4 Finite Element Model in PLAXIS

PLAXIS Version 8 may be used to carry out two-dimensional finite element analyses. Finite element models may be either *Plane strain* or *Axisymmetric*. Separate PLAXIS programs are available for 3D analyses. The default setting of the *Model* parameter is *Plane strain*.

While a three-dimensional finite element analysis is frequently used in structural or mechanical applications, it is rarely used in geotechnical engineering. There are two types of geometry models in PLAXIS 2D named i) plane strain model and ii) axisymmetric model shown in Figure 5.3. Most of the geotechnical problems can be assumed to be either 'plane strain' or 'axisymmetric' without significant loss of the accuracy of the solution (S. Springman, 2014).To carry out each finite element analysis using the PLAXIS 2D program, a two dimensional geometry model has been created composed of points, lines and cluster (area), in the X-Y plane and specify the material properties and boundary conditions. Also some general assumptions with regards to material behaviour, stress states, geometry and parameter selection must be made.

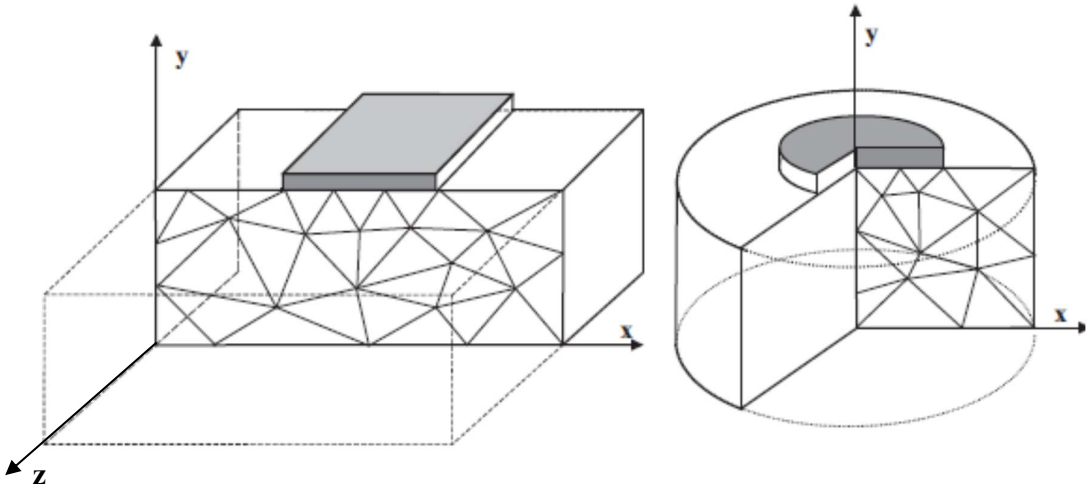

(a) (b)

Figure 5.3 (a) Plane strain, (b) Axisymmetric model (Brinkgreve et al., 2011).

An elongated footing foundation which support load bearing walls or a single row of columns are generally referred to as strip footings. The characteristic feature of a Plane Strain 2D Analysis (Figure 5.3a) is the dimension along the z-axis is considerably very large compared with the other two dimensions. Hence, loads and boundary conditions are independent of the largest dimension. As a result, the strains in the direction of z-axis are considered to be zero. Therefore, we only have to solve for strains in the x-y plane and the problem reduces to a plane strain problem. For plane strain problems, the numerical integration is performed for a unit section (1 unit length) along the z-axis.

If it is considered that the shallow foundation has a width B and a length L and B/L is equal to zero (that is, $L = \infty$), a plane strain case will exist in the soil mass supporting the foundation. For most practical cases when B/L =1/5 to 1/6, the plane strain theories will

yield fairly good results. Typical examples of plane strain geotechnical problems are continuous strip footings, retaining walls, long straight tunnels and mines.

5.5 General Settings of Input in Analysis with PLAXIS

In starting the analysis the general settings window was used to create the geometry and the element type and the dimensions are selected in it. The general model used is plane strain, the elements used in the model are 15-noded triangular elements, the gravity angle is -90^{o} and gravitational constant is 9.8 m/s^2.

The plane strain model has been chosen here, because the model has a uniform cross section and corresponding direction of vertical stress and loading are perpendicular to the cross section and it is assumed that the strains and deformations in the z-direction which is normal to the cross section are zero but normal stresses in that direction are taken into account.

An optimum size of geometry has been chosen because too large size of geometry leads to a major computational effort. Besides, the results given on distant points may be not relevant, since these are out of the influence range. On the other hand too small size of geometry may lead to wrong results, as these are under the influence of the boundary conditions.

After specifying the model type, and dimension the general procedure when modelling in PLAXIS is to; define the geometry with elements and corresponding materials, define loads and boundary conditions, create a FEM-mesh, define the initial condition, perform the FEM-calculation.

5.6 Creation of Geometry

The generation of a finite element model begins with the creation of a geometry model, which is a representation of the problem of interest. A geometry model consists of points, lines and clusters. Points and lines are entered by the user, whereas clusters are generated by the program. In addition to these basic components, structural objects or special conditions can be assigned to the geometry model to simulate tunnel linings, walls, plates, soil-structure interaction or loadings.

5.7 Boundary Conditions

After creating geometry and assigning material properties, boundary conditions have to be assigned to do the calculation of the problem. For current analysis the "standard fixities" option has been used as boundary condition which is commonly used in many geotechnical problems and this is quick and comfortable. This boundary type restrict both horizontal and vertical displacements to zero at the bottom boundary and horizontal displacements to zero at the side boundaries.

5.8 Loads

After assigning boundary conditions specific load have to assigned to the geometry model. Two types of load can be applied in PLAXIS, i.e. distributed load and point load, and these may be applied in *x*- and *y*-direction. Since the model is two dimensional, the point load is in fact a one meter line load in the out-of-plane direction, in kN/m. Likewise, the distributed load is applied over one meter in the out-of-plane direction, in kN/m^2.

5.9 Mesh generating

PLAXIS has implemented an automatic mesh generator developed by Sepra (Ingenieursbureau Sepra, Park Nabij 3, 2267 AX Leidschendam (NL)). This mesh generator generates an unstructured mesh with the chosen type of element such as 15-node element. The user can choose from five different coarseness of the global mesh and can also make the mesh finer in local parts of the model. The latter option is a convenient way to ensure sufficient elements in parts exhibiting great stress and strain gradients, without creating a heavy (i.e. time consuming) mesh.

The division of the finite element domain in which to perform the subsequent calculations is the discretization of the problem and is represented by the mesh. At first the mesh is generated by using a coarse mesh (few elements). Then, points or areas with concentrations of stress are found, or strain or phenomena where better accuracy is desired are identified. The global mesh of the model in these areas is adjusted to take into account possible local phenomena, maintaining a certain balance with the time consuming calculation. Fine mesh has been provided at surrounding location of footing plate for better accuracy of results and the coarseness has been increased gradually at distant location.

5.10 Initial Condition in PLAXIS

Prior to the main calculations in PLAXIS, the initial condition of the soil has been determined. This includes calculating both the initial effective stress-state and the initial water pressures in the soil. In PLAXIS the initial water pressures can be generated in two manners, either directly from the phreatic level or by a steady state groundwater calculation. In both methods the user must define the phreatic levels and in the latter it is possible to prescribe the groundwater head or discharge (only possible to set the discharge to zero). The groundwater calculation is based on the finite element method and uses the generated mesh, the permeability of the soil and the boundary conditions to calculate the water pressures. Closed consolidation boundaries are set at the sides and at the bottom boundary and an open consolidation boundary is set at the top of the geometry.

Defining the initial conditions has been done to assign the history of the soil (through assignment of proper overconsolidation ratio, *OCR* or pre-overburden pressure, *POP*), the soil water conditions (steady state) and if relevant the influence of existing constructions. The initial conditions within the ground (K_0, *OCR/POP* parameters, water conditions etc.) are considered when using non linear constitutive models for the soil. After developing the geometry of the model, initial situation and initial stress state has been stated. This was done in the initial conditions part of the input program. The elements that are not active in the initial situation has been deselected. Initial stresses are developed by the K_0-procedure.

The initial condition also implies the soil being at rest and no external loads and the vertical stresses are therefore calculated using the soils unit weight. At the initial moment, the stress state is characterised by a vertical effective stress (σ'_{v0}).The horizontal stresses are therefore calculated using the at-rest coefficient of lateral earth pressure, i.e. K_o. The default value of this coefficient is $K_o = 1 - \sin\phi$ (Jaky's formula), but could also be chosen by the user. K_0^{NC} is the K_0 -value associated with normally consolidated states of stress. For the Hardening-Soil model the default parameter settings is same as the Jaky formula. For the Soft-Soil-Creep model, the default setting is slightly different.

5.11 Initial Stress Generation

When setting the initial stresses the program by default switches off all the different elements to the soil type prior to any action. At all times it has been assumed normally consolidated soil represented by a zero value of *OCR* (overconsolidation ratio) and *POP* (pre-overburden pressure) parameters corresponding to the degree of overconsolidation and preconsolidation pressure respectively.

The at-rest coefficient may be introduced manually, and then assigned to each cluster. Otherwise, the program automatically introduces a value of the coefficient calculated from Jacky's formula. After this step, the initial stresses are generated in the model (Figure 5.4).

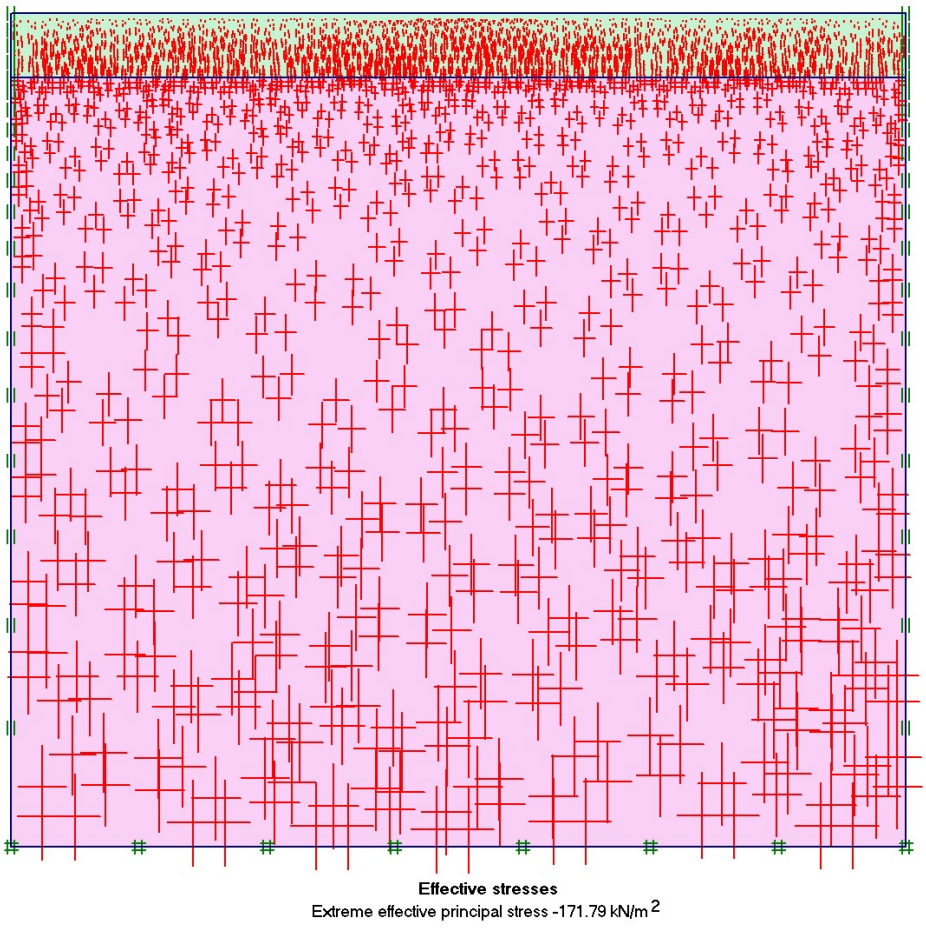

Figure 5.4 Initial effective stresses (Extreme effective principle stress at bottom)

The initial stresses in a soil body depend on the weight of the material and the history of its formation. In normally consolidated soils, K_0 is constant and depends on the soil friction angle. When introducing manually the value of K_0, the program PLAXIS warns of selecting very high or very low K_0-values, since this values may cause initial plasticity.

5.12 Material Models and Allowable Drainage Types

PLAXIS analysis with both Drained and Undrained behavior of soil is not possible in all Material model. The Material Models and Material Types available in PLAXIS are presented in Table 5.1.

Table 5.1. The Material Models and Material Types available in PLAXIS

Material model	Material type
Mohr-Coulomb model	Drained Undrained (A) Undrained (B) Undrained (C) Non-porous
Hardening Soil model HS small model	Drained Undrained (A) Undrained (B)
Soft Soil model Soft Soil Creep model	Drained Undrained (A)
A, B, C means different type of undrained analysis as per PLAXIS 2D-Version 8 - Manual	

5.13 Deciding When to Use Which Model

When the material at hand is a granular one and the pore pressures dissipate quickly relative to the speed of loading, the added load is carried by the soil skeleton and not pore pressures. Such a situation is better described as a drained one and effective stresses should be used in the analysis. On the other hand when loading a saturated material that does not allow the porewater to dissipate quickly compared to the speed of loading, the load will be carried by the pore pressures rather than the soil skeleton and the situation is better described using undrained analysis.

The key considerations in selecting material model are the speed of loading and the mediums ability to release porewater and transfer the added stress to its skeleton. The two methods are different but are connected by a process called consolidation. Consolidation is the time dependent process of pushing the porewater from the soil and thus transferring the excess pore pressures caused by the added loading to the soil skeleton. Because water can be assumed as incompressible in comparison with soil, this process will control the rate of the primary settlements after the load has been added.

5.14 Calculations

When the geometry is set, the material properties to all clusters from the data sets are defined, the drainage conditions are assigned to impermeable layers and the initial condition is calculated by K_0 procedure. This is the first calculation phase (initial phase). After the initial conditions, the main finite element analysis is performed. There are different types of calculations available in PLAXIS 2D, e.g. Plastic calculation, Consolidation analysis, Phi-c reduction and dynamic analysis. Additionally updated mesh analysis is used in this dissertation to account large displacements. The different calculation types are presented here.

5.14.1 Plastic Calculation

'Plastic calculation' process is used for calculation of elastic-plastic deformation. It is used when failure and stability of the object are analysed. Plastic calculation does not account for the time dependent decay of excess pore pressure, and is therefore not appropriate when analysing settlement in low permeable soil. On the other hand, plastic calculation type could be used when calculating settlement in highly permeable soil or when the final settlement of a structure is calculated.

5.14.2 Consolidation Analysis

The consolidation analysis is used in PLAXIS 2D when it is necessary to evaluate the development or dissipation of excess pore water pressure in water-saturated clay-type soils as a function of time. Consolidation settlement (or primary consolidation settlement) happens when an increase in the effective vertical stress occurs which gives rise to a decrease in the volume of the voids. If the soil is saturated (S_r =100%) reduction in volume occurs only if some of the pore water is squeezed out of the soil. The volume of solids remains constant because the compression of individual particles is negligible. (Coduto, 1999). PLAXIS allows for true elastic-plastic consolidation analyses. It is possible to consolidate with and without additional loading. In general, a consolidation analysis without additional loading is performed after an undrained plastic calculation. It is also possible to apply loads during a consolidation analysis. However, care should be taken when a failure situation is approached, since the iteration process may not converge in such situations. It is possible to apply construction stages in time using a consolidation

analysis. Moreover, consolidation analyses can be performed in the framework of large deformations.

Water-saturated soil must drain water to develop settlement (due to water's incompressibility). In low permeable soil, such as clay, this is a time-consuming process and it is important to account for this process when analysing settlement. That is accounted in the consolidation calculation. Hence, this calculation type is suitable for analysing time-dependent settlement for water-saturated and low permeable soil. Here, the important parameter is not the drainage type of the material set but rather the permeability parameters specified.

5.14.3 Phi-c Reduction (Safety analysis)

Phi-c reduction is a safety analysis in PLAXIS which is desired in a calculation of the safety factor. *Phi-c reduction* is not in the scope of this research work.

5.15 Staged Construction

A construction is, in practice, made in stages or phases. To resemble and simulate this, the calculation process in PLAXIS 2D is also divided into phase or stages that are called calculation phases. This is mainly to avoid failure during construction and to simulate excavation processes. The first calculation phase is always the earlier defined initial condition. After the initial phase adequate number of phases could be added according to the planned construction process. It is also possible to modify or change the material parameter data and the water condition and to activate or deactivate loadings, soil clusters and structural objects and also to change pre-stress anchors.

5.16 Iterative Settings

5.16.1 Desired Minimum and Desired Maximum

The iterative parameters 'Desired minimum' and 'Desired maximum' are primarily meant to determine when the calculation should take larger steps or smaller steps. For a Plastic analysis or Safety analysis there is no influence on the results when changing the Desired minimum or Desired maximum. As long as the calculation converges in every step it (changes this parameters) is unimportant if the calculation uses a lot of small steps with few iterations or a limited amount of larger steps with more iterations per step.

For a consolidation analysis, however, there is a small influence. In a consolidation analysis during a load step (time step) water flows out of the soil, and generally the flow is slightly higher at the beginning of the step than at the end of the step. This means that on average the flow rate (constant within the step) during a time step is slightly underestimated, leading to a slightly higher consolidation time for calculation. With larger steps this effect is bigger than calculation with smaller steps.

In practice, when a consolidation analysis takes several hundred steps, the influence on the consolidation time will be very small. However, for very specific cases where consolidation analysis only takes few steps, for instance when modelling laboratory tests on high permeable soils, there may be an influence of several percent. In that case lowering the Desired minimum and Desired maximum in order to force the calculation to use smaller steps will improve the results.

A more common reason to change the Desired minimum and Desired maximum in a consolidation analysis is the calculation time. In a consolidation analysis the stiffness matrix depends on the time step and so the time step must be know before composing the stiffness matrix. For almost any calculation step a new stiffness matrix has to be made, which is very time consuming. In this case slightly increasing the Desired minimum and Desired maximum can cause the calculation to change step size less frequent, which may give a significant improvement to the calculation speed.

5.16.2 Arc Length Control

During the calculation if the load to be applied is larger than the failure load then calculation would try to apply the load defined by the user over and over again without converging to a solution as the load can simply not be applied. When using the arc-length control the calculation will in fact accurately find how much of the load can really be applied. In principle using arc-length control or not makes no difference for the result of the calculation if no failure occurs. Without using arc-length control the failure load is overestimated typically in a Safety factor determination (phi/c reduction). Since arc-length control is meant to determine failure accurately, it’s recommended to always do Safety analysis with arc-length control.

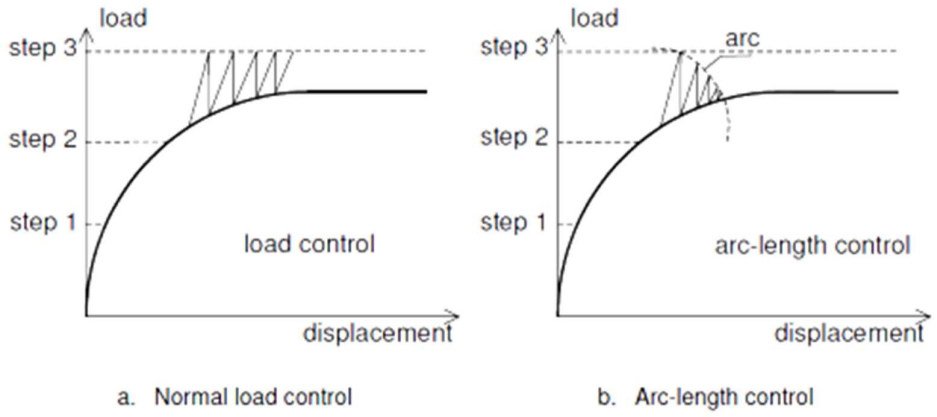

Figure 5.5 Arc Length Control

Additionally, in PLAXIS the use of arc-length control (Figure 5.5) is combined with an automatic failure detection which says that if in 5 successive calculation steps the applied load has to be decreased in order for the calculation to converge, failure is assumed and the calculation stops. Without arc-length control there is no automatic failure detections. By using arc-length control it is possible for the calculation to determine accurately how much load is really applied from a load step determined by the user. This implies that the calculation won't know how much load is really applied until the calculation has converged. For a plastic calculation this is fine, but for consolidation this is a problem. Arc-length control cannot be used for a consolidation analysis.

5.17 Calculation Types in Consolidation Analysis

There are three calculation options for a consolidation analysis in PLAXIS:

In Staged construction we set the time interval and we can activate/deactivate soil, structures and loads, or change load values.

In *minimum excess pore pressure*, setting of time interval and I activating/deactivating of soil, structures and loads are not included. These settings are kept the same as the previous stage while the calculation continues until the maximum (absolute) value of the excess pore pressure is below the specified value for the excess pore pressure, |P-stop|. One of the results is then the time it needs to consolidate. The value of *Minimum excess pore pressure* value has been used is 1 kN/m^2 in all analysis during this research work.
The calculation was stoped when the maximum absolute excess pore pressure is below this value of *Minimum excess pore pressure*.

5.18 Manually Controlling Load Stepping

A special option to control the load advancement scaling (size of the step) exists for setting these desired minimum and maximum values to specific values. When the desired minimum is set to 2 and the desired maximum to the maximum iterations, there will be no scaling up or down and a constant load step for each step can be seen. The initial load step size can be controlled using a Incremental Multipliers phase. With arc-length control, the actual load step may be smaller. For plastic calculations with arc-length control, the load steps may differ in size a bit.

5.19 Delete Intermediate Steps

This option is by default selected to save disk space. As a result, all additional output steps within the calculation phase, except for the last one, are deleted when a calculation phase has finished successfully. If desired, the option can be de-selected to retain all individual output steps. This enables a stepwise evaluation of the cause of the problem.

5.20 Calculation and Result

A nodes or stress point has been selected at midpoint of footing before start of calculation to get deformation output at that point which is settlement at center point of strip footing. Stage construction option has been used that allows change of material sets of a cluster to simulate ground improvement. Phase wise calculation details is discussed later. Updated mesh analysis required has been used large deformation problems of soft soil. Input value of load has been changed and activated/deactivated according to requirement. Footing plate has been activated/deactivated in earlier phases (natural condition). Material data set has been reassigned (in a set material properties is not possible to be changed during calculation stages) to clusters to simulate its appropriate condition in different phases during various stages of construction. Automatic load stepping and load advancement was allowed. Additional load step was needed. Calculation phases was selected by double clicking on each for calculation and this selection is indicated by blue arrow '→'. When the calculations are finished, PLAXIS supplies the user with several different illustrations of the stress and deformation distribution. This is done in two different programs called Output and Curves. The Output program illustrates the stress and deformation distribution by arrows, contour lines or shades. The user is also provided with the final stresses and deformation for all nodes in tables. In the Curves program the user is provided with curves and tables of the variation of displacement in specific points

(chosen by the user). No 'numerical difficulties' are found near the point of minimum displacement. In calculating each case, the maximum number of iterations was never reached and the accuracy condition was fulfilled.

5.21 2D Modeling of Strip Footing on Sand Layer over Clay Deposit

The aim of this research is to analyze a strip footing on a sand layer underlain by clay using advanced soil models in the two-dimensional finite element program PLAXIS 8.0. The Advanced soil model, that is, Hardening Soil Model, Soft Soil Model, Soft Soil Creep Model are used as a material model for simulation in this thesis.

PLAXIS 8.0 is used to calculate the settlement of plate as shallow footing or foundation. During the modeling in PLAXIS, various trial analyses are performed to assess the model behavior. A natural clay deposit of 15m thickness and 18m width has been used. A cement treated or untreated compacted sand layer of varying thickness is considered over the natural clay deposit. A 2.5m wide concrete strip footing is installed at the center of top surface of the sand layer. Ground water level is at top level of clay deposit that make this fully saturated. Uniformly distributed vertical load of varying value is applied to the strip footing. A lots of analysis of this foundation system has been carried out using PLAXIS 8.0 to get a better understanding of the primary and secondary settlement.

The displacements are prescribed to zero in both x- and y-direction in the bottom and only in the x-direction at the sides. The width of the model is chosen so that the boundary conditions did not introduce constrain, this was controlled by observing a normal shear stress distribution at the boundaries. The clusters were arranged so that the provision of artificial sand layer could be simulated, using a staged calculation. This cluster's thickness is changing from 0.0 to 2.0 m by 0.25 m and a set of calculations is performed for each thickness. Three different elements are present in the model; 15-node element for the soil clusters, plate element for the strip footing and interface element for the interaction between the soil and structural elements.

5.21.1 Model Geometry and Load

Distributed load has been applied in *y*-direction only. Loads were activated firstly in the second plastic calculations phase and secondly in the creep calculations phase.

5.21.2 Material Model

The material model, drainage condition and material properties parameters used in different cases are given in Table 4.10 and Table 4.11. Only the effective soil parameters are used in both types of material drained or undrained. Too large or too small values of E may cause numerical problems. A Poisson's coefficient (ν) of 0.3 has been adopted, which is suitable for drained conditions. Usually this value is adopted for drained soils, when variations in the volume are significant. Alternative stiffness parameters are automatically calculated from the Young modulus and the Poisson's ratio.

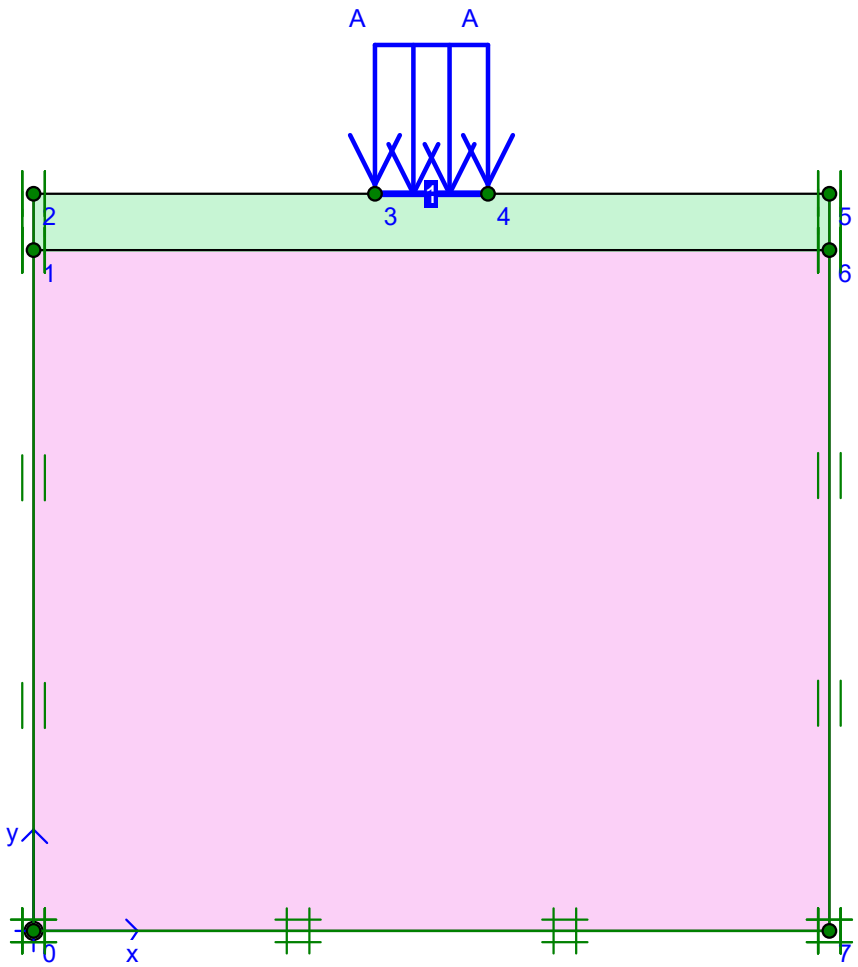

Figure 5.6 PLAXIS Model Geometry.

5.21.3 Material Sets for Plates

Material type for plate element has been selected "elastic" for all the cases analysed. This selection simplifies the calculations and is in accordance with the reality, since strip footings are designed to have an elastic response. Material properties parameters have

been given in Table 4.12. Weight (w) is obtained by multiplying the unit weight of the plate material by the thickness of the plate. Therefore, it has units of force per unit area. For thin and flexible structures a Poisson's coefficient (ν) of value of zero is recommended for the direction normal to the plane.

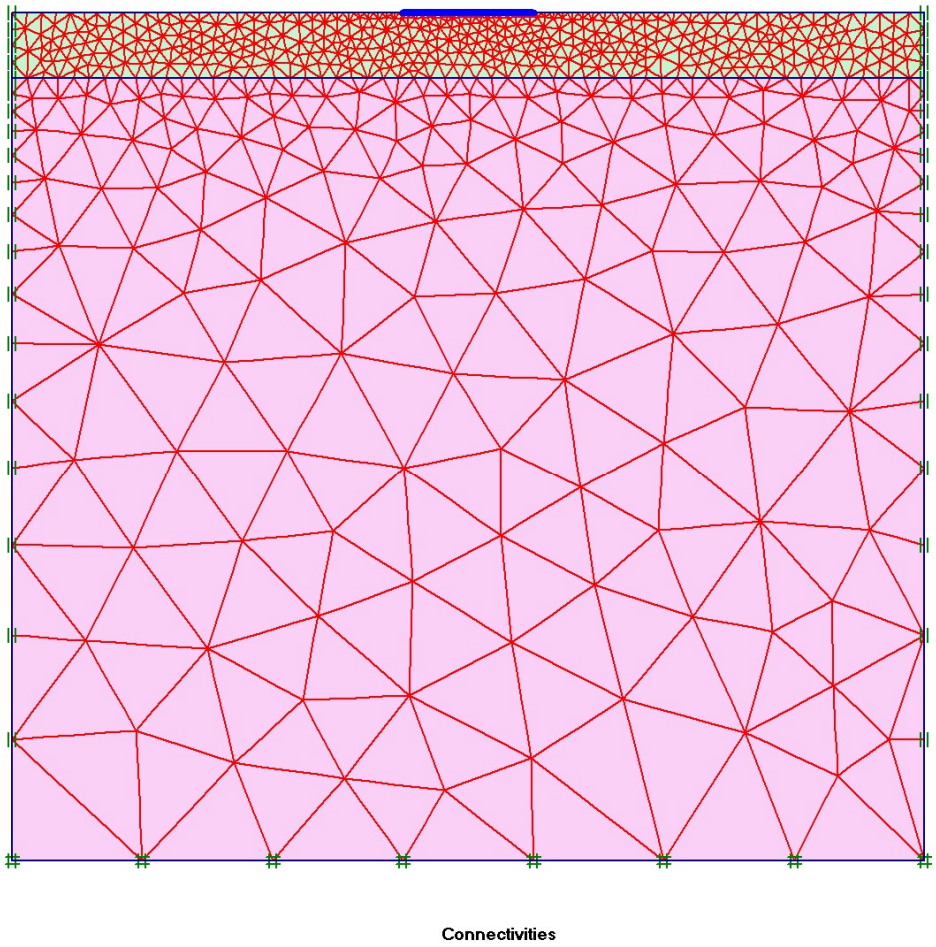

Figure 5.7 Finite element (FE) mesh for the geometry model.

5.21.4 Modelling Strip Footing

Strip Footing has been modelled through the element "plate". Plates are geometrical lines as well. The beam element has three degrees of freedom per node and has three respective five nodes when used with 6 noded volume elements and 15 noded volume elements. Elastoplastic behaviour has been chosen which requires two limit parameters for which plastic behaviour occurs, i.e. maximum bending moment and maximum axial force. The equivalent plate thickness is calculated through the following transformation: $d_{eq} = \sqrt{12\frac{EI}{EA}}$ and the data for plates is summarised in Table 4.12.

5.21.5 Mesh Generation

To carry out a finite analysis using PLAXIS, a finite element mesh has been generated (Figure 5.8) and the material properties and boundary conditions are specified. To set up a FEM, geometry model composed of points, lines and other components has been created in the XY-plane for PLAXIS 2D.

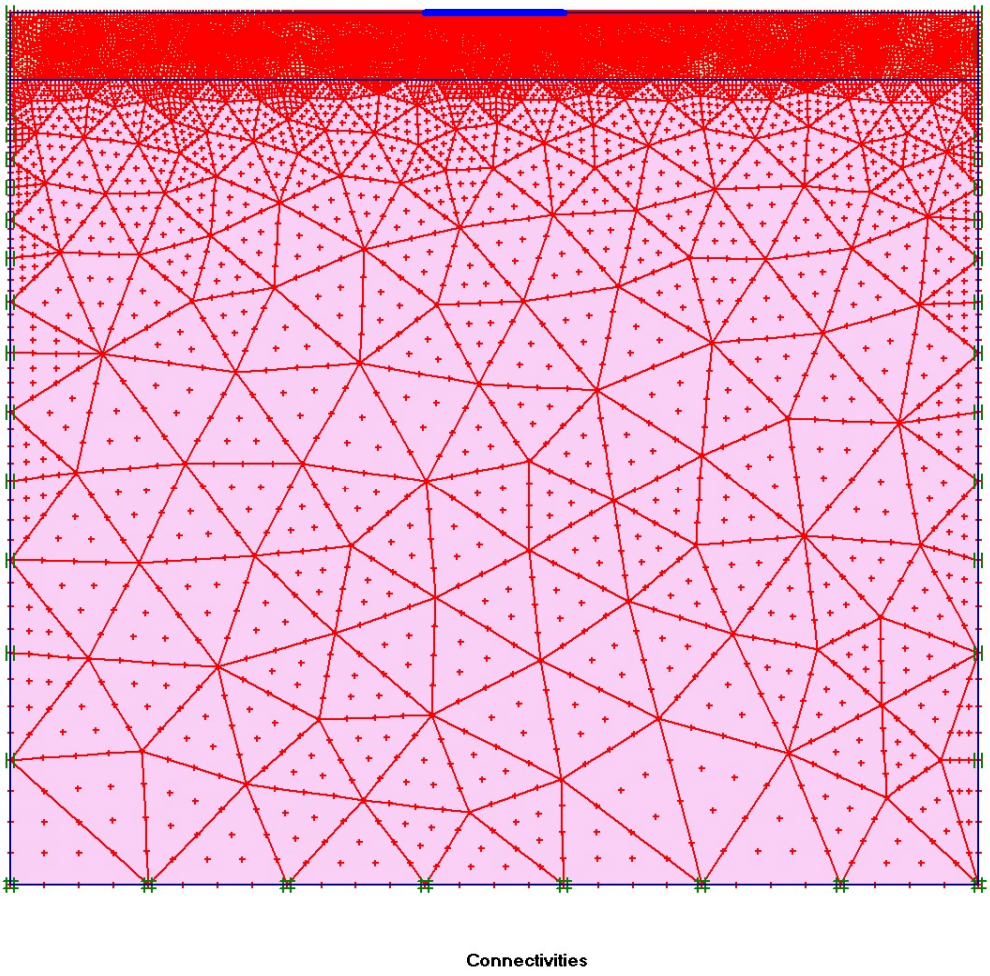

Figure 5.8 Finite element mesh with stress points for the geometry model.

The elements requiring special attention such as strip footing, which have demanded greater precision of the results for further analysis, the mesh is refined by local refinement factor that reduces the size of the elements in proportion to the value introduced. In general, the overall level of refinement type is "fine" with a local refinement in displays. The mesh was defined as coarse and refined upper sand cluster and refined further around the Concrete strip footing, as large stress gradients are expected there. The same mesh was used in all models.

5.21.6 Initial Condition

The initial stress-state was calculated with the K_0-procedure and the initial water condition was calculated by the direct method, using the phreatic level. The phreatic level (groundwater table) is at the top surface of clay later. For this calculation plate and load elements were deactivated. In the initial conditions, the hydrostatic pore water pressures are based on a general phreatic level. For the consolidation analysis, closed consolidation boundary has been chosen at the left and right side of the geometry (two vertical boundary). The bottom horizontal boundary is automatically closed consolidation boundary and the top of the geometry is kept open for consolidation.

5.21.7 Calculation

Soil is considered a two-phase material consisting of soil skeleton and pore water. First the stress increases and immediate deformations are computed using an elastoplastic plane strain analysis assuming no drainage. Resulting excess pore pressures are calculated by the computer code from the volumetric strains assuming saturated conditions. This is followed by the consolidation stage based on Biot's theory providing the dissipation of excess pore pressures and the resulting consolidation settlements. The calculation was performed as a plastic and consolidation calculation and with standard and manual settings for the iterative procedure.

In an updated mesh analysis the finite element mesh is updated after every displacement increment, so that every nodal point (x, y) will be updated to a new coordinate ($x+\Delta x, y+\Delta y$). The 'Updated mesh analysis' was chosen for all phases, as large deformations were expected. In such a case the traditional stress-strain relation will not be accurate. 'Updated water pressure analysis' was used for strip footing for lowering of water head. Period of secondary compression is 10 - 30 years. *'Ignore undrained behavior'* has not been selected with *K_0 -procedure*. PLAXIS distinguishes between drained and undrained soils to model permeable sands as well as almost impermeable clays. Excess pore pressures are computed during plastic calculations when undrained soil layers are subjected to loads.

5.21.8 Calculation Phases

Each calculation is carried out with an initial phases and three subsequent phases which are described below:

Initial phase: This phase is an initial stage of calculation and this incorporates the initial conditions defined earlier.

Phase 1: This phase is strip foundation on a sand mat underlain by natural clay deposit. In this phase the lower layer is 'Undrained Clay' (SS Model) and the upper layer is Drained Sand or Undrained Cemented Sand (HS Model). Strip footing plate and load is activated in this phase. Elastoplastic deformation of the problem geometry under assigned load is calculated in this phase.

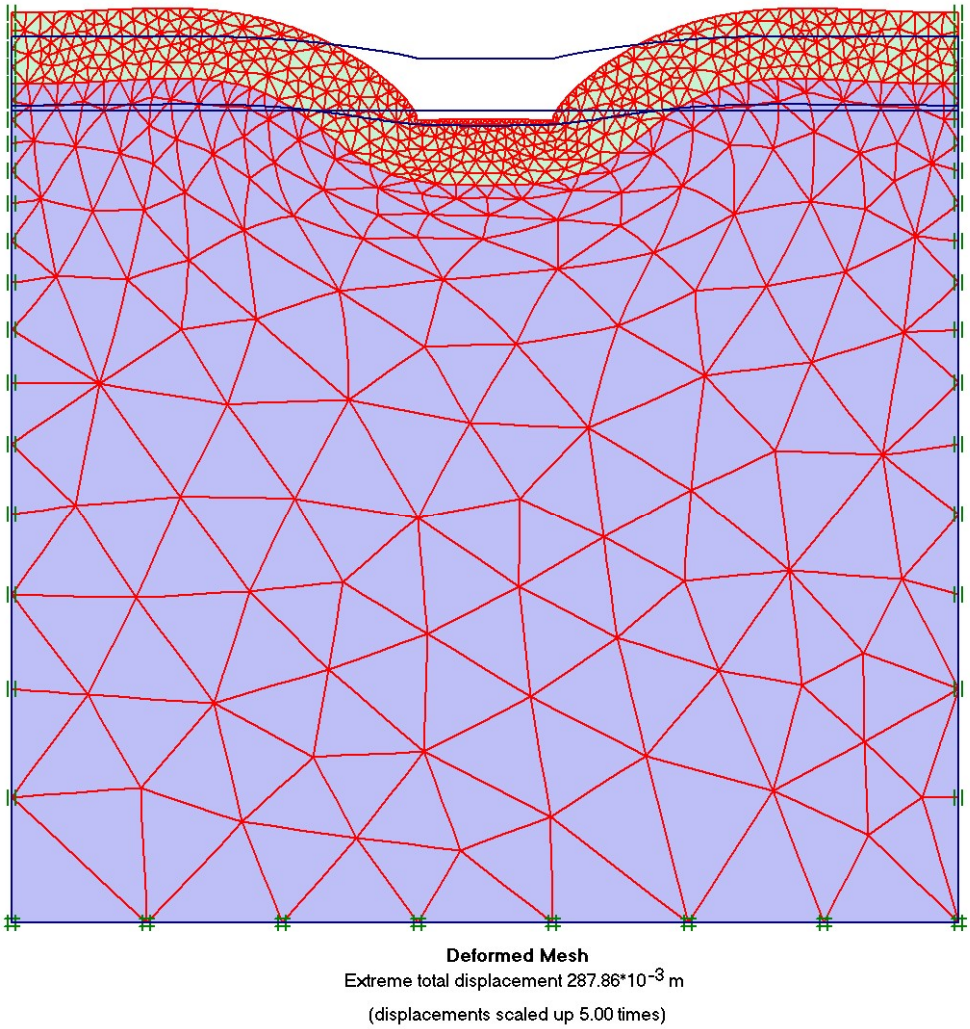

Figure 5.9 The deformed mesh for the final stage

Phase 2: In this phase the lower layer is 'Undrained Clay' (SS Model) and the upper layer is 'Drained Sand' or 'Undrained Cemented Sand' (HS Model). No additional load is activated in this phase. Deformation of the problem geometry due to consolidation under the load applied at 'Phase 1' is calculated in this phase. The consolidation settlement occurred in this phase through dissipation of pore water pressure up to a very small value which is 1.0kN/m^2.

Phase 3: In this phase the lower layer is 'Undrained Clay' (SSC Model) and the upper layer is same as 'Phase 3'. No additional load is activated in this phase. After about full dissipation of pore water pressure inter particle rearrangement or creep is occurred without application of any additional load. Creep deformation of the problem geometry under load applied at 'Phase 2' is calculated in this phase.

5.21.9 Output

After completion of calculation through above mentioned phases the 'Output Program' was run and the deformed at the end of 'Phase 4' has been recorded. A sample deformed mesh for the final stage is illustrated in Figure 5.9. The vertical displacements may be illustrated with shading.

5.22 Footing on Surface

The strip footing used in current analysis is on ground surface. The load that causes bearing capacity failure or soil body collapse of surface footing is less than that for footing embedded into ground. Consolidation settlement of surface footing is more than that of embedded footing under the same load.

5.23 Components of Settlement and Comparison with Classical Analysis

Three Components of Settlement found from PLAXIS analysis are: i) Elasto-plastic Settlement ii) Consolidation Settlement and iii) Creep Settlement. For soft inorganic soil Consolidation Settlement is the major component of total settlement and Elasto-plastic Settlement is also a considerable component. Creep Settlement is very little for inorganic soft soil compared to total settlement. Consolidation Settlement and Elasto-plastic Settlement obtained from PLAXIS analysis and calculated values of these from classical theory are presented in Table 5.2.

Table 5.2. Components of Settlement and Comparison with Classical Analysis

Footing Pressure, q(kN/m^2)	100.0	200.0	100.0	200.0	100.0	200.0
Footing Width, B(m)	2.5	2.5	2.5	2.5	2.5	2.5
Footing Length, L(m)	30	30	30	30	30	30
Sand Layer Thickness, H_i(m)	1.0	1.0	1.5	1.5	2.0	2.0
Clay Layer Thickness, H_c(m)	15.0	15.0	15.0	15.0	15.0	15.0
Consolidation Pressure at Top, ΔP_t	68.7	137.3	59.0	118.0	51.6	103.1
Consolidation Pressure at Bottom, ΔP_b	8.7	17.4	8.7	17.4	8.7	17.4
Consolidation Pressure at Mid Depth, ΔP_m	17.4	34.9	16.9	33.9	16.5	32.9
Average Consolidation Pressure, ΔP_{avg}	24.5	49.0	22.6	45.1	21.0	42.0
Depth of footing, D_f	0.0	0.0	0.0	0.0	0.0	0.0
Saturated Unit Weight, γ_{sat}	20.0	20.0	20.0	20.0	20.0	20.0
Effective Overburden Pressure, σ'_0	86.4	86.4	86.4	86.4	86.4	86.4
Compression Index, C_c	0.36	0.36	0.36	0.36	0.36	0.36
Natural Void Ratio, e_0	1.23	1.23	1.23	1.23	1.23	1.23
$(\Delta P+\sigma'_0)$	2.94	3.45	2.96	3.43	2.98	3.41
$(\Delta P+\sigma'_0)/\sigma'_0$	1.21	1.42	1.19	1.38	1.17	1.34
$Log[\Delta P/(\Delta P+\sigma'_0)]$	0.08	0.15	0.08	0.14	0.07	0.13
Consolidation Settlement,S_c(mm)	263	473	230	417	203	371
Consolidation Settlement S_c(mm)(PLAXIS)	168	311	148	272	132	245
$q= \gamma_{sat} D_f$	0.32	0.32	0.32	0.32	0.32	0.32
C_1	0.91	0.96	0.91	0.96	0.91	0.96
C_2	1.00	1.00	1.00	1.00	1.00	1.00
I_z	0.30	0.30	0.30	0.30	0.30	0.30
Triaxial Stiffness, $E_{s,sand}$(kN/m^2)	5.0E+4	5.0E+4	5.0E+4	5.0E+4	5.0E+4	5.0E+4
Elasto-plastic Settlement, $S_{e,sand}$(mm)	0.60	1.20	0.90	1.80	1.20	2.40
$H_c/(B+H_i)$	4.36	4.36	3.68	3.68	3.15	3.15
$D_f/(B+H_i)$	0.44	0.44	0.39	0.39	0.34	0.34
A_1	0.50	0.50	0.50	0.50	0.50	0.50
A_2	0.95	0.95	0.95	0.95	0.95	0.95
Triaxial Stiffness, $E_{s,clay}$(kN/m^2)	5.0E+3	5.0E+3	5.0E+3	5.0E+3	5.0E+3	5.0E+3
Elasto-plastic Settlement, $S_{e,clay}$(mm)	22.5	45.0	22.1	44.3	21.8	43.6
Elasto-plastic Settlement, $S_{e,total}$(mm)	23.1	46.2	23.0	46.1	23.0	46.0
S_{e-p}(mm) (PLAXIS)	20.0	39.0	18.0	36.0	14.0	28.0

CHAPTER-6
RESULTS OF ANALYSIS

6.1 Introduction

Parametric Study has been done using PLAXIS and the results are presented in graphical form in this chapter. Vertical displacement fields for different thickness of upper sand layer are also presented here for untreated cement treated Sand. Conclusions have been drawn on the basis of these parametric study and displacement fields.

6.2 Parametric Study with PLAXIS

The settlement of the shallow foundation resting on layered soils, with an upper untreated or treated sand layer and bottom clay layer, depends on related parameters. These parameters include the initial void ratio, e_{init}, upper layer thickness, H_i, and foundation pressure, q. In the presentation of the results, dimensionless form for a wide range of values are used to generalize their effect. Here, H_i/B is the non-dimensional layer thickness, $q/\gamma_{sat}B$ is the non-dimensional loads on strip footings, γ_{sat} is saturated unit weight of the bottom Clay layer. B is the width of strip footing which is kept constant for all the analysis done in this study. c and ϕ of natural clay deposit and ϕ of sand mat are also kept constant for all the analysis done in this study. Values of various soil properties used in analysis are represented in Table 4.10 and Table 4.11. Model geometry used in analysis is represented in Figure 4.4. In the analysis footing pressure q, sand layer thickness H_i was varied. Calculation phases that was required in the analysis by PLAXIS are described in Section 5.23.8.

From each analysis total vertical settlement at footing centre and deformation field of the subsoil was obtained from PLAXIS analyses. Analysis was done for different footing pressure q, vertical settlement S and void ratio e_{init} for different thickness of upper sand mat layer, H_i. The values of e_{init} are 1.0, 1.15, 1.3, 1.45, values of H_i (m) are 0.75, 1.0, 1.25, 1.5, 1.75, 2.0 and q (kN/m^2) are 50, 75, 100, 125, 150, 175, 200 used in analysis which are similar to foundation pressure of three to eight storied residential or commercial buildings. The values of relative depth H_i/B used are 0.3, 0.4, 0.5, 0.6, 0.7, 0.8 and 0.9 and normalizes footing pressure $q/\gamma_{sat}B$ used are 1, 1.5, 5, 2.5, 3, 3.5 and 4. Settlement (downward vertical displacement) of footing centre (midpoint of footing plate) is denoted as S when H_i (m)=0.75, 1.0, 1.25, 1.5, 1.75 and 2.0m. Analyses were

conducted by changes of the thickness of upper sand layer from 0.25 to 2.00m. Settlement at midpoint of footing plate when H_i=0.25m is S_0. It was tried to analyze the current problem without any sand mat and in this case bearing capacity failure occured before completion of application of total load. Hence, a small thickness of upper sand layer equal to 0.25m has been used which is the minimum thickness to avoid soil body collapses during application of total amount of load in a PLAXIS analysis and to get the total settlement due to that load. Sand layer thichness, H_i=0.75m or more has been used for improvement purpose of the ground. Settlement of the footing on improved ground is S and this is always less than S_0. So that, $S/S_0<1.0$. The relative settlement (S/S_o) of the center point of the footing was calculated, where S_o is the settlement for the case with H_i= 0.25m and S is the settlement for other H_i values. It is to be noted that a larger value of relative settlement S/S_o indicates larger difference of settlement between the cases of small and larger thickness of sand layer. This is the definition and significance of the term relative settlement, S/S_0 introduced by this research.

6.3 Results for Untreated Sand as Upper Layer

The results of untreated sand as upper layer are presented in Fig. 6.1a through 6.3d as plots of S/S_0 (the relative settlement) against $q/\gamma_{sat}B$, e_{init} and H_i.

6.3.1 Variation of S/S_0 with $q/\gamma_{sat}B$ for different e_{init}

Fig. 6.1 shows that for a single thickness of upper sand layer with the range of H_i used, the relative settlement, S/S_0 decreases with increase of $q/\gamma_{sat}B$ for different value of e_{init}. This decreasing rate (slope) is not constant for all $q/\gamma_{sat}B$. Effect of initial void ratio on the relative settlement is not significant.

It is observed for Fig. 6.1a through 6.1f that the relative settlement decreases at a high rate with the increase of normalized footing pressure upto a certain value of normalized footing pressure. After this particular value of normalized footing pressure, this rate of decrease of relative settlement is smaller. In general three distinct zones can be identified in the relationship of S/S_o vs $q/\gamma_{sat}B$ for different e_{init}. At left zone up to $q/\gamma_{sat}B$=2.5 the S/S_o decreases rapidly and at middle zone from $q/\gamma_{sat}B$=2.5 to 3.5 S/S_o decreasing rate of S/S_o is low and at right zone for $q/\gamma_{sat}B$>3.5 there is no decrease of S/S_o that is sand mat is no longer effective to reduce settlement. The difference of relative settlement for different

normalized footing pressure remains more or less same for different value of relative thickness of upper sand mat at right zone.

It may be noted that both S_o and S changes when footing pressure changes. For a given H_i/B , with a given increase in S_o is higher compared to the increase in S. As a result S/S_o decrease. Stated in a different way in figures 6.1a to 6.1f, a larger relative settlement means that the sand mat is more effective in controlling the settlement.

For a given thickness of sand mat and clay layer, the effectiveness of the sand mat reduces with increase of footing pressure and after a certain value of footing pressure the sand mat appears to be no longer effective. Similar observation can be made from figures 6.1a to 6.1f for all thickness (H_i = 0.75m to 2.0m i. e. H_i/B = 0.3 to 0.8) of sand layer.

For a given H_i as $q/\gamma_{sat}B$ is increased up to a value of 2.5 the relative settlement decreases indicating the effectiveness of the sand layer in settlement reduction. S/S_o may be considered as the index for the effectiveness of the sand layer.

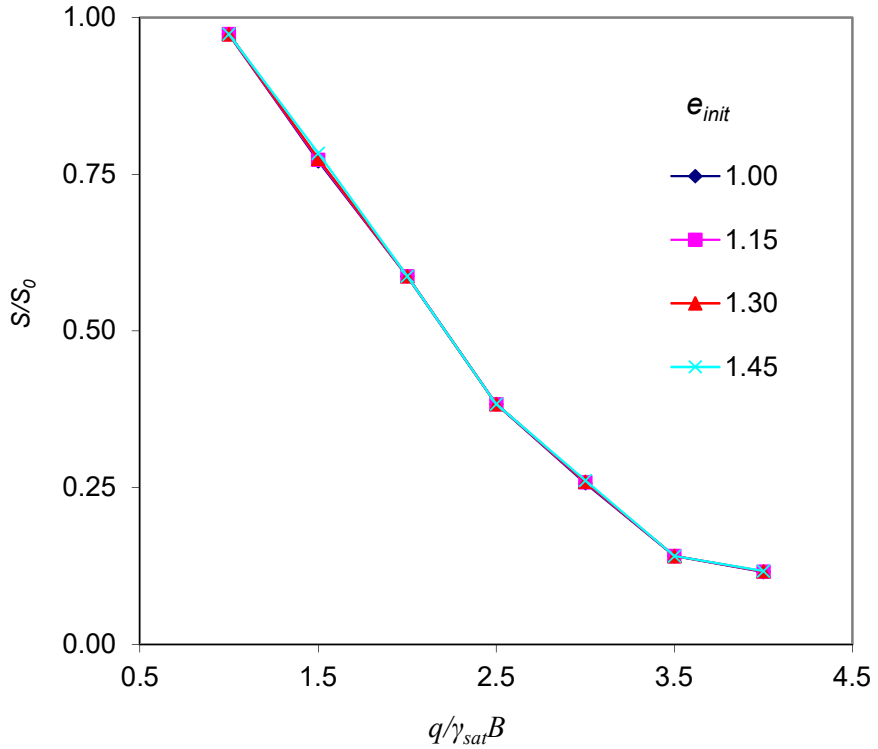

Fig. 6.1a Variation of S/S_0 with $q/\gamma_{sat}B$ for different e_{init} at H_i/B=0.30

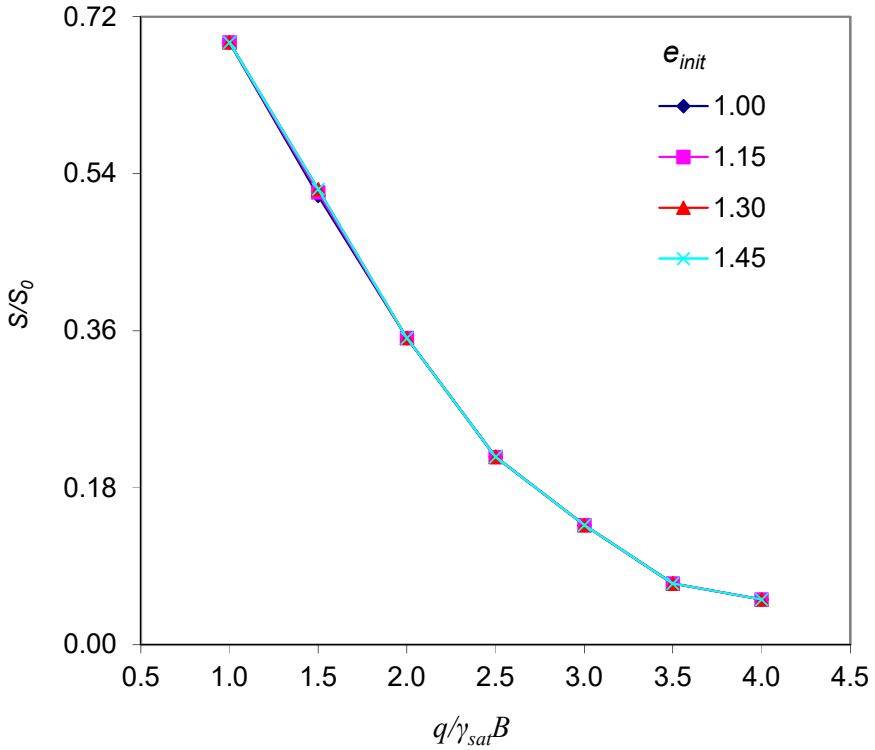

Fig. 6.1b Variation of S/S_0 with $q/\gamma_{sat}B$ for different e_{init} at H_i/B=0.40

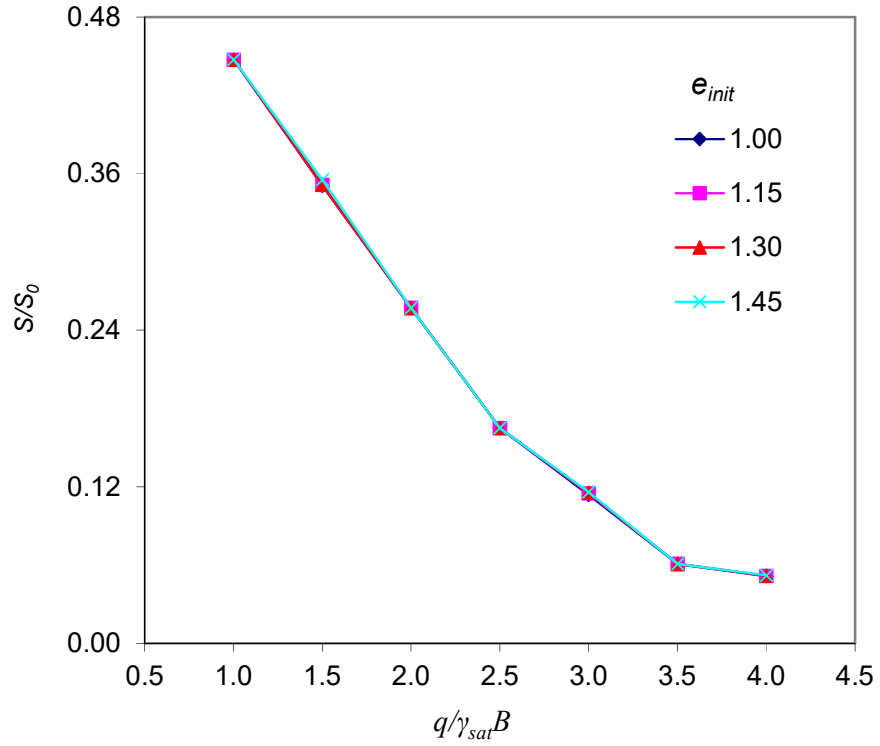

Fig. 6.1c Variation of S/S_0 with $q/\gamma_{sat}B$ for different e_{init} at H_i/B=0.50

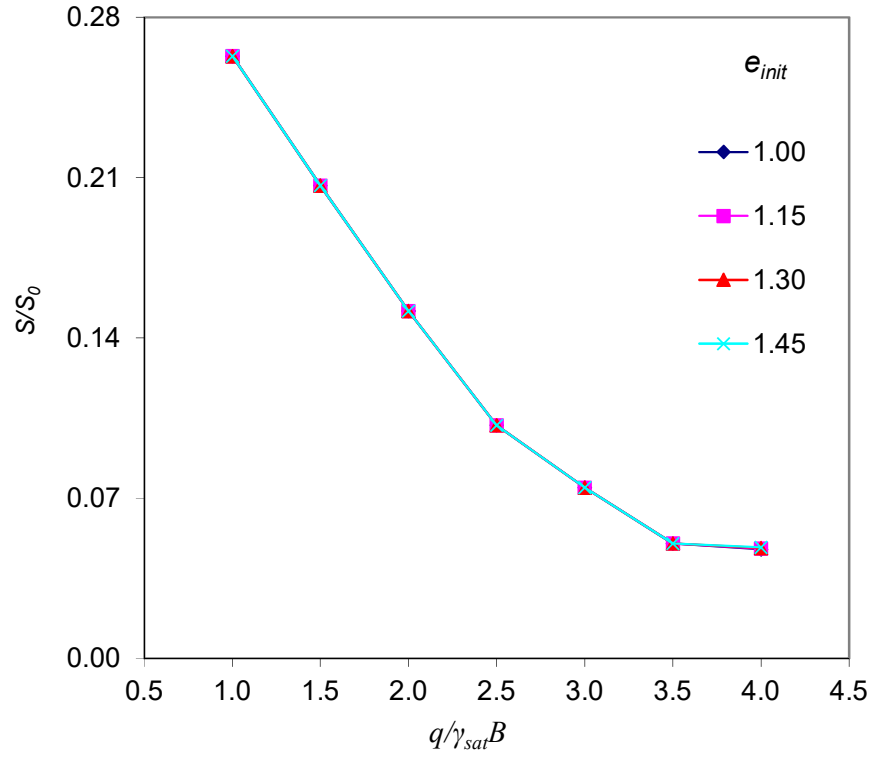

Fig. 6.1d Variation of S/S_0 with $q/\gamma_{sat}B$ for different e_{init} at H_i/B=0.60

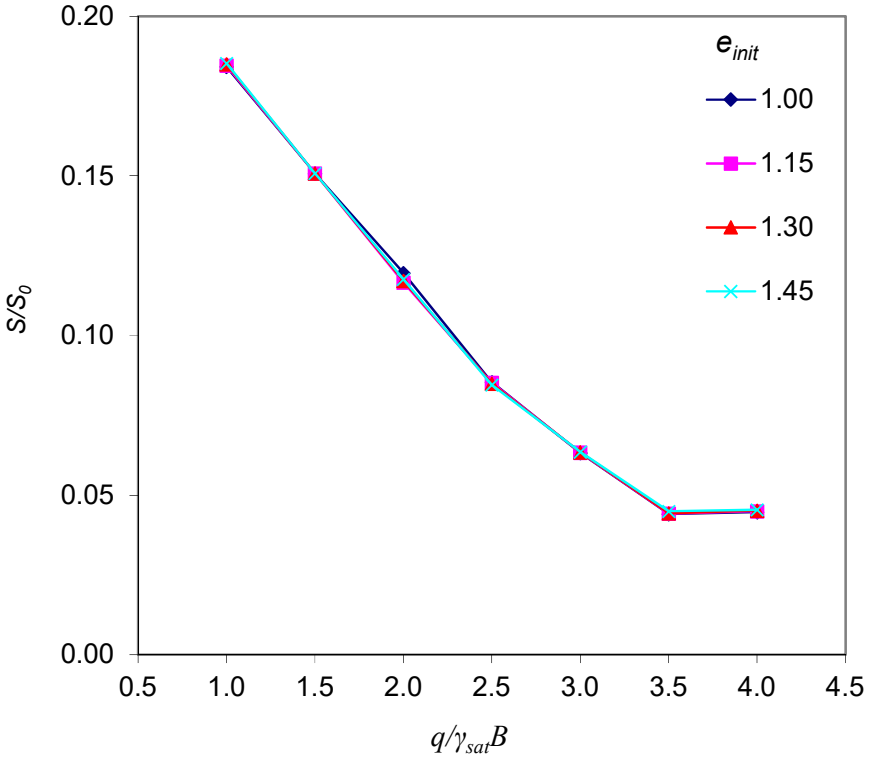

Fig. 6.1e Variation of S/S_0 with $q/\gamma_{sat}B$ for different e_{init} at H_i/B=0.70

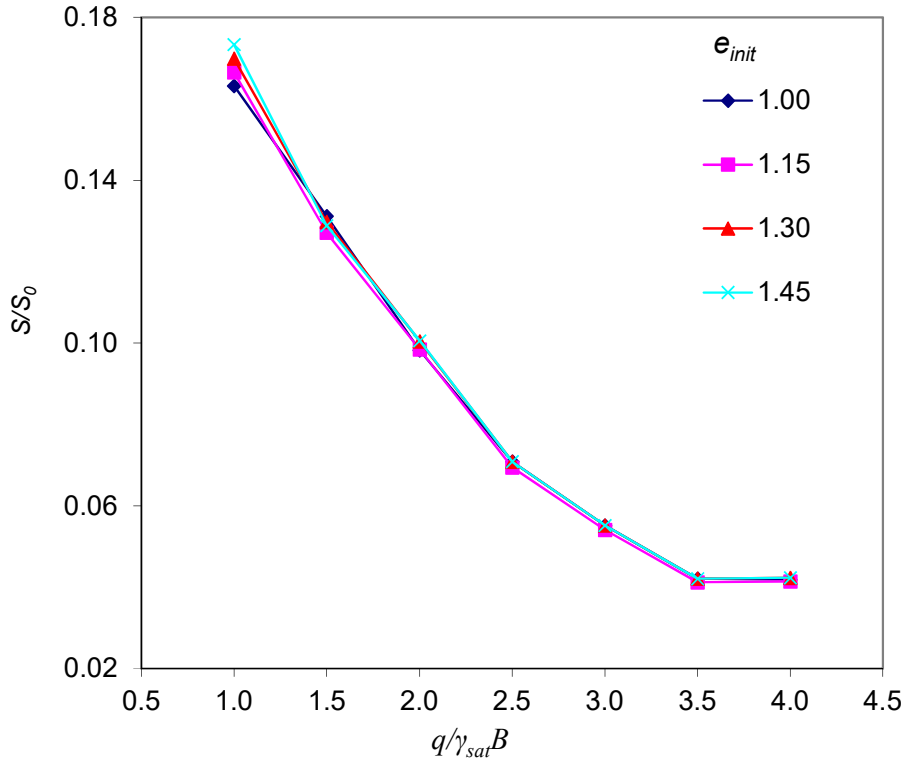

Fig. 6.1f Variation of S/S_0 with $q/\gamma_{sat}B$ for different e_{init} at H_i/B=0.80

6.3.2 Variation of S/S_0 with H_i/B for different $q/\gamma_{sat}B$

For a particular value of normalized footing pressure, $q/\gamma_{sat}B$, S_0 is same and therefore decrease of relative settlement, S/S_0 implies decrease of settlement, S. THus, in figures 6.2a to 6.2d reduction in S/S_0 with increase in H_i/B for a given $q/\gamma_{sat}B$ indicates better settlement control (reduction) by the sand mat..

Fig. 6.2a through 6.2d presents the variation of S/S_0 against H_i/B for different $q/\gamma_{sat}B$ for different void ratios. It can be observed from these graphs that for all value of e_{init}, S/S_0 decreases with increase of normalized value of thickness of upper sand layer *i. e.* H_i/B for a particular $q/\gamma_{sat}B$. However, the rate of decrease (slope) is not constant for all values of H_i/B.

Fig. 6.2a through 6.2d also shows that for a value of $H_i/B \leq 0.6$, increase of S/S_0 with $q/\gamma_{sat}B$ is more significant for values of $q/\gamma_{sat}B$ equal to 2.5 and above. On the other hand for $H_i/B > 0.6$, there is little change of S/S_0 with $q/\gamma_{sat}B$. For values of $q/\gamma_{sat}B$ less than 2.5, changes in S/S_0 for different $q/\gamma_{sat}B$ are small for any H_i/B.

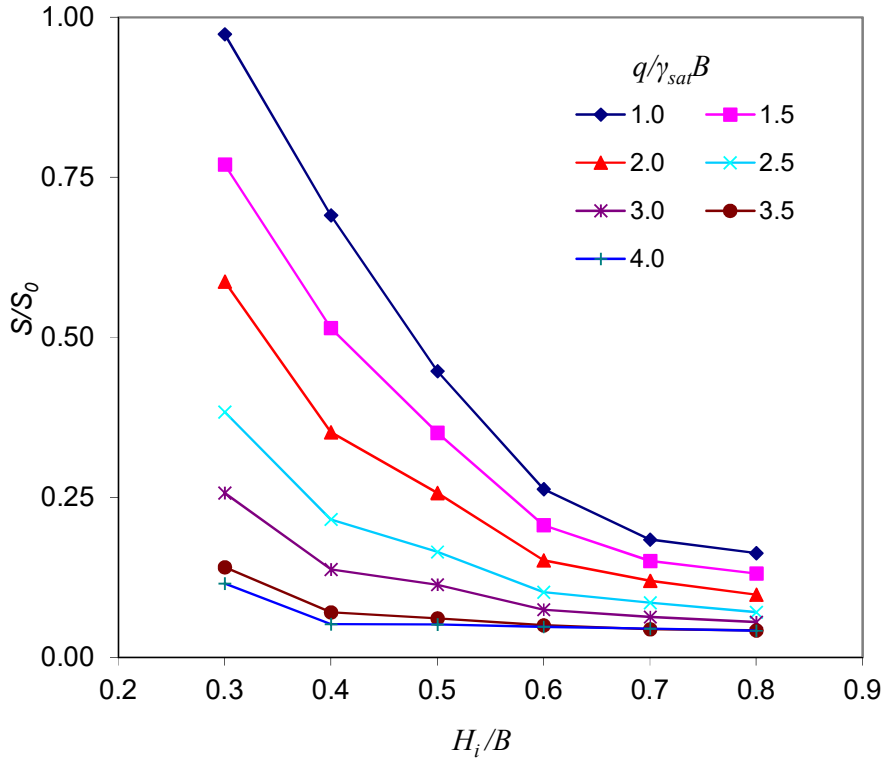

Fig. 6.2a Variation of S/S_0 with H_i/B for different $q/\gamma_{sat}B$ at e_{init}=1.0

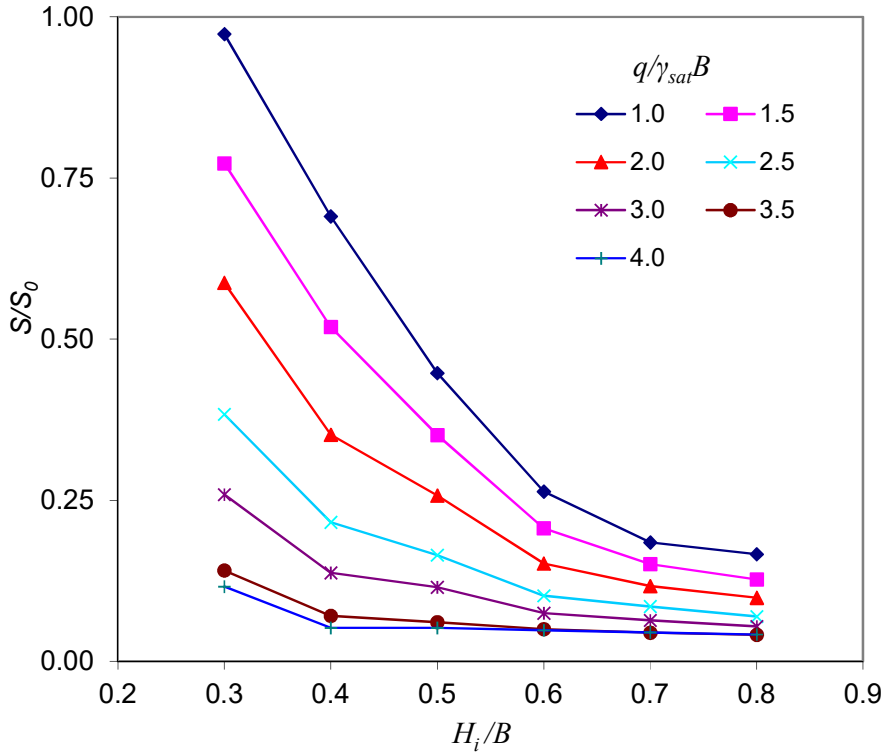

Fig. 6.2b Variation of S/S_0 with H_i/B for different $q/\gamma_{sat}B$ at e_{init}=1.15

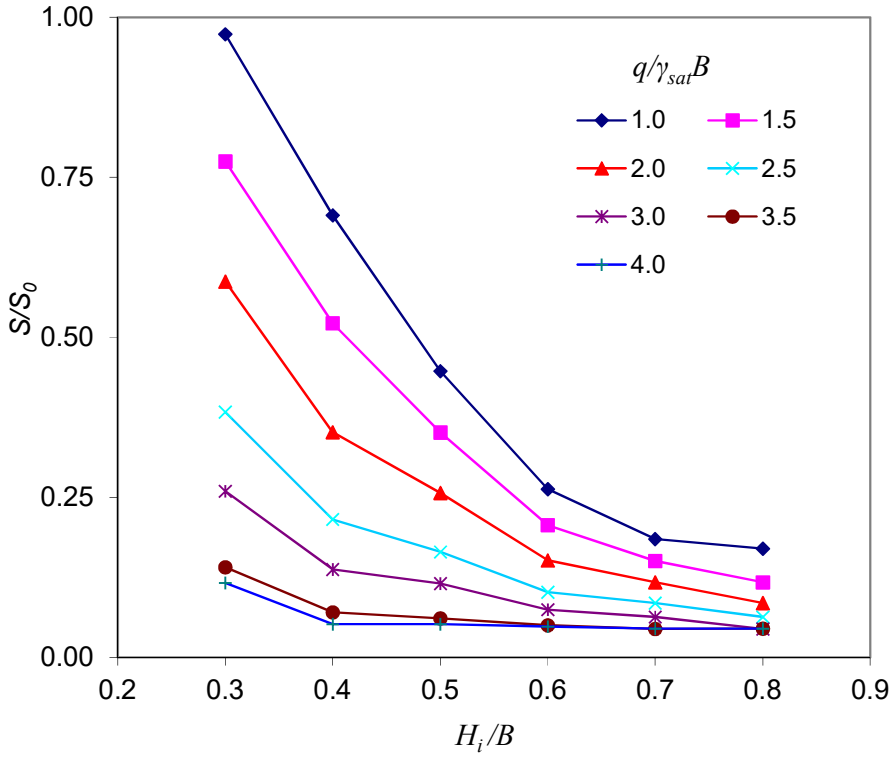

Fig. 6.2c Variation of S/S_0 with H_i/B for different $q/\gamma_{sat}B$ at e_{init}=1.3

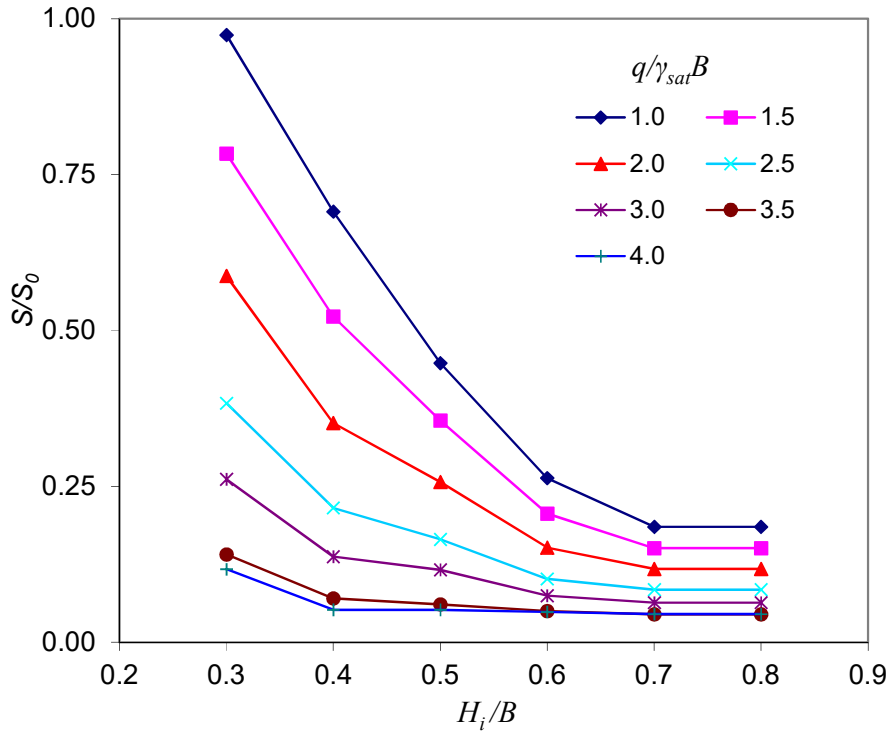

Fig. 6.2d Variation of S/S_0 with H_i/B for different $q/\gamma_{sat}B$ at e_{init}=1.45

6.3.3 Variation of S/S_0 with $q/\gamma_{sat}B$ for different H_i/B

Fig. 6.3a through 6.3d presents the effect of $q/\gamma_{sat}B$ on relative settlement S/S_0 for various H_i/B and at a given void ratio e_{init}. It is observed that for all value of e_{init}, S/S_0 decreases with increase of different $q/\gamma_{sat}B$ for normalized value of thickness of upper sand layer H_i/B. This decreasing rate (slope) is not constant for all value of $q/\gamma_{sat}B$.

It is observed for these graph that the relative settlement decreases at a high rate with the increase of thickness of upper sand layer H_i/B upto a certain value of normalized footing pressure which is 2.5. After this particular value of footing pressure, this rate of decrease of relative settlement is smaller.

Fig. 6.3a through 6.3d also shows for a particular value of H_i/B, decrease of S/S_0 with $q/\gamma_{sat}B$ is more significant for value of $q/\gamma_{sat}B$ less than 2.5. For values of $q/\gamma_{sat}B$ more than 2.5, S/S_0 at different $q/\gamma_{sat}B$ are quite closer.

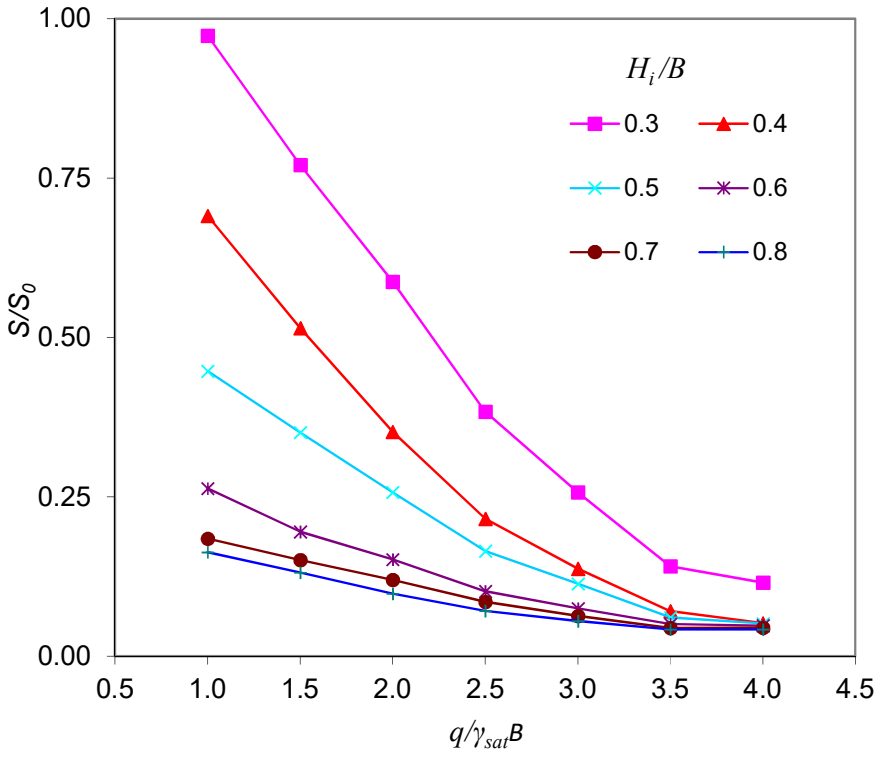

Fig. 6.3a Variation of S/S_0 with $q/\gamma_{sat}B$ for different H_i/B at e_{init}=1.0

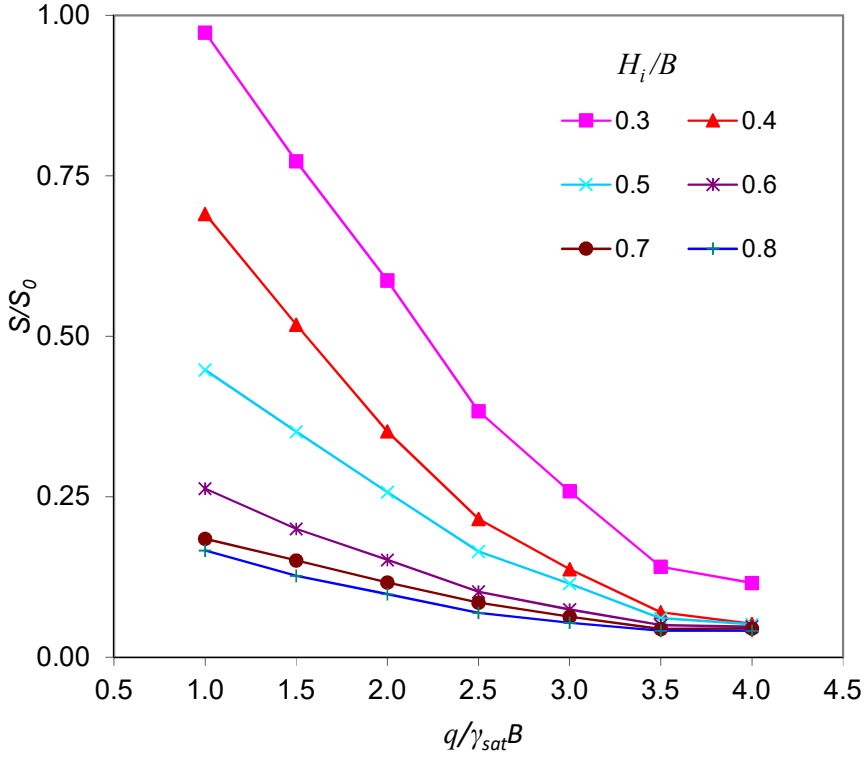

Fig. 6.3b Variation of S/S_0 with $q/\gamma_{sat}B$ for different H_i/B at e_{init}=1.15

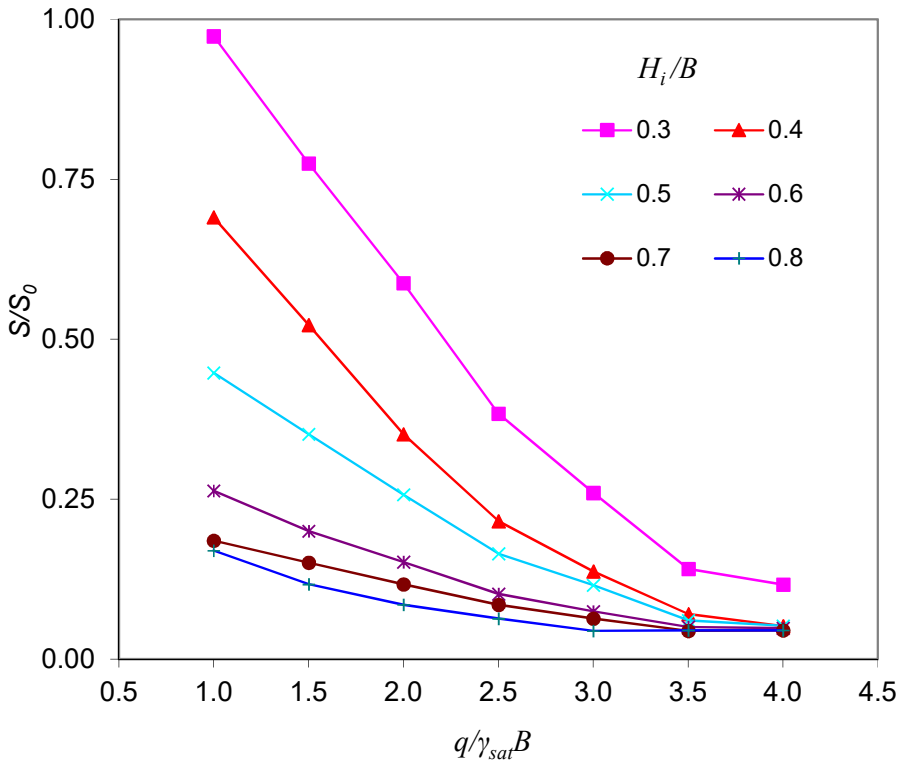

Fig. 6.3c Variation of S/S_0 with $q/\gamma_{sat}B$ for different H_i/B at e_{init}=1.3

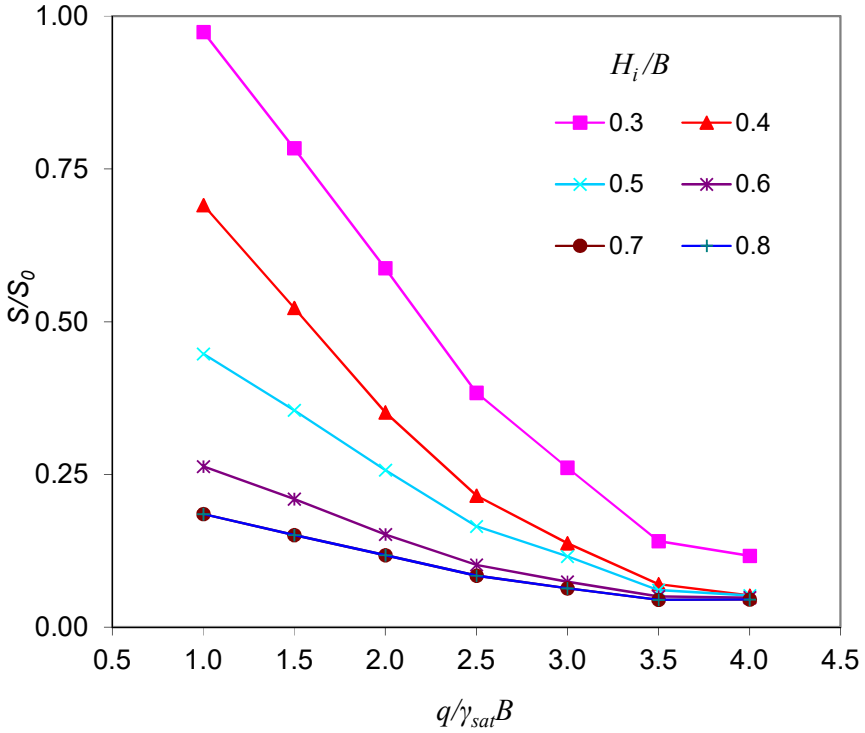

Fig. 6.3d Variation of S/S_0 with $q/\gamma_{sat}B$ for different H_i/B at e_{init}=1.45

6.4 Results for Cement Treated Sand as Upper Layer

The results of untreated sand as upper layer are presented in Fig. 6.4 through 6.6 as plots of S/S_0 (the relative settlement) against $q/\gamma_{sat}B$, e_{init} and H_i.

6.4.1 Variation of S/S_0 with $q/\gamma_{sat}B$ for different e_{init}

Fig. 6.4a through 6.4f shows that for a single thickness of upper sand layer with the range of H_i used, S/S_0 decreases with increase of $q/\gamma_{sat}B$ for different value of e_{init}. This decreasing rate (slope) is not constant for all $q/\gamma_{sat}B$.

It is observed for Fig. 6.4a through 6.4f that the relative settlement decreases at a high rate with the increase of normalized footing pressure upto a certain value of normalized footing pressure. After this particular value of normalized footing pressure, this rate of decrease of relative settlement is smaller. In general three distinct zones can be identified in the relationship of S/S_o vs $q/\gamma_{sat}B$ for different e_{init}. At left zone up to $q/\gamma_{sat}B$=2.5 the S/S_o decreases rapidly and at middle zone from $q/\gamma_{sat}B$=2.5 to 3.5 S/S_o rate of decrease of S/S_o is low and at right zone for $q/\gamma_{sat}B$>3.5 there is no decrease of S/S_o. Thus for

$q/\gamma_{sat}B$>3.5, sand mat is no longer effective to reduce settlement. The difference of relative settlement for different normalized footing pressure remains more or less same for different value of relative thickness of upper sand mat at right zone. As has been stated earlier both S_o and S changes when footing pressure changes. A higher value of S/S_o implies smaller difference between S and S_o.

For a given thickness of sand mat and clay layer, the effectiveness of the sand mat reduces with increase of footing pressure and after a certain value of normalized footing pressure 3.5 the sand mat appears to be no longer effective. Similar observation can be made from figures 6.4a to 6.4f for all other thickness (0.75m – 2.0m) of sand layer.

For a given H_i if the $q/\gamma_{sat}B$ is increased up to a value of 2.5 the relative settlement S/S_o decreases indicates increasing effectiveness of the sand layer in reducing the settlement. However, beyond the value of $q/\gamma_{sat}B$=2.5, there is little reduction in relative settlement.

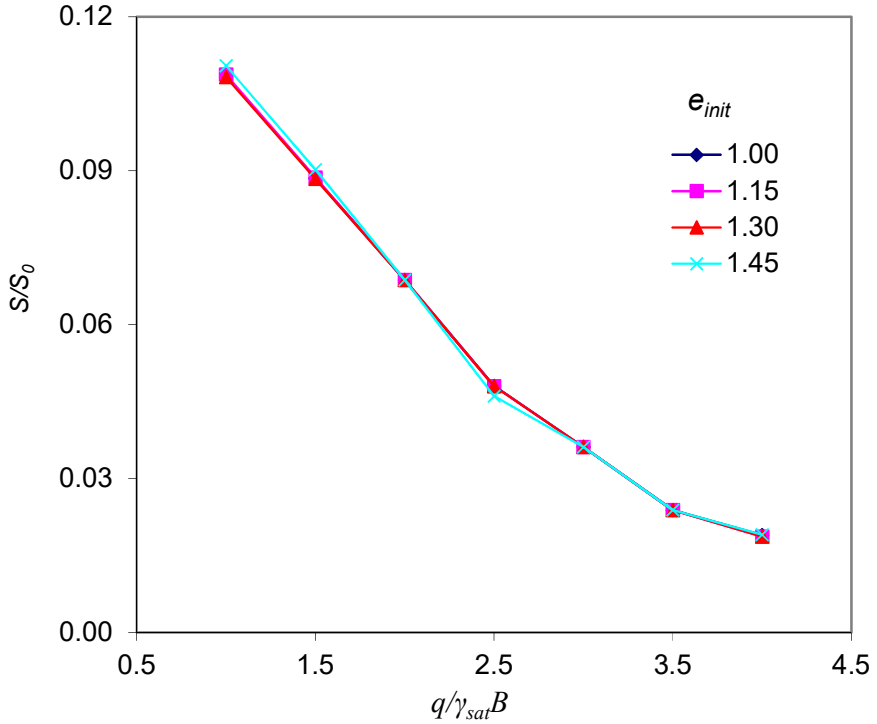

Fig. 6.4a Variation of S/S_0 with $q/\gamma_{sat}B$ for different e_{init} at H_i/B=0.30

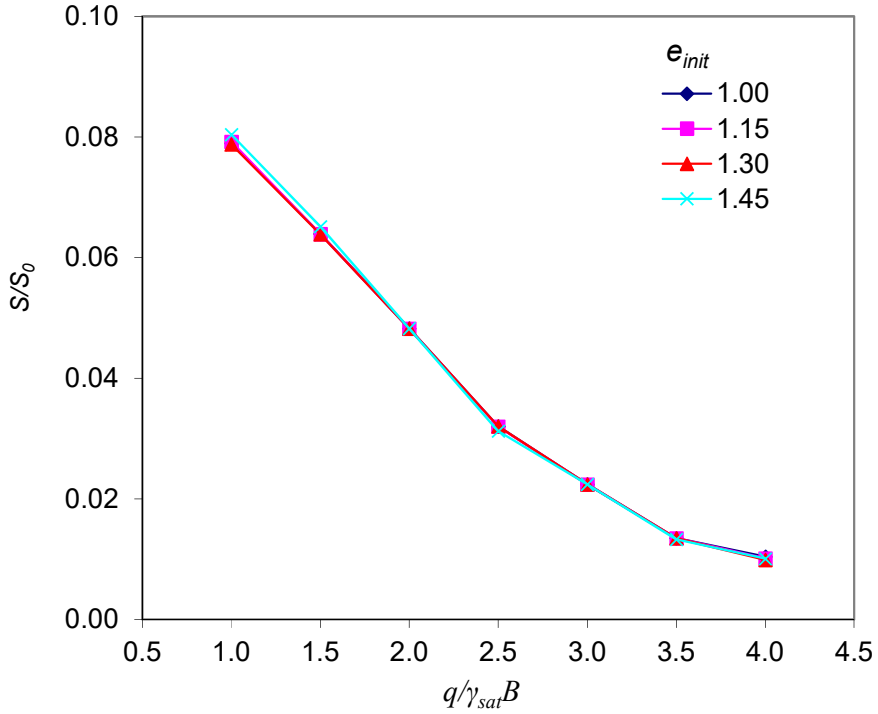

Fig. 6.4b Variation of S/S_0 with $q/\gamma_{sat}B$ for different e_{init} at H_l/B=0.40

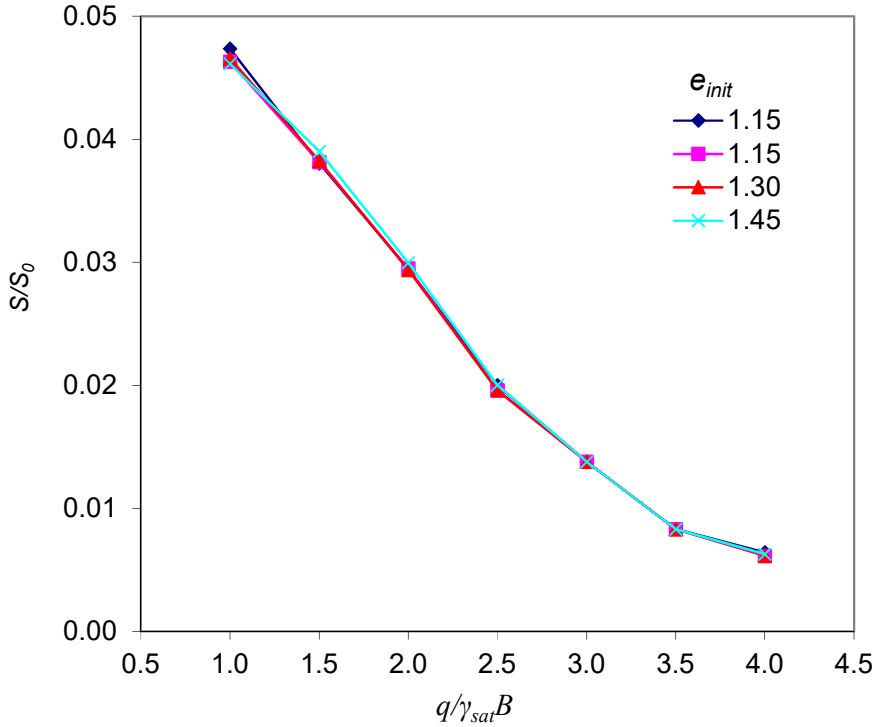

Fig. 6.4c Variation of S/S_0 with $q/\gamma_{sat}B$ for different e_{init} at H_l/B=0.50

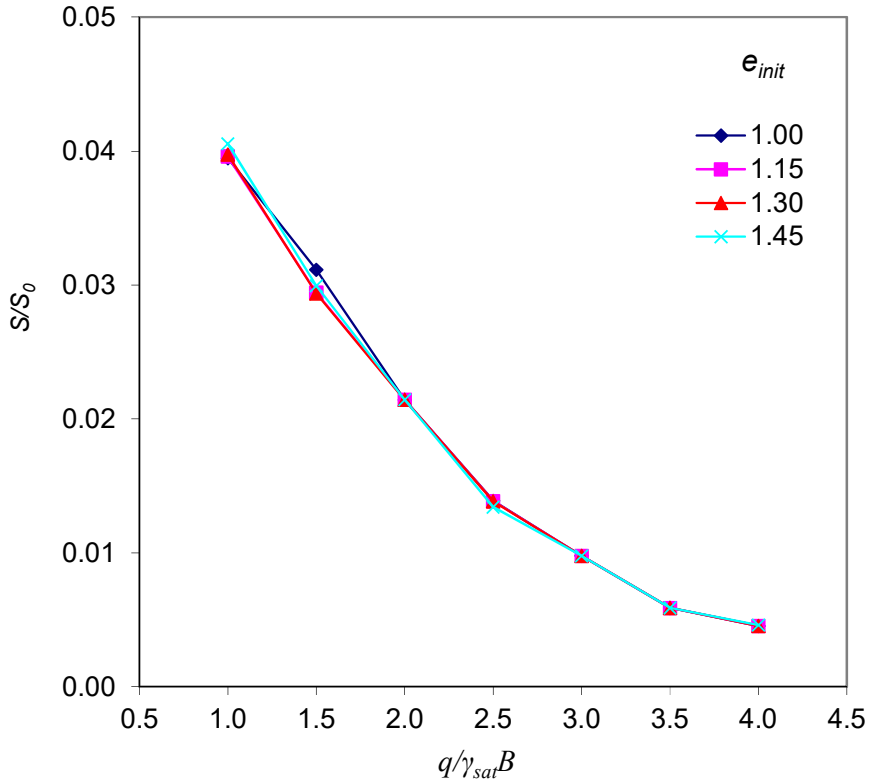

Fig. 6.4d Variation of S/S_0 with $q/\gamma_{sat}B$ for different e_{init} at H_f/B=0.60

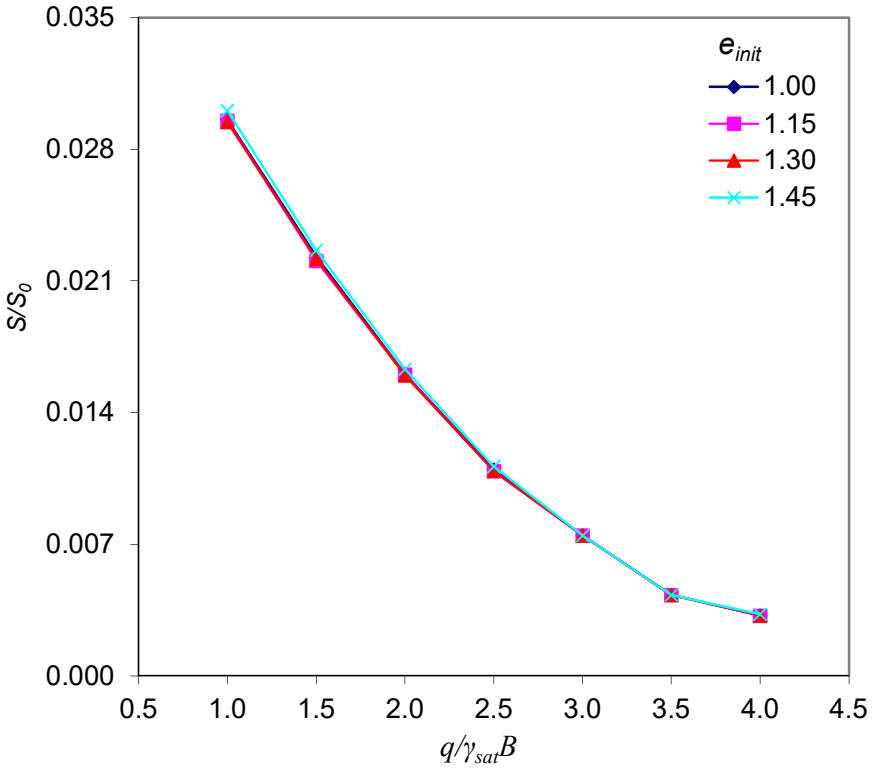

Fig. 6.4e Variation of S/S_0 with $q/\gamma_{sat}B$ for different e_{init} at H_f/B=0.70

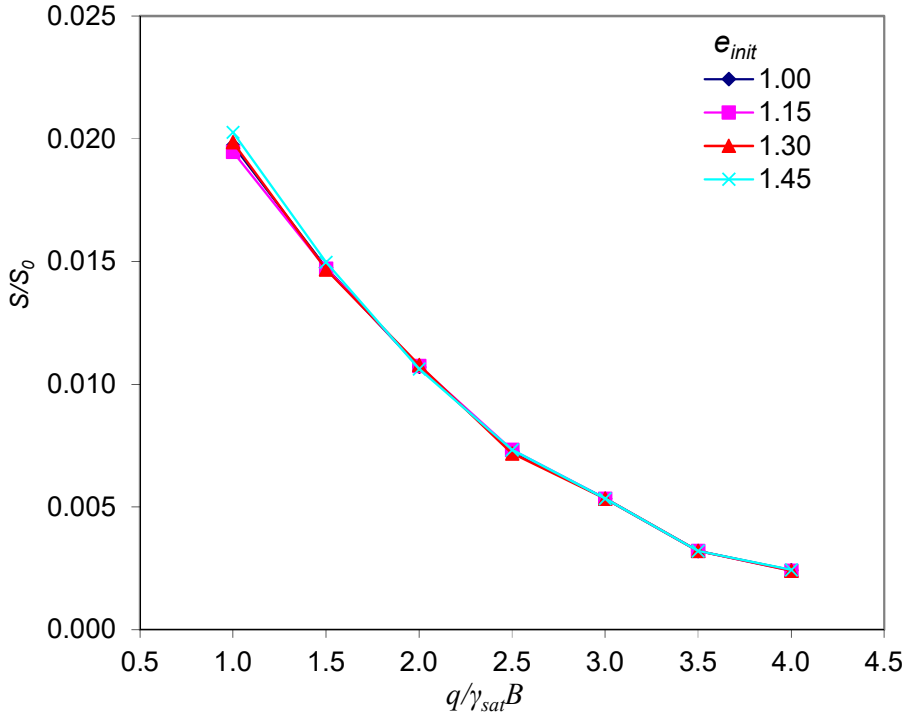

Fig. 6.4f Variation of S/S_0 with $q/\gamma_{sat}B$ for different e_{init} at H_i/B=0.80

6.4.2 Variation of S/S_0 with H_i/B for different $q/\gamma_{sat}B$

For a particular value of normalized footing pressure, $q/\gamma_{sat}B$, S_0 is same and therefore decrease of relative settlement, S/S_0 implies decrease of settlement, S. THus, in figures 6.5a to 6.5d reduction in S/S_0 with increase in H_i/B for a given $q/\gamma_{sat}B$ indicates better settlement control (reduction) by the sand mat..

Fig. 6.5a through 6.5d presents the variation of S/S_0 against H_i/B for different $q/\gamma_{sat}B$ for different void ratios. It can be observed from these graphs that for all value of e_{init}, S/S_0 decreases with increase of normalized value of thickness of upper sand layer *i. e.* H_i/B for a particular $q/\gamma_{sat}B$. However, the rate of decrease (slope) is not constant for all values of H_i/B.

Fig. 6.5a through 6.5d also shows that for a value of $H_i/B \leq 0.6$, increase of S/S_0 with $q/\gamma_{sat}B$ is more significant for values of $q/\gamma_{sat}B$ equal to 2.5 and above. On the other hand for $H_i/B > 0.6$, there is little change of S/S_0 with $q/\gamma_{sat}B$. For values of $q/\gamma_{sat}B$ less than 2.5, changes in S/S_0 for different $q/\gamma_{sat}B$ are small for any H_i/B.

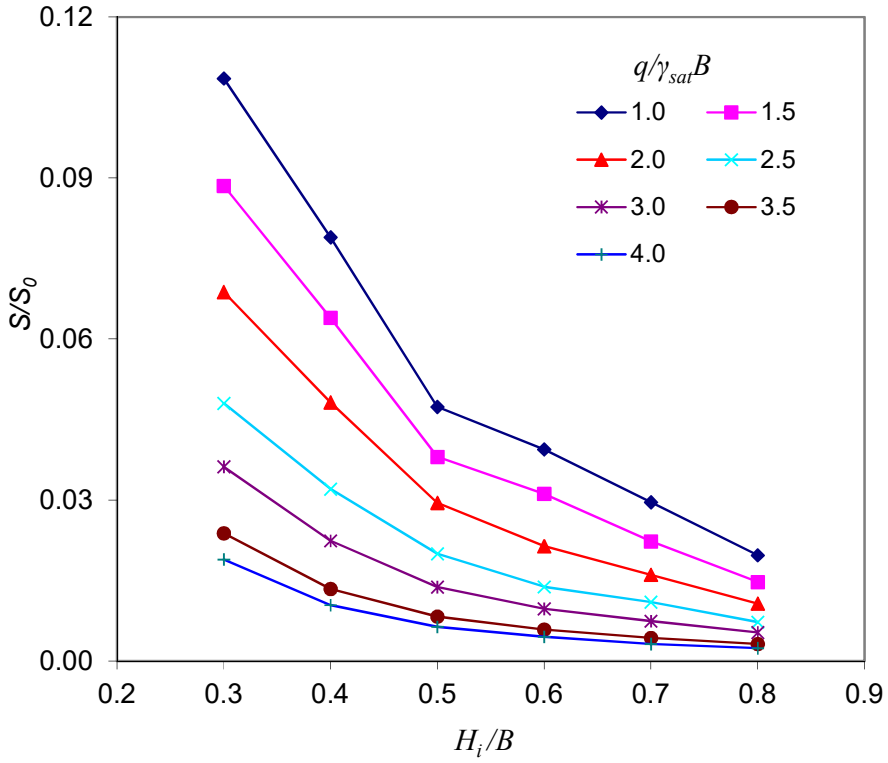

Fig. 6.5a Variation of S/S_0 with H_i/B for different $q/\gamma_{sat}B$ at e_{init}=1.00

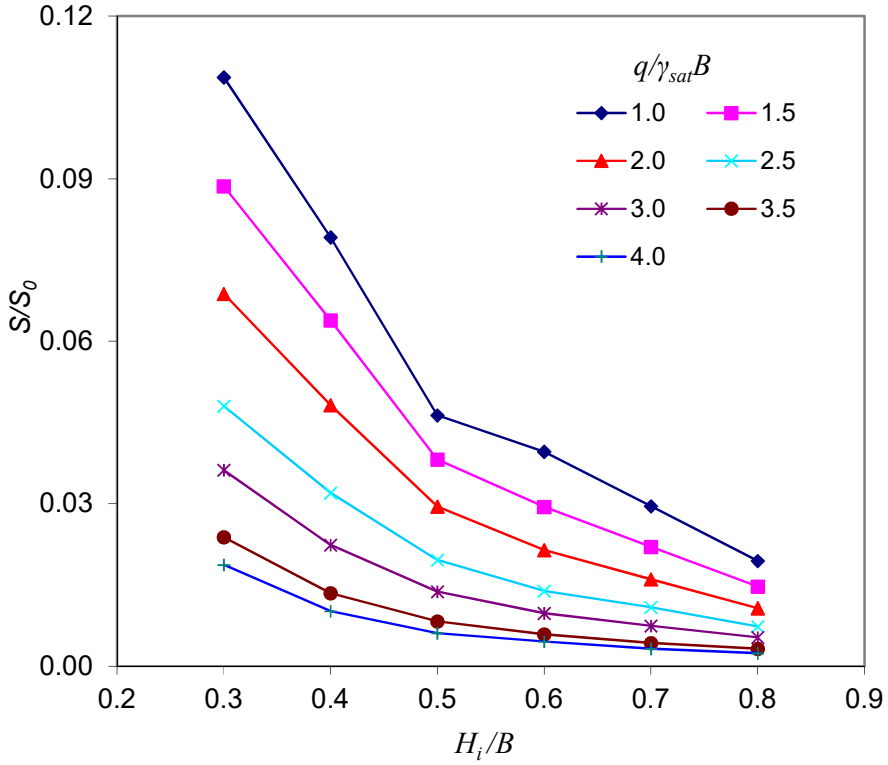

Fig. 6.5b Variation of S/S_0 with H_i/B for different $q/\gamma_{sat}B$ at e_{init}=1.15

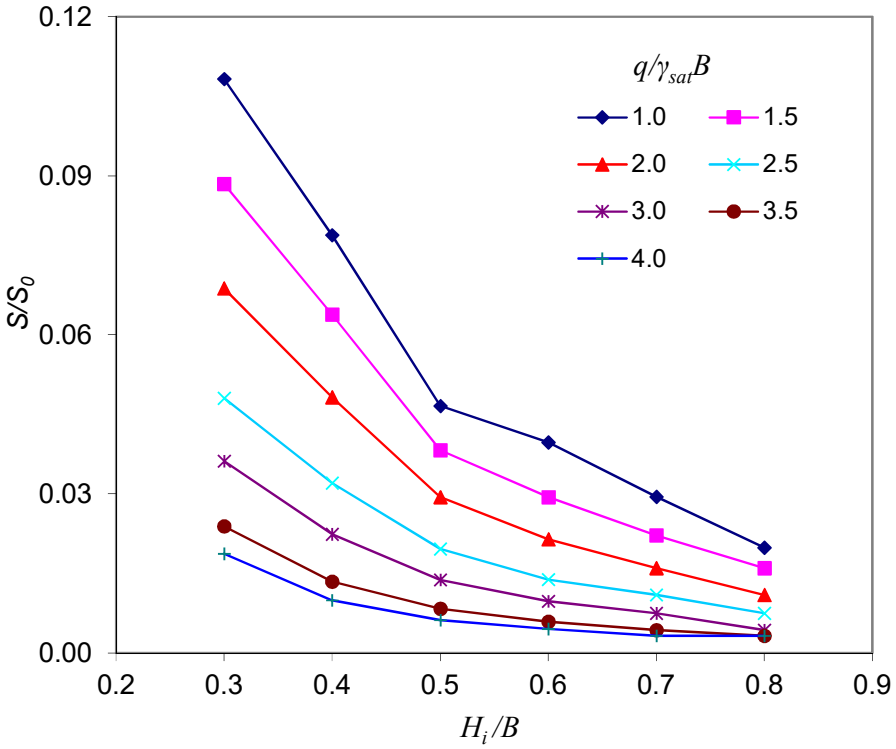

Fig. 6.5c Variation of S/S_0 with H_i/B for different $q/\gamma_{sat}B$ at e_{init}=1.30

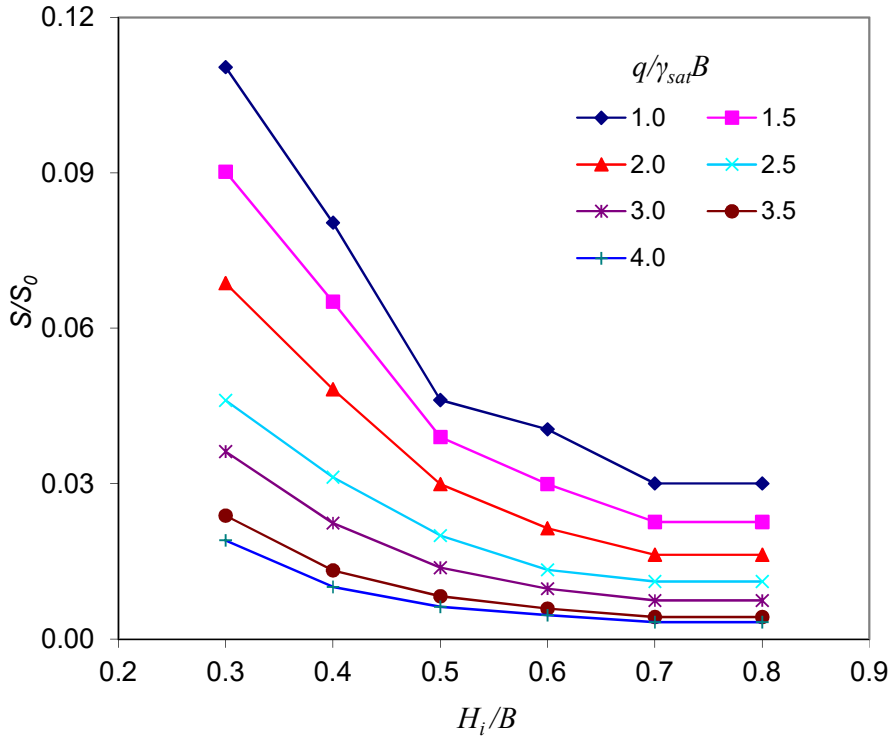

Fig. 6.5d Variation of S/S_0 with H_i/B for different $q/\gamma_{sat}B$ at e_{init}=1.45

6.4.3 Variation of S/S_0 with $q/\gamma_{sat,1}B$ for different H_i/B

Fig. 6.6a through 6.6d presents the effect of $q/\gamma_{sat}B$ on relative settlement S/S_0 for various H_i/B and at a given void ratio e_{init}. It is observed that for all value of e_{init}, S/S_0 decreases with increase of different $q/\gamma_{sat}B$ for normalized value of thickness of upper sand layer H_i/B. This decreasing rate (slope) is not constant for all value of $q/\gamma_{sat}B$.

It is observed for these graph that the relative settlement decreases at a high rate with the increase of thickness of upper sand layer H_i/B upto a certain value of normalized footing pressure which is 2.5. After this particular value of footing pressure, this rate of decrease of relative settlement is smaller.

Fig. 6.6a through 6.6d also shows for a particular value of H_i/B, decrease of S/S_0 with $q/\boldsymbol{\gamma}_{sat}B$ is more significant for value of $q/\boldsymbol{\gamma}_{sat}B$ less than 2.5. For values of $q/\gamma_{sat}B$ more than 2.5, S/S_0 at different $q/\gamma_{sat}B$ are quite closer.

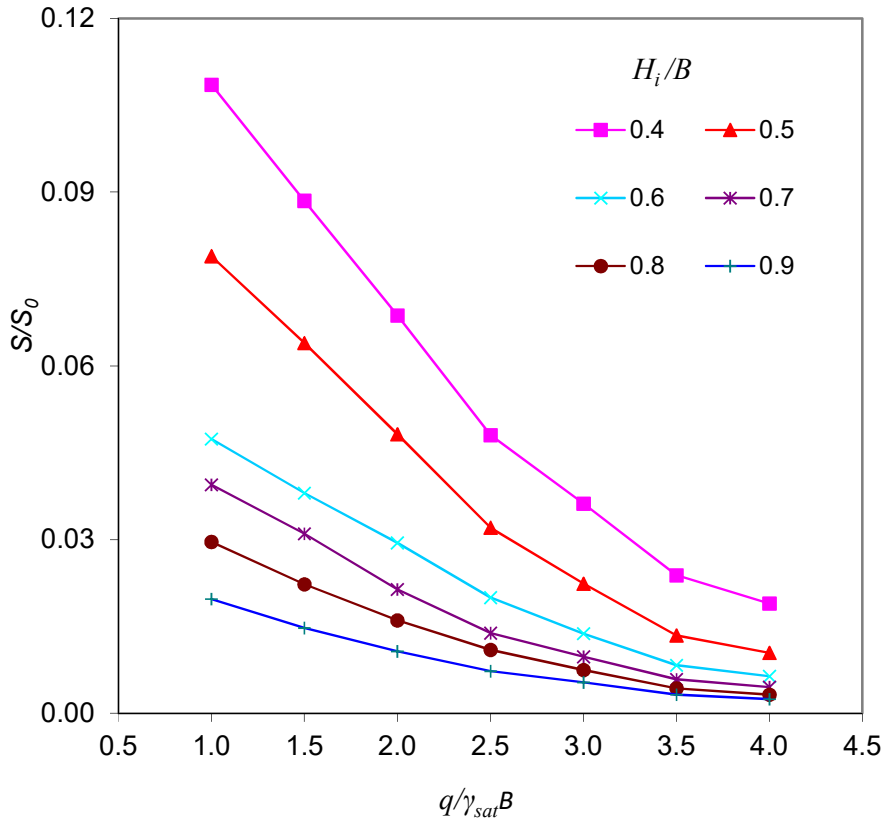

Fig. 6.6a Variation of S/S_0 with $q/\gamma_{sat}B$ for different H_i/B at e_{init}=1.00

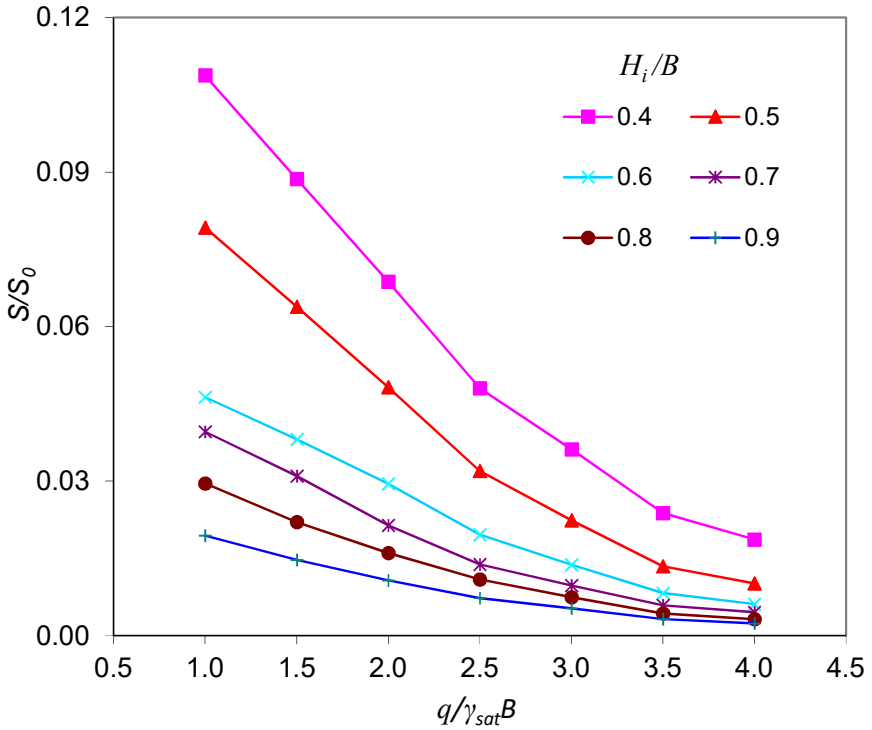

Fig. 6.6b Variation of S/S_0 with $q/\gamma_{sat}B$ for different H_i/B at e_{init}=1.15

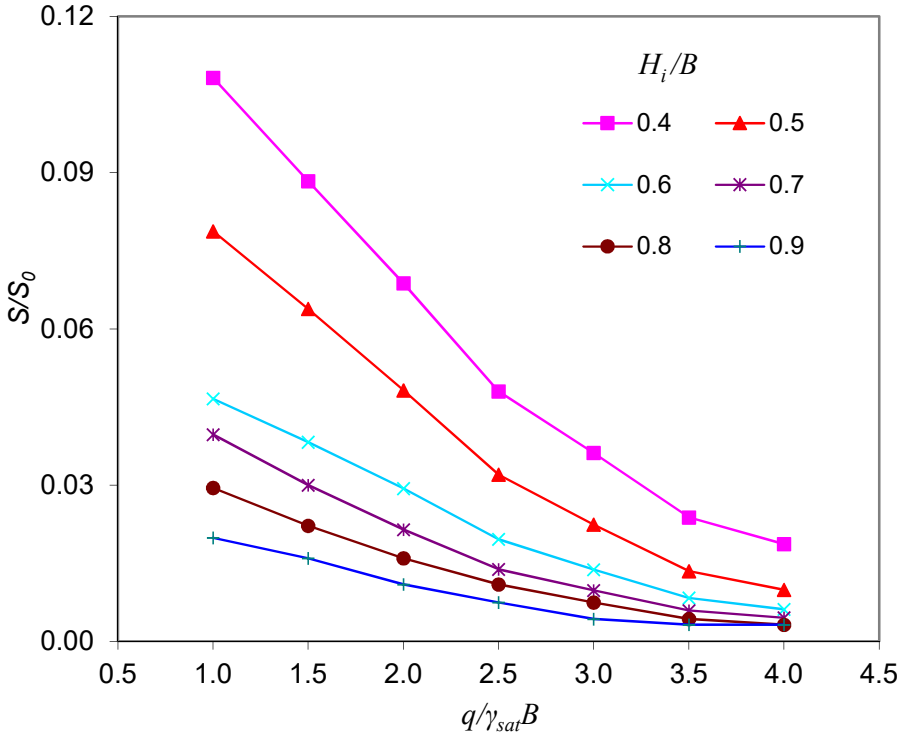

Fig. 6.6C Variation of S/S_0 with $q/\gamma_{sat}B$ for different H_i/B at e_{init}=1.30

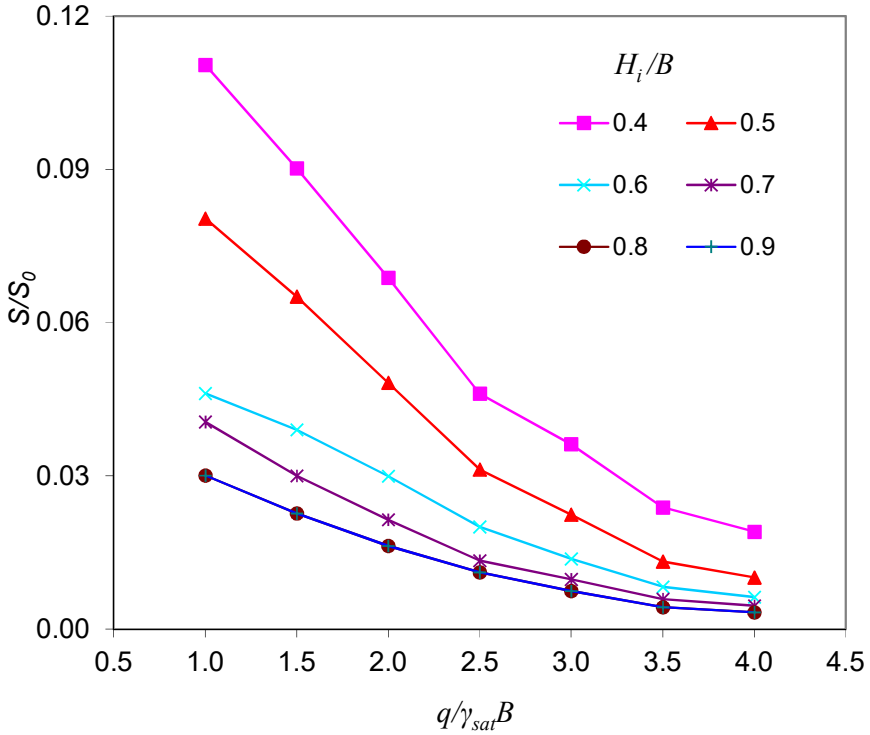

Fig. 6.6d Variation of S/S_0 with $q/\gamma_{sat}B$ for different H_i/B at e_{init}=1.45

6.5 Comparison between Effectiveness of Untreated and Cement Treated Upper Sand Layer

6.5.1 Comparison of Effectiveness as S/S_0 vs $q/\gamma_{sat}B$

For e_{init}=1.0 the effectiveness of untreated upper sand layer and cement treated upper sand layer is presented in Fig. 6.7a through 6.7f as variation of S/S_0 with $q/\gamma_{sat}B$ for different Sand Type at different H_i/B.

From Fig. 6.7a through 6.7f it is observed that for value of $q/\gamma_{sat}B$ smaller than 2.5 the cement treated upper sand layer is more effective than untreated upper sand layer in reducing relative settlement S/S_0 and for value of $q/\gamma_{sat}B$ higher than 2.5 the effectiveness of untreated upper sand layer and cement treated upper sand layer is about similar in reducing relative settlement S/S_0.

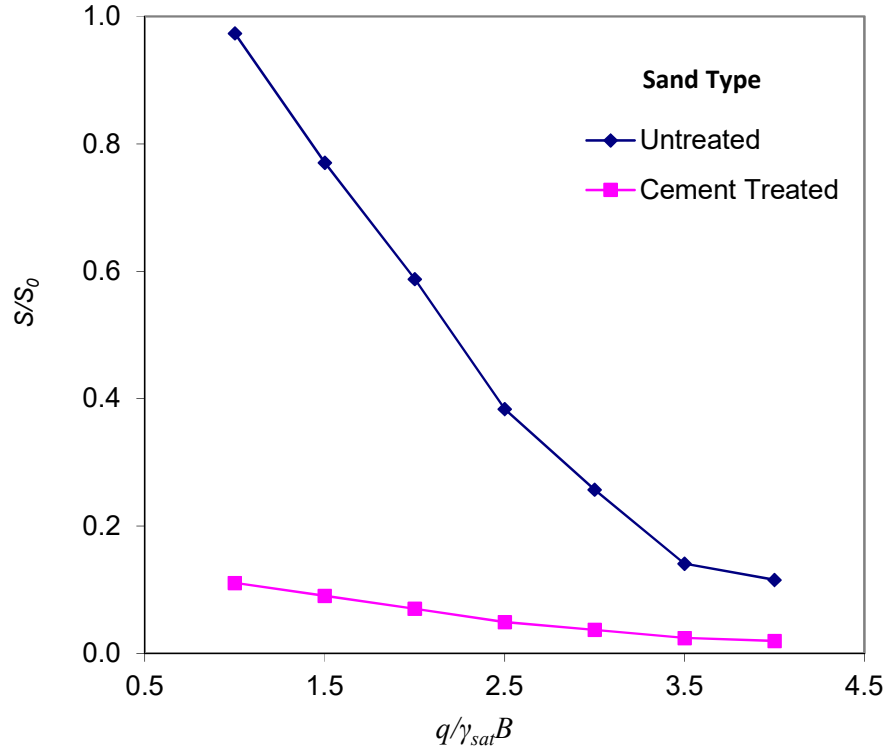

Fig. 6.7a Variation of S/S_0 with $q/\gamma_{sat}B$ for different Sand Type at H_i/B=0.3

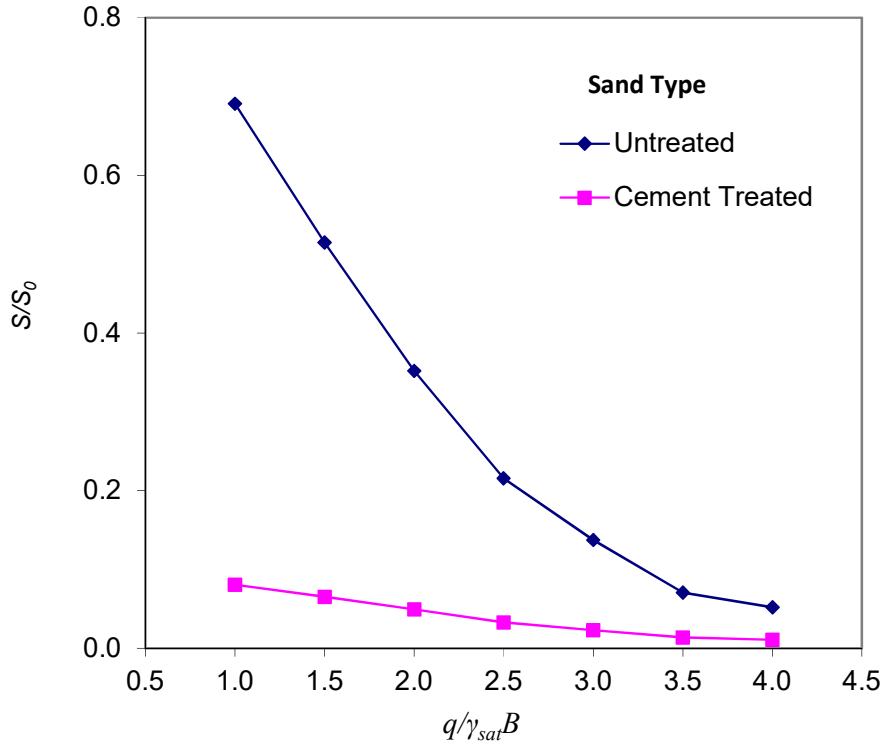

Fig. 6.7b Variation of S/S_0 with $q/\gamma_{sat}B$ for different Sand Type at H_i/B=0.4

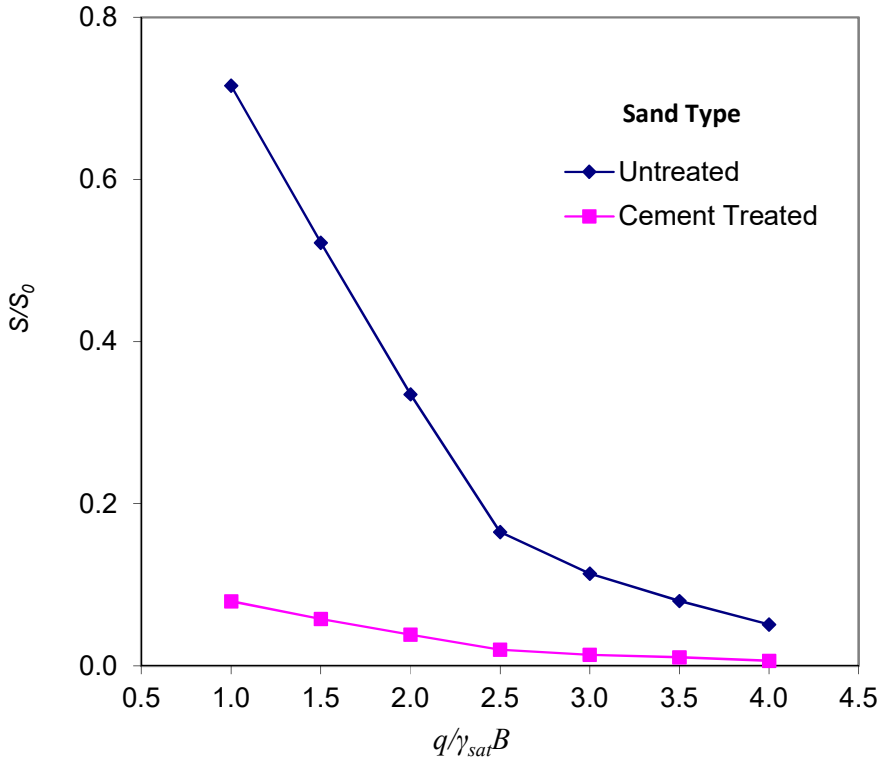

Fig. 6.7c Variation of S/S_0 with $q/\gamma_{sat}B$ for different Sand Type at H_i/B=0.5

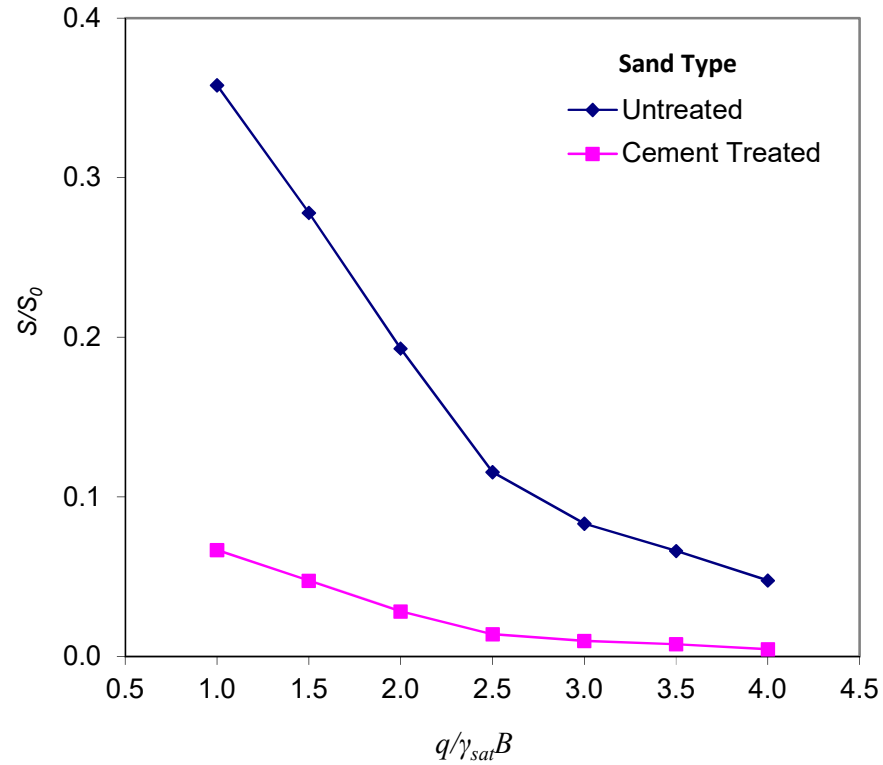

Fig. 6.7d Variation of S_B/S_{0B} with $q/\gamma_{sat}B$ for different Sand Type at H_i/B=0.6

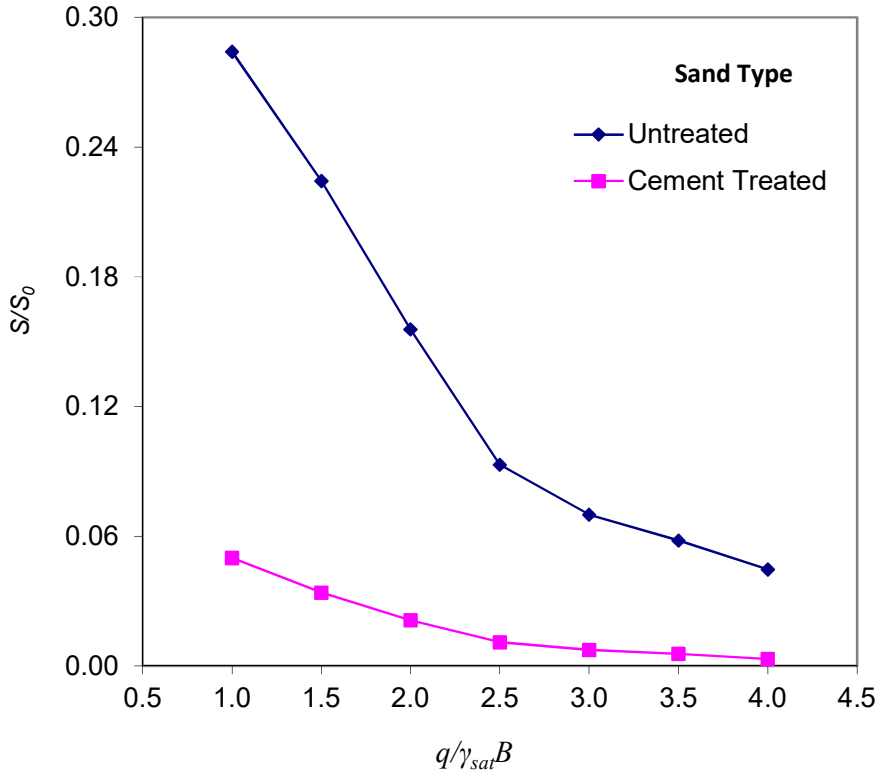

Fig. 6.7e Variation of S/S_0 with $q/\gamma_{sat}B$ for different Sand Type at H_i/B=0.7

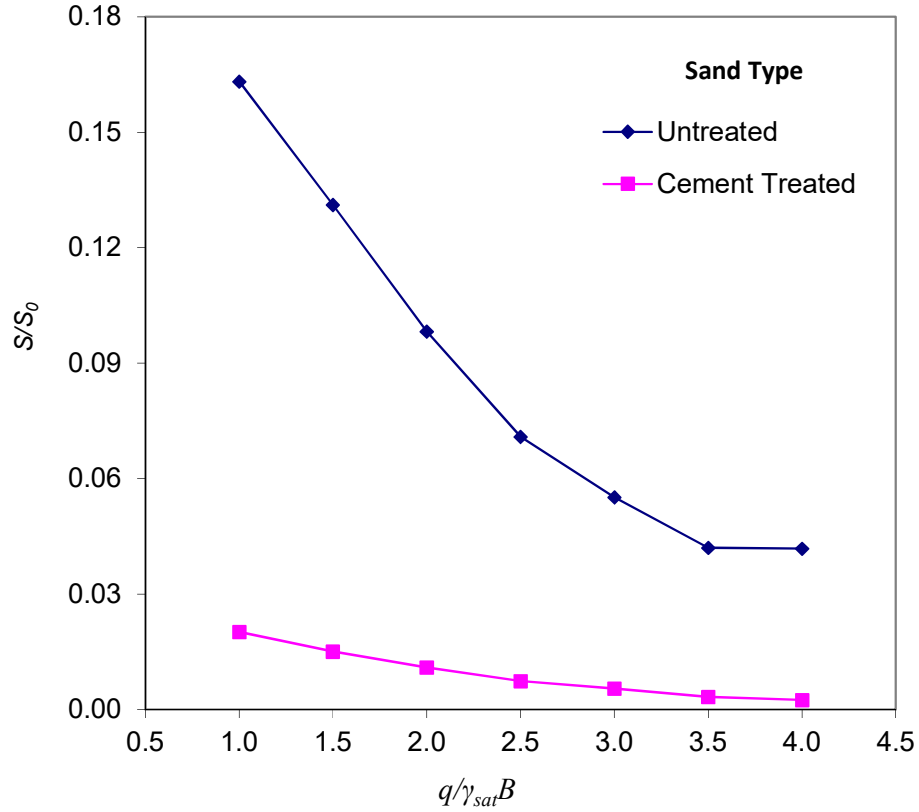

Fig. 6.7f Variation of S_B/S_{0B} with $q/\gamma_{sat}B$ for different Sand Type at H_i/B=0.8

6.5.2 Comparison of Effectiveness as S/S_0 vs H_i/B

For e_{init}=1.0 the effectiveness of untreated upper sand layer and cement treated upper sand layer is presented in Fig. 6.8a through 6.8d as variation of S/S_0 with H_i/B for different Sand Type at different $q/\gamma_{sat,1}B$.

From Fig. 6.8a through 6.8d it is observed that for value of H_i/B smaller than 0.5 the cement treated upper sand layer is more effective than untreated upper sand layer in reducing relative settlement S/S_0 and for value of H_i/B higher than 0.5 the effectiveness of untreated upper sand layer and cement treated upper sand layer is about similar in reducing relative settlement S/S_0.

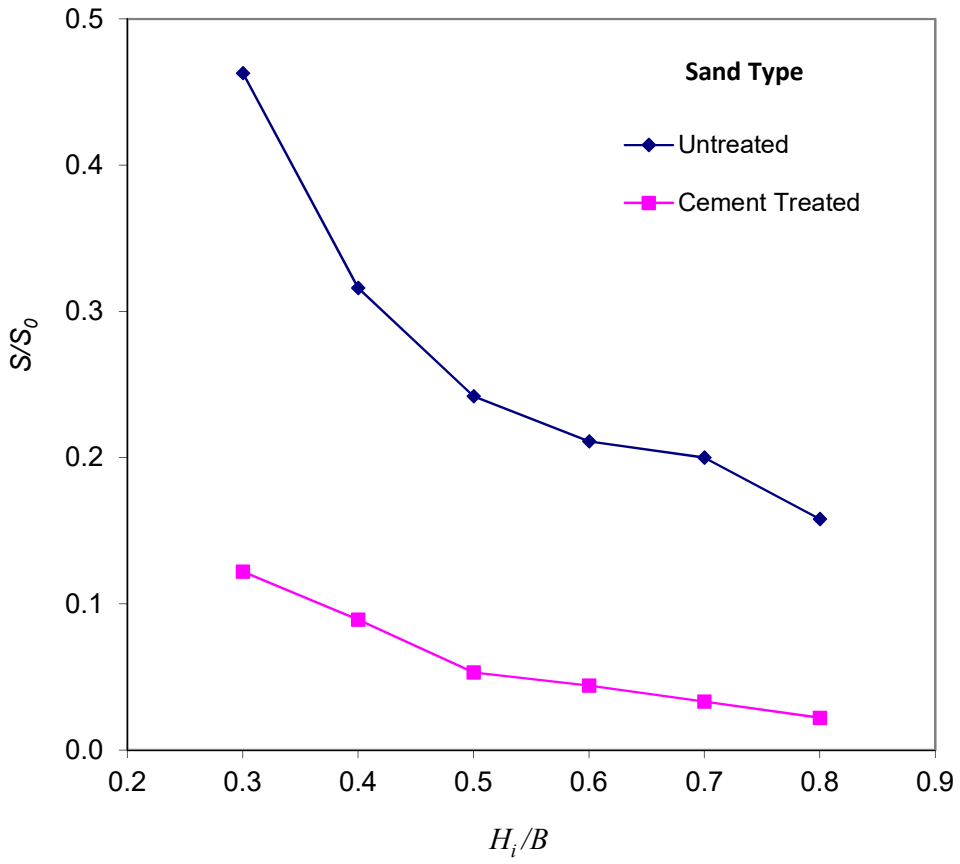

Fig. 6.8a Variation of S/S_0 with H_i/B for different Sand Type at $q/\gamma_{sat}B$=1.0

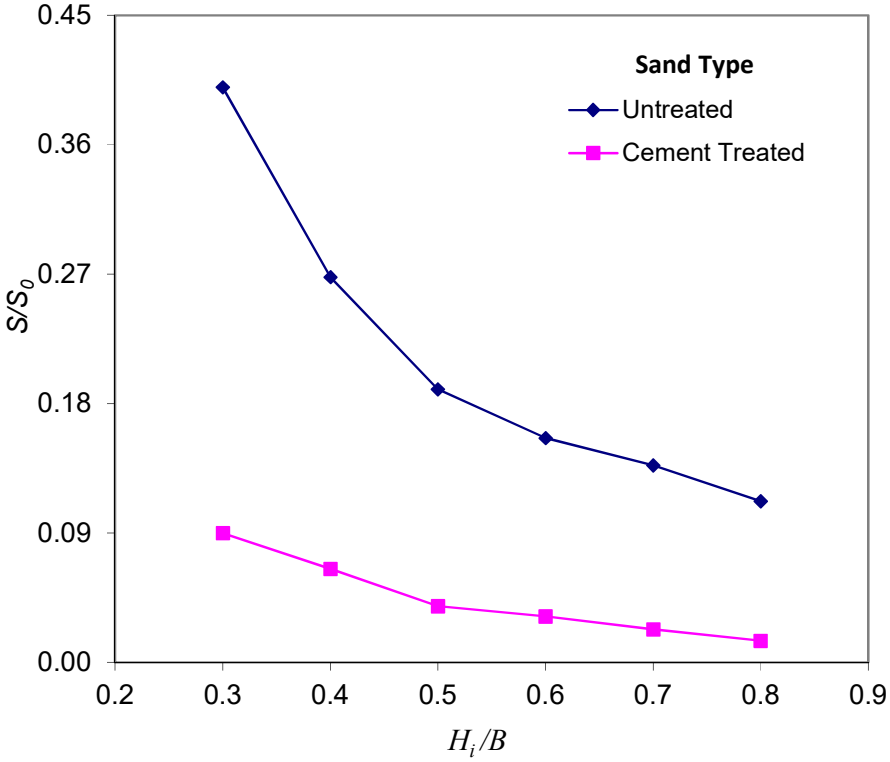

Fig. 6.8b Variation of S/S_0 with H_i/B for different Sand Type at $q/\gamma_{sat}B$=1.5

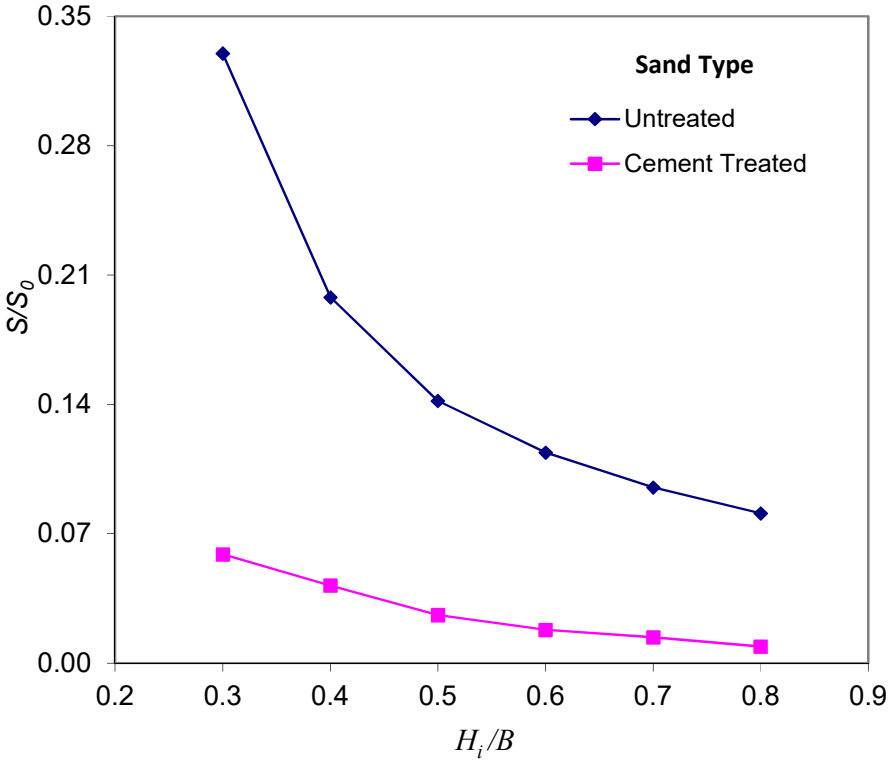

Fig. 6.8c Variation of S/S_0 with H_i/B for different Sand Type at $q/\gamma_{sat,1}B$=2.0

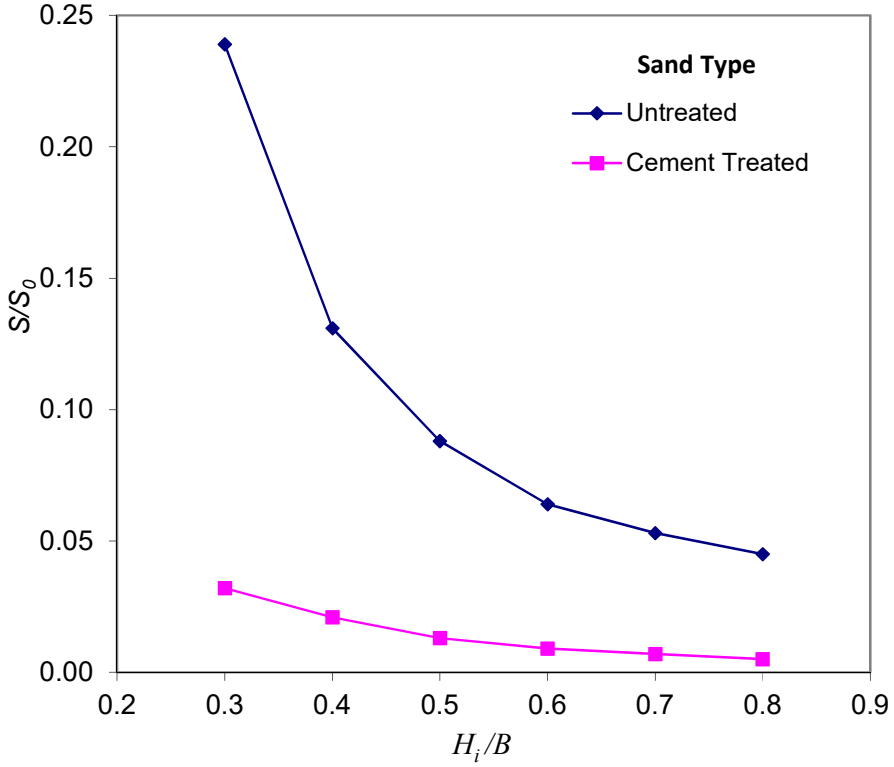

Fig. 6.8d Variation of S/S_0 with H_i/B for different Sand Type at $q/\gamma_{sat,1}B$=2.5

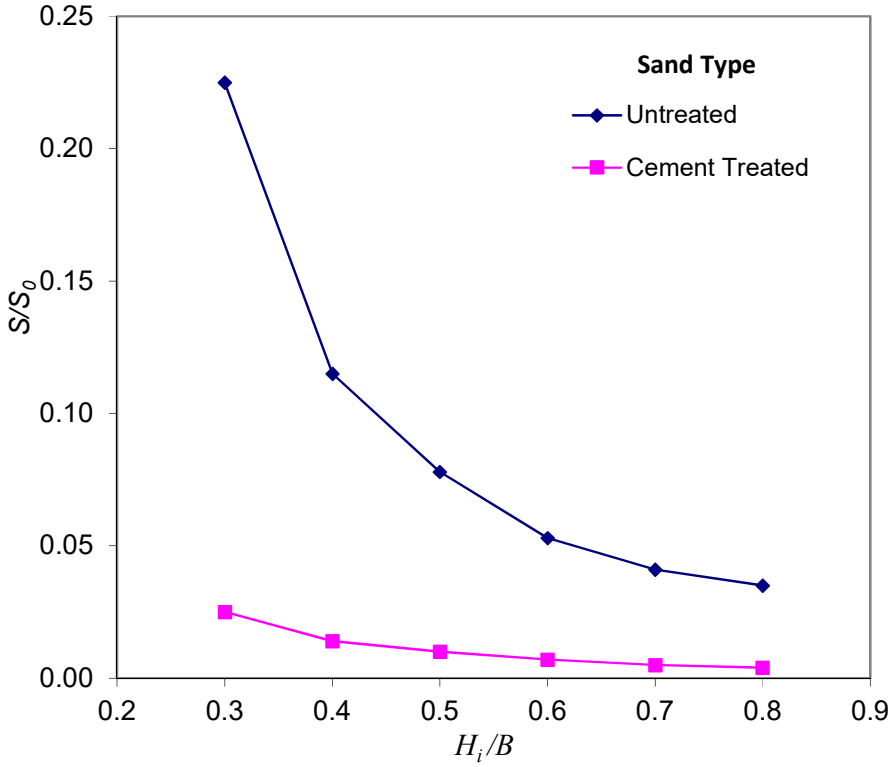

Fig. 6.8e Variation of S/S_0 with H_i/B for different Sand Type at $q/\gamma_{sat}B$=3.0

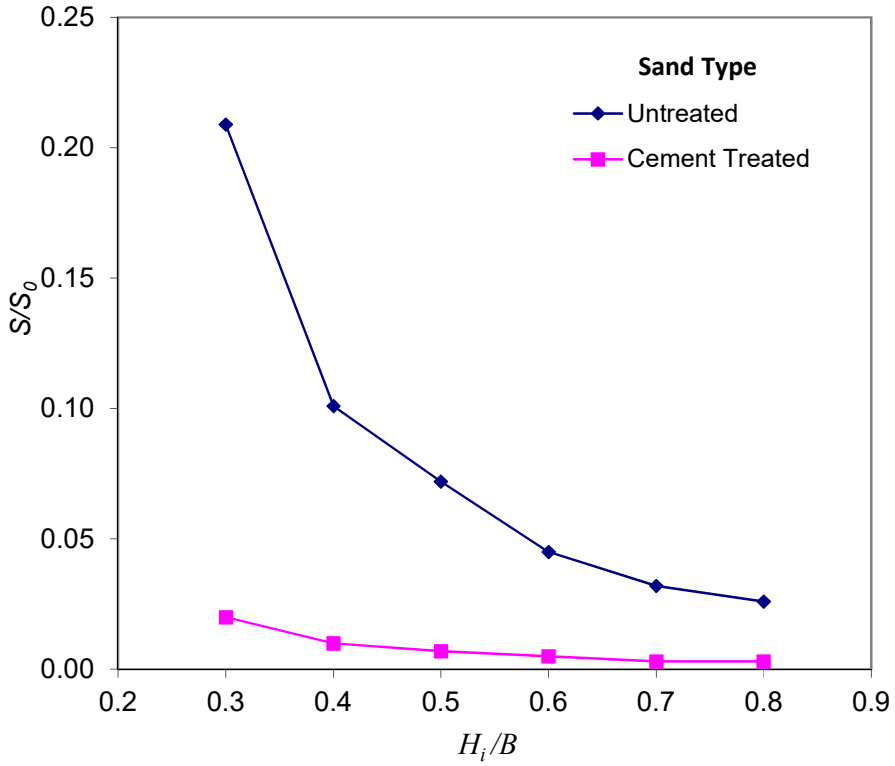

Fig. 6.8f Variation of S/S_0 with H_i/B for different Sand Type at $q/\gamma_{sat,1}B$=3.5

6.6 Design Guideline for Untreated Sand Mat

Design Guideline for ground improvement by providing untreated sand mat has been developed. This guideline is developed for strip footing on soft inorganic NC soil of Bangladesh having void ratio 1.0 to 1.45. The research work was limited on a single E' and ϕ' value of soft clay layer and also a single ϕ' value of sand mat.

These design charts may be used to obtain total settlement for particular values of footing pressure (q), Sand mat thickness (H_i), footing width (B) and initial void ratio ($\boldsymbol{e_{init}}$).

6.6.1 Design Charts in form of S/H_i vs $q/\gamma_{sat}B$ for different e_{init}

These design charts may be used to obtain total settlement, S for particular values of footing pressure (q), Sand mat thickness (H_i), footing width (B) and initial void ratio ($\boldsymbol{e_{init}}$) using different chart for different H_i/B.

From S/H_i vs $q/\gamma_{sat}B$ graphs for different e_{init} is presented in Fig. 6.9a through 6.9f this have been observed that for a particular $q/\gamma_{sat}B$ values of S/H_i for different void ratio, $\boldsymbol{e_{init}}$

are almost same. To avoid the very little effect of void ratio S/H_i for average void ratio have been plotted and is presented in Fig 6.10a and 6.10b.

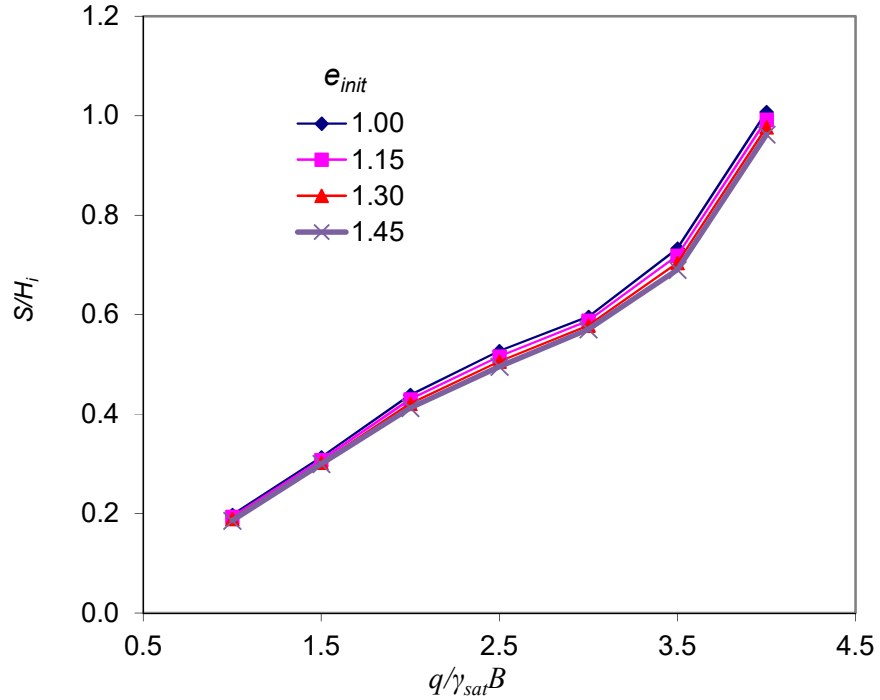

Fig. 6.9a Variation of S/H_i with $q/\gamma_{sat}B$ for different e_{init} at H_i/B=0.30

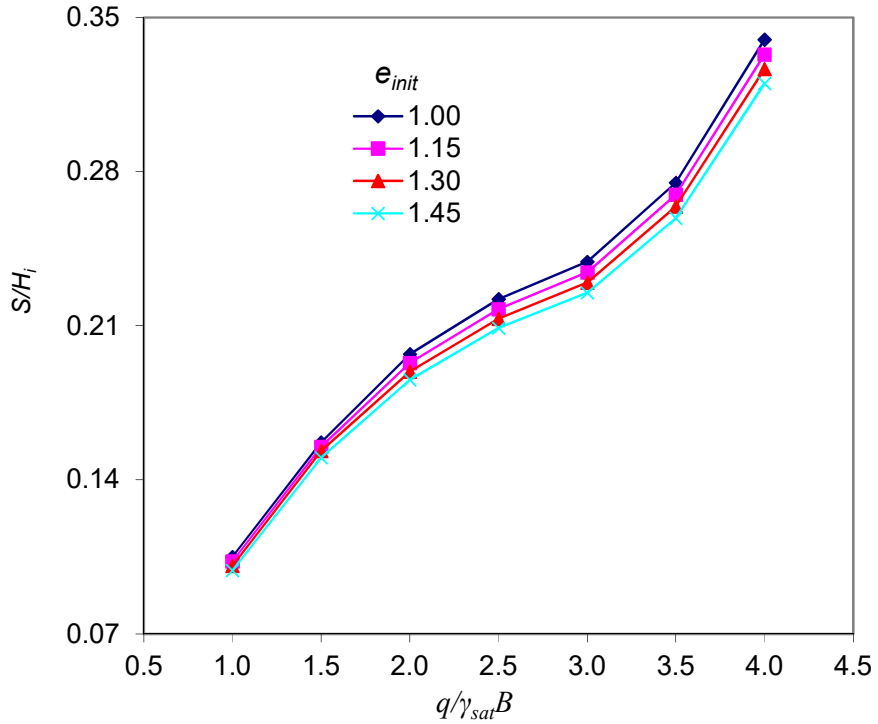

Fig. 6.9b Variation of S/H_i with $q/\gamma_{sat}B$ for different e_{init} at H_i/B=0.40

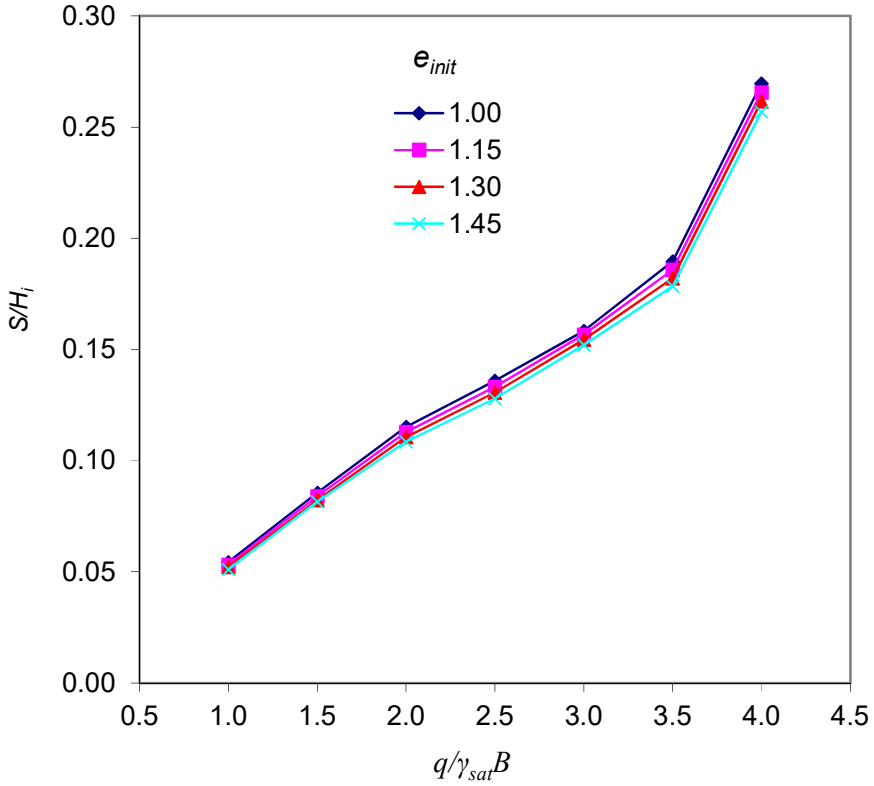

Fig. 6.9c Variation of S/H_i with $q/\gamma_{sat}B$ for different e_{init} at H_i/B=0.50

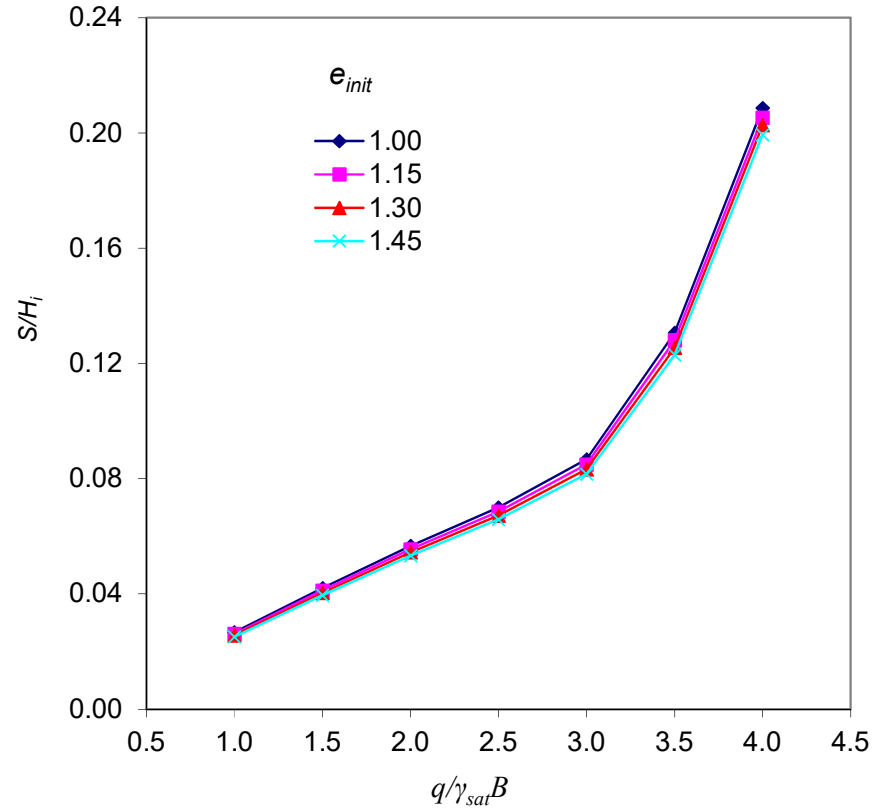

Fig. 6.9d Variation of S/H_i with $q/\gamma_{sat}B$ for different e_{init} at H_i/B=0.60

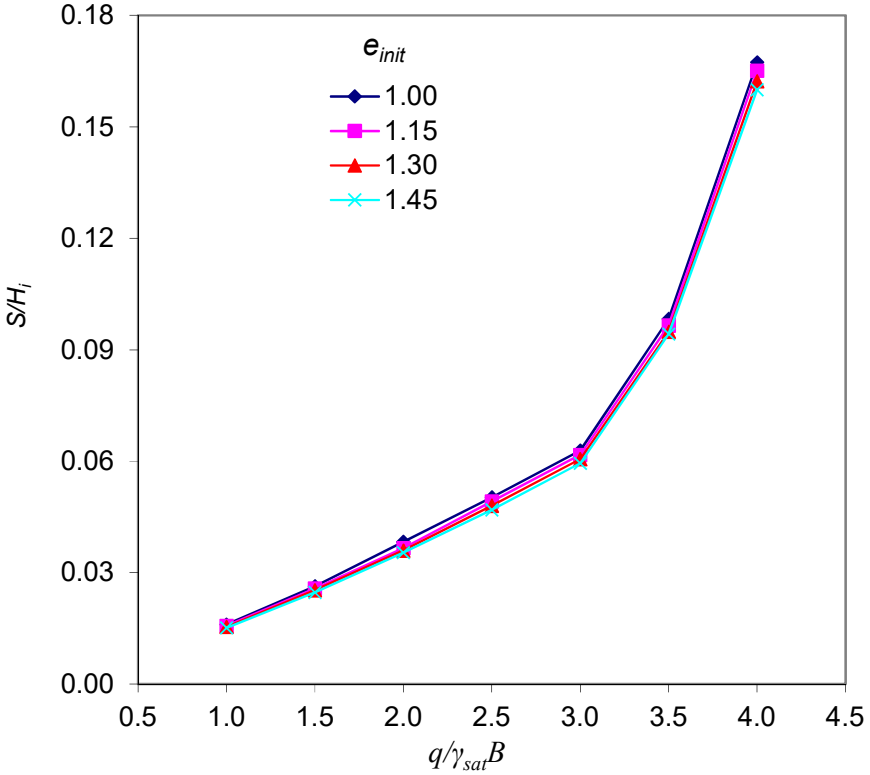

Fig. 6.9e Variation of S/H_i with $q/\gamma_{sat}B$ for different e_{init} at H_i/B=0.70

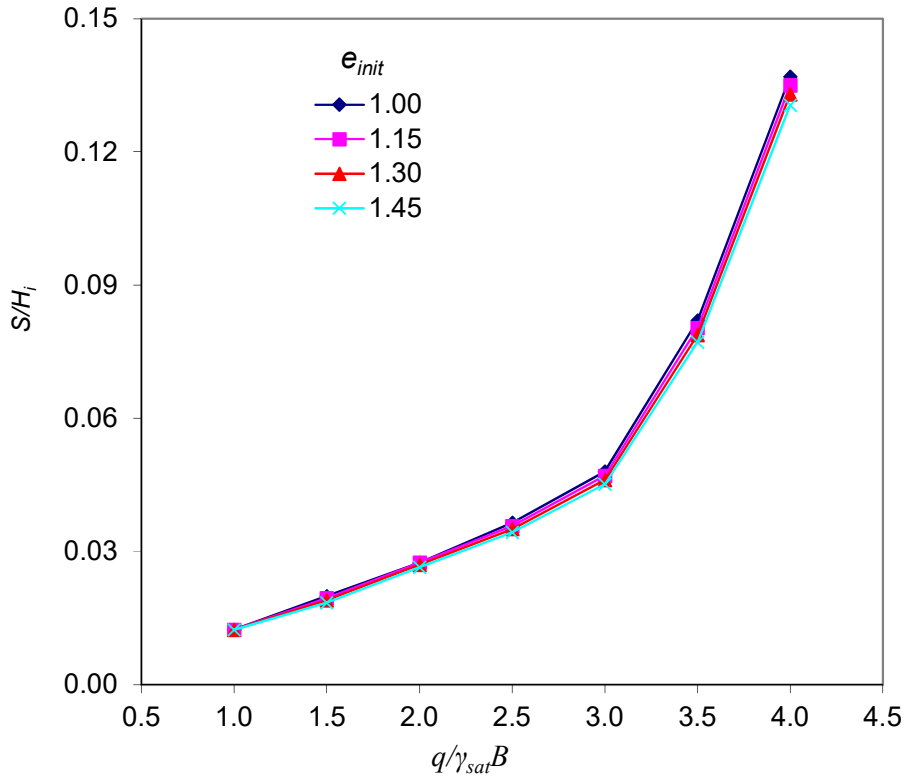

Fig. 6.9f Variation of S/H_i with $q/\gamma_{sat}B$ for different e_{init} at H_i/B=0.80

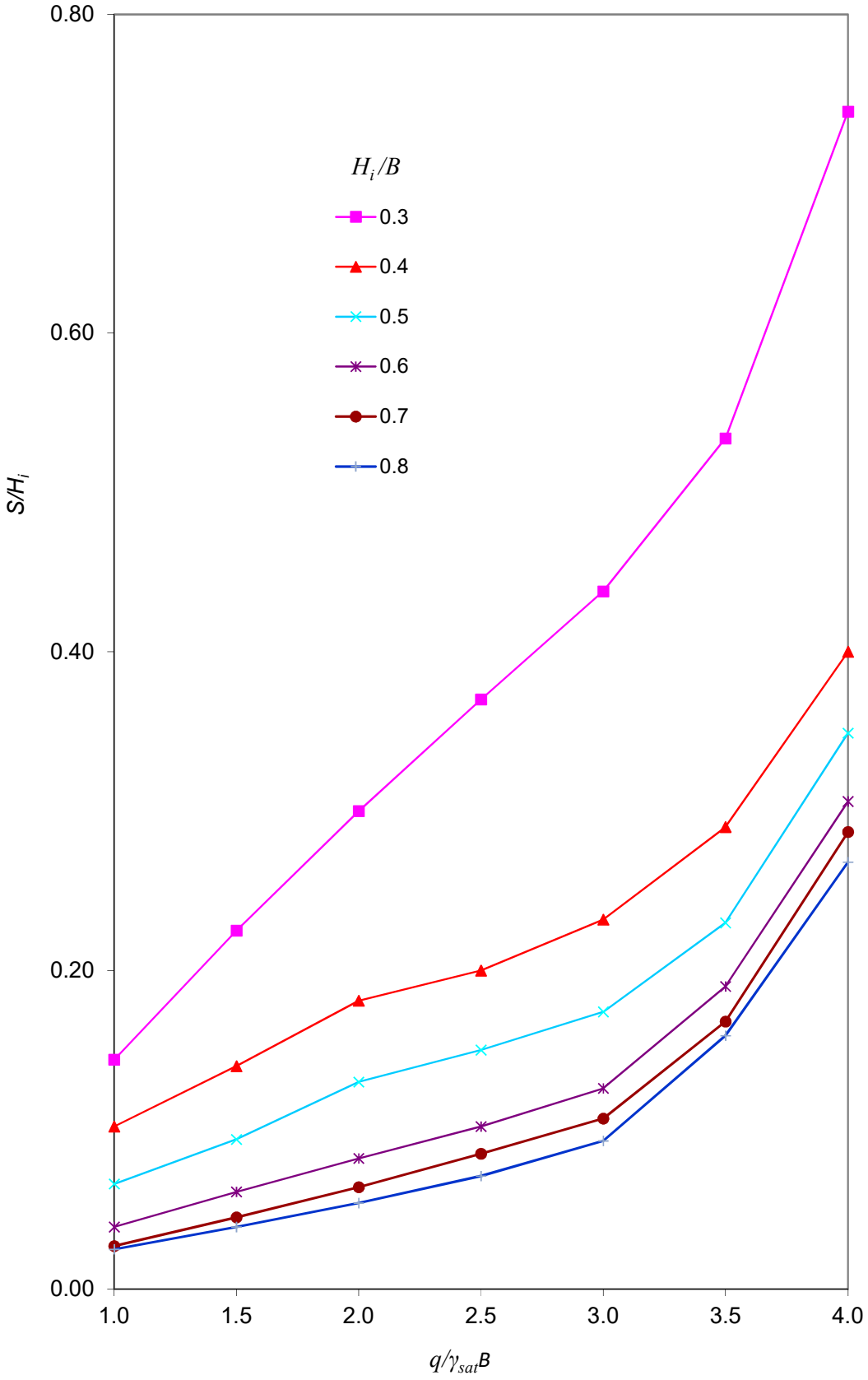

Fig. 6.10a Variation of S/S_0 with $q/\gamma_{sat}B$ for different H_i/B

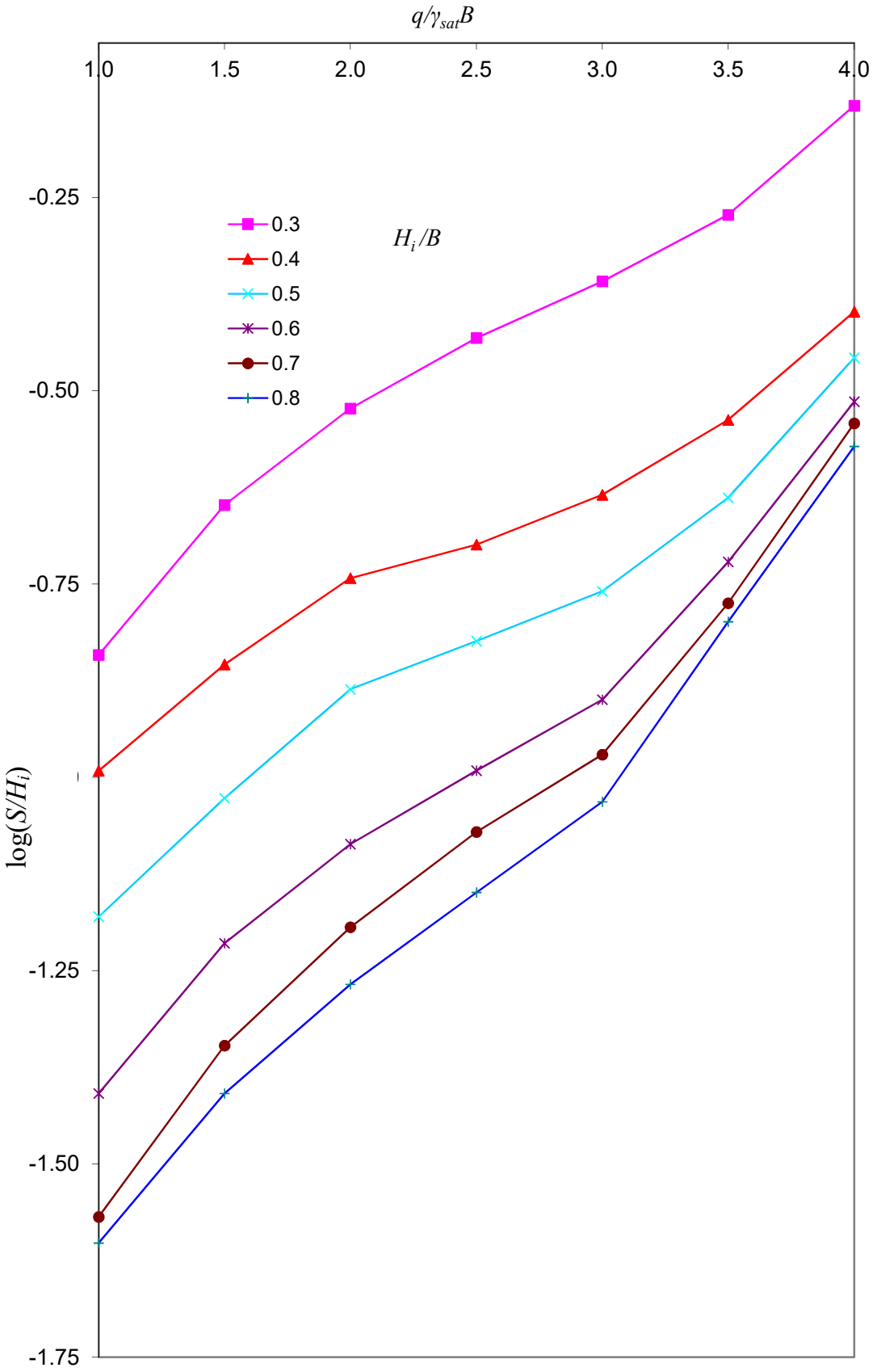

Fig. 6.10b Variation of S/S_0 with $q/\gamma_{sat}B$ for different H_i/B

6.6.2 Design Charts in form of S/H_i vs H_i/B for Different $q/\gamma_{sat}B$

These design charts may be used to obtain total settlement, S for particular values of footing pressure (q), Sand mat thickness (H_i) and footing width (B) using different chart for different initial void ratio (e_{init}).

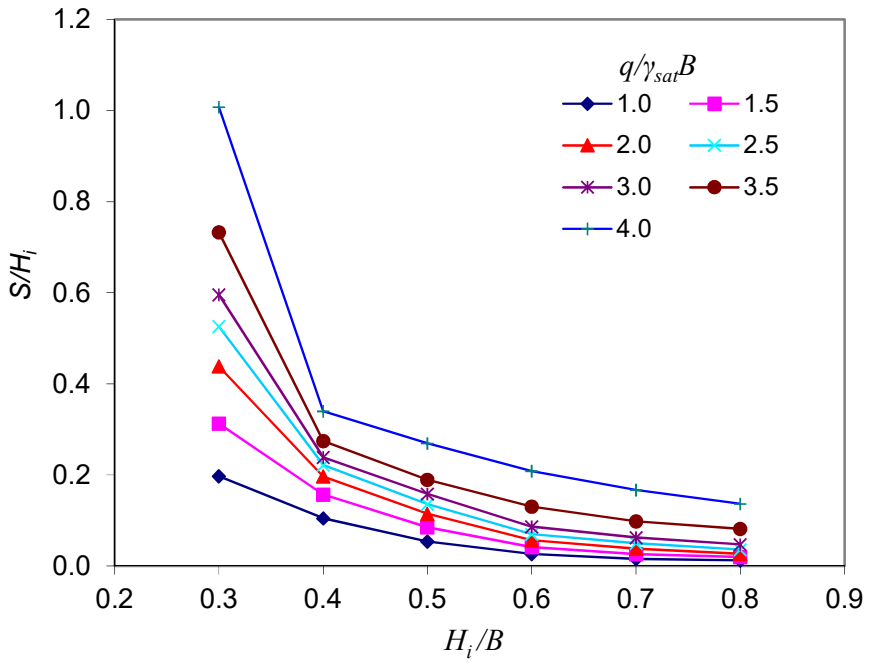

Fig. 6.11a Variation of S/H_i with H_i/B for different $q/\gamma_{sat}B$ at e_{init}=1.0

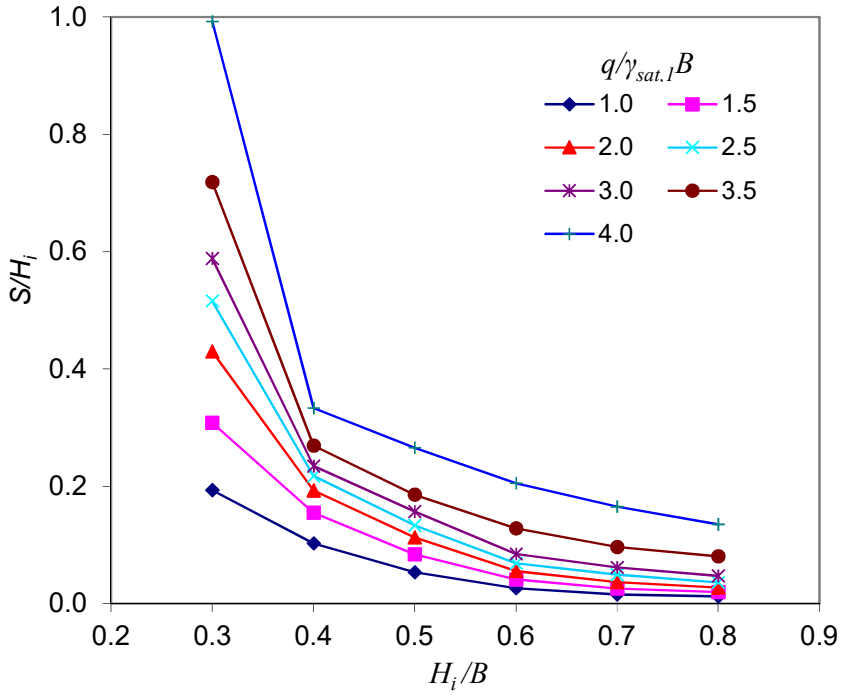

Fig. 6.11b Variation of S/H_i with H_i/B for different $q/\gamma_{sat}B$ at e_{init}

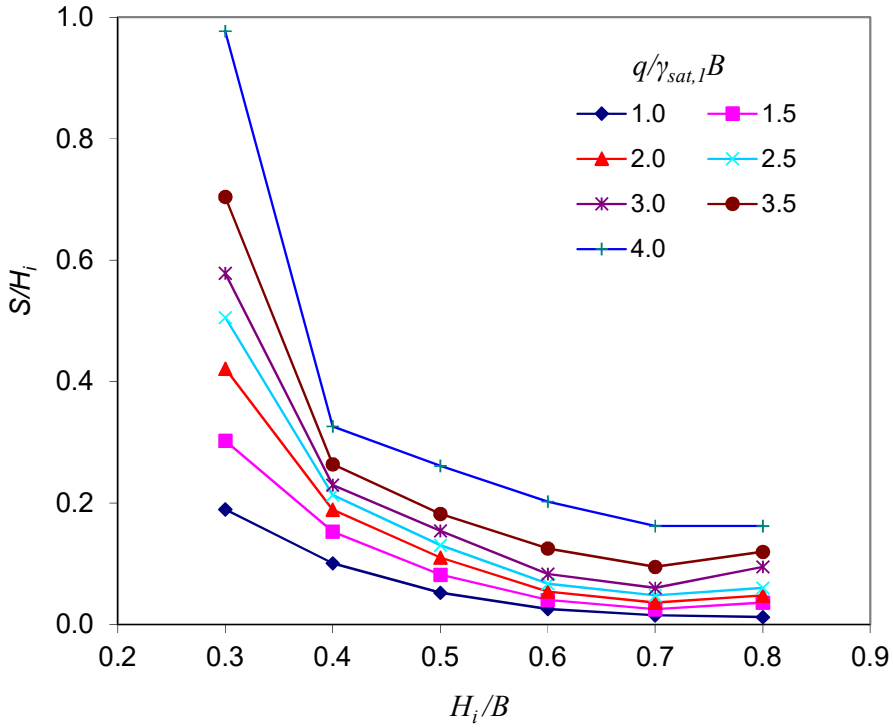

Fig. 6.11c Variation of S/H_i with H_i/B for different $q/\gamma_{sat}B$ at e_{init}=1.3

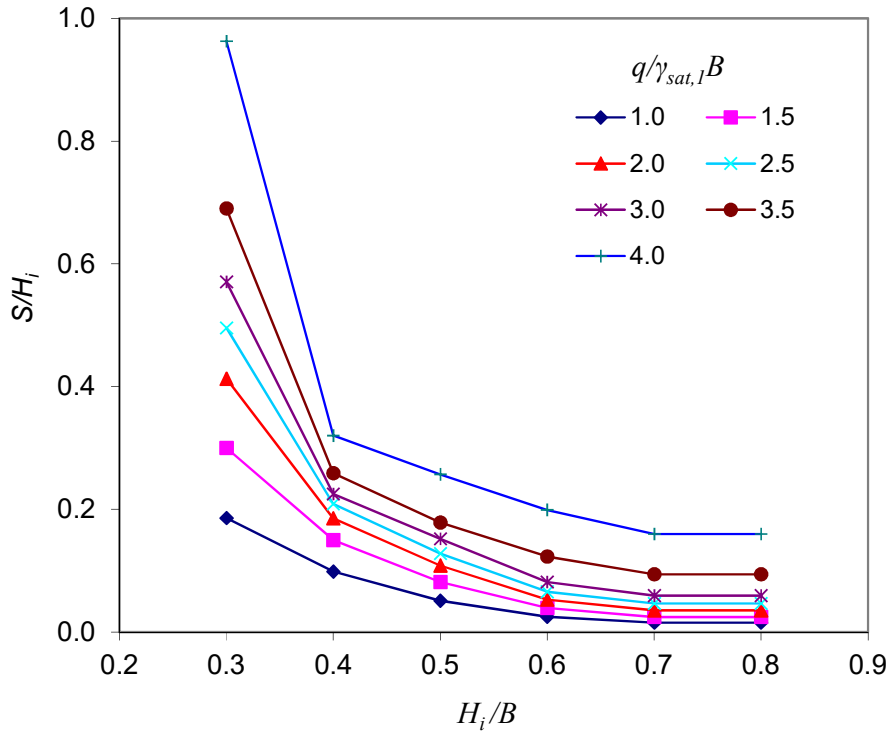

Fig. 6.11d Variation of S/H_i with H_i/B for different $q/\gamma_{sat}B$ at e_{init}=1.45

6.6.3 Design Charts in form of S/H_i vs $q/\gamma_{sat}B$ for different H_i/B

These design charts may be used to obtain total settlement, S for particular values of footing pressure (q), Sand mat thickness (H_i) and footing width (B) using different chart for different initial void ratio (e_{init}).

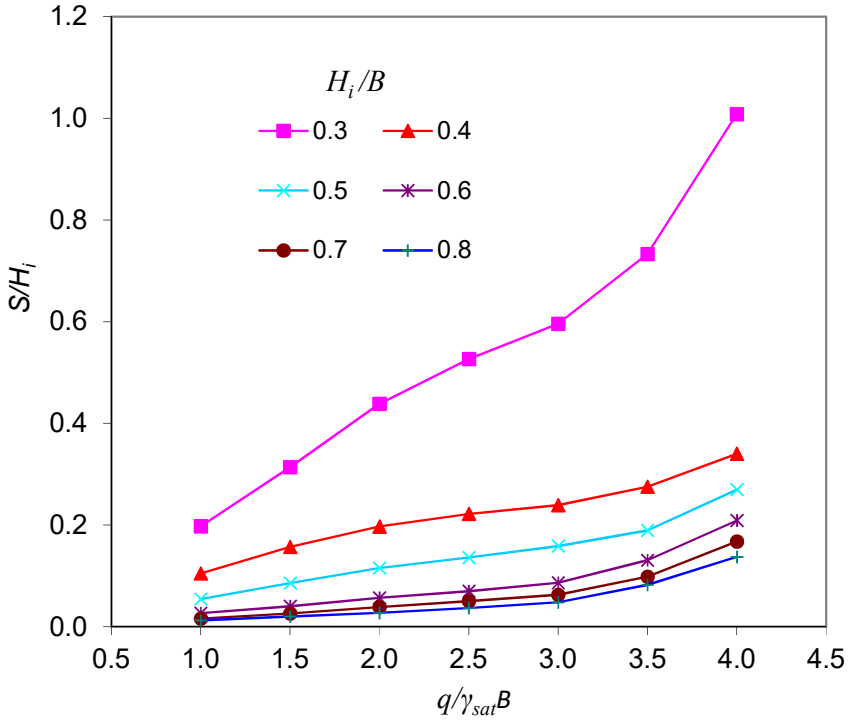

Fig. 6.12.a Variation of S/H_i with $q/\gamma_{sat}B$ for different H_i/B at e_{init}=1.0

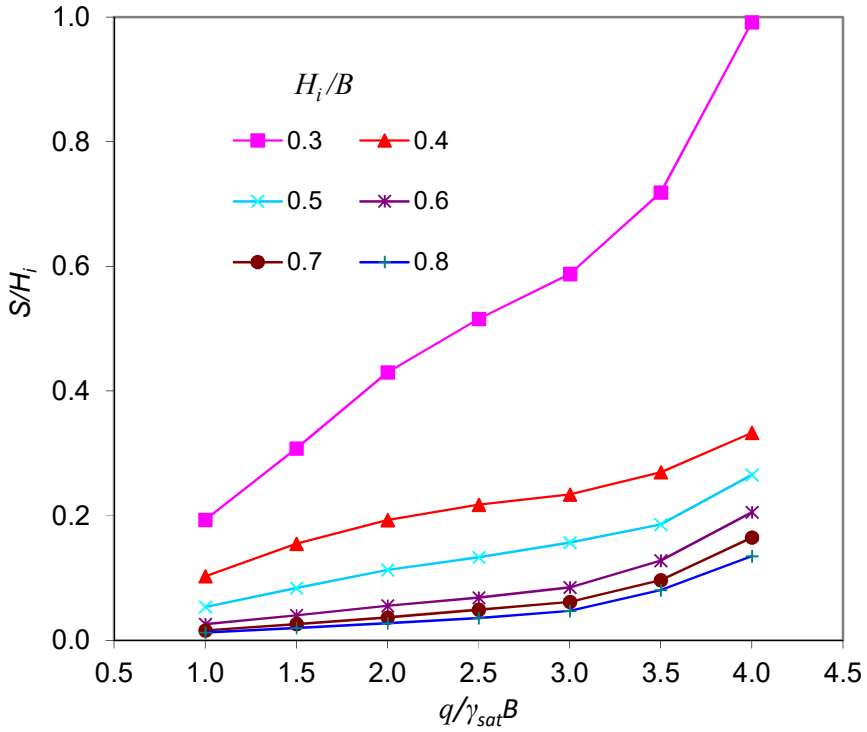

Fig. 6.12b Variation of S/H_i with $q/\gamma_{sat}B$ for different H_i/B at e_{init}=1.15

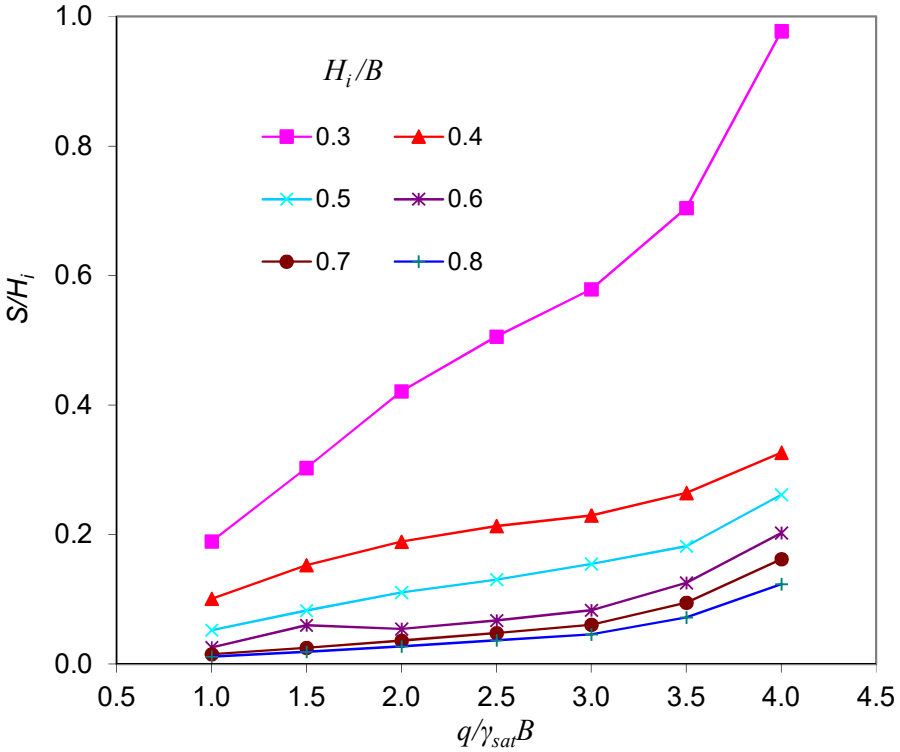

Fig. 6.12c Variation of S/H_i with $q/\gamma_{sat}B$ for different H_i/B at e_{init}=1.3

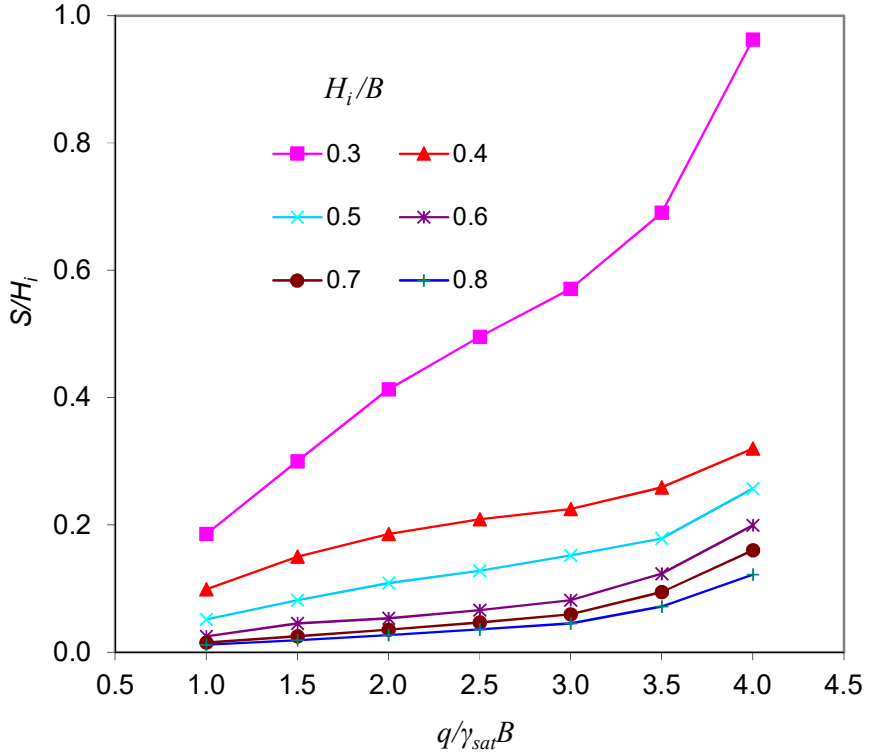

Fig. 6.12d Variation of S/H_i with $q/\gamma_{sat}B$ for different H_i/B at e_{init}=1.45

6.7 Design Guideline for Cement Treated Sand Mat

Design Guideline for ground improvement by providing Cement Treated sand mat has been developed. This guideline is developed for strip footing on soft inorganic NC soil of Bangladesh having void ratio 1.0 to 1.45.

The research work was limited on a single E' and ϕ' value of soft clay layer and also a single ϕ' value of sand mat.

These design charts may be used to obtain total settlement for particular values of footing pressure (q), Sand mat thickness (H_i), footing width (B) and initial void ratio (e_{init}).

6.7.1 Design Charts in form of S/H_i vs $q/\gamma_{sat}B$ for different e_{init}

These design charts may be used to obtain total settlement, S for particular values of footing pressure (q), Sand mat thickness (H_i), footing width (B) and initial void ratio (e_{init}) using different chart for different H_i/B.

From S/H_i vs $q/\gamma_{sat}B$ graphs for different e_{init} is presented in Fig. 6.13a through 6.13f this have been observed that for a particular $q/\gamma_{sat}B$ values of S/H_i for different void ratio, e_{init} are almost same.

To avoid the very little effect of void ratio S/H_i for average void ratio have been plotted and is presented in Fig 6.14a and Fig 6.14b.

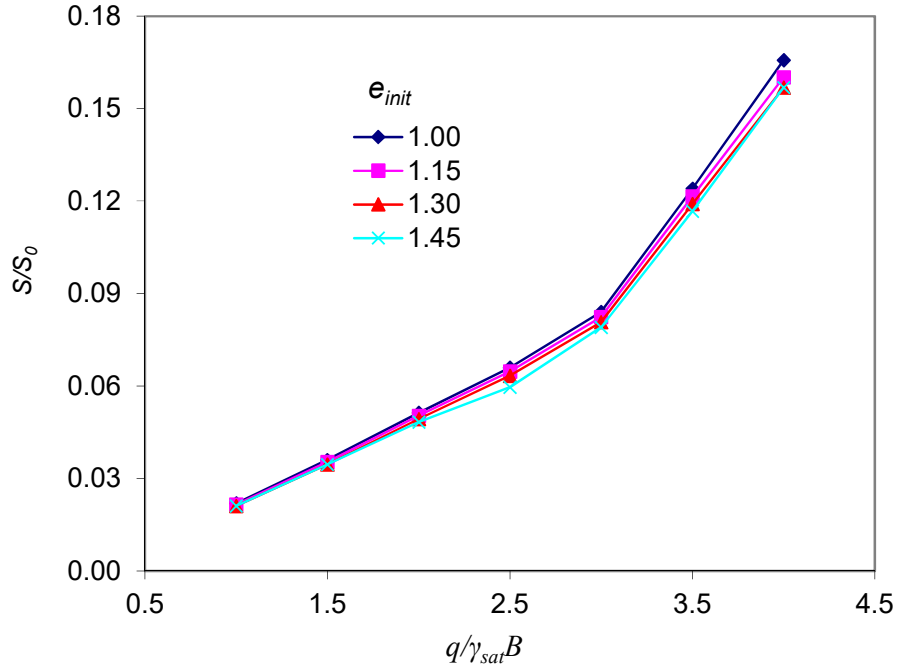

Fig. 6.13a Variation of S/S_0 with $q/\gamma_{sat}B$ for different e_{init} at H_i/B=0.30

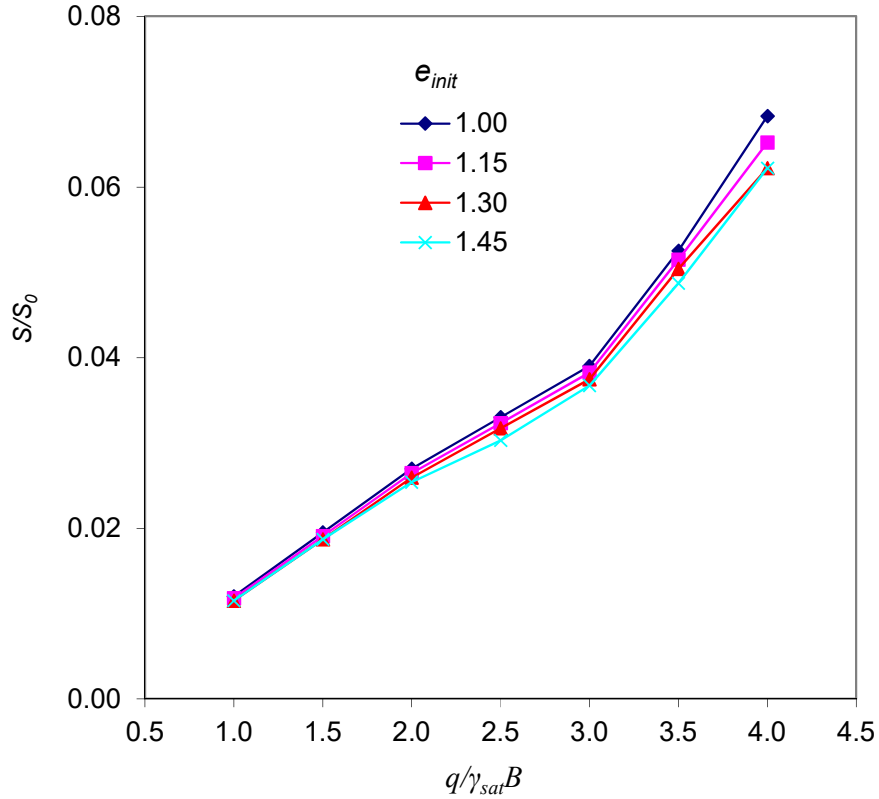

Fig. 6.13b Variation of S/S_0 with $q/\gamma_{sat}B$ for different e_{init} at H_i/B=0.40

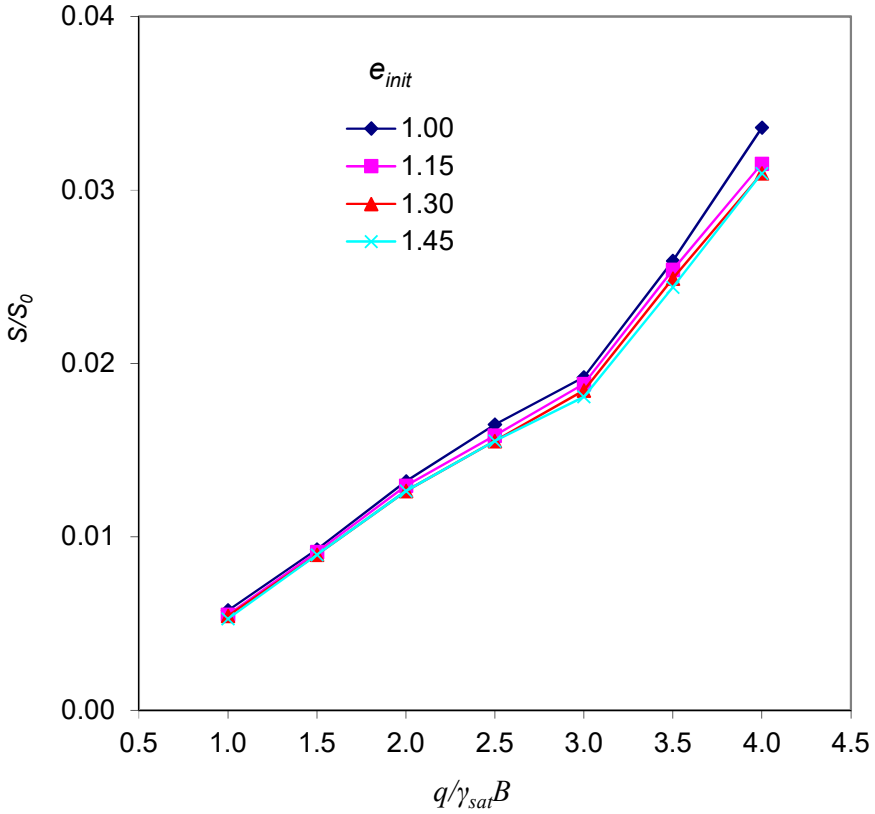

Fig. 6.13c Variation of S/S_0 with $q/\gamma_{sat}B$ for different e_{init} at H_t/B=0.50

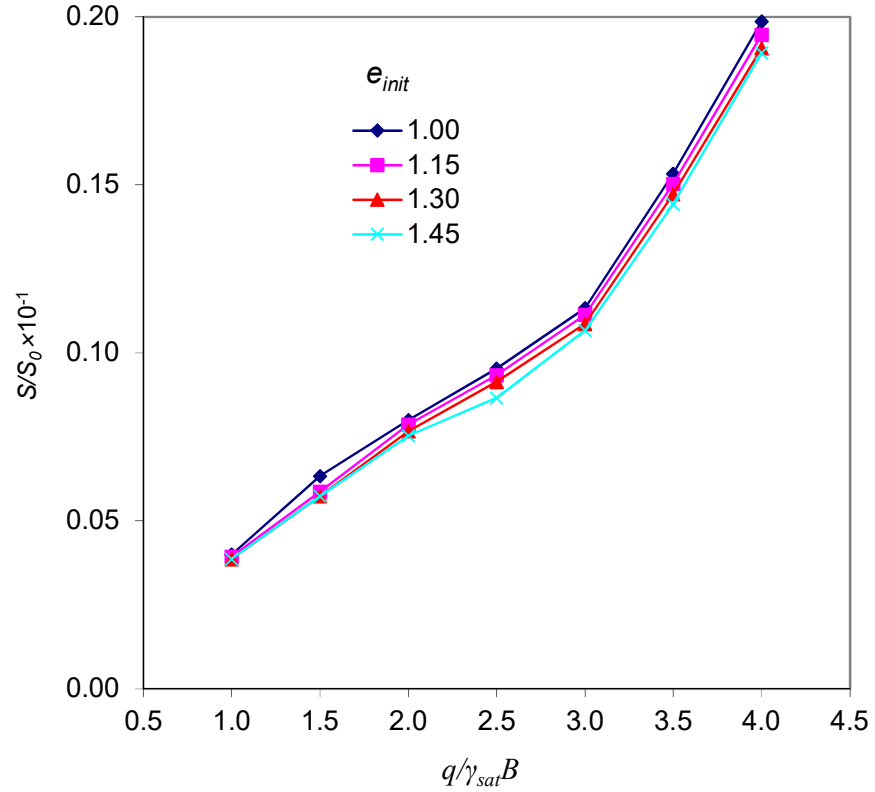

Fig. 6.13d Variation of S/S_0 with $q/\gamma_{sat}B$ for different e_{init} at H_t/B=0.60

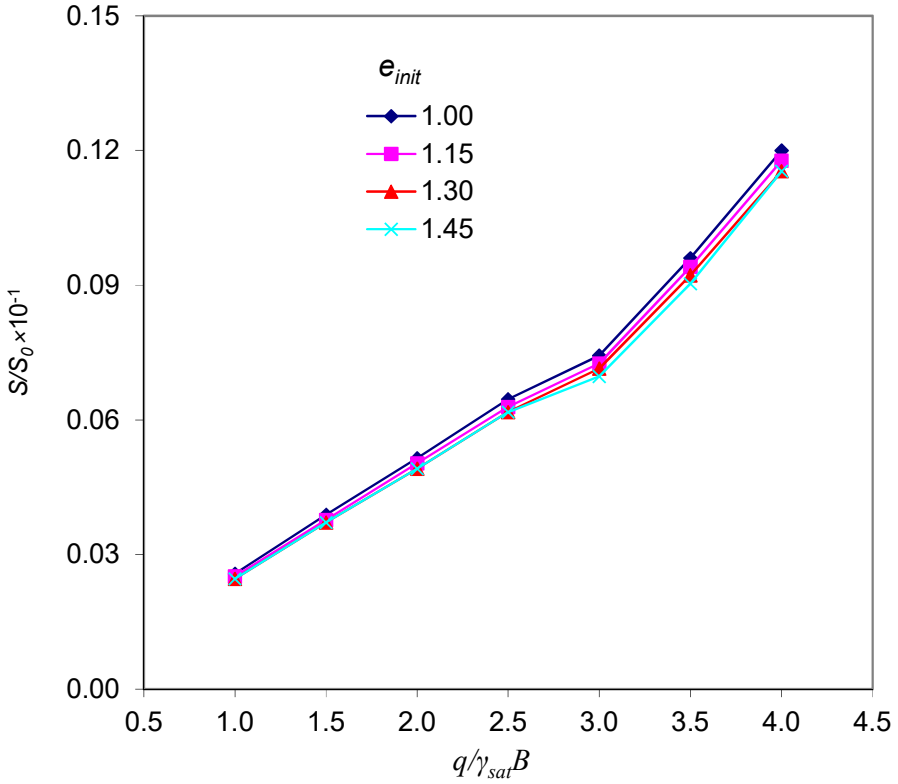

Fig. 6.13e Variation of S/S_0 with $q/\gamma_{sat}B$ for different e_{init} at H_t/B=0.70

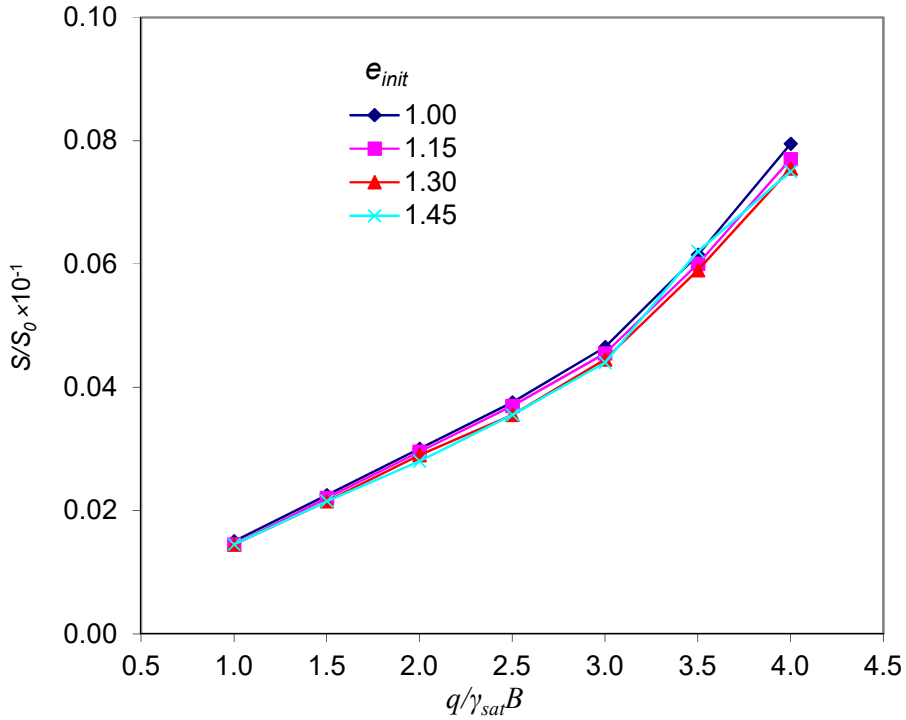

Fig. 6.13f Variation of S/S_0 with $q/\gamma_{sat}B$ for different e_{init} at H_t/B=0.80

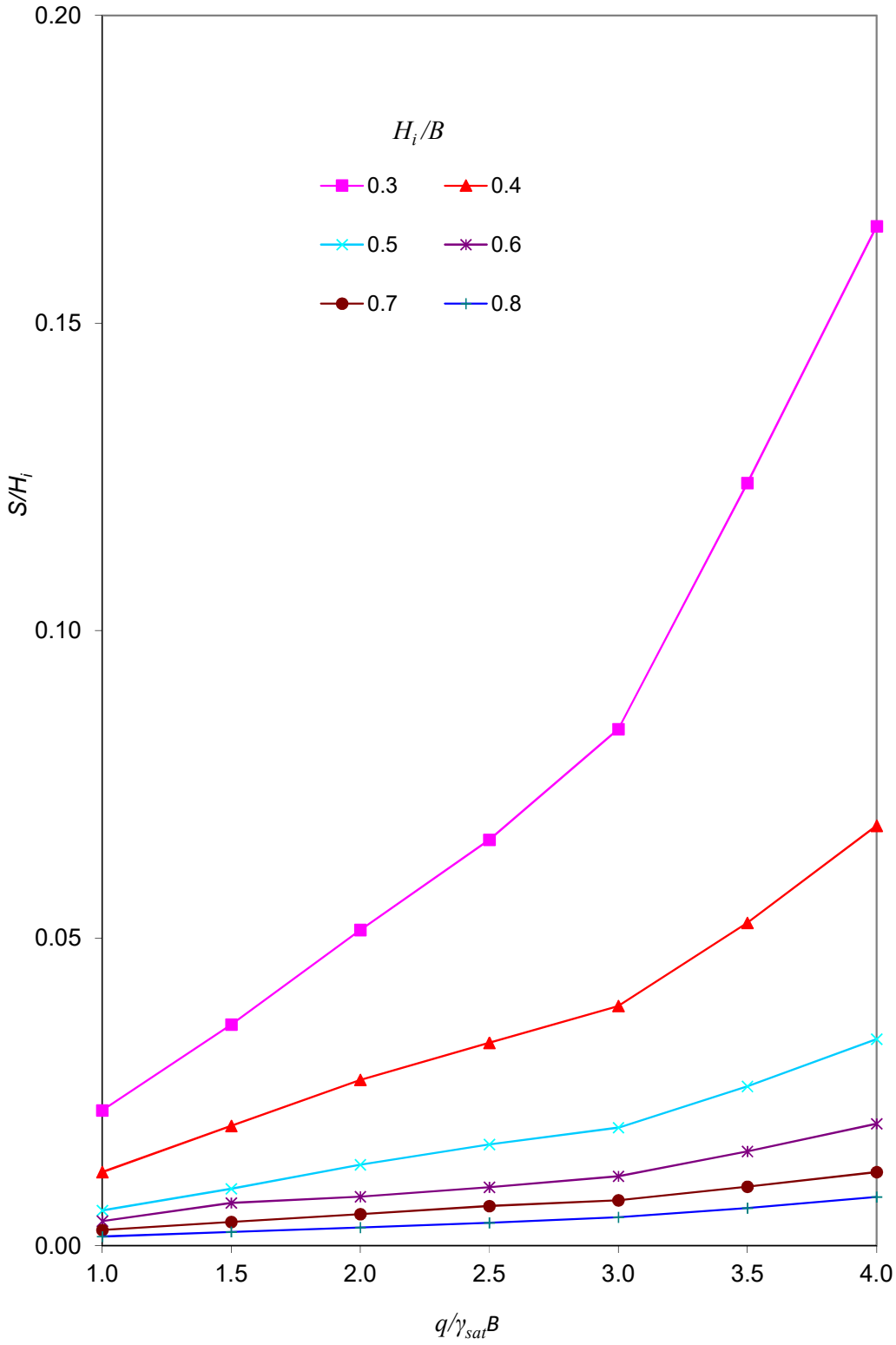

Fig. 6.14a Variation of S/S_0 with $q/\gamma_{sat}B$ for different H_i/B at e_{init}=1.00

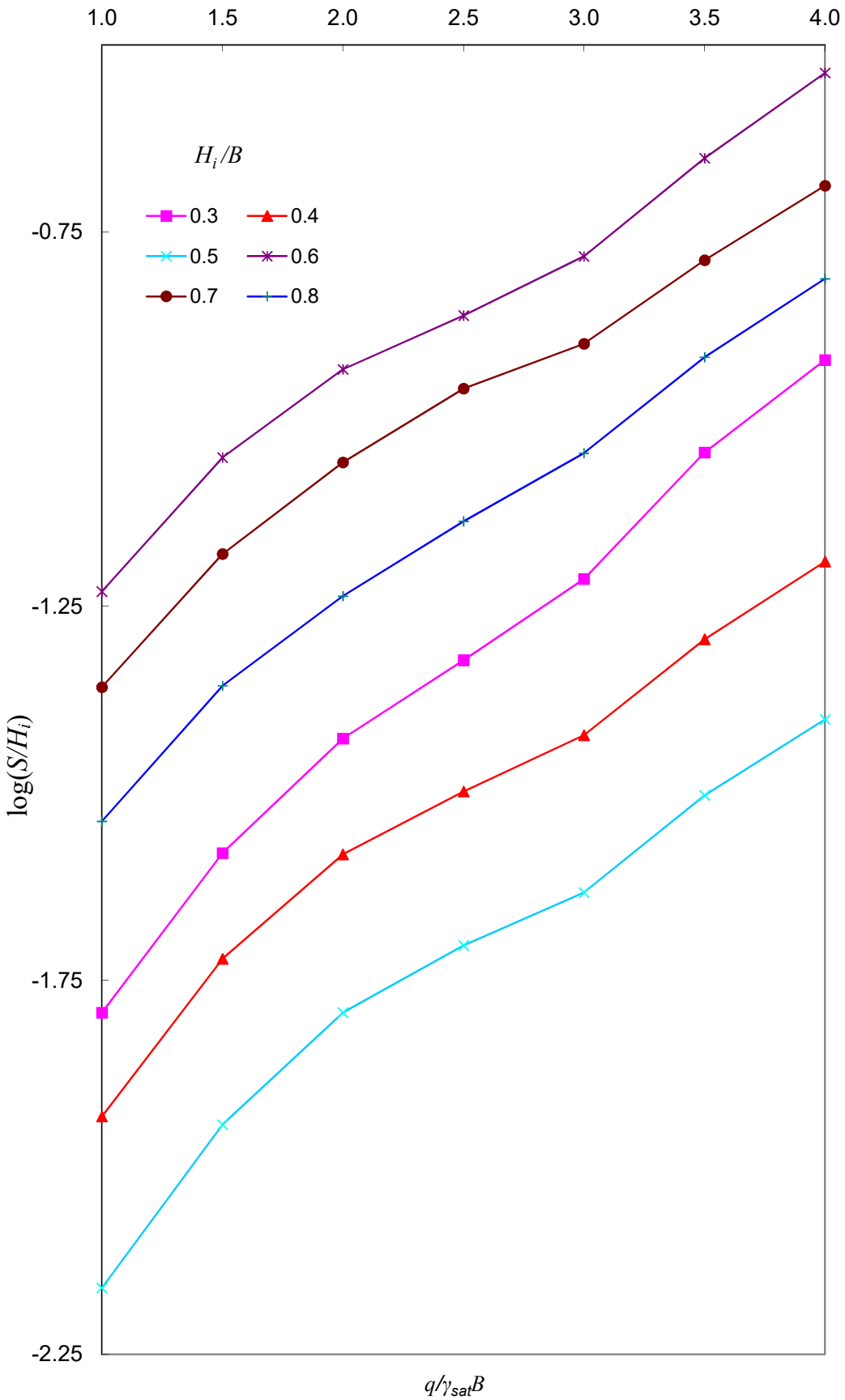

Fig. 6.14b Variation of $\log(S/H_i)$ with $q/\gamma_{sat}B$ for different H_i/B at e_{init}=1.00

6.7.2 Design Charts in form of S/H_i vs H_i/B for different $q/\gamma_{sat}B$

These design charts may be used to obtain total settlement, S for particular values of footing pressure (q), Sand mat thickness (H_i) and footing width (B) using different chart for different initial void ratio (e_{init}).

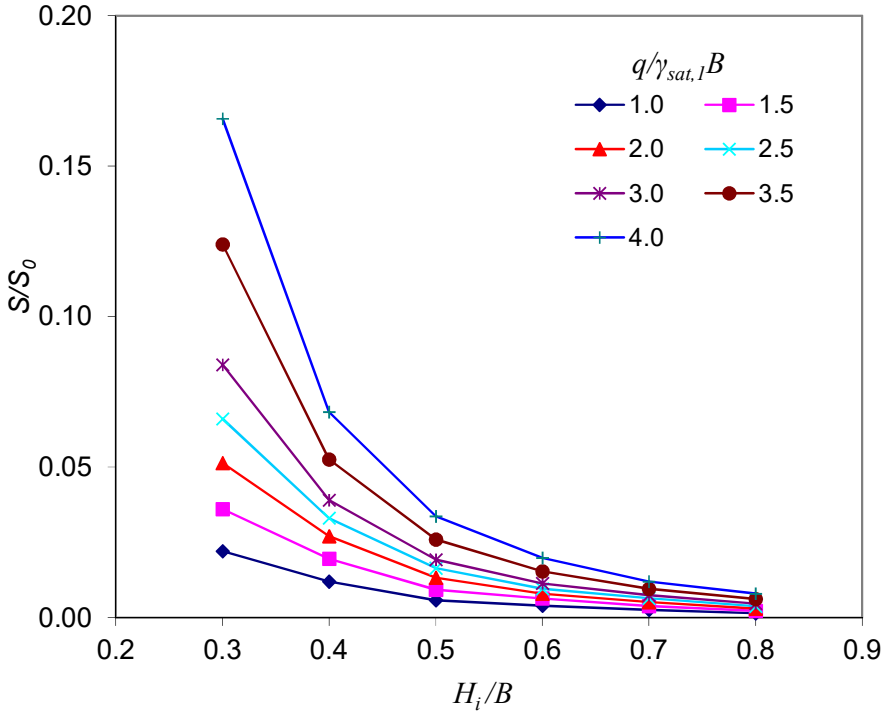

Fig. 6.15a Variation of S/S_0 with H_i/B for different $q/\gamma_{sat}B$ at e_{init}=1.00

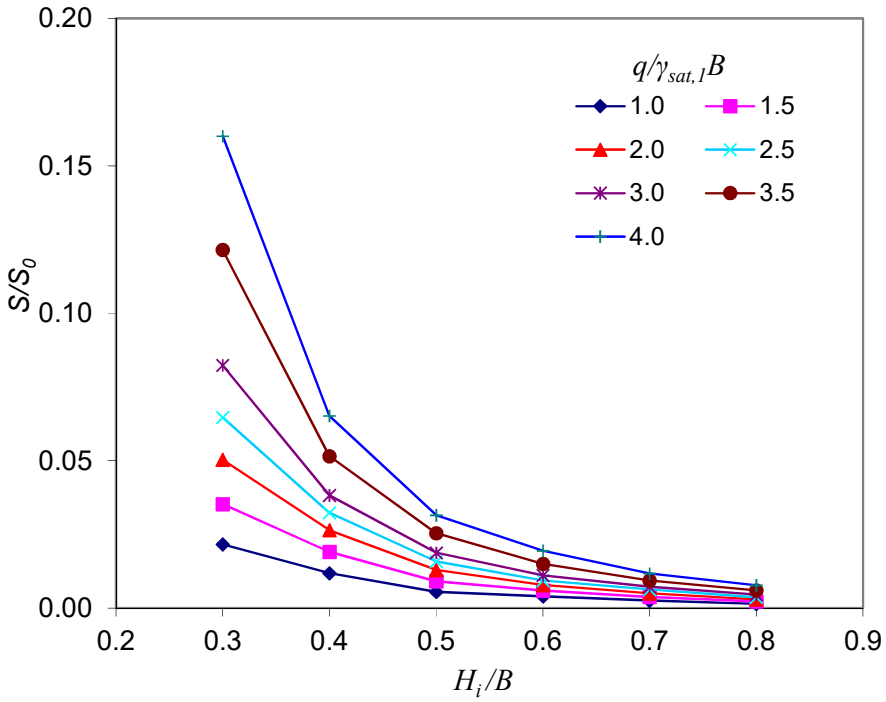

Fig. 6.15b Variation of S/S_0 with H_i/B for different $q/\gamma_{sat}B$ at e_{init}=1.15

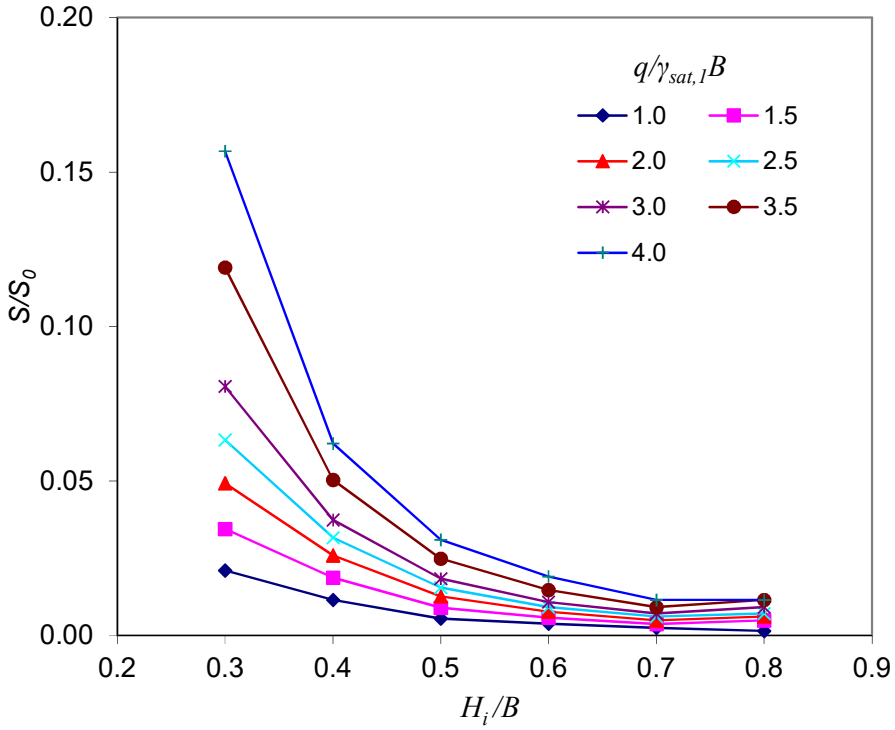

Fig. 6.15c Variation of S/S_0 with H_i/B for different $q/\gamma_{sat}B$ at e_{init}=1.30

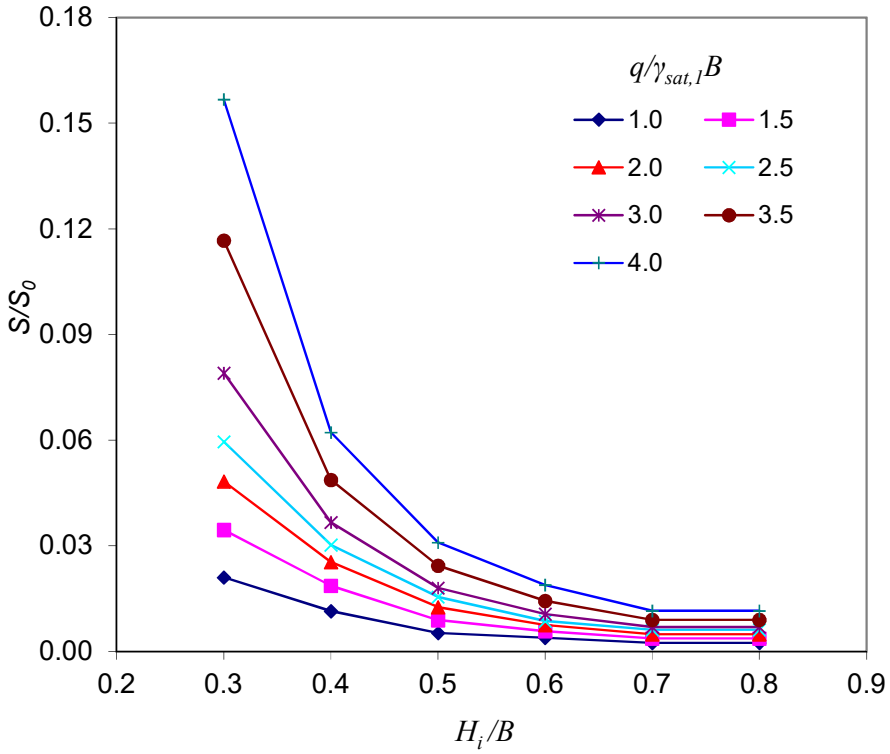

Fig. 6.15d Variation of S/S_0 with H_i/B for different $q/\gamma_{sat}B$ at e_{init}=1.45

6.7.3 Design Charts in form of S/H_i vs $q/\gamma_{sat}B$ for different $q/\gamma_{sat}B$

These design charts may be used to obtain total settlement, S for particular values of footing pressure (q), Sand mat thickness (H_i) and footing width (B) using different chart for different initial void ratio (e_{init}).

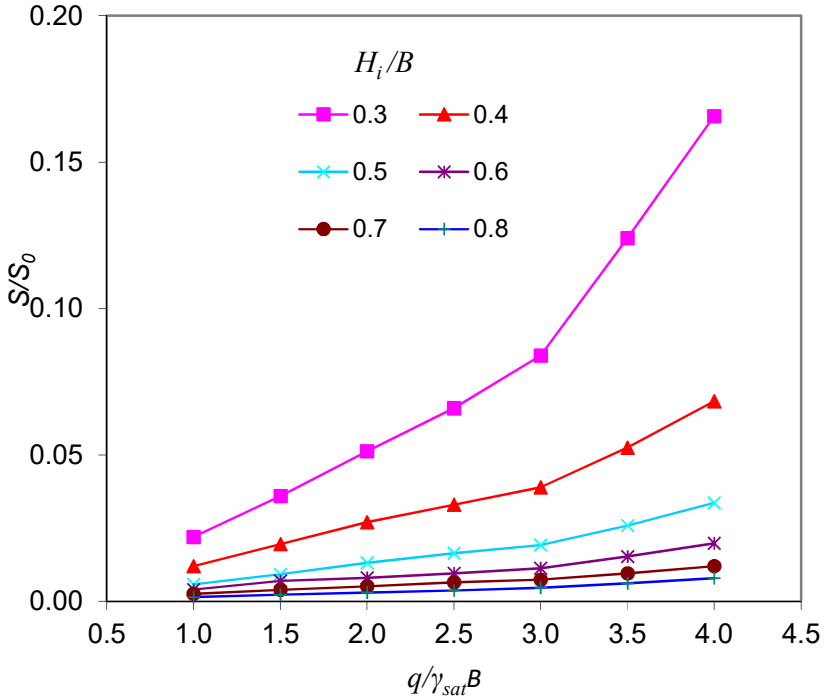

Fig. 6.16a Variation of S/S_0 with $q/\gamma_{sat}B$ for different H_i/B at e_{init}

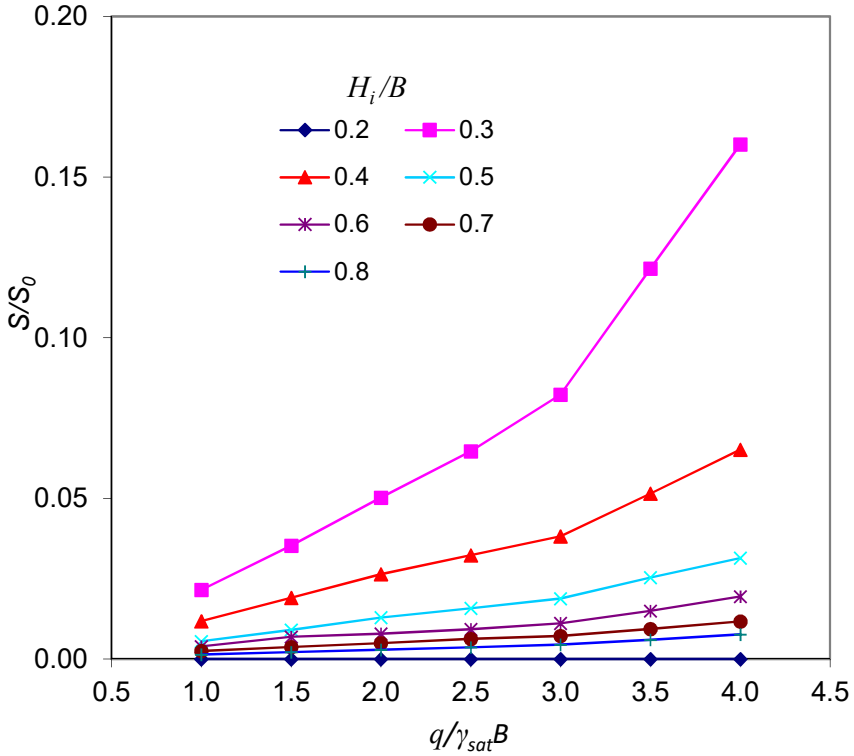

Fig. 6.16b Variation of S/S_0 with $q/\gamma_{sat}B$ for different H_i/B at e_{init}=1.15

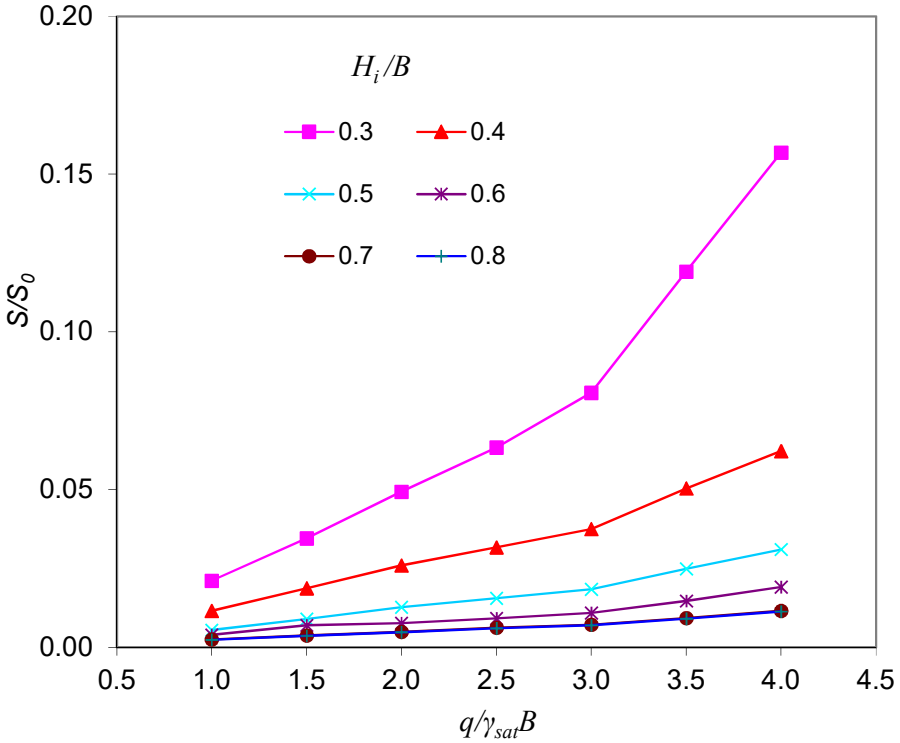

Fig. 6.16c Variation of S/S_0 with $q/\gamma_{sat}B$ for different H_i/B at e_{init}=1.30

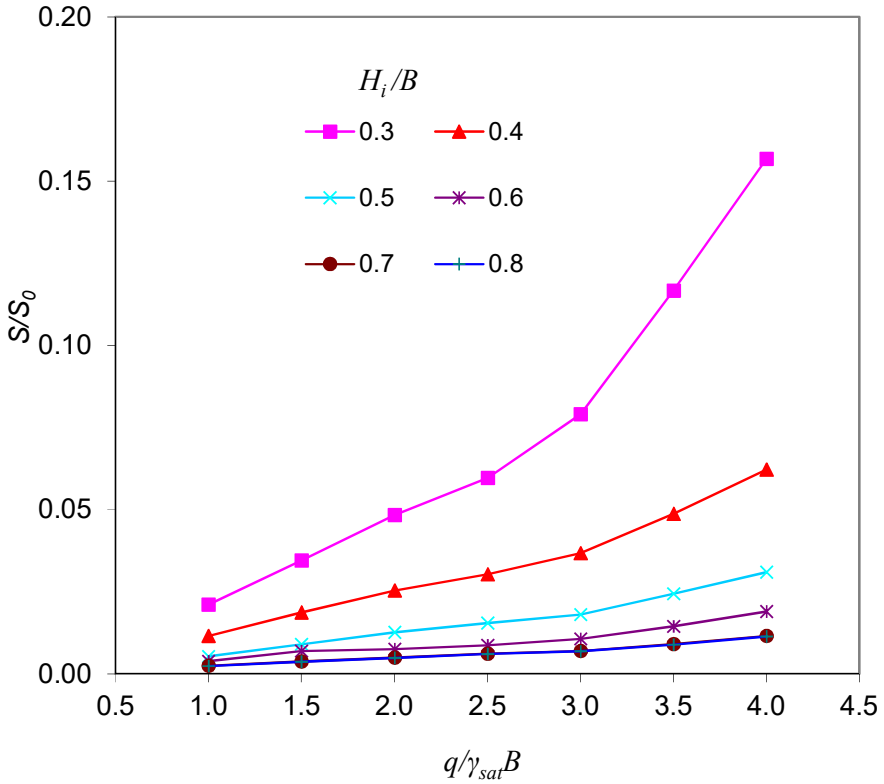

Fig. 6.16d Variation of S/S_0 with $q/\gamma_{sat}B$ for different H_i/B at e_{init}=1.45

6.8 Equation for Design

6.8.1 Equation for Design H_i for Untreated Sand as Upper Layer

Combined logarithmic design chart for untreated sand is as upper layer presented in Fig. 6.10. The curves in that chart for different $\frac{S}{H_i}$ may be converted to exponential equation. The common equation for untreated sand is as upper layer obtained and given below as Equation 6.1. This equation may be written another form specifying the value of settlement equal to a permissible value and this form of that equation is also given below as Equation 6.2.

For untreated sand as upper layer settlement of strip footing may be calculated for particular value of H_i, q, B and γ_{sat} using design chart or equations presented in fig. 6.20 and Equation 6.1.

$$\frac{S}{H_i} = a\left(10^{b\frac{q}{\gamma_{sat}B}}\right) \qquad \mathbf{6.1}$$

where,

H_i/B	0.3	0.4	0.5	0.6	0.7	0.8
a	0.0995	0.0719	0.0424	0.0216	0.0138	0.0117
b	0.217	0.180	0.219	0.275	0.317	0.324

For a specific value of settlement the design thickness of sand mat may be obtained using Equation 6.2.

$$H_i = \frac{1}{a}\left(10^{-b\frac{q}{\gamma_{sat}B}}\right)S \qquad \mathbf{6.2}$$

The permissible settlement as per BNBC 2015 is 50mm. The equations has been converted to equations 6.3 for unique settlement. Design thickness of sand mat for possible settlement of 50mm may be obtained using this equations.

$$H_i(mm) = \frac{50}{a}\left(10^{-b\frac{q}{\gamma_{sat}B}}\right) \qquad \mathbf{6.3}$$

6.8.2 Equation for Design H_i for Cement Treated Sand as Upper Layer

Combined logarithmic design chart for Cement Treated sand is as upper layer presented in Fig. 6.10. The curves in that chart for different $\frac{S}{H_i}$ may be converted to exponential equation. The common equation for Cement Treated sand is as upper layer obtained and given below as Equation 6.4. This equation may be written another form specifying the value of settlement equal to a permissible value and this form of that equation is also given below as Equation 6.6.

For Cement Treated sand as upper layer settlement of strip footing may be calculated for particular value of H_i, q, B and γ_{sat} using design chart or equations presented in fig. 6.20 and Equation 6.4.

$$\frac{S}{H_i} = a\left(10^{b\frac{q}{\gamma_{sat}B}}\right) \qquad \mathbf{6.4}$$

where,

H_i/B	0.3	0.4	0.5	0.6	0.7	0.8
a	0.0394	0.0304	0.0187	0.00944	0.00472	0.0117
b	0.216	0.211	0.231	0.278	0.231	0.237

For a specific value of settlement the design thickness of sand mat may be obtained using Equation 6.5.

$$H_i = \frac{1}{a}\left(10^{-b\frac{q}{\gamma_{sat}B}}\right)S \qquad \mathbf{6.5}$$

The permissible settlement as per BNBC 2015 is 50mm. The equations has been converted to equations 6.6 for unique settlement. Design thickness of sand mat for possible settlement of 50mm may be obtained using this equations.

$$H_i(mm) = \frac{50}{a}\left(10^{-b\frac{q}{\gamma_{sat}B}}\right) \qquad \mathbf{6.6}$$

6.9 Study on Displacement Field

6.9.1 Total Displacement in Untreated Sand as Upper Layer

Total displacement in Untreated Sand as Upper Layer for q=200kN/m^2, e_{init}=1.15 are presented in this section.

Total displacement is shown separately by arrows in Figure. 6.17a through 6.17f and by shadings in Figure. 6.19a through 6.19f.

6.9.1.1 Total Displacement Shown by Arrows for Untreated Upper Sand Mat

For H_i =1.5 or above settlement of upper layer into bottom clay layer is very small which represented the distribution of major deformation with in upper layer and the function of footing is limited in upper layer and this indicates complete effectiveness of upper layer in bearing the foundation effectively.

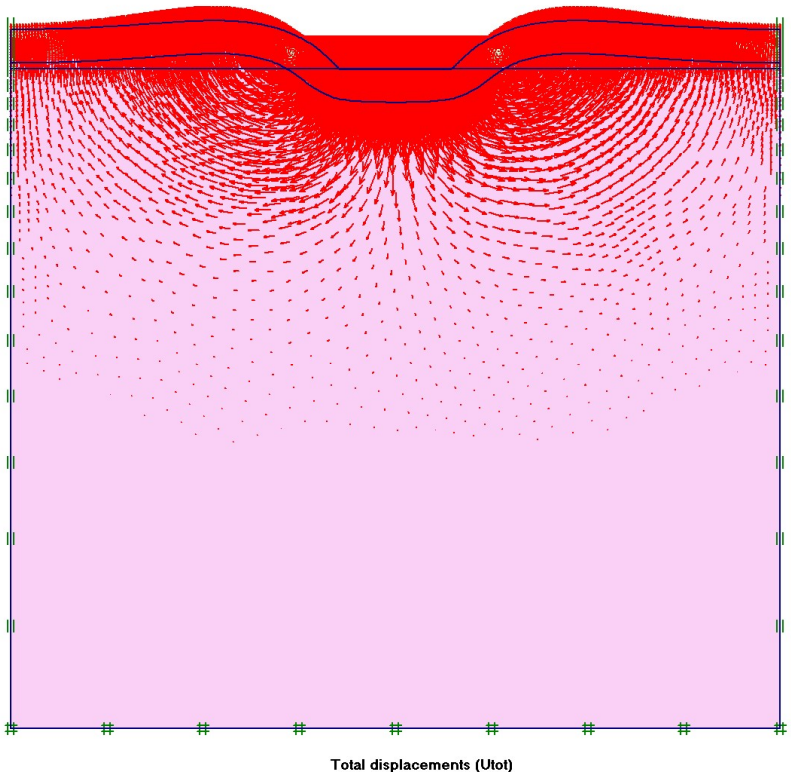

Fig. 6.17a Total Displacement arrows for H_i =0.75m, U_{tot}=0.744m

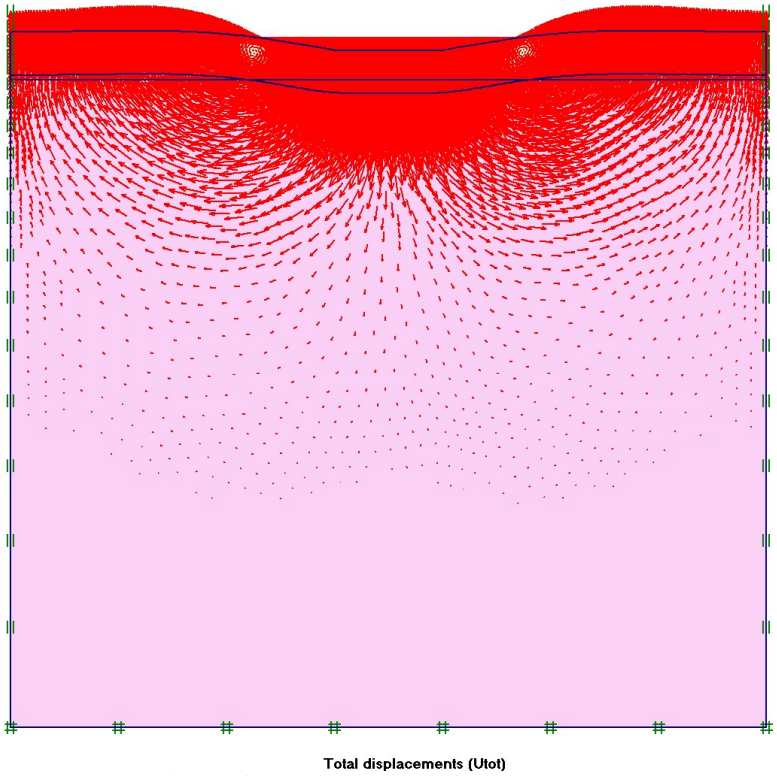

Fig. 6.17b Total Displacement arrows for H_i =1.0m, U_{tot}=0.333m

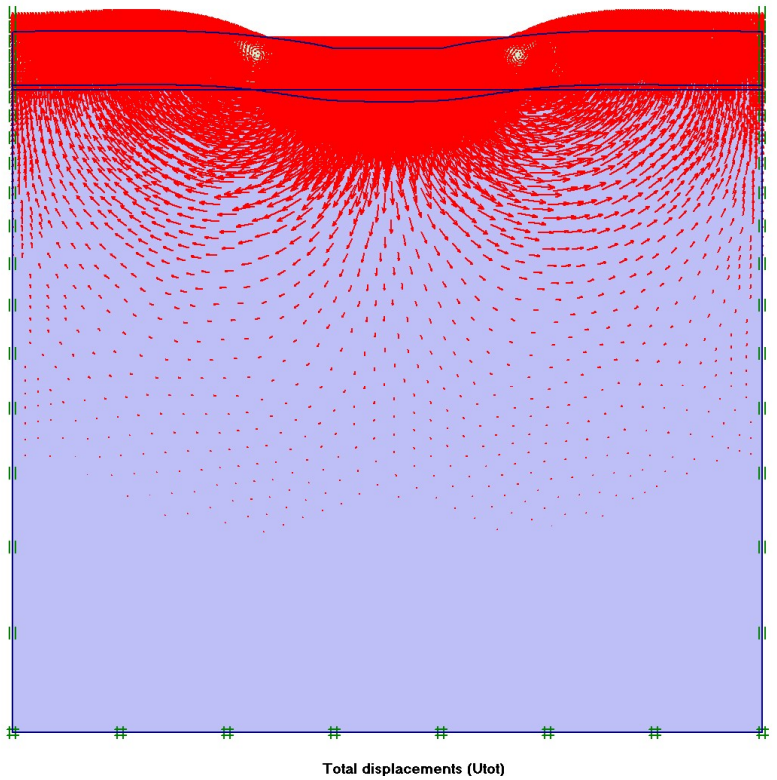

Fig. 6.17c Total Displacement arrows for H_i =1.25m, U_{tot}=0.332m

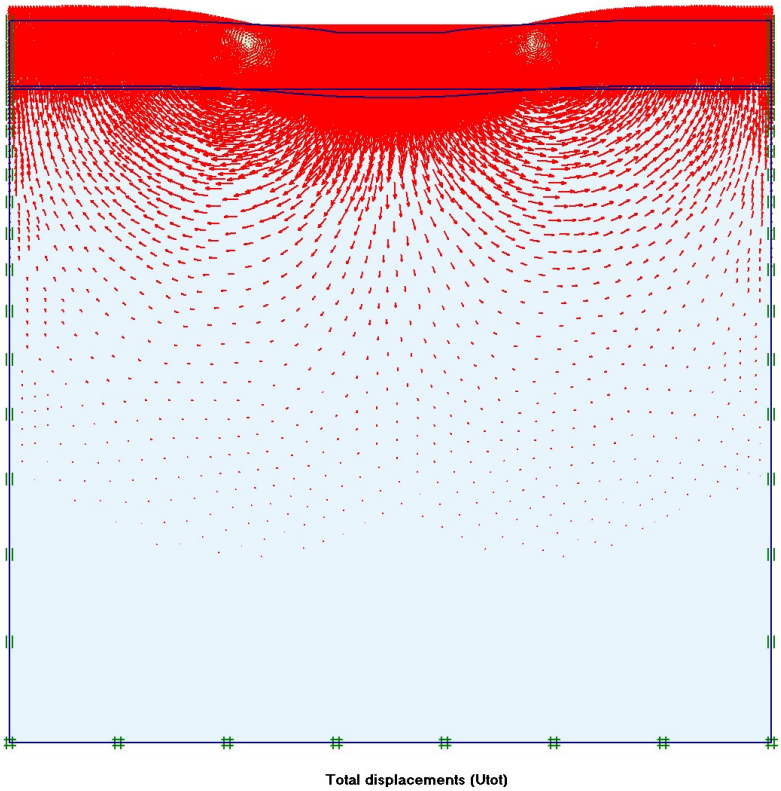

Fig. 6.17d Total Displacement arrows for H_i =1.5m, U_{tot}=0.308m

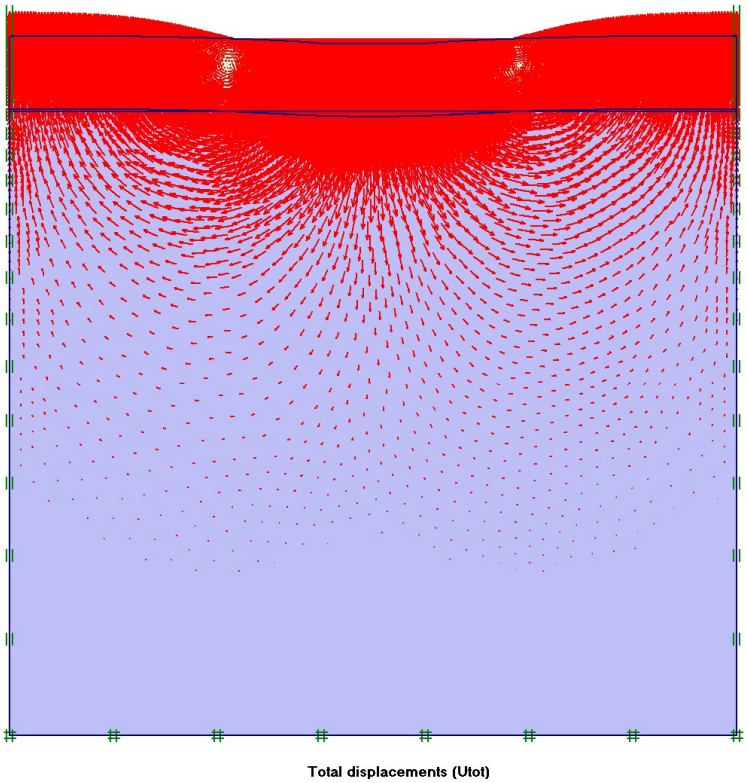

Fig. 6.17e Total Displacement arrows for H_i =1.75m, U_{tot}=0.289m

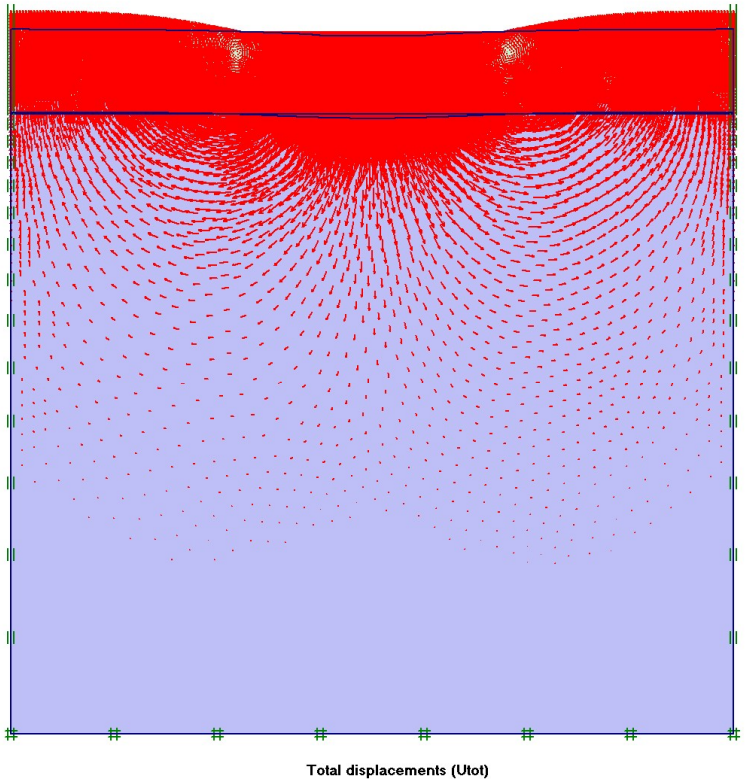

Fig. 6.17f Total Displacement arrows for H_i =2.0m, U_{tot}=0.27.m

6.9.1.2 Total Displacement Shown by Shadings for Untreated Upper Sand Mat

Legend of shadings is kept same for all H_i to compare the displacements with same scale. For H_i=0.5 and H_i/B=0.2 or less the strip footing penetrates into the bottom soft clay layer. For up to H_i=0.75 and H_i/B=0.3 the strip footing settles up to of bottom soft clay layer. For H_i=1.00 and H_i/B=0.4 or above settlement of strip footing is limited within upper sand mat.

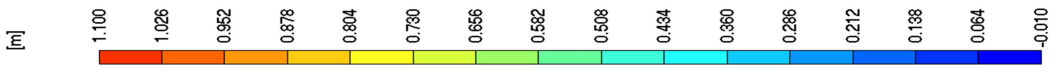

Fig. 6.18 Legend of shadings for Untreated Upper Sand Mat

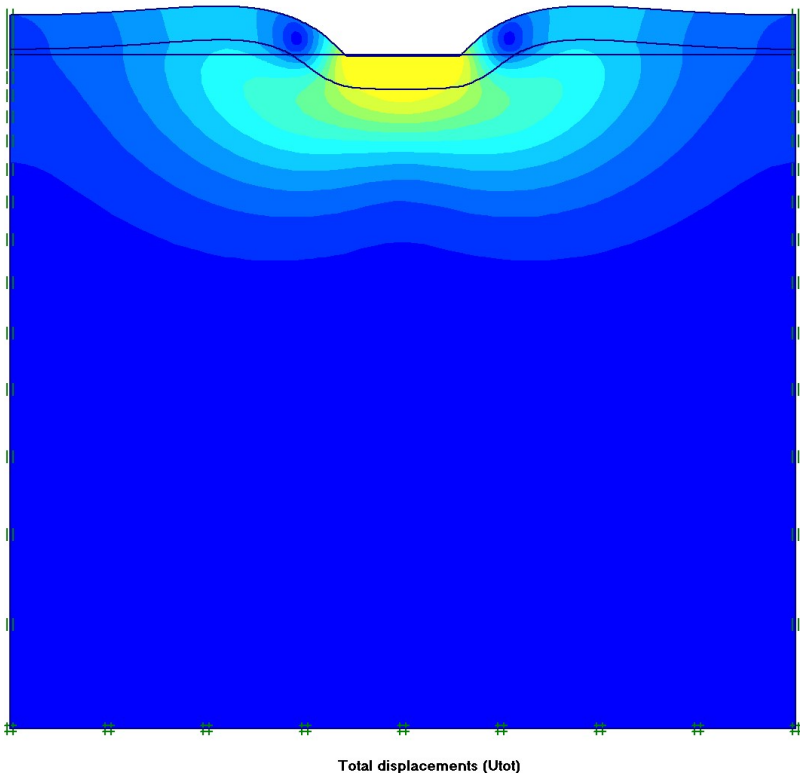

Fig. 6.19a Total Displacement shadings for H_i =0.75m, U_{tot}=0.744m

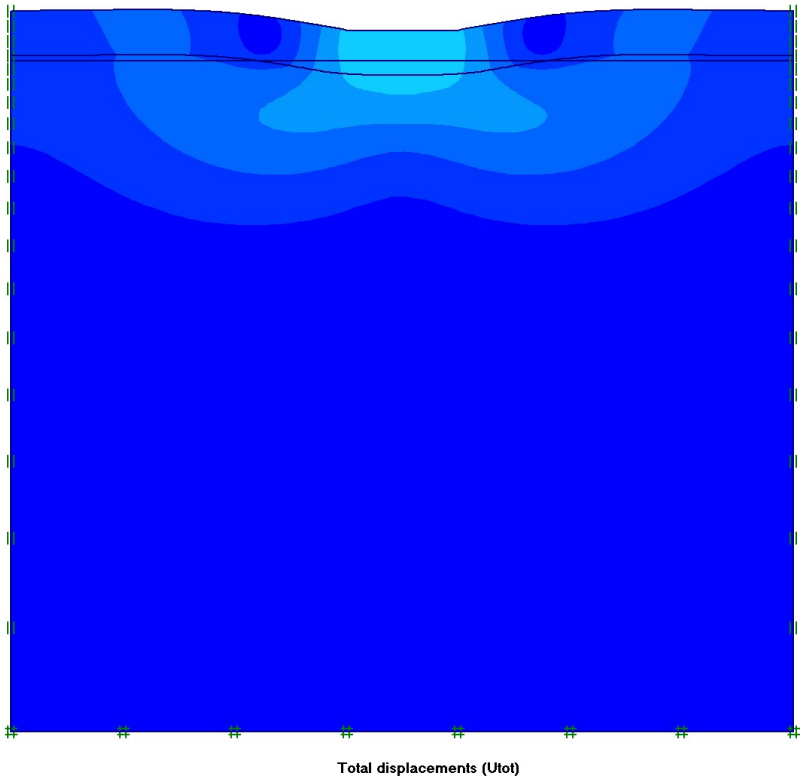

Fig. 6.19b Total Displacement shadings for H_i=1.00m, U_{tot}=0.333m

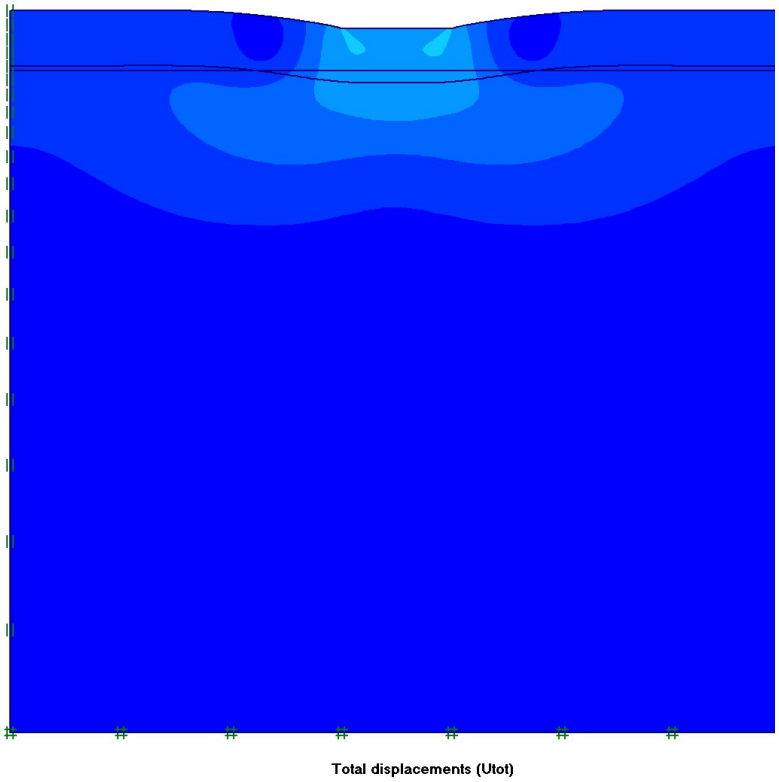

Fig. 6.19c Total Displacement shadings for H_i =1.25m, U_{tot}=0.332m

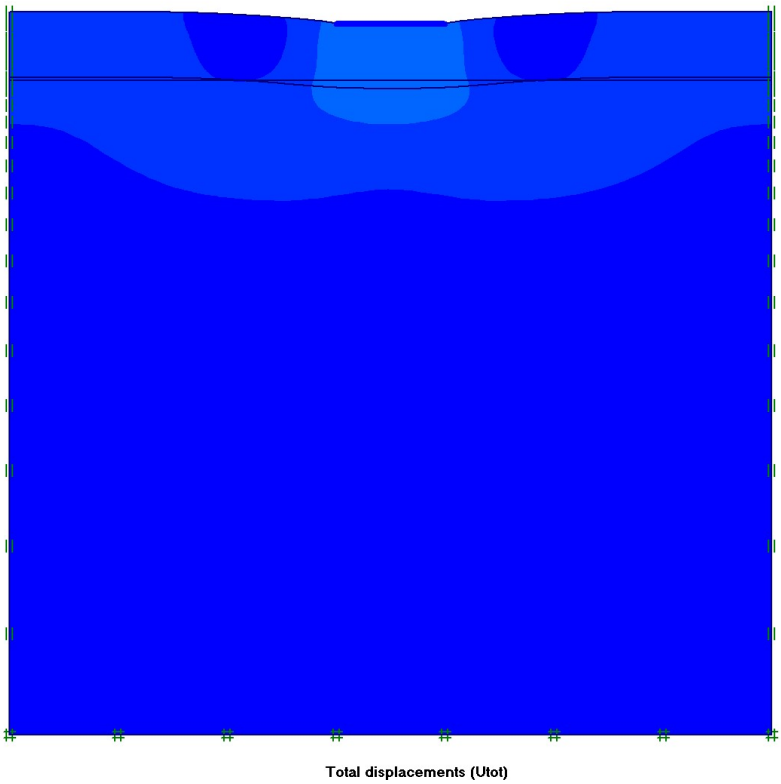

Fig. 6.19d Total Displacement shadings for H_i =1.50m, U_{tot}=0.308m

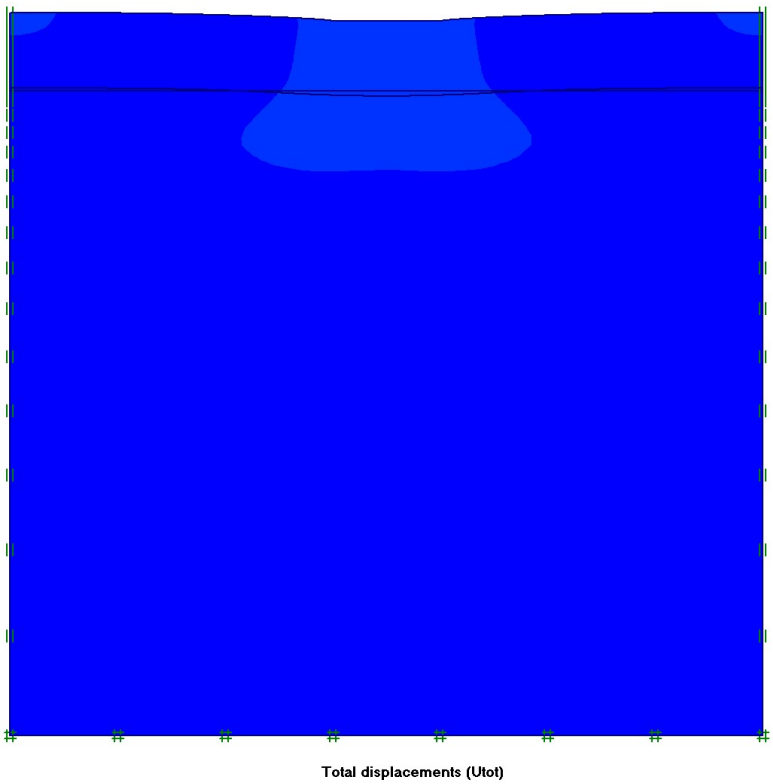

Fig. 6.19e Total Displacement shadings for H_i =1.75m, U_{tot}=0.289m

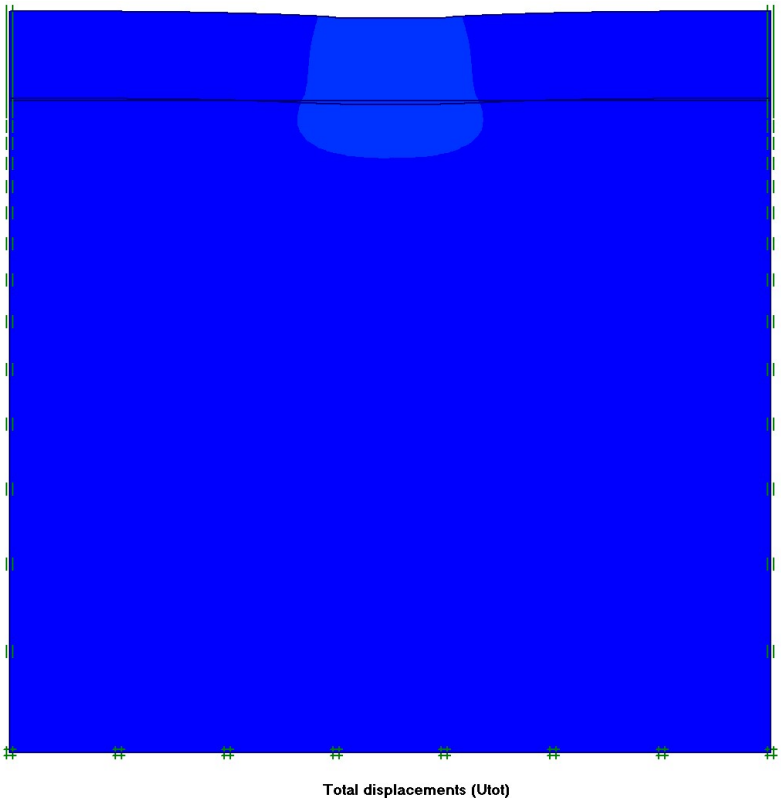

Fig. 6.19f Total Displacement shadings for H_i =2.00m, U_{tot}=0.270m

6.9.2 Total Displacement in Cement Treated Sand as Upper Layer

Total displacement in Cement Treated Sand as Upper Layer for q=200kN/m^2, e_{init}=1.225 are presented in this section.

Total displacement is shown separately by arrows in Figure. 6.20a through 6.20f and by shadings in Figure. 6.22a through 6.22f.

6.9.2.1 Total Displacement Shown by Arrows for Cemented Upper Sand Mat

For H_i =0.75 or above settlement of upper layer into bottom clay layer is very small which represented the distribution of major deformation with in upper layer and the function of footing is limited in upper layer and this indicates complete effectiveness of upper layer in bearing the foundation effectively.

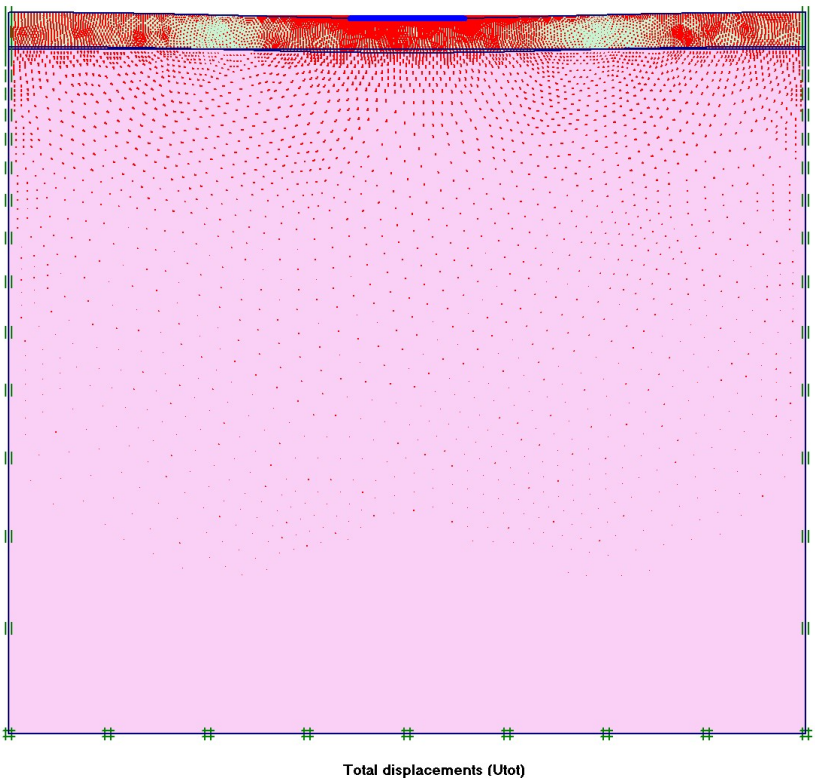

Fig. 6.20a Total Displacement arrows for H_i =0.75m, U_{tot}=0.120m

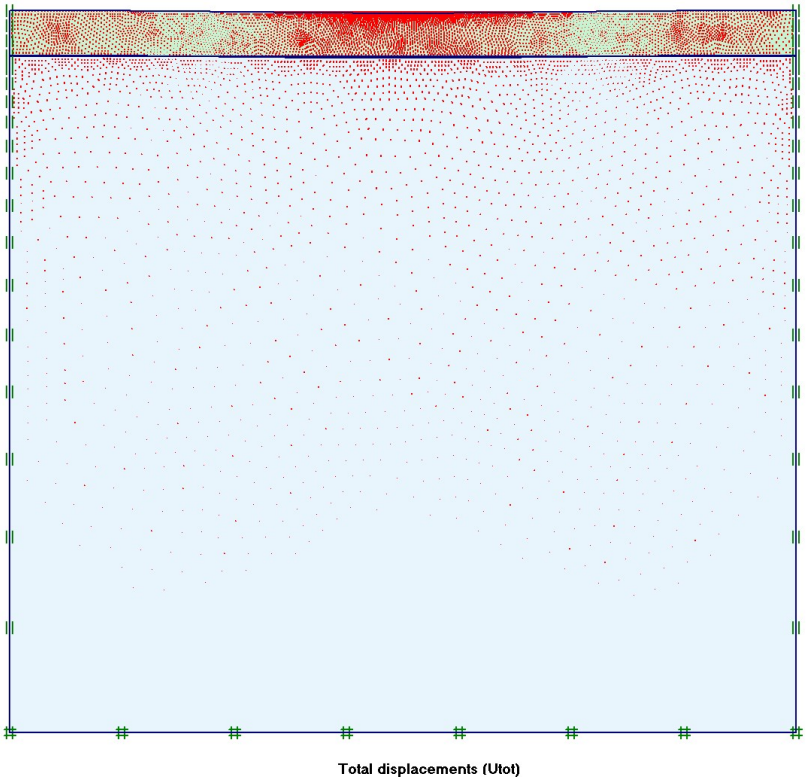

Fig. 6.20a Total Displacement arrows for H_i =1.0m, U_{tot}=0.065m

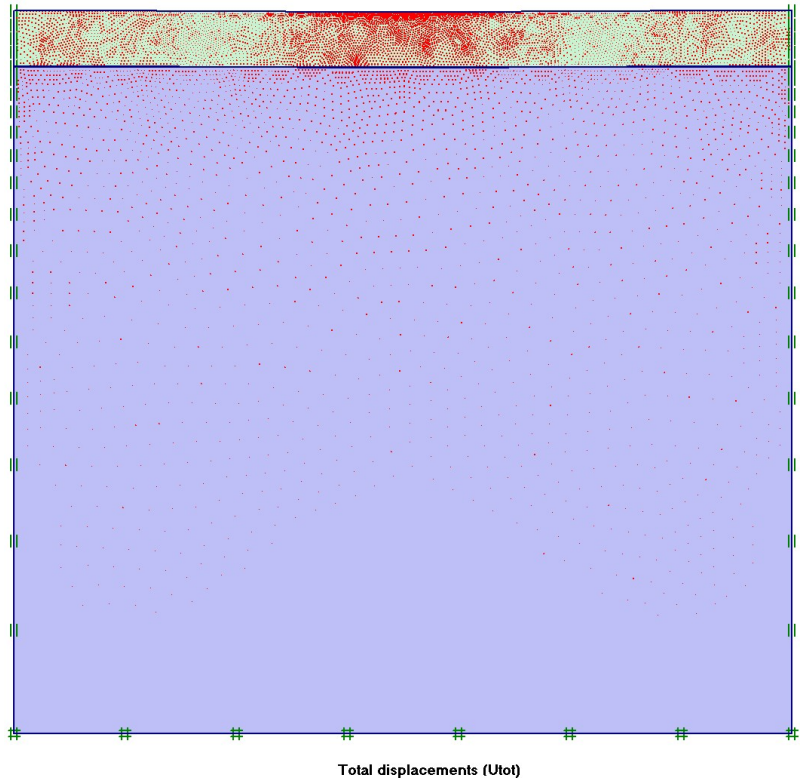

Fig. 6.20a Total Displacement arrows for H_i =1.25m, U_{tot}=0.039m

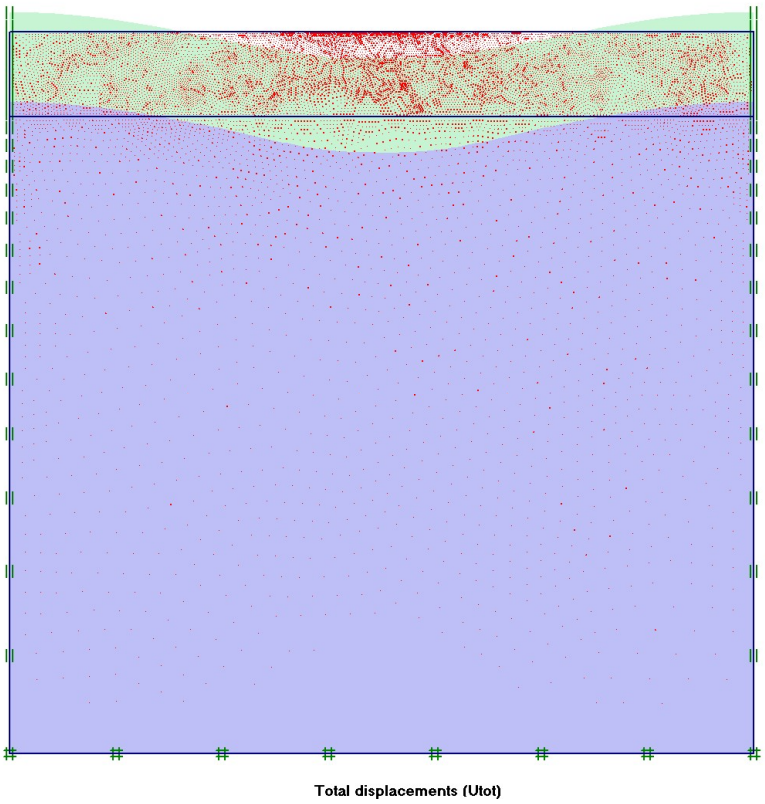

Fig. 6.20a Total Displacement arrows for H_i =1.5m, U_{tot}=0.029m

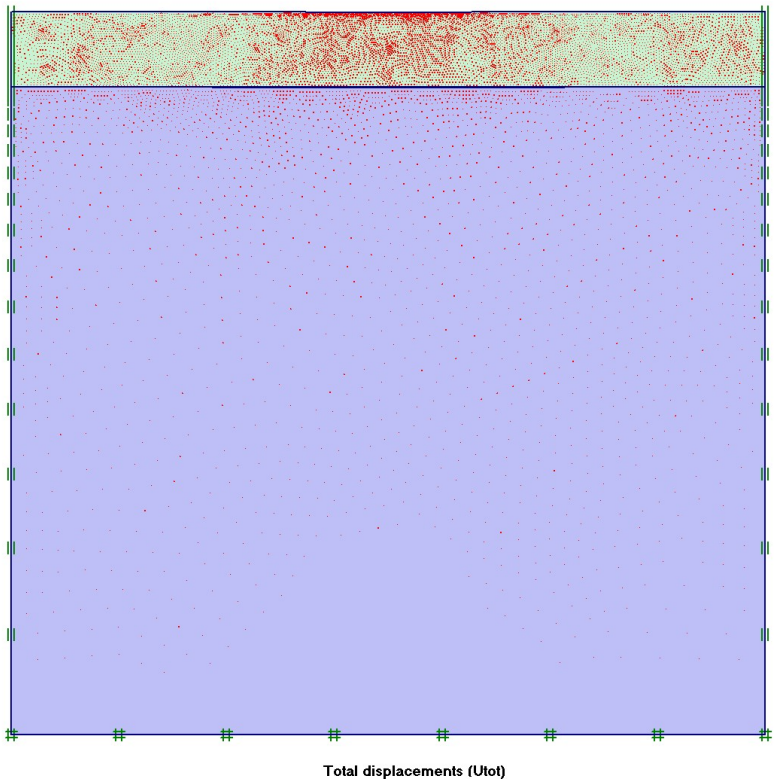

Fig. 6.20a Total Displacement arrows for H_i =1.75m, U_{tot}=0.021m

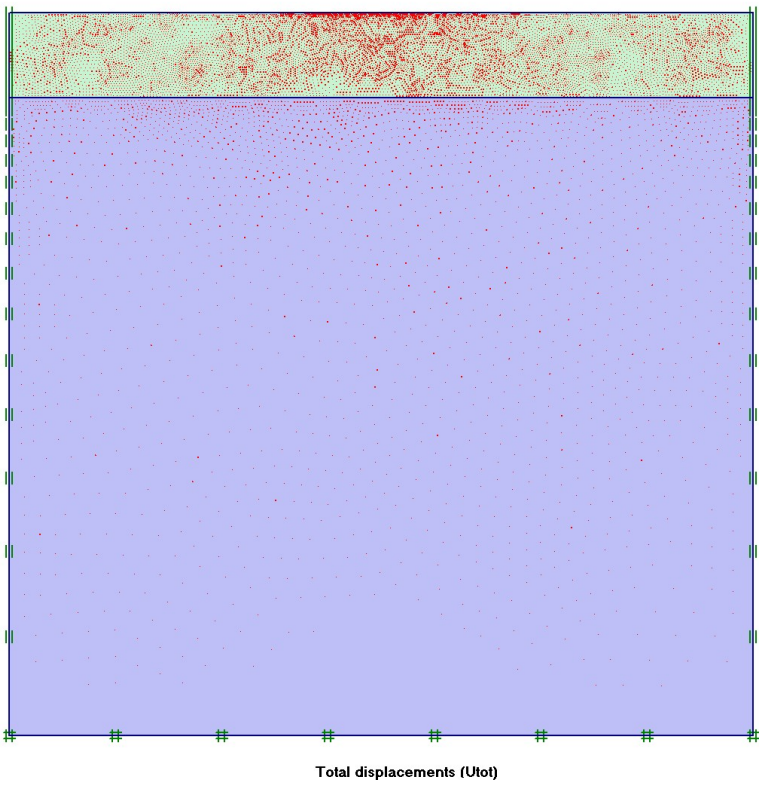

Fig. 6.20a Total Displacement arrows for H_i =2.0m, U_{tot}=0.015m

6.9.2.2 Total Displacement Shown by Shadings for Cement Treated Upper Sand Mat

Legend of shadings is kept same for all H_i to compare the displacements with same scale. For H_i=0.5 and H_i/B=0.2 or above the strip footing does not penetrate in bottom soft clay layer. For up to H_i=0.75 and H_i/B=0.3 or above settlement of strip footing is limited within upper sand mat.

Fig. 6.21 Legend of shadings for Cement Treated Upper Sand Mat

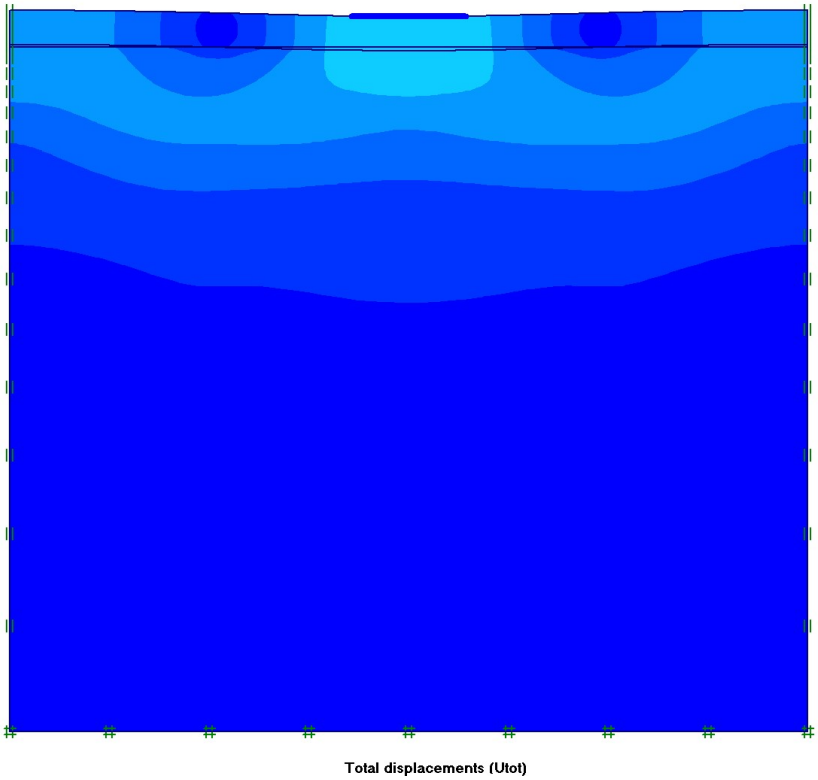

Fig. 6.22a Total Displacement shadings for H_i =0.75m, U_{tot}=0.120m

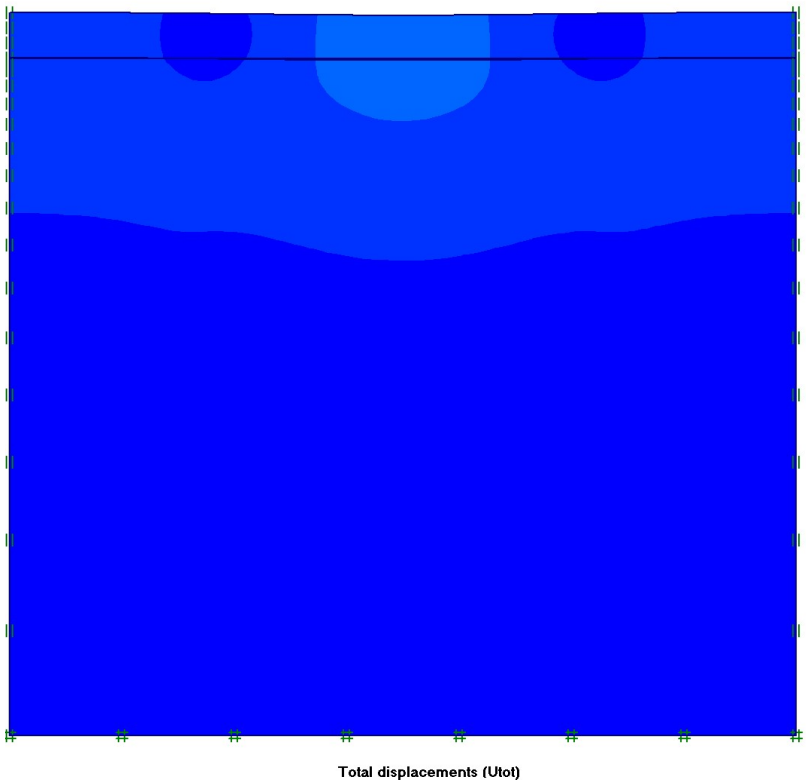

Fig. 6.22b Total Displacement shadings for H_i=1.00m, U_{tot}=0.065m

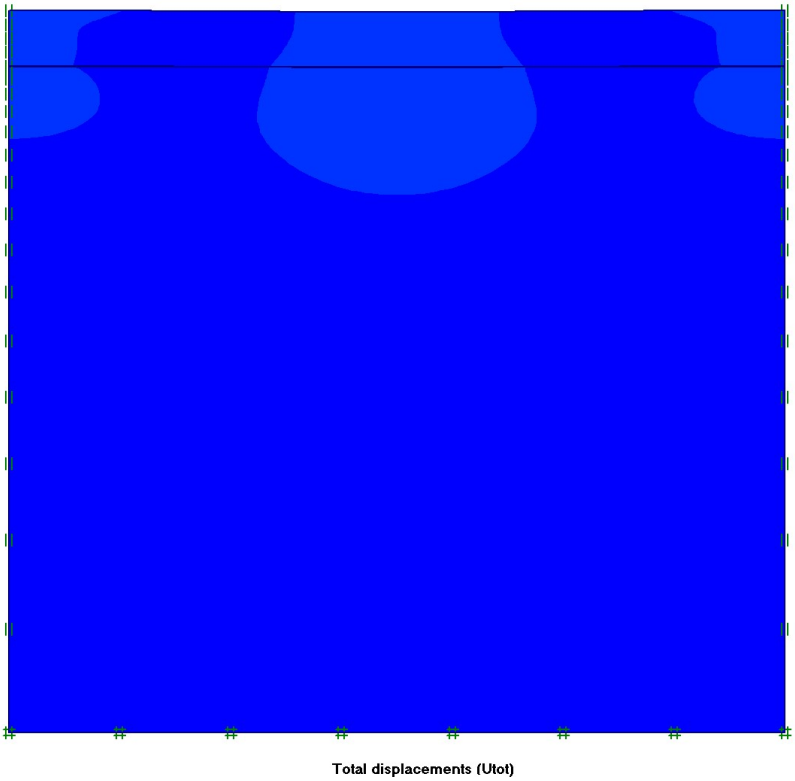

Fig. 6.22c Total Displacement shadings for H_i =1.25m, U_{tot}=0.039m

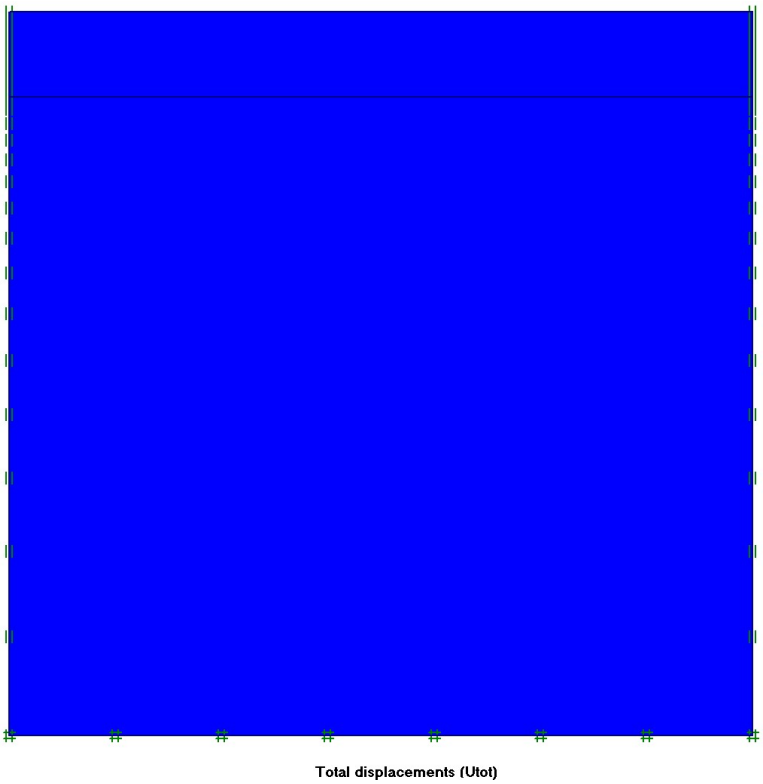

Fig. 6.22d Total Displacement shadings for H_i =1.50m, U_{tot}=0.029m

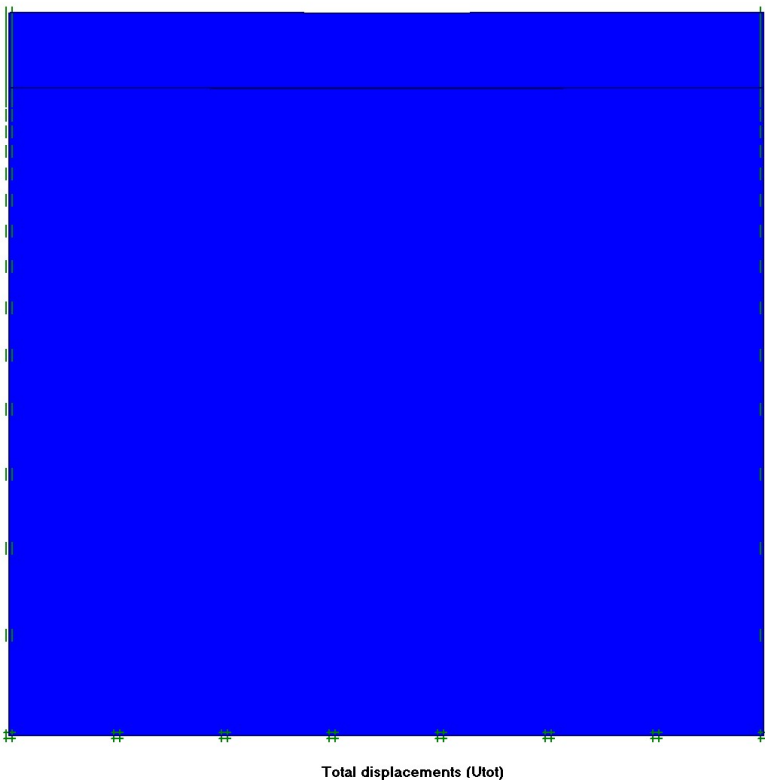

Fig. 6.22e Total Displacement shadings for H_i =1.75m, U_{tot}=0.021m

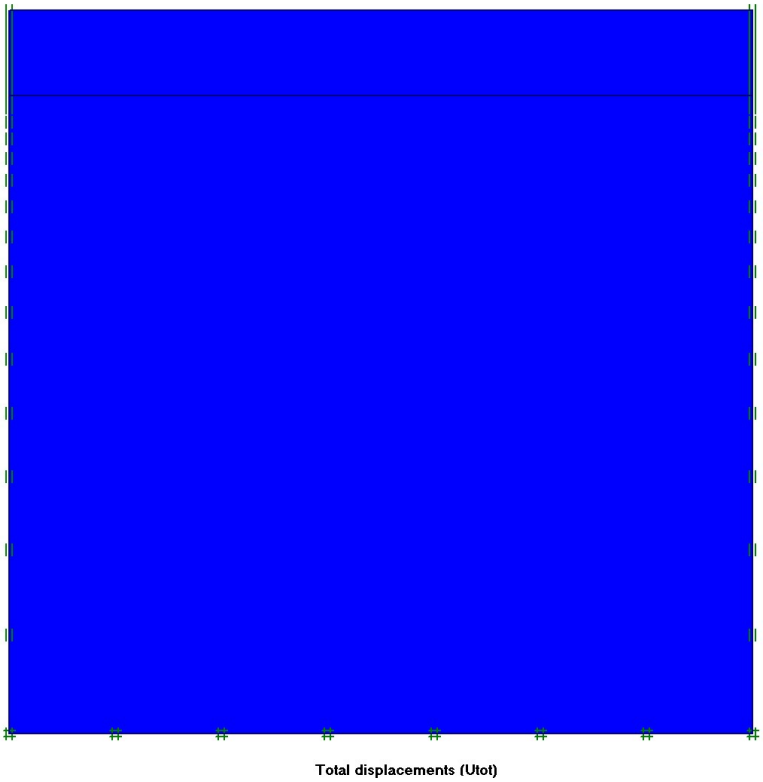

Fig. 6.22f Total Displacement shadings for H_i =2.00m, U_{tot}=0.015m

CHAPTER-7
CONCLUSIONS

7.1 Summary and Conclusions

The settlement of the shallow strip foundation resting on layered soils, with untreated or treated sand layer as upper and bottom clay layer has been analyzed in this research work. Parametric study has been conducted to determine the effect of thickness, density, cementation of sand mat and density, shear strength of the soft clay layer on the settlement of strip foundation. A better insight of elasto-plastic, consolidation & creep settlements of a strip footing on sand mat under different footing pressure equivalent to low or moderately loaded low to medium rise residential or commercial building loads has been developed. Guidelines have been established for designing shallow strip footing with sand mat on thick soft clay deposit determining the thickness of sand mat for different material characteristics to avoid punching shear failure and to limit the settlement to an allowable level. The conclusions from this study are summarized below in article 7.1.1 to 7.1.3.

7.1.1 Significance of Relative Settlement S/S_0

The relative settlement (S/S_o) at the center point of the footing for both untreated or cement treated upper sand layer was calculated, where S_o is the settlement for the case with H_i= 0.25m and S is the settlement for others H_i value. A larger value of relative settlement S/S_o indicates this larger difference of settlement between the cases of small and larger thickness of sand layer. This is the definition and significance of relative settlement S/S_0 introduced by this research. The effect S/S_o is presented below:

- For both untreated or cement treated upper sand layer the relative settlement decreases at a high rate with the increase of normalized footing pressure upto a certain value of normalized footing pressure. After this particular value of footing pressure, this rate of decrease of relative settlement is smaller. In general three distinct zone can be identified in the relationship of S/S_o vs $q/\gamma_{sat}B$ for different e_{init}. At left zone up to $q/\gamma_{sat}B$=2.5 the S/S_o decreases rapidly and at middle zone from $q/\gamma_{sat}B$=2.5 to 3.5 the S/S_o decreasing rate of S/S_o is low and at right zone for $q/\gamma_{sat}B$>3.5 there is no decrease of S/S_o that is sand mat is no longer effective to reduce settlement. The difference of relative settlement for different normalized

footing pressure remains more or less same for different value of relative thickness of upper sand mat at right zone.

- Both S_o and S changes when footing pressure changes. Thus a higher value of S/S_o implies larger difference between S and S_o. Stated in a different way a larger relative settlement means that the sand mat is more effective in controlling the settlement.

- For a given thickness of sand mat and clay layer, the effectiveness of the sand mat reduces with increase of footing pressure and after a certain value of footing pressure the sand mat appears to be no longer effective. Similar observation can be made for both untreated or cement treated upper sand layer.

- For a given H_i if the $q/\gamma_{sat}B$ is increased up to a 2.5 certain value the relative decreases means the effectiveness of the sand layer in controlling settlement reduces for both untreated or cement treated upper sand layer. S/S_o may be considered as the index of the effectiveness of sand layer.

- For all value of e_{init}, S/S_0 decreases with increase of normalized value of thickness of upper sand layer *i. e.* H_i/B for particular $q/\gamma_{sat}B$. This rate of decrease (slope) is not constant for all value of H_i/B. It is observed from the graphs that the relative settlement decreases at the same rate with the increase of thickness of upper sand layer H_i/B. For a particular value of H_i/B increase of S/S_0 with $q/\gamma_{sat}B$ is more significant for values of $q/\gamma_{sat}B$ higher than 2.5. For values of $q/\gamma_{sat}B$ less than 2.5 S/S_0 at different $q/\gamma_{sat}B$ are closer.

- For all value of e_{init}, S/S_0 decreases with increase of different $q/\gamma_{sat}B$ for normalized value of thickness of upper sand layer H_i/B. This decreasing rate (slope) is not constant for all value of $q/\gamma_{sat}B$.

- The relative settlement decreases at a high rate with the increase of thickness of upper sand layer H_i/B upto a certain value of normalized footing pressure which is 2.5. After this particular value of footing pressure, this rate of decrease of relative settlement is smaller. For a particular value of H_i/B increase of S/S_0 with $q/\gamma_{sat}B$ is

more significant for value of $q/\gamma_{sat}B$ higher than 2.5. For values of $q/\gamma_{sat}B$ less than 2.5 S/S_0 at different $q/\gamma_{sat}B$ are closer.

- For value of $q/\gamma_{sat}B$ smaller than 2.5 the cement treated upper sand layer is more effective than untreated upper sand layer in reducing relative settlement S/S_0 and for value of $q/\gamma_{sat}B$ higher than 2.5, the effectiveness of untreated upper sand layer and cement treated upper sand layer is about similar in reducing relative settlement S/S_0. For value of H_i/B smaller than 0.5 the cement treated upper sand layer is more effective than untreated upper sand layer in reducing relative settlement S/S_0 and for value of H_i/B higher than 0.5 the effectiveness of untreated upper sand layer and cement treated upper sand layer is about similar in reducing relative settlement S/S_0.

7.1.2 Design Guideline

Design guidelines are developed for strip footing on soft inorganic NC soil of Bangladesh having void ratio 1.0 to 1.45. The research work was limited on a single E' and ϕ' value of soft clay layer and also a single ϕ' value of sand mat. These design charts may be used to obtain total settlement for particular values of footing pressure (q), Sand mat thickness (H_i), footing width (B) and initial void ratio (e_{init}). For untreated or cement treated sand as upper layer settlement of strip footing may be calculated for particular value of H_i, q, B and γ_{sat} using developed design chart or equations. For a specific value of settlement the design thickness of sand mat may be obtained using different Equations. The permissible settlement as per BNBC 2015 is 50mm. Design thickness of sand mat for possible settlement of 50mm may be obtained using separate equations.

Provision of untreated or cement treated upper sand layer immediately below footings may offer a ground improvement technique that, depending on local labour costs, may be a cost-effective alternative to piled foundations for light to moderate foundation loads. The approach should be considered as replacement of weak top soil or for low fills needed to reach a specified ground level to carry load of footings for low or medium rise buildings constructed on this artificial layer.

7.1.3 Deformation Behaviour

For H_i/B =0.6 or above settlement of Untreated Sand as upper layer into bottom clay layer is very small which represented the distribution of major deformation with in upper layer and the function of footing is limited in upper layer and this indicates complete effectiveness of upper layer in bearing the foundation effectively. For H_i=0.5 and H_i/B=0.3 or less the strip footing penetrates in bottom soft clay layer. For up to H_i=0.75 and H_i/B=0.3 the strip footing settles up to of bottom soft clay layer. For H_i=1.00 and H_i/B=0.4 or above settlement of strip footing is limited within upper sand mat.

For H_i =0.3 or above settlement of cement treated Sand as upper layer into bottom clay layer is very small which represented the distribution of major deformation with in upper layer and the function of footing is limited in upper layer and this indicates complete effectiveness of upper layer in bearing the foundation effectively. For H_i=0.5 and H_i/B=0.3 or above the strip footing does not penetrate in bottom soft clay layer. For up to H_i=0.75 and H_i/B=0.3 or above settlement of strip footing is limited within upper sand mat.

7.2 Limitation of Analysis

Brittle behavior of cemented sand and fracture or cracks is not considered in this analysis.

Various correlation are available for C_c in literature but only a particular correlation has been used in this analysis.

No site specific parameter has been used in analysis. Arbitrary parameter of soil reported in previous literature has been used.

7.3 Recommendations for Future Research

Similar analysis may be conducted with different stiffness of cemented sand, sand using different amount of cement and use of aggregate with cement.

Analysis may also be conducted using reinforced sand layer.

Using design guideline different type structure may be designed and comparison of cost between treated and untreated sand mat and with deep foundation may be made.

Model test may be carried out and displacement field observed from model test may be compared with the displacement field obtained in this research.

REFERENCES:

Adhikari, D. K., Roy, M. K., Datta, D. K., Roy, P. J., Roy, D. K., Malik A. R. and Alam, A. K. M. B. (2006), "Urban Geology: A Case Study of Khulna City Corporation, Bangladesh", J. Life Earth Sci., Vol. 1(2): 17- 29, ISSN 1990-4827@2006, JLES, RU.

Ahamed, S. (2005), "Soil characteristics and liquefaction potential of selected reclaimed areas of Dhaka city", M.Sc. Engg. Thesis, Department of Civil Engineering, Bangladesh University of Engineering and Technology, Dhaka, Bangladesh.

Anisuzzaman, M., Arifuzzaman and Ridha (2013), "Sub - Soil Characteristics of Selected Coastal Regions of Bangladesh", International Journal of Chemical, Environmental & Biological Sciences (IJCEBS) Volume 1, Issue 5, ISSN 2320-4079; EISSN 2320–4087.

Arifuzzaman and Hasan, A. (2013), "Evaluation of Foundation Difficulties over Soft Organic Soil", Jordan Journal of Civil Engineering, Volume 7, No. 4, 2013.

Axelsson, O. (1994), "Iterative Solution Methods", Cambridge University Press, New York.

Augustesen, A., Liingaard, M. and Lade, P.V. (2004), "Evaluation of Time-Dependent Behavior of Soils", International Journal of Geomechanics, vol 4, no. 3.

Berengo, V. (2010),"Constitutive modelling of the time-dependent behaviour of Venice heterogeneous silts", Ph.D. thesis, Department of Geotechnical Engineering, University of Padova, Italy.

Bowles, J. E. (1996), "Foundations Analysis and Design", McGraw-Hill Publishing Company, New York.

Bowles, J. E. (1997), "Foundation Analysis and Design", McGraw-Hill, International Edition, New York.

Brinkgreve, R. B. J. and Broere, W. (2002), "PLAXIS 2D-Version 8 - Manual", Delft University of Technology & PLAXIS b.v., The Netherlands, A.A. Balkema Publishers, http://www.plaxis.nl.

Burd, H. J. and Frydman, S. (1997). Bearing capacity of plane-strain footings on layered soils. Canadian Geotechnical Journal. Vol. 34.

Bujang, B. K., Asadi, A. and Kazemian, S. (2009), "Experimental Investigation on Geomechanical Properties of Tropical Organic Soils and Peat", American J. of Engineering and Applied Sciences 2 (1):184-188 .

Charbit, B. (2009), "Numerical analysis of laterally loaded lime/cement columns", M. Sc. Thesis 09/05, Division of Soil and Rock Mechanics, Department of Civil and Architectural Engineering, Stockholm, Sweden, Royal Institute of Technology (KTH).

Chen, W. F. and Davidson, H. L. (1972), "Bearing Capacity Determination by Limit Analysis", Fritz Engineering Laboratory, Department of Civil Engineering, Lehigh University, Bethlehem, Pennsylvania, Fritz Engineering Laboratory Report No. 355.15.

Das, B. M. (1999), "Shallow Foundations Bearing Capacity and Settlement", CRC Press LLC, Boca Raton, London, NewYork, Washington, D.C.

Duraisamy, Y. B., Huat, B. K. and Aziz, A. A. (2007), "Engineering Properties and Compressibility Behavior of Tropical Peat Soil", Science Publications, American Journal of Applied Sciences 4 (10): 768-773.

Fattah, M. Y., Hadidi, M. T. A. and Shammary, A. S. A. (2012), "Effect of Change in the Coefficient of Permeability on Consolidation Characteristics of Clays", Journal of Engineering, Volume 18 January, 2012, Number 1, Building and Construction Engineering Dept., University of Technology and Civil Engineering Dept., College of Engineering, University of Baghdad, Baghdad, Iraq.

Fernando, S., Pedro, D. M. P. and Nilo, C. C. (2000), "Characterization of Cemented Sand in Triaxial Compression", Porto Alegre, Rio Grande do Sul, Brazil.

Ferdous, S. M. (2007), M. Sc. Engg Thesis, Abdul Jabbar Khan, pp-5.

Haan, E. J. D. (1996), "A compression model for non-brittle soft clays and peat", Int. J. Rock Mech. Min. Sci. Geomech., 33.

Hanna, A. M. and Meyerhof, G. G. (1980), Design charts for ultimate bearing capacity for sands overlying clays, *Canadian Geotech. J.*, 17(2).

Haan, E. J. D. (1997), "An overview of the mechanical behavior of peats and organic soils and some appropriate construction techniques", Proceedings of Conference on Recent Advances in Soft Soil Engineering. Huat & Bahia (ed), Kuching, Sarawak.

Hossain, M. M. and Rahman, M. N. (2005), 'Sub-soil Investigation Report at the Proposed Site for the Construction of Residential Building of S. I. and A.S.I. at Sonadanga Thana (KMP, Khulana)', Department of Civil Engineering, KUET, pp-7.

Huat, B. K. (2004), "Organic and Peat Soils Engineering", Serdang: University Putra Malaysia Press.

Islam, M. S., Siddique, A. and Muqtadir, A. (2004), "Mechanical Properties of Soft Organic Dhaka Clay", Journal of Civil Engineering (IEB), 32(2) (2004) 143-161.

Kenny, M. J. and Andrawes, K. Z. (1999), "The bearing capacity of footings on a sand layer overlying soft clay", G e′otechnique 49, No. 4, 553-555.

Khan, A. J. and Ferdous, S. M. (2004). "Geotechnical Characteristics of Subsoil in Khulna City Corporation (KCC) Area", Journal of the Institute of Engineers, Bangladesh, Vol. Mul-dis 29, No.1, December, pp. 37-58.

Kuo, Y. L. (2008), "Effect Of Soil Variability on The Bearing Capacity of Footings on Multi-Layered Soil", Thesis Submitted for the Degree of Doctor of Philosophy (Ph. D.), School of Civil, Environmental And Mining Engineering, University Of Adelaide, Australia.

Mashad, M. E. and Hashad, A. (2013), "Improving the strength of sandy silt soils by mixing with cement kiln dust", Journal of Engineering Sciences, Assiut University, Faculty of Engineering, Vol. 41, No. 4, July, 2013, PP. 1421 - 1431.

Massih, Y. A. D., El-Hachem, E. and Soubra, A. H. (2005), "Bearing Capacity of Eccentrically and or Obliquely Loaded Strip Footing over Two-Layer Foundation Soil by a Kinematical Approach", VIII International Conference on Computational Plasticity, Complas VIII, Ó Cimne, Barcelona, 2005.

Meyerhof, G. G. and Hanna, A. M. (1978), Ultimate bearing capacity of foundations on layered soils under inclined load, *Canadian Geotech. J.*, 15(4).

Michalowski, R. L. and Shi, L. (1995). Bearing capacity of footings over two-layer foundation soils. Journal of Geotechnical Engineering, 121(5).

Mitchell, J. K. (1976), The properties of cement-stabilized soils. Proceeding of Residential Workshop on Materials and Methods For Low Cost Road, Rail, and Reclamation Works, Australia: 365–404.

Muhunthan, B. and Sariosseiri, F. (2008), "Interpretation of Geotechnical Properties of Cement Treated Soils", Research Report FHWA Contract DTFH61-05-C-00008, Compaction Control of Marginal Soils in Fills, The Federal Highway Administration U.S. Department of Transportation.

Murthy, B. R. S., Sridharan, A. and Vinod, P. (1995), "Analyses Of Two-Layer Soil Systems Beneath Rigid Footings", Division of Earth and Environmental Sciences, Indian Institute of Science, Civil Engineering, G14426, Jul-1995.

Ozcoban, S., Berilgen M. M. H. Kilic, T. B. E. and Ozaydin, I. K. (2007), "Staged Construction and Settlement of a Dam Founded on Soft Clay", Journal of Geotechnical and Geoenvironmental Engineering, ASCE, August 2007, Page-1103-1016.

Pantelidis, L. (2008), "Determining of The Soil Strength Characteristics Through The Plate Bearing Test", Foundations of Civil and Environmental Engineering, No. 11, Aristotle University of Thessaloniki, Greece.

Razzaque and Alamgir (1999), 'Long-Term Settlement Observation of a Building in a Peat Deposit of Bangladesh', International Conference of AIT, Thailand, Dr. Abdul Jabbar Khan, P-5.

Sharma, M. S. R., Baxter, C. D. P., Wilhelm, H., Moran, K. and Vaziri, H. (2010) "Characterization of Weakly Cemented Sands using Nonlinear Failure Envelopes".

Serajuddin, M. (1998), "Some Geotechnical studies on Bangladesh soils: A Summary of papers between 1957-96",Journal of civil engineering, The institution of engineers, Bangladesh, Vol. CE 26, No-2, 1998.

Serajuddin, M. and Chowdhury, M. A. (1967),'Studies on Engineering Properties of East Pakishsan Soil', Proc, First Southest Asian Regional Conference on Soil Engineering, Bangkok Thailand, pp9-12.

Serajuddin, M. and Ahmed, A. (1998),'Correlation between SPT and Unconfined Compressive Strength of Cohesive Soil Deposit of Bangladesh', Journal of CE, IEB, Vol. CE 24, no 1, 1996, pp69-81.

Shenawy, A. O. A. and Karni, A. A. A. (2005), "Derivation of Bearing Capacity Equation for a Two Layered System of Weak Clay Layer Overlaid by Dense Sand Layer", Pertanika J. Sci. & Techno!. 13(2): 213 - 235, Universiti Putra Malaysia Press, King Saud University, Civil Eng. Dept., P. O. Box 800, Riyadh, 11421, Saudi Arabia.

Skempton, A. W. and Petley, D. J. (1970), "Ignition loss and other properties of peats and clays from Avonmouth", King's Lynn & Cranberry Moss, Geotechnique. Vol 20, no. 4.

Sorensen, K. K. and Okkels, N. (2013), "Correlation Between Drained Shear Strength and Plasticity Index of Undisturbed Overconsolidated Clays", Proceedings of the 18th International Conference on Soil Mechanics and Geotechnical Engineering, Paris 2013, vol. 1.

Springman, S. M. (2014), "Modelling in Geotechnics - Script(Part 1)", ETH Zürich, Institute of Geotechnical Engineering, *http://igtcal.ethz.ch/mig*.

Sture, S. (2004), "Determination of Soil Stiffness Parameters", Short Course on Computational Geotechnics and Dynamics, University of Colorado, Boulder, U.S. state of Colorado, U. S. A.

Szypcio, Z. and Dołżyk, K. (2006), "The Bearing Capacity of Layered Subsoil", Studia Geotechnica et Mechanica, Vol. XXVIII, No. 1.

Thomé, A., Donato, M., Consoli, N. C. and Graham, J. (2005), "Circular footings on a cemented layer above weak foundation soil", Can. Geotech. J. 42: 1569–1584, NRC Canada.

Tuncer, B. E. and Craig, H. B. (2009), "Comparison of Basic Laboratory Test Results With More Sophisticated Laboratory and In-Situ Tests Methods on Soils In Southeastern Wisconsin", Department of Civil and Environmental Engineering University of Wisconsin-Madison, Submitted To The Wisconsin Department of Transportation.

Waterman, D. and Broere, W. (2004), "Application of the SSC model - part I", Delft University of Technology/Plaxis BV.

Waterman, D. and Broere, W. (2004), "Application of the SSC model - part II", Delft University of Technology/Plaxis BV.

Waterman, D. and Broere, W. (2004), "Application of the SSC model - part III", Delft University of Technology/Plaxis BV.

Willemsen, L. A. (2011),"Validation And Verification of Thermo- Hydro-Mechanical (THM) Coupling In Plaxis", Master's Thesis, Department of Civil, Environmental And Natural Resources Engineering, Luleå University of Technology.

Wood, D. M. (1990), "Soil behaviour and critical state soil mechanics", Cambridge University Press, Cambridge, UK.

Wood, D. M. (2004), "Geotechnical Modeling", Version 2.2.

Yasin, S. J. M. and Shafiullah, A. M. M. (2003), "Effect of Particle Characteristics on the Strength and Volume Change Behaviour of Sand", Journal of Civil Engineering, The Institution of Engineers, Bangladesh, Vol. CE 31, No. 2, 2003.